An *in vivo* Approach to Elucidating the Function of Mitochondrial Porin by the Characterisation of *Neurospora crassa* Strains Deficient in Porin

by

William Anthony Theodore Summers

A Thesis submitted to the Faculty of Graduate Studies of

The University of Manitoba

in partial fulfilment of the requirements of the degree of

DOCTOR OF PHILOSOPHY

Department of Microbiology

University of Manitoba

Winnipeg

Defended August 16, 2010

Abstract

The mitochondria are the primary energy providers for most eukaryotic cells. The substrate and products of the mitochondria need to be translocated across the semi-permeable mitochondrial outer membrane (MOM). Mitochondrial porin is an aqueous channel in the MOM thought to provide the primary pathway for metabolite translocation. Porin is a nuclear encoded protein and therefore needs to be transported to the mitochondria, translocated across and assembled within the MOM. Of all the recognition signals required for successful transport, import and assembly, only the β-sorting signal used in assembly is known. In addition, this protein possesses the ability to gate, and in doing so can preferentially allow the passage of anions in the open state and cations in the closed state. However, the precise mechanism by which gating of porin occurs and a complete understanding of porin's function in vivo remains elusive.

The essentiality of porin was examined by constructing a strain of *Neurospora crassa* deficient for porin. This strain, denoted as WS004, exists as evidence that porin is non-essential for the survival of *Neurospora crassa*. However, the loss of porin results in a reduction in growth rate due to the dysfunction of the cytochrome mediated respiratory pathway, which was made evident by the reduction of cytochrome *b* and almost complete lack of cytochrome aa_3. WS004 survives by inducing the expression of alternative oxidase, which funnels the electrons from the Q pool directly to oxygen, bypassing the cytochrome b and aa3 containing complexes III and IV respectively. Additional phenotypic differences observed included loss in ability to produce aerial hyphae, reduced amount of conidia produced and strains that were female sterile. It was determined, that additional genetic factors influenced the resulting phenotype due to the

loss of porin. LC-MS/MS, in combination with iTRAQ labelling, was utilized to examine changes in the proteome profiles of porin containing and porin lacking mitochondria and showed several different proteins as significantly up- or down-regulated which lend to an explanation to some of the phenotypes observed. Taken together, these results demonstrate the central role of porin in regulating both mitochondrial and cellular processes.

Acknowledgements

I would like to thank the following people who have provided me with technical support, plasmids and *Neurospora crassa* strains. Dr. F. Nargang for supplying *N. crassa* αTOM70 antibody, several different plasmids and the collection of *mus* mutant *N. crassa* strains. Dr. K. Hell for supplying *N.crassa* αTOM22, αTOM40, αTOM70 and αTIM44 antibodies. A thank you to P. Ezzati for performing the iTRAQ analysis and A. Dufresne for technical support with fluorescent microscopy. I would like to thank all of my committee members for valuable guidance throughout the course of my studies, and the department members for experimental assistance and nerdy chit chat. A thank you to K. Hamill and S. Craig for their much appreciated assistance with experimental preparation and clean up. A special thanks to my supervisor, Dr. Deborah A. Court, without whom none of this would have been possible, words can't do the experience justice. NSERC and the Faculty of Science for funding. Lastly, but most certainly not least, I would like to acknowledge my father and his better half, my mommy, for making me the man i am today; Denise, Jordann, William and Emily and of course my little bro Peewee, for their unfaltered support during this long and trying road.

Table of Contents

List of Figures

List of Tables

List of Abbreviations

2D	two dimensional
A	adenine
Å	angstrom
ade	adenine
ADP	adenosine diphosphate
ATP	adenosine triphosphate
bp	base pair
BSA	bovine serum albumin
C	cytosine
cDNA	complimentary deoxyribonucleic acid
COX	cytochrome c oxidase
Δ	deletion
Da	Dalton
DDM	dodecylmaltoside
DIC	differential interference contrast
DIG	deoxygenin
DMSO	dimethylsulfoxide
DNA	deoxyribonucleic acid
DOC	deoxycholic acid
E. coli	*Escherichia coli*
eGFP	enhanced green fluorescent protein
EM	electron microscopy
FADH2	flavin adenine dinucleotide, reduced form
Fe-S	iron sulfur

G	guanine
GTP	guanosine triphosphate
his	histidine
HRP	horse radish peroxidase
Hsp	heat shock protein
hyg	hygromycin
hVDAC	human voltage-dependent anion-selective channel
IM	inner membrane
IMS	intermembrane space
iTRAQ	isobaric tag for relative and absolute quantitation
kb	kilo base pair
kDa	kilo Dalton
l	litre
LB	Luria-Bertani
LG	linkage group
lys	lysine
µg	microgram
µl	microlitre
µm	micrometer
M	molar
mg	milligram
ml	milliltre
mM	millimolar
min	minute
MOM	mitochondrial outer membrane

MOPS	4-morpholinepropanesulfonic acid
mRNA	messenger ribonucleic acid
mtDNA	mitochondrial DNA
mVDAC	mouse voltage-dependent anion-selective channel
NADH	nicotinamide adenine dinucleotide, reduced form
N. crassa	*Neurospora crassa*
NcVDAC channel	*Neurospora crassa* voltage-dependent anion-selective
Ni-NTA	nickel-nitrilotriacetic acid
NMR	nuclear magnetic resonance imaging
OD	optical density
PAGE	polyacrylamide gel electrophoresis
PCR	polymerase chain reaction
PK	proteinase K
PLB	planar lipid bilayer
PMSF	phenylmethylsulfonyl fluoride
RIP	repeat-induced point mutation
RNA	ribonucleic acid
rpm	revolutions per minute
SAM	sorting and assembly machinery
S. cerevisiae	*Saccharomyces cerevisiae*
ScVDAC	*S. cerevisiae* voltage-dependent anion-selective channel
SDS-PAGE	sodium dodecyl sulfate polyacrylamide gel electrophoresis
T	thymine
TCA	tricarboxylic acid cycle

TIM	translocase of the mitochondrial inner membrane
Tris	tris (hydroxymethyl) aminomethane
trp	tryptophane
TOB proteins	topogenesis of mitochondrial outer membrane β-barrel
UTR	untranslated region
VM	Vogel's minimal

NRC RESEARCH PRESS LICENSE
TERMS AND CONDITIONS

Jul 09, 2010

This is a License Agreement between William AT Summers ("You") and NRC Research Press ("NRC Research Press") provided by Copyright Clearance Center ("CCC"). The license consists of your order details, the terms and conditions provided by NRC Research Press, and the payment terms and conditions.

All payments must be made in full to CCC. For payment instructions, please see information listed at the bottom of this form.

License Number	2464920591068
License date	Jul 09, 2010
Licensed content publisher	NRC Research Press
Licensed content publication	Biochemistry and Cell Biology
Licensed content title	Origami in outer membrane mimetics: correlating the first detailed images of refolded VDAC with over 20 years of biochemical data
Licensed content author	William A.T. Summers and Deborah A. Court
Licensed content date	Jun 1, 2010
Volume number	88
Issue number	3
Type of Use	Thesis/Dissertation
Requestor type	Author (original work)
Format	Print and electronic
Portion	Full article
Order reference number	
Title of your thesis / dissertation	An in vivo approach to elucidating the function of mitochondrial porin by the characterisation of Neurospora crassa strains deficient in porin
Expected completion date	Aug 2010
Estimated size(pages)	309
Total	0.00 CAD
Terms and Conditions	

General Terms & Conditions

Permission is granted upon the requester's compliance with the following terms and conditions:

1. A credit line will be prominently placed in your product(s) and include: for books the author, book title, editor, copyright holder, year of publication; for journals the author, title of article, title of journal, volume number, issue number, and the inclusive pages. The credit line must include the following wording: "© 2008 NRC Canada or its

licensors. Reproduced with permission," except when an author of an original article published in 2009 or later is reproducing his/her own work.

2. The requester warrants that the material shall not be used in any manner that may be derogatory to the title, content, or authors of the material or to National Research Council Canada, including but not limited to an association with conduct that is fraudulent or otherwise illegal.
3. Permission is granted for the term (for Books/CDs-Shelf Life; for Internet/Intranet-In perpetuity; for all other forms of print-the life of the title) and purpose specified in your request. Once term has expired, permission to renew must be made in writing.
4. Permission granted is nonexclusive, and is valid throughout the world in English and the languages specified in your original request. A new permission must be requested for revisions of the publication under current consideration.
5. National Research Council Canada cannot supply the requester with the original artwork or a "clean copy."
6. If the National Research Council Canada material is to be translated, the following lines must be included: The authors, editors, and National Research Council Canada are not responsible for errors or omissions in translations.

v1.3

Gratis licenses (referencing $0 in the Total field) are free. Please retain this printable license for your reference. No payment is required.

If you would like to pay for this license now, please remit this license along with your payment made payable to "COPYRIGHT CLEARANCE CENTER" otherwise you will be invoiced within 48 hours of the license date. Payment should be in the form of a check or money order referencing your account number and this invoice number RLNK10813084.
Once you receive your invoice for this order, you may pay your invoice by credit card. Please follow instructions provided at that time.

Make Payment To:
Copyright Clearance Center
Dept 001
P.O. Box 843006
Boston, MA 02284-3006

If you find copyrighted material related to this license will not be used and wish to cancel, please contact us referencing this license number 2464920591068 and noting the reason for cancellation.

Questions? customercare@copyright.com or +1-877-622-5543 (toll free in the US) or +1-978-646-2777.

Chapter 1: Introduction

The focus of this study was the mitochondrial porin of *Neurospora crassa* with specific focus on its purpose in the mitochondrial outer membrane and how the organism might function without it. Therefore, a brief introduction in *Neurospora crassa* and its genetics will be given, followed by a review of mitochondrial porin structure. This review was recently published (Summers and Court, 2010) and proposed a possible mechanism for the voltage-dependent gating ability mitochondrial porins are known to exhibit.

1.1 *Neurospora crassa as a Model Organism*

Neurospora crassa is a filamentous fungus most recognizable as an orange bread mould, which belongs to the phylum Ascomycota. A sound knowledge base has been developed from over a century of research, into the genetics, cell biology and biochemistry of the organism. Historically, *Neurospora* was employed in experiments by George Wells Beadle and Edward Tatum for which they were awarded the Nobel Prize in physiology or medicine. This work established the "one gene, one enzyme" hypothesis (Horowitz, 1991). The *Neurospora crassa* genome, consisting of seven chromosomes, has been sequenced in its entirety (Galagan et al., 2003). These seven chromosomes, consisting of about 43 megabase pairs, encode for approximately 10,000 genes.

1.1.1 *The Asexual Life Cycle*

Vegetative growth results from hyphal tip extension, with lateral branching occurring behind the tip and fusion of contacting hyphae. The extending hyphae are compartmentalized by incomplete septa and therefore allow for cytoplasmic streaming of

all cellular components. Each compartment can contain 3 to 4 nuclei, and up to a 100 in some mutant strains (Davis and De Serres, 1970). As a result of hyphal fusion of compatible strains, the nuclei are not always genotypically identical. The life cycle of *Neurospora crassa* is predominated by the haploid state, reproducing via asexual conidiation or spore formation. Differentiation of the hyphal tips results in the production of macroconidia predominantly, although uninucleated microconidia are also a possibility; macroconidia contain an average of 2-3 nuclei per spheroid cell. This haploid life cycle makes genetic analysis relatively simple given that recessive traits will be expressed in offspring. Additionally, the genome is devoid of duplication due to a phenomenon known as repeat-induced point mutation (RIP; Selker et al., 1987).

The haploid life cycle contains several processes that are linked to light. Several physiological effects in *Neurospora crassa* are induced by blue light, a phenomena in fungi referred to as photomorphogenesis. The processes that are light-induced are summarized as follows: (i) synthesis of carotenoids in the mycelia, (ii) induction of conidiation, (iii) phase shifting in the circadian rhythm of conidiation, (iv) production of protoperithecia on nitrogen-deficient media (Innocenti et al., 1983). For this reason, vegetative cultures are typically grown in complete darkness to allow for vegetative growth prior to moving the culture into a lit environment to induce conidiation.

1.1.2 *The Sexual Life Cycle*

All strains of *Neurospora crassa* are one of two mating types (a or A), yet strains of either mating type possess the ability to produce the female reproductive structures known as protoperithecia when grown on nitrogen-poor (Westergaard's) media slants under continuous light (Davis and De Serres, 1970). The diploid phase of its life cycle

occurs during sexual reproduction, where the protoperithecia of one mating type is fertilized with conidia of the opposite mating type. The product of a sexual cross between two compatible *Neurospora crassa* strains is 4 pairs of genetically diverse ascospores that are present within the ascus in a linear, ordered arrangement resulting from two meiotic events followed by a single mitotic event. This ordered arrangement of ascospores facilitates the analysis of genetic recombination, i.e. tetrad analysis (Davis and De Serres, 1970).

1.1.3 *Genetic Manipulations of Neurospora crassa*

Classical genetics, combined with random mutagenesis, provided extensive information about the *Neurospora crassa* genome (Davis and De Serres, 1970). Other methods such as RIP, have been used to knock out specific genes (Selker, 1990). Essential genes can be destroyed by using RIP and then" sheltering" the mutant nucleus in a heterokaryon (Harkness et al., 1994). While effective, the RIP-based methods are time consuming and only allow knock-outs to be produced; they do not allow the generation of genetic replacements, unless the replacement gene is integrated into an ectopic site in the genome. "Sheltered disruption" techniques were also developed to produce targeted gene replacements (Nargang et al., 1995), but require the gene replacement to be flanked by large fragments of target DNA sequence and still only about 10% of selected isolated contain the correct mutation. There is currently a project being undertaken to generate a collection of strains that include knockout mutants of every gene (Colot et al., 2006). This project coincides with a recent discovery leading to a highly efficient method of gene replacement in *Neurospora crassa* (Ninomiya et al., 2004).

Neurospora crassa employs a DNA repair mechanism known as non-homologous end joining. In the event of a double-stranded break, the first two available blunt-ended fragments of DNA found are joined. This process involves homologues of the human *Ku70* and *Ku80* proteins, which in *Neurospora crassa* have been identified as MUS51 and MUS52 (Ninomiya et al., 2004). The MUS51 and MUS52 proteins together form a heterodimer that interacts with a second heterodimer to bring the DNA ends together to be ligated. With the loss of these proteins, the frequency of homologous integration of exogenous DNA is increased. With a strain of *Neurospora crassa* that is capable of homologous recombination similar to that of the yeast system, a genome knock-out project is feasible due to the time required per disruption is now several weeks as opposed to months. This strain also makes investigation of proteins involved in mitochondrial function possible given that the majority of the proteins comprising the mitochondria are nuclear encoded.

1.2 *The Mitochondrion*

The word mitochondrion comes from the Greek *μίτος* or *mitos* meaning thread and *χονδρίον* or *khondrion* meaning granule (http://en.wikipedia.org/wiki/Mitochondria). The number of mitochondria varies from organism to organism, some containing only a single mitochondrion, and others upwards of thousands, as is the case for *Neurospora crassa* (Davis and De Serres, 1970). A double-membrane-enclosed organelle present in most eukaryotic cells, the mitochondrion can be described as the "cellular power plant" for the organism in which it resides. As this implies, mitochondria generate most of the cells supply of ATP using the large number of proteins present in the inner membrane

(IM) specifically for the task of oxidative phosphorylation. Metabolic processes such as glycolysis, the Kreb's cycle and β-oxidation of fatty acids all produce NADH + H^+ and $FADH_2$. Some of the NADH produced by the Kreb's cycle within the mitochondria is derived from the oxidation of pyruvate provided by glycolysis which occurs in the cytoplasm. Therefore, this substrate needs to be brought in through the outer membrane (OM) and actively transported across the IM into the matrix.

An idea first introduced in 1890 by Richard Altmann had mitochondria derived from the invasion of anaerobic photosynthetic or aerobic bacteria into ancestral prokaryotic cells. This would become the central concept behind the endosymbiotic theory introduced by Konstantin Mereschkowski in 1905. There is evidence for and against the theory. Phylogenetic analysis of protein coding genes and ribosomal RNA (rRNA) genes housed by the mitochondrial DNA (mtDNA) has identified the α-proteobacteria as the closest relatives of mitochondria. Shared amongst all mitochondria is the production of ATP via coupled electron transport which can be directly traced back to the α-proteobacteria (Gray et al., 2001). An argument against the endosymbiotic theory is that the mitochondria cannot survive outside the cell having lost many genes required for survival. The majority of the genes missing from the mitochondrial DNA were argued to have been transferred to the host genome. However, it is the genes that remained a part of the mitochondrial genome that argue against the endosymbiotic theory; raising the question of why the entire mitochondrial genome was not transferred to the host genome? In either case, the majority of the proteins comprising the mitochondria of *Neurospora crassa* are nuclear encoded and imported as precursors after their production on cytosolic ribosomes (reviewed in Bohnert et al., 2007). The

mitochondrial DNA of *Neurospora crassa* contains genes that encode only some of the components of the respiratory chain (seven subunits of NADH:ubiquinone oxidoreductase (complex I), one subunit of ubiquinol:cytochrome *c* oxidoreductase (complex III), three subunits of cytochrome *c* oxidase (complex IV) and three subunits of ATP synthase (complex V)), a minimal set of tRNAs and rRNAs necessary for the synthesis of the respiratory components, and the S5 protein of the small ribosomal subunit and maturases (Kennell et al., 2004). Therefore, mutations in either nuclear or mitochondrial DNA can result in respiratory deficient strains.

The study of extranuclear *Neurospora crassa* mutants that developed in continuously growing cultures showed that some respiratory defects are inheritable through non-nuclear genetic determinants (Bertrand and Pittenger, 1969). This finding implicated mitochondrial DNA as the source of respiratory defects caused by the altered cytochrome content of the mutant strains when compared to a wild-type strain. The apoprotein of cytochrome *b* and three of the seven polypeptides of cytochrome aa_3 are produced on mitochondrial ribosomes, suggesting a lack of functional mitochondrial ribosomes was the cause of the reduced capacity for protein synthesis observed in the mitochondria of these strains (discussed in Bertrand and Kohout, 1977).

As expected, nuclear mutations have been identified in respiratory defective strains, such as the nuclear mutation that results in a lack of subunit 1 of COX (Nargang et al., 1978). Conversely, nuclear mutations have also been a source of suppressors of respiratory defects caused by mitochondria DNA mutations in some *Neurospora crassa* strains (Bertrand and Kohout, 1977). Thus, the nuclear genome plays a major role in regulating mitochondrial function given that more than 99% of the proteins comprising

the mitochondria are nuclear-encoded. The mitochondrial protein of interest for the current studies is porin, which is also nuclear-encoded.

1.3 *Mitochondrial Porin*

The products and substrates of mitochondrial metabolism traverse the outer membrane via aqueous proteinaceous channels, the mitochondrial porins, or voltage-dependent, anion-selective channels (VDAC). In addition to this role in basic eukaryotic biology, mitochondrial porins interact with numerous mitochondrial and cytosolic proteins (for example, Roman et al., 2006 and references therein), suggesting multiple additional roles in processes ranging from glucose metabolism to apoptosis.

Mitochondrial porins are very abundant in the outer membrane (for examples see, Schmitt et al., 2006; Goncalves et al., 2007). Although many organisms harbour multiple isoforms of porin, all seem to have at least one variant (VDAC1) with the "canonical" properties of moderate anion-selectivity (pA/pC of ~1.5) and voltage-dependent gating (reviewed by Benz, 1994; Young et al., 2007 and references therein). The latter property has been studied extensively in planar artificial bilayers (PLB, also known as black lipid bilayers (Benz, 1994) and is characterized by conversion of the pore to a partially-closed form with cation-selectivity under applied fields of about –30 or +30 mV. Recent work has suggested that the anion-selective open state may also transition to a cation-selective open state without a change in conductance (Pavlov et al., 2005).

The first primary sequences of VDACs were deduced from the cDNA sequences of fungal VDACs (Mihara and Sato, 1985; Kleene et al., 1987). It was noted that the primary sequences lacked regions that would be predicted to form hydrophobic,

transmembrane α-helices, and it was hypothesized that the protein traversed the membrane as a series of β-strands (Kleene et al., 1987). The β-strand nature of purified porins solubilized in detergent and in liposomes was confirmed about 10 years later (Shao et al., 1996; Koppel et al., 1998). With the advent of "his-tagging" the termini of proteins with multiple histidine residues, fungal, plant and human porins could be expressed in Escherichia coli and "refolded" in detergent (Popp et al., 1996; Popp et al., 1997; Koppel et al., 1998; Malia and Wagner, 2007), maintaining their β-strand rich character. Depending on the detergent, protein and method used for analysis, the estimates of β-strand content varied from 30-70% (see Bay and Court, 2002; Malia and Wagner, 2007; Shanmugavadivu et al., 2007; Bay et al., 2008), precluding precise prediction of the amount of β-strand and therefore the testing of structural models.

In the last 20 years, numerous models for the transmembrane arrangement of mitochondrial porins have been generated (see Table 1.1). These models have been based either entirely or in part on in silico searches for regions with β-strand propensity. Some models have used this information, and layered on data obtained from porin variants in artificial membranes (to be discussed below). Two basic types of barrel composition emerged: i) 12 or 13 β-strands and the N-terminal α-helix; ii) 15-19 β-strands, with 16 being the most common value (see Table 1.1 for references). Based on the organization of bacterial β-barrel proteins, it was thought by some (for example Young et al., 2007) that an even number of β-strands would be needed to meet the hydrogen bonding requirements of a barrel structure (reviewed by Koebnik et al., 2000). In fact, the solved structures of thirty-two other β-barrel proteins from prokaryotic sources all contained an even number of anti-parallel β-strands (discussed in Hiller et al., 2008).

Table 1.1 *Models for the transmembrane topology of mitochondrial porins.*

Reference	No. of β-strands	Location of N-terminus	Organism	Method
(Forte et al., 1987)	19	EM[a]	*Saccharomyces cerevisiae*	Delphi algorithm-β-strands and contacts with membrane
(Kleene et al., 1987)	15	nc[b]	*Neurospora crassa, S. cerevisiae*	predictions of sided β-strands via hydropathy plots
(Blachly-Dyson et al., 1990)	12	TM[c]	*S. cerevisiae*	point mutations changing charged residues-effects on conductance and reversal potential in artificial bilayers
(Peng et al., 1992)	12	TM	*S. cerevisiae*	point mutations as above- effects on open and closed states
(Thomas et al., 1993)	12	TM	*S. cerevisiae*	point mutations as above- effects on voltage dependence parameters
(De Pinto et al., 1991)	16	EM	human	protease digestion, antibody binding and hydropathy plots
(Benz, 1994)	16	EM	*S. cerevisiae*	predictions of hydropathy and "sided" β-strands
(Rauch and Moran, 1994)	16	EM	human, *S. cerevisiae*	predictions of hydropathy plots and avoidance of β-strand "breakers"

(Song et al., 1998a)	13	TM	*N. crassa*	biotinylation at unique cysteines and analysis in artificial membranes; measurement of conductance and gating
(Song et al., 1998b)	12	TM	*N. crassa*	biotinylation at unique cysteines and analysis in artificial membranes; measurement of conductance and gating
(Casadio et al., 2002)	16	EM	*N. crassa*, *S. cerevisiae*, human	neural network based prediction
(Runke et al., 2006)	16	EM	*N. crassa*	pore characteristics of variants lacking short segments of the protein
(Young et al., 2007)	19 (16)[d]	EM	animals, plants, fungi	PRALINE alignment followed by SSPRO structure predictions
(Bayrhuber et al., 2008; Hiller et al., 2008; Ujwal et al., 2008)	19	EM	human, mouse	NMR, x-ray crystallography

Note: The estimated number of β-strands and the location of the predicted N-terminal helix are given.

[a] EM, extramembrane

[b] nc, not considered

[c]TM, transmembrane

[d] SSPRO alignment obtained through the PRALINE server predicted 19 β-strands, but experimental data and strand length were used to argue against three of those strands (Young et al., 2007).

Three reports in 2008 presented the high-resolution structures of mitochondrial porins (Bayrhuber et al., 2008; Hiller et al., 2008; Ujwal et al., 2008; Figure 1.1). An NMR solution structure of human VDAC isoform 1 (hVDAC1) was obtained from the protein refolded in lauryl dimethylamine oxide (LDAO) micelles and NMR and x-ray diffraction were used together to solve the structure of hVDAC1 refolded in either LDAO or Cymal-5. Mouse VDAC1 (mVDAC1) was crystallized following folding in 1,2-Dimyristoyl-sn-Glycero-3-Phosphocholine (DMPC)/3-[3-cholamidopropyl)dimethylammonio]-2-hydroxy-1-propanesulfonate (CHAPSO) bicelles.

All three groups demonstrated, remarkably, that mammalian mitochondrial porin (VDAC1) folds into a unique arrangement in which 19 antiparallel β-strands are closed by two parallel strands. The β-strands identified in the structural studies are referred to as β1-β19 in this review (Figure 1.1). It was clearly shown that the N-terminal segment does not form part of the barrel, although its precise location and interactions with the barrel differed slightly among the forms (Figure 1.1 and see discussion below). With these structures, it is now possible to re-evaluate the experimental data that were obtained to delineate porin structure and mechanisms of ion selectivity and gating. Most of these data were obtained with fungal mitochondrial porins, but structural predictions from alignments of almost 300 porin primary sequences suggest that the 19 β-strand arrangement is common to all VDACs, in spite of significant differences in predicted primary sequences (Young et al., 2007; and see Figure 1.1G). In addition, the functionality of mitochondrial porins is strikingly similar. For instance, VDAC from fungi, amoebae and mammals, when reconstituted into artificial, planar lipid bilayers (PLB) bathed in 1 M KCl, yield single channels with conductance of about 4 nS

Figure 1.1 *Comparison of mammalian mitochondrial porin structures and sequences*. Upper panel is the cartoon representation of A) hVDAC1 structure solved with NMR (Hiller et al., 2008; PDB ID code 2K4T). B) hVDAC1 structure solved conjointly with NMR and crystallography (Bayrhuber et al., 2008; 2JK4) C) mVDAC1 structure solved with X-ray diffraction (Ujwal et al., 2008; 3EMN). In all structures the N- and C-termini are facing away from the viewer and the N-terminal segment of the protein is located within the lumen of the barrel. Structures A and B were aligned to C using PyMOL with RMSD values of 1.694 Å and 1.240 Å respectively. The second row shows the vacuum electrostatics calculated for the structures above it using APBS Tools in PyMOL (Version1.1r1). Negative charges are depicted in red and positive charges in blue. All cartoon representations were created with PyMOL . The third panel shows the alignment of VDAC sequences from human (hVDAC1), mouse (mVDAC1), *Neurospora crassa* (NcVDAC) and *Saccharomyces cerevisiae* (ScVDAC1). In the human and mouse sequences, α-helical secondary structure is indicated in yellow and β-sheet in purple, based on the recent structural data. For hVDAC1, the letters in parenthesis indicate whether the model was presented by Bayrhuber et al., (2008) (B) or Hiller et al., (2008) (H). Underlining indicates the secondary structure predicted by the SSPRO option within PRALINE alignment (Young et al., 2007). For the fungal VDAC sequences, residues in gray and green indicate predicted α-helical and β-sheet, respectively. The number above the sequences indicates the position within the alignment and the β-strands are numbered as β1-β19.

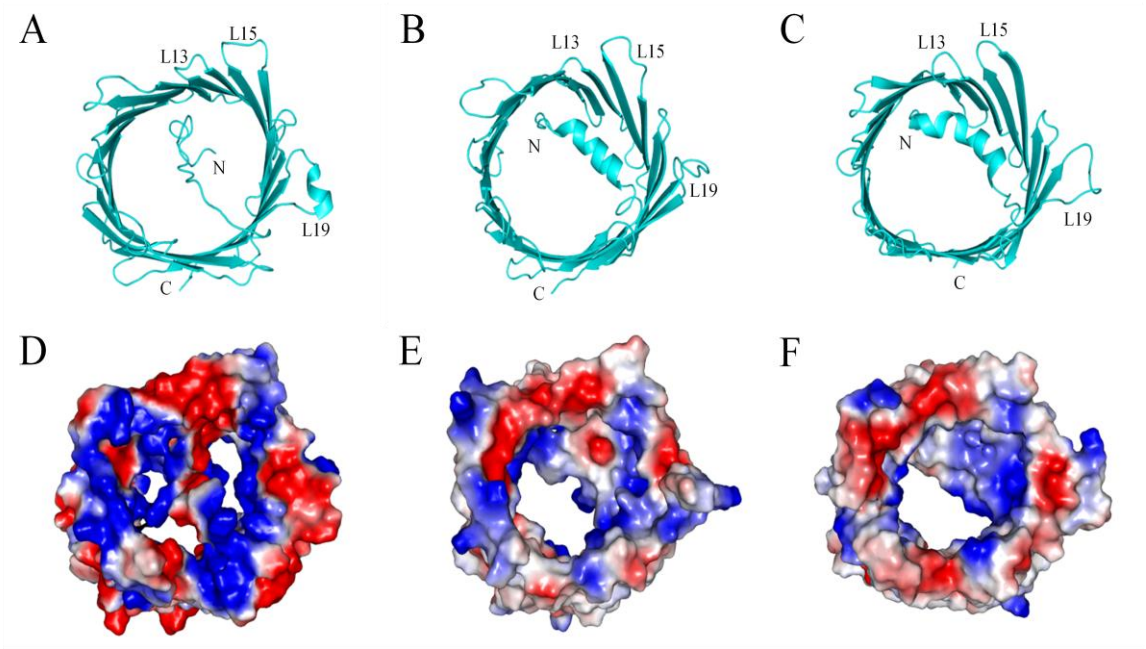
A
L15
L13
N
L19
C
B
L13
L15
N
L19
C
C
L13
L15
N
L19
C
D
E
F

G


20 40 60 80
β1 β2 β3 β4 β5
hVDAC1 (B): MAVPPTYADLGKSARDVFTKG-YGFGLIKLDLKTKSENGLEFTSSGSANTETTKVTGSLETKYRWTEYGLTFTEKWNTDNTLGTEITVEDQLARGLK
hVDAC1 (H): MAVPPTYADLGKSARDVFTKG-YGFGLIKLDLKTKSENGLEFTSSGSANTETTKVTGSLETKYRWTEYGLTFTEKWNTDNTLGTEITVEDQLARGLK
mVDAC1 : MAVPPTYADLGKSARDVFTKG-YGFGLIKLDLKTKSENGLEFTSSGSANTETTKVNGSLETKYRWTEYGLTFTEKWNTDNTLGTEITVEDQLARGLK
NcVDAC : MA-VPAFSDIAKSANDLLNKDFYHLAAGTIEVKSNTPNNVAFKVTGK-STHDKVTSGALEGKFTDKPNGLTVTQTWNTANALETKVEMADNLAKGLK
ScVDAC1 : MS-PPVYSDISRNINDLLNKDFYHATPAAFDVQTTTANGIKFSLKAKQPVKDGPLSTNVEAKLNDKQTGLGLTQGWSNTNNLQTKLEFAN-LTPGLK
100 120 140 160 180
β6 β7 β8 β9 β10 β11 β12
hVDAC1 (B): LTFDSSFSPNTGKKNAKIKTGYKREHINLGCDMDFDIAGPSIRGALVLGYEGWLAGYQMNFETAKSRVTQSNFAVGYKTDEFQLHTNVND-GTEFG
hVDAC1 (H): LTFDSSFSPNTGKKNAKIKTGYKREHINLGCDMDFDIAGPSIRGALVLGYEGWLAGYQMNFETAKSRVTQSNFAVGYKTDEFQLHTNVND-GTEFG
mVDAC1 : LTFDSSFSPNTGKKNAKIKTGYKREHINLGCDVDFDIAGPSIRGALVLGYEGWLAGYQMNFETSKSRVTQSNFAVGYKTDEFQLHTNVND-GTEFG
NcVDAC : AEGIFSFLPATNARGAKFNLHFKQSNFHGRAFFDL-LKGPTANIDAIVGHEGFLAGASAGYDVQKAAITGYSAAVGYHAPTYSAAITATDNLSVFS
ScVDAC1 : NELITSLTPG-VAKSAVLNTTFTQPFFTARGAFDLCLKSPTFVGDLTMAHEGIVGGAEFGYDISAGSISRYAMALSYFAKDYSLGATLNN-EQITT
200 220 240 260 280
β13 β14 β15 β16 β17 β18 β19
hVDAC1 (B): GSIYQKVNK-KLETAVNLAWTAG-NSNTRFGIAAKYQIDPDACFSAKVNNSSLIGLGYTQTLKPGIKLTLSALLDGKNVNAGGHKLGLGLEFQA
hVDAC1 (H): GSIYQKVNK-KLETAVNLAWTAG-NSNTRFGIAAKYQIDPDACFSAKVNNSSLIGLGYTQTLKPGIKLTLSALLDGKNVNAGGHKLGLGLEFQA
mVDAC1 : GSIYQKVNK-KLETAVNLAWTAG-NSNTRFGIAAKYQVDPDACFSAKVNNSSLIGLGYTQTLKPGIKLTLSALLDGKNVNAGGHKLGLGLEFQA
NcVDAC : ASYYHKVNSQVEAGSKATWNSKT-GNTVGLEVATKYRIDPVSFVKGKINDRGVAAIAYNVLLREGVTLGVGASFDTQKLDQATHKVGTSFTFES
ScVDAC1 : VDFFQNVNAFLQVGAKATMNCKLPNSNVNIEFATRYLPDASSQVKAKVSDSGIVTLAYKQLLRPGVTLGVGSSFDALKLSEPVHKLGWSLSFDA

(reviewed by Benz, 1994). Hence, the data from a variety of porins can be placed, cautiously, within the context of other VDAC structures. The purpose of this review is to fit the large body of biochemical and biophysical data into these structures, and determine if they shed light on the functional properties of mitochondrial porins, including pore formation, ion selectivity and voltage-dependent gating.

1.3.1 *Estimation of Pore Size*

The internal area of the pore has to be large enough for passage of metabolites. Early studies of the shrinking and reswelling of proteoliposomes in response to various osmolytes suggested a pore size of 2 nm for fungal VDAC (Colombini, 1980). Reconstitution of VDAC into PLBs allowed estimation of an inner diameter of about 1.7 nm, based on the specific conductance of the channel (see Table 1.2 and references therein). This estimate refers specifically to the lumen, and assumes a perfectly cylindrical opening and a pore height of 6 nm. If the pore size is re-estimated using the electrophysiological data and the average pore height of 3.5 nm determined from the recent structures, the resulting lumen diameter (1.3 nm) is in good agreement with that obtained from the structural data (Table 1.2). A four-sided cylindrical channel was indicated from electron microscopic analysis of frozen-hydrated and gold-glucose-embedded membrane crystals of VDAC. Due to limited resolution, the beta-barrel nature of the protein could not be directly observed, but the projected density map was shown to be consistent with a β-barrel having a diameter of 3.6-3.8 nm at the C-alpha backbone (Mannella, 1982; Guo et al., 1995). Atomic force microscopy of whole mitochondrial outer membranes (MOM) from *Saccharomyces cerevisiae* revealed 3.8 x 2.7 nm, eye-shaped pores (Goncalves et al., 2007). These microscopic data correlate well with the

Table 1.2 *Estimates of VDAC pore size*.

Reference	Porin and Organism	Method for Estimation	Pore Size
(Colombini, 1980)	Neurospora crassa VDAC	Planar lipid bilayer	2 nm (L)[a]
(Freitag et al., 1982)	N. crassa VDAC	Planar lipid bilayer	1.8 nm (L) [1.4 nm][b]
(Mannella, 1982)	N. crassa VDAC	Electron microscopy	2-3 nm
(Ludwig et al., 1988)	Saccharomyces cerevisiae VDAC1	Planar lipid bilayer	1.7 nm (L) [1.3 nm]
(Blachly-Dyson et al., 1994)	Homo sapiens VDAC1 expressed in yeast	Planar lipid bilayer	1.3 nm (L)
(Dolder et al., 1999)	H. sapiens VDAC1	Cryo-electron microscopy of 2D-crystals	3.7 nm 1.7-2.0 nm (L)
(Goncalves et al., 2007)	S. cerevisiae VDAC1	Atomic force microscopy	3.8 x 2.7 nm
(Hiller et al., 2008)	H. sapiens VDAC1	NMR[c]	2.5 nm (L)
(Bayrhuber et al., 2008)	H. sapiens VDAC1	NMR and X-ray crystallography	3.5 x 3.1 nm 1.5 x 1 nm (L)
(Ujwal et al., 2008)	H. sapiens VDAC1	X-ray crystallography	2.7 x 2.4 nm 2.7 x 1.4 nm (L)

Note: Outer diameters are given unless indicated.

[a] L, lumen diameter

[b] values in square brackets were recalculated using an average pore height of 3.5 nm for recalculation of pore estimation. The original values were calculated with an value of 6 nm for pore height. Values were calculated using the formula $\Lambda=\sigma\pi r^2/l$, where Λ is average single-channel conductance, σ is the specific conductivity, r is the radius (in nm) and *l* is the pore height in nm (Dihanich et al., 1990).

[c] NMR, nuclear magnetic resonance

outer dimensions of mVDAC1 presented by Bayrhuber et al., (2008), outlining the pore to be 3.5 x 3.1 nm. The dimensions of mVDAC1, in a bicelle environment (Ujwal et al., 2008), and hVDAC1 in LDAO (Hiller et al., 2008) were slightly smaller (Table 1.2). The composition of the membrane or membrane mimetic, as well as the experimental approach, likely contributes to these small variations in size and shape.

1.3.2 *Prediction of β-strand arrangement*

Numerous approaches have been taken to the prediction of β-strands on the basis of sequence alone (see Table 1.1; Bay and Court, 2002; Casadio et al., 2002; Young et al., 2007). Predictions have been generally consistent for the six N-terminal β-strands, and these fit with the published structural data. For the remainder of the protein, the approach that predicted all of the remaining β-strands was secondary structure prediction using SSPRO analysis (Pollastri et al., 2002) of about 300 VDAC sequences previously aligned with PRALINE (Simossis and Heringa, 2005). However, some experimental data and the bacterial porin model requiring an even number of strands led Young et al., (2007) to discount three of the strands since confirmed by structural analysis.

1.3.2.1 *Ion Selectivity of the Barrel Wall*

Most models combined *in silico* predictions with experimental data. Reconstitution of VDAC, and variants thereof, into PLB was used to assign β-strands within the overall topology of the barrel. In one approach to defining transmembrane strands, the fact that the open state of mitochondrial porin is slightly anion selective was used. The principle theory for ion selectivity is that residues affecting it would reside within the barrel wall, and non-influential residues would be located outside of this region (Blachly-Dyson et al., 1990). Analysis of the involvement of 29 residues in ion selectivity was addressed by site-directed mutagenesis of the *S. cerevisiae* VDAC1

(ScVDAC1) gene to replace individual charged residues with ones of opposite charge, or uncharged with charged residues. Fourteen replacements affected selectivity (Figure 1.2, upper row). Modeling these data over the 19 β-strand models gives an almost perfect fit: of the residues now known to reside in β-strands, all but two affected selectivity (Figure 1.2). However, these two residues are oriented toward the hydrophobic tails of the phospholipid bilayer as opposed to the lumen of the pore, possibly explaining the lack of effect on selectivity.

1.3.2.2 Accessibility of Streptavidin to Covalently Linked Biotin

In a second approach, site-directed mutagenesis was used to make a collection of variants, each with a single residue substituted by cysteine. These studies utilized the single *N. crassa* VDAC (NcVDAC) as it is naturally devoid of cysteines. For each variant, the cysteine residue was covalently linked to biotin via the thiol group. The biotinylated VDAC molecules, when reconstituted into PLB, showed channel formation characteristic of the wild-type protein. Addition of streptavidin to either the cis or trans side of the chamber (with respect to the side of porin addition), was predicted to modify pore function only if the biotinylated residue was exposed to the side of streptavidin addition. These experiments revealed sites, that when bound to streptavidin, either reduced conductance (type 1 pores) or locked the channel in a closed state (type 2 pores). The relative positions, across the membrane, of the biotinylated sites were then determined by examining molecules with two cysteine substitutions (Figure 1.2, lower row). Residues were defined as cis or trans with respect to one reference residue (T53 in the *N. crassa* protein). Using the alignment of NcVDAC with mVDAC (Figure 1.1G), the biotinylated residues reported by Song et al. (1998a) were placed onto the structure produced by Ujwal et al. (2008) with the T53C reference residue (yellow in Figure 1.2).

Figure 1.2 *Sites of single amino acid replacements and modification used for modeling VDAC structure.*

Upper row: Residue substitutions tested for their affect on ScVDAC ion selectivity were highlighted on the mVDAC structure (PDB ID code 3EMN), according to the alignment in Figure 1.1G. The image was created using PyMOL. Residues affecting ion selectivity are coloured in red (clockwise from the N-terminus: D16, K20, D30, S46, K61, T65, E84, K96, G126, H181, S234, T248, K256 and Q282) and those not affecting selectivity are coloured in blue (T51, K110, A134, E158, D176, V206, A212, G220, K252, N267 and K274). Data were taken from (Blachly-Dyson et al., 1990). The structure in panel A is oriented as in Figure 1.1, and panels B and C show the half pore view of A with the asterisks indicating adjacent residues connecting the N-terminus to β1. The lower row (D, E) is a cartoon representation of the results of biotinylation experiments of Song et al., (1998b), using NcVDAC. The residues were superimposed onto the mVDAC structure created with PyMol (PDB ID code 3EMN) according to the alignment in Figure 1.1G. Residues reported to be cis or trans to the reference residue NcVDAC T53 (yellow, V54 in HsVDAC1) are coloured red and blue, respectively. The two residues coloured in magenta were shown to be trans to T53 and cis to each other. To clearly show all residues, panel D shows the N-terminal helix and β-strands 1-10; β-strands 10-19 are shown in E. The darker blue bands on the β-strands on the right side of each image are "shadows" generated by PyMOL. Loops are labelled with the number of the following β-strand; for example, loop L13 separates β12 and β13.

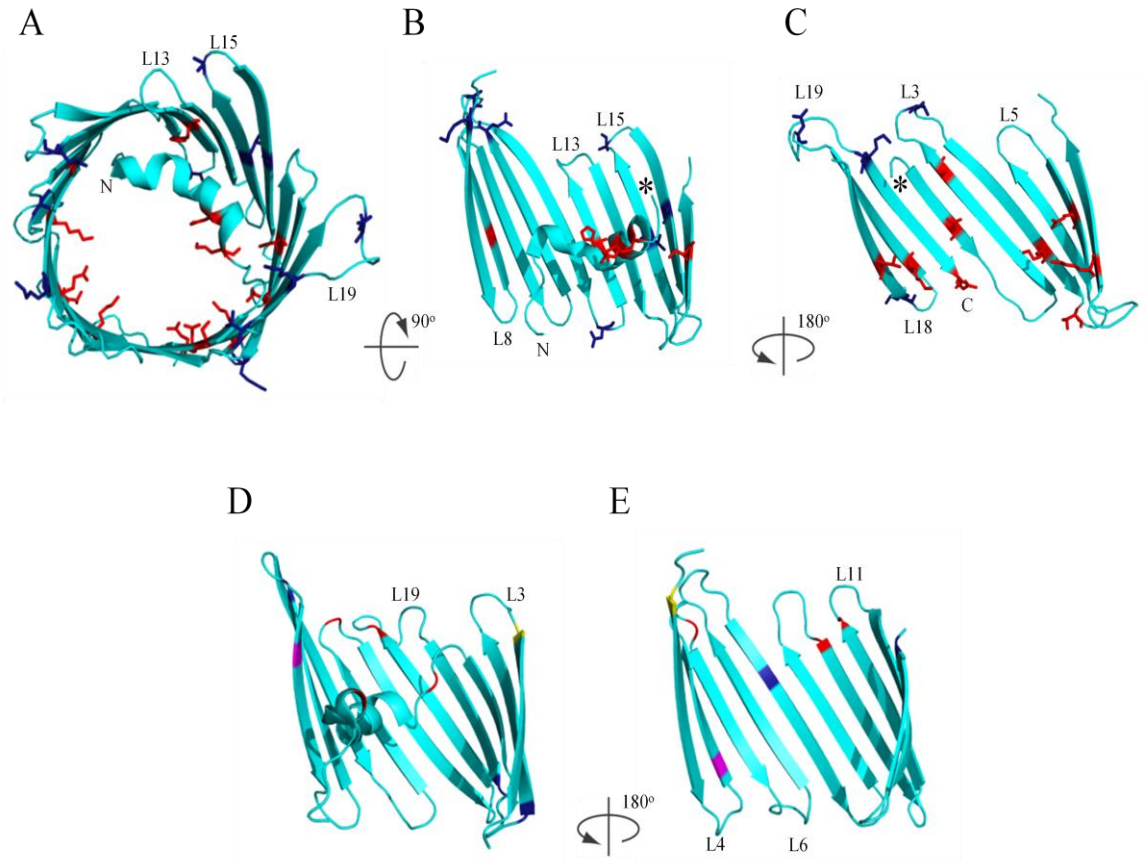
A
L13
L15
N
L19
90°
B
L15
L13
*
L8
N
C
L19
L3
L5
*
180°
C
L18
D
L19
L3
E
L11
180°
L4
L6

Prediction of residue placement was generally accurate when a type 1 residue was examined in conjunction with a type 2 residue (exceptions are discussed below). However, due to the complexity involved in interpreting the results of pairing two type 2 residues, the predictions from this type of experiment are less accurate, calling about half of the residues to be trans to T53, when they are on the same side of the membrane according to the Ujwal et al. (2008) model (Figure 1.2).

1.3.2.3 *Deletion Variants*

Another approach used to test various models was to create *N. crassa* porin variants lacking short segments and to determine their ability to create pores in PLB (Popp et al., 1996; Koppel et al., 1998; Runke et al., 2006). The hypothesis was that deletions of β-strand regions would prevent pore formation, while removal of loop regions could be tolerated (Figure 1.3, upper row). Variants of fungal porins lacking the N-terminal eight (Koppel et al., 1998) or 23 (Popp et al., 1996) residues formed pores with wild-type conductance, supporting models in which the N-terminus did not form an essential part of the pore.

In agreement with the known structures, variants lacking segments near or encompassing the loops between β13 and β14 (ΔHKVN, see Figure 1.1G for sequence), β15 and β16 (ΔDPVSF), and β16 and β17 (ΔNDRGV), displayed high to moderate pore forming ability, in agreement with the structures of mammalian porins. Deletions within regions encompassing β10(ΔFLAGA), β11 (ΔSAAVG), β12 (ΔAAITA), and part of β13 (ΔLSFS) had very weak pore-forming ability, and the resulting pores likely represented alternatively-folded structures. However, ΔVAAIAYN is an outlier, as it encompasses β17. This variant was capable of generating pores of wild-type dimensions, with up to 4

Figure 1.3 *Variants of fungal VDAC used to examine pore structure and gating*. Panels A and B describe deletion variants of NcVDAC. The residues corresponding to the deletions were mapped onto the mVDAC1 structure (PDB ID code 3EMN), using the alignment in Figure 1.1G. The regions absent from the termini of these variants are indicated in red (Δ2-12 and Δ269-283). The segment absent in a variant that formed wild-type pores (βNDRGV) is shown in blue. Intermediate pore-forming ability was noted for variants lacking the regions shown in light purple (βDPVSF, βVAAIAYN and βHKVN). Variants βFLAGA, βSAAVG, βSAAITA, and βLSVFSA (yellow) formed small pores at low frequency. Data taken from (Popp et al., 1996; Runke et al., 2006). The lower panel shows representative sites that were tested for their effect on ScVDAC voltage-dependent gating. These residues are highlighted on the mVDAC structure (PDB ID code 3EMN), according to the alignment in Figure 1.1G. Sites at which amino acid substitutions affected (red, clockwise from the N-terminus, D16, K20, S46, K61, T65, E84, Q154 and Q282) and did not affect (blue, D30, T51, K96, G126, A134, E158, V206, A212, S234, T248, K252 and N267) voltage-dependent gating are indicated. The orientation of the molecule in C is the same as that shown in Figure 1.1C. Panels D and E show the half pore view and are labelled as described for Figure 1.2. Data taken from Thomas et al. (1993).

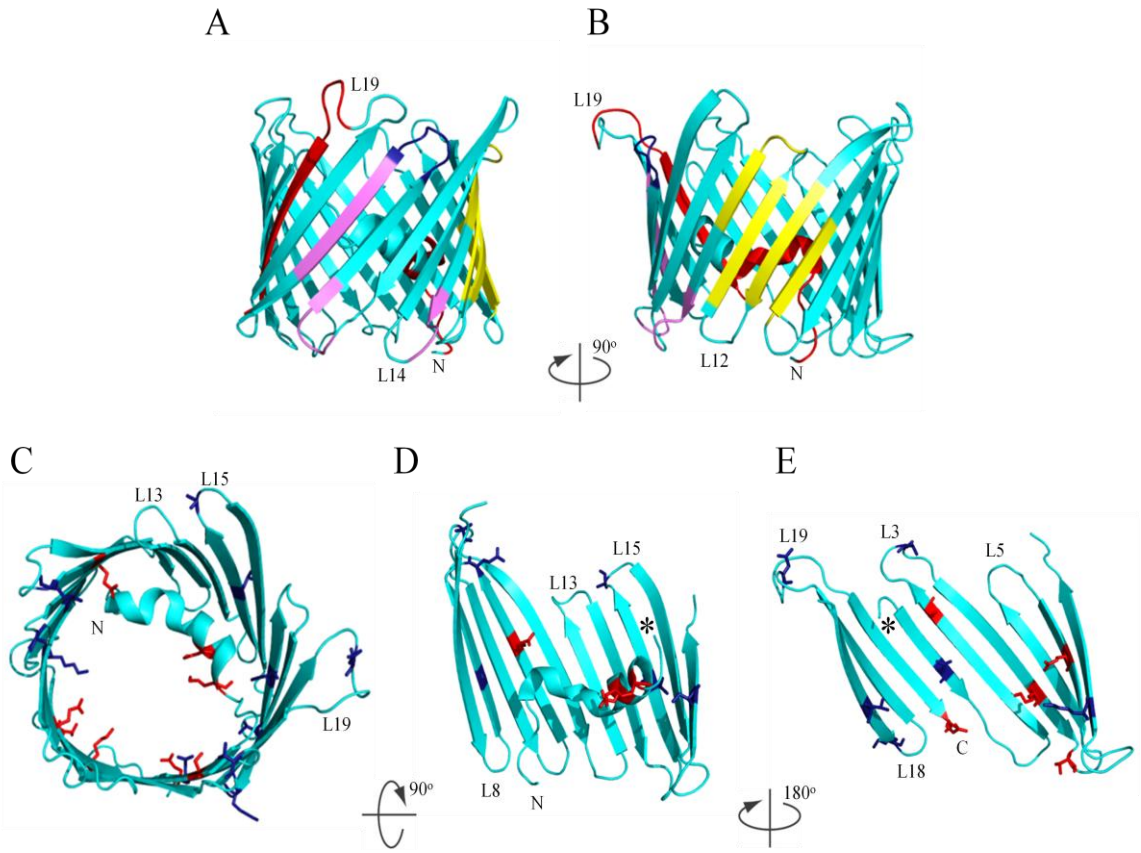
A
B
L19
L14
N
L19
90°
L12
N
C
D
E
L13
L15
N
L19
90°
L8
N
L15
L13
*
L19
L3
L5
*
C
L18
180°

nS conductance. However, it did not display voltage-dependent gating suggesting that it may adopt an alternative topology (Runke et al., 2006).

All *in silico* analyses have predicted that the C-terminus of VDAC creates a β-strand that resides in the membrane. This was supported by the D282K variant of ScVDAC1, which possesses altered ion selectivity. However, deletion of the C-terminal 15 residues of NcVDAC created a molecule that can form stable pores in PLB (Popp et al., 1996), which is unexpected if the C-terminus forms a β-strand, and particularly one that is involved in "sealing" the N-terminal and C-terminal parts of the pore. These pores were of lower conductance (up to 3 nS), suggesting that an alternative structure was formed, but they retained voltage-dependent gating and anion-selectivity, as might be expected if important residues for ion selectivity and gating do not reside in β19. While potentially interesting, this variant is not biologically relevant, as it does not import into mitochondria (Court et al., 1996), because the C-terminal β-strand contains the β-signal motif required for interaction with the sorting and assembly complex (SAM) that mediates insertion of VDAC into the MOM (Kutik et al., 2008).

In summary, the data from these electrophysiological experiments generally fit well with the solved structures, but using any one approach, a much more exhaustive analysis would have been required to generate precise structural information.

1.3.3 *Orientation of the Pore Across the Membrane*

1.3.3.1 *Localization of the N- and C-terminus*

The question of the orientation of the pore across the MOM has been addressed in several ways. With detailed structural data now available, localization of one terminus or loop should be sufficient to orient the molecule across the MOM. The C-terminus is

embedded in the membrane (see Figure 1.1 and references therein), and not accessible to protease from either side of the bilayer (De Pinto et al., 1991). Conflicting data have been reported regarding the localization of the N-terminus, although the current structural information provides a potential explanation for the inconclusive results. In mitochondria, the N-terminus of the protein has been shown to be accessible (bovine VDAC1, De Pinto et al., 1991) or not accessible (NcVDAC, Stanley et al., 1995; rat VDAC1, Konstantinova et al., 1995) to antibodies directed against residues 1-20 of the protein. Likewise, a FLAG-epitope engineered into position 11 of the *Saccharomyces* protein is not accessible to anti-FLAG antibody in intact organelles (McDonald et al., 2009). Assuming that in mitochondria the N-terminus resides in the barrel lumen, as in the conformations used for structural studies, these conflicting results may reflect subtle differences in the location and exposure of the epitopes detected by these antibodies.

1.3.3.2 *Monoclonal Antibody Accessibility*

Alternatively, a single internal site could be used to "set" the orientation. Peptide-specific antibodies have been used to probe the topology of the internal parts of the protein. Antibodies generated against residues 195-210 (β13-loop-β14), 251-268 (β18 and subsequent loop) and 272-283 (β19) of NcVDAC showed effective binding to their corresponding epitopes only when the mitochondria were lysed in hypotonic solution (Stanley et al., 1995). This observation is not informative as all of the peptides used for antibody generation include both membrane-spanning and extra-membrane segments. In addition, they correspond mainly to transmembrane segments that would likely not be accessible in mitochondrial membranes, either in intact or lysed mitochondria. In an approach that potentially avoids this difficulty, ScVDAC1 was engineered to contain FLAG epitopes in several turns and loops (McDonald et al., 2009). Epitopes engineered

into either loop 2 or 5 were detected only following mitochondrial lysis; according to the published structures, these positions should reside on opposite sides of the membrane. It is possible that, in the ScVDAC1 experiments, one loop is not available for antibody binding in intact mitochondria, but that lysis of the MOM in detergent exposes the epitope.

1.3.3.3 *Protease Fragmentation Patterns*

Protease digestion of intact mitochondria has been used as another approach to address this question. Trypsin digestion of intact bovine mitochondria cleaves VDAC into a 12-kDa and an 18-kDa fragment (De Pinto et al., 1991). The smaller fragment is detectable with an antibody raised against the N-terminus of the protein, placing a potential cleavage site at K109 (based on NCBI Sequence: NP_003365), which is in loop 7 (see Figure 1.1G). This cleavage site would place K109 on the cytosolic side of the membrane. However, similar experiments with chymotrypsin support the opposite conclusion. Chymotrypsin digestion created 12.5- and 19.5-kDa fragments, which could be produced by cleavage at Y119 and F178. However, if K109 is exposed to the cytosol, the latter residues would reside on the intermembrane space (IMS)-side of the membrane. It is possible that cleavage by one of the enzymes occurred at a site(s) further from the N-terminus, and subsequent unfolding of the protein exposed IMS-proximal cleavage sites.

1.3.3.4 *Accessibility of Interacting Proteins*

A third approach to determining orientation may lie in the identification of sites through which porin interacts with cytosolic proteins. A well-studied example is hexokinase binding to hVDAC1. Variant porins harbouring E72Q or E202Q replacements were unable to bind hexokinase (Zaid et al., 2005; Abu-Hamad et al., 2008; Arzoine et al., 2009). The N-terminus of human hexokinase I forms an 11-residue,

hydrophobic α-helix that inserts into the mitochondrial membrane (Xie and Wilson, 1988), where it could interact with VDAC. Presumably other contacts between the two proteins could occur at the cytosolic face of the membrane. Glutamate 72 resides in the middle of β-strand 4, exposed to the lipid rather than the lumen barrel, in a region of the protein that may exhibit some flexibility (see below). This may be a candidate for interaction with the hydrophobic tail of hexokinase. E202 is at the N-terminal part of β14 and thus it may be more likely to interact with hexokinase from the cytosolic side of the membrane. However, determination of the hexokinase sequences interacting with these two regions of VDAC is required before a definitive conclusion can be reached.

1.3.4 *Gating*

The mechanism of gating has been in question since VDAC first was subjected to PLB experiments that demonstrated voltage-dependant open and closed states (Schein et al., 1976). Several mechanisms have been proposed, ranging from conformational changes in the barrel wall, to movement of the soluble amphipathic helical N-terminus. One long-standing model for gating of VDAC involved transmembrane strand rearrangements (see Colombini, 1989; Peng et al., 1992).

1.3.4.1 *β-strand Rearrangment*

The transmembrane structure was predicted to contain 12 β-strands and the N-terminal α-helix; initially it was proposed that the pore was comprised of a pair of porin molecules in order to conform to biophysical data that were available at the time (Colombini, 1989). Later, the model was refined to involve a single molecule (Peng et al., 1992), based analysis of the surface density of two-dimensional VDAC crystals, which indicated that each channel was composed of one VDAC polypeptide (Thomas et al., 1991; and see discussion in Peng et al., 1992). Depending on the potential presented to

the outer membrane (positive or negative), the C-terminal six β-strands would be displaced from the barrel wall and into the cytosol or the IMS. This change would result in a reduction of the overall diameter of the pore, and leave a barrel with altered ion selectivity. Such a gating mechanism has not been observed for bacterial porins, and it would appear to be energetically-expensive, requiring repeated cycles of disruption of hydrophobic interactions between the protein and the membrane during removal of β-strands, and of lipid-lipid contacts during reinsertion of segments of the protein into the membrane. Nonetheless, the notion of some flexibility within the N-terminal six β-strands of the barrel is supported by several observations. In the biotinylation experiments using NcVDAC discussed above (Song et al., 1998a), two residues, N38 (G38 in mouse) and T69 (in both) were accessible on both sides of the PLB. However, these residues occupy locations within or near the N-terminal end of β2 and β4, respectively, and would be expected to be accessible from the one side (Figure 1.1G). Similarly, a FLAG epitope engineered into each one of the opposing loops 2 and 5 of ScVDAC1 were most accessible to antibody in solubilized mitochondria, as would be expected if they resided on the same side of the membrane (McDonald et al., 2009). In the latter experiment, these results could indicate flexibility in these strands, or may reflect increased accessibility of the epitope tags when mitochondria were lysed in detergent. Alternatively, they could result from altered folding or stability due to introduction of a highly-charged tag (DYKDDDDK in single letter code) into the protein, although when assessed by the level of cellular oxygen consumption, the pores were assumed to function normally.

1.3.4.2 *Barrel Flexibility*

The structural analyses have also suggested some flexibility in the barrel. Twenty slightly different structural conformers were analyzed by Hiller et al., (2008); these forms

ranged from circular to ovoid shapes. In NMR analysis of LDAO or Cymal-5-solubilized hVDAC1, β-strands 1-4 show rapid amide proton exchange, suggesting switching between conformations that involves transient splitting of hydrogen bonds (Bayrhuber et al., 2008). It should be noted that these structures were obtained in detergent micelles, which lack the rigidity of the outer membrane. Furthermore, movement of the soluble N-terminus in solution may be capable of providing the energy required for hydrogen bond rearrangement. This segment is anchored to β1; therefore movement of the N-terminus could result in shifting of β1, which in turn would destabilize the hydrogen bonding network about β2-β1-β19. Nonetheless, while the current studies do not support energetically-expensive large-scale movement of strands in and out of the membrane, it remains that the pore may not be a completely rigid structure, and that some movement within the lumen of the barrel may be involved in gating, or interactions with proteins such as hexokinase.

1.3.4.3 *The Role of Intramolecular Loop*

It is interesting to note that, although bacterial porins have served as structural models for VDAC, gating via a large intramolecular loop (such as the 36-residue loop 3 of the porin OmpF of *E. coli*) received limited support (Bainbridge et al., 1998), in spite of the predictions of several large loops in some models (Casadio et al., 2002; Runke et al., 2006). In the recently published structures, the largest loop is only 8-9 residues. Interestingly, there is an α-helical structure within this loop (Hiller et al., 2008); see Figure 1.1A), reminiscent of OmpF loop 3, but the relatively short turn regions separating this helix from the adjacent β-strands make gating via this loop unlikely. However, when the structure of hVDAC1 in LDAO is superimposed over the OmpF structure, the N-

terminal segment is placed near the equivalent site of the gating loop of the bacterial porin, suggesting a role in gating (Bayrhuber et al., 2008).

1.3.4.4 *Movement of the N-terminus*

Models of gating that involve movement of the N-terminus have been suggested by the authors of all of the recent structural studies. However, a unified model cannot be generated, as there is no common position or structure identified for the N-terminus with respect to the barrel (Figure 1.1). The reason for the different placements of the N-terminus is not clear, but in part they may reflect differences in the versions of the protein used for the structural studies. For example, all were isolated in denatured form from *E. coli*, but purified with either an N- or C- terminal tag, with additional differences in the methods used for refolding. The hVDAC1 used by Hiller et al., (2008) and Bayrhuber et al., (2008) possessed an C-terminal hexahistidyl (His_6) tag and were folded at pH 6.8, while the mVDAC1 (Ujwal et al., 2008) carried an N-terminal His_6-tag and crystallized best at pH 8.5. In PLB experiments conducted at pH 6.0-7.0, the N-terminally His_6-tagged NcVDAC (Popp et al., 1996) and ScVDAC1 (Koppel et al., 1998), along with the version with a C-terminal tag (Hiller et al., 2008) are indistinguishable from the corresponding porin isolated from mitochondria, suggesting that the His_6-tag does not impair the gating mechanism *in vitro*. However, it has yet to be confirmed that either of these tagged molecules function *in vivo*. Furthermore, it cannot be known with certainty whether the refolded proteins used for the structural studies were in conformations similar to the cation- or anion-selective open state, or a closed state.

The specific role of the N-terminus has been investigated in PLB experiments. Deletion of all or part of the N-terminal domain (Δ2-12 and Δ3-20 of NcVDAC (Popp et

al., 1996) and Δ1-8 of ScVDAC1 (Koppel et al., 1998) generated channels with "noisy" transitions between states. The two *N. crassa* variants retained gating capacity while open states were rarely observed for the yeast variant. These conflicting observations are not readily explained but support models in which there are contacts between residues in the N-terminus and the barrel that stabilize the open state. However, only the NcVDAC variants retained the N-terminal His-tags used for their purification from E. coli. It is possible that this tag and the residues added with it (MRGSHHHHHHGS) can mimic some of the function of the N-terminus if all or part of it is deleted. These observations suggest the importance of analyzing N-terminal variants in the absence of the His_6-tag.

1.3.4.5 *Voltage Dependence*

Key to the concept of voltage gating is the presence of voltage sensor domain(s). Voltage-dependent gating was known to be abolished at low pH, and by treatment that converts amino groups to carboxyl groups, suggesting that positively-charged residues were involved in sensing voltage (discussed in Thomas et al., 1993). Based on this observation, individual charged residues were replaced with a residue of the opposite charge through site-directed mutagenesis of the yeast VDAC gene (Thomas et al., 1993). A second approach to evaluate the voltage sensor region used a similar rationale to select residues for replacement with cysteine, to be used in streptavidin binding studies with NcVDAC (Song et al., 1998b). Residues that did or did not impact voltage gating are summarized in Table 1.3. It can be noted that modifications to the N-terminal residues at positions 7, 12, 15, 19, and 23 impacted voltage dependence, which would agree with the idea that changes in conformation or placement of the N-terminus are involved in gating.

The remaining critical residues are scattered throughout the polypeptide, and

Table 1.3 *Residues tested for involvement in voltage-dependent gating*.

Residues involved in gating	Corresponding residue in other fungal VDAC[a]	Corresponding residue in hVDAC1	Position in hVDAC1 structure
S7 (Nc) [b]	S7 (Sc)	A8	N-terminal strand
S12 (Nc) [b]	N12 (Sc)	S13	N-terminal strand
D15 (Sc) [c]	D15 (Nc)	D16	N-terminal strand
K19 (Sc) [c]	K19 (Sc)	K20	N-terminal strand
H23 (Nc) [b]	H23 (Sc)	G23	N-terminal strand
K46 (Sc) [c]	K46 (Nc)	S46	β2
T53 (Nc) [c]	L54 (Sc)	V54	β3
E58 (Nc) [c]	E59 (Sc)	E59	β3
K61 (Sc) [c]	K60 (Nc)	K61	β3
K65 (Sc) [c]	K65 (Nc)	T65	loop after β3
T69 (Nc) [b]	G70 (Sc)	T70	β4
A79 (Nc) [b]	N80 (Sc)	T80	β5
K84 (Sc) [c]	K84 (Nc)	E84	β5
E152 (Sc) [c]	S152 (Nc)	Q154	β10
T183 (Nc) [b]	T182 (Sc)	N183	β12
S190 (Nc) [b]	T190 (Sc)	G191	β13
E282(Nc) [b]	D282 (Sc)	Q282	β19

Residues not involved in gating	Corresponding residue in other fungal VDAC[a]	Corresponding residue in hVDAC1	Position in hVDAC1 structure
D30 (Sc) [c]	E30 (Nc)	D30	β1
N38 (Nc) [b]	G38 (Sc)	G38	loop after β1
D51 (Sc) [c]	D50 (Nc)	T51	loop after β2
K92 (Nc) [b]	P92 (Sc)	R93	loop after β5
K112 (Nc) [b]	V111 (Sc)	K113	end of β7d
R124 (Sc) [c]	R125 (Nc)	G126	β8
T135 (Nc) [b]	T136 (Sc)	S137	end of β9
D156 (Nc) [b]	D157 (Sc)	E158	end of β10
K205 (Sc) [c]	K206 (Nc)	V206	β14
S211 (Nc) [b]	C211 (Sc)	T211	end of β14
K234 (Sc) [c]	K234 (Nc)	K236	β16
R240 (Nc) [b]	D240 (Sc)	N239	loop after β16
K248 (Sc) [c]	K248 (Nc)	Q249	β17
R252 (Sc) [c]	R252 (Nc)	K252	loop after β17
D264 (Nc) [b]	D265 (Sc)	D264	end of β18

K267 (Sc) c	K267 (Nc)	N267	loop after β18

Note: Corresponding residues were chosen according to the alignment shown in Figure 1.1G

[a] Sc, *Saccharomyces cerevisiae* VDAC1; Nc, *Neurospora crassa* VDAC

[b] data taken from Song et al., (1998b)

[c] data taken from Thomas et al., (1993)

[d] within two residues of the end of the β-strand

localized to two regions of the protein: β19 and β1-5, and β10-13 (for examples see Figure 1.3). Equally interesting are the residues that do not affect gating (Table 1.3), most of which are not embedded deep within the barrel. NcVDAC ΔNDRGV (loop after β16) follows this trend by forming pores with wild-type conductance and gating properties (Runke et al., 2006). The deletion includes R240 that does not affect gating (Table 1.3). In contrast, NcVDAC ΔDPVSF (loop after β15) is locked in a cation-selective, high conductance state. The explanation for this observation is not clear; the latter variant may fold into an alternative structure in PLB. Point mutations in this and other small loops have not been examined to more precisely test the role of these regions in gating.

The current structural data all place the N-terminus of VDAC within the barrel lumen, where it could be interacting with components of the voltage sensor. In the NMR analysis of hVDAC1 described by Hiller et al., (2008) (Figure 1.1A), residues 7-10 in the N-terminus are involved in nuclear Overhauser effect (NOE) contacts with a hydrophobic region of the barrel, specifically residues V143 (β9) and L150 (β10). The N-terminal residues would protrude from the barrel on the same side as the C-terminus. With this organization the N-terminal segment would bisect the lumen (Figure 1.1A) and negatively-charged residues in β3-β6 are aligned near the centre of the pore wall as noted by Hiller et al., (2008). In comparison to the other structures shown in Figure 1.1, the pore is relatively small, which is compatible with a closed state. The calculated vacuum electrostatic potential of this structure reveals clusters of positively- and negatively-charged residues. It is not clear whether this form would be anion- or cation-selective, as there are several possible pathways for small ions.

1.3.4.6 *Conserved Residues*

The uniform gating properties of VDAC1 from different sources suggest a universal gating mechanism that might be reflected in conserved residues in the voltage sensor or the N-terminal helical segment. Based on the alignment presented by Young et al., (2007), an aromatic residue (Y,F,W) and an acidic residue (D,E) in positions 7 and 9, respectively, are found in almost all VDAC sequences (Figure 1.4). A hydrophobic, branched-chain amino acid (I,L,V) is found at position 143 in most VDAC, but less frequently at position 150. The NcVDAC biotinylated variant S7C and the ScVDAC E152C both showed altered gating properties. Together, these observations are consistent with this set of residues participating in one of the possible gated states.

In the model for mVDAC1 presented by the Abramson lab (Ujwal et al., 2008), and the hVDAC1 model from the Zeth lab (Bayrhuber et al., 2008), a portion of the N-terminal sequence is placed horizontally against the barrel wall, parallel to the membrane. In the hVDAC1 model (Bayrhuber et al., 2008), residues 7 to 17 form a helix that lies against the barrel wall and residues 3-6 are directed toward the opening of the pore. Residues Y7, D9, L10 and R15 are chemically conserved in most VDAC (Figure 1.4). These residues contact H181 (β12), S193 and Y195 (β13), and K224 (β15), but only S193 and Y195 are highly conserved (see Figure 1.4). Based on the calculated electrostatic surface (Figure 1.1E), the resulting pore is lined with mainly positively-charged residues, implying an anion-selective state. The pore opening appears larger than that in the structure from the Wagner lab (Hiller et al., 2008; Figure 1.1A), suggesting that the protein was locked in an open state under the experimental conditions used by Bayrhuber et al., (2008).

The position of the N-terminus was most-clearly resolved for the mouse protein

Figure 1.4 *Conservation of residues of VDAC involved in intramolecular interactions*. 245 VDAC sequences were analyzed for residue conservation using GENEDOC base composition analysis (v2.5.010; Nicholas and Nicholas, 1997) of the PRALINE alignment generated by Young et al., (2007). Light grey bars indicate the percentage of sequences in which a chemically-conserved amino acid was present at a given position, and dark grey bars indicate the percentage of sequences containing residues identical to that in the mVDAC1 and hVDAC1 sequences.

A

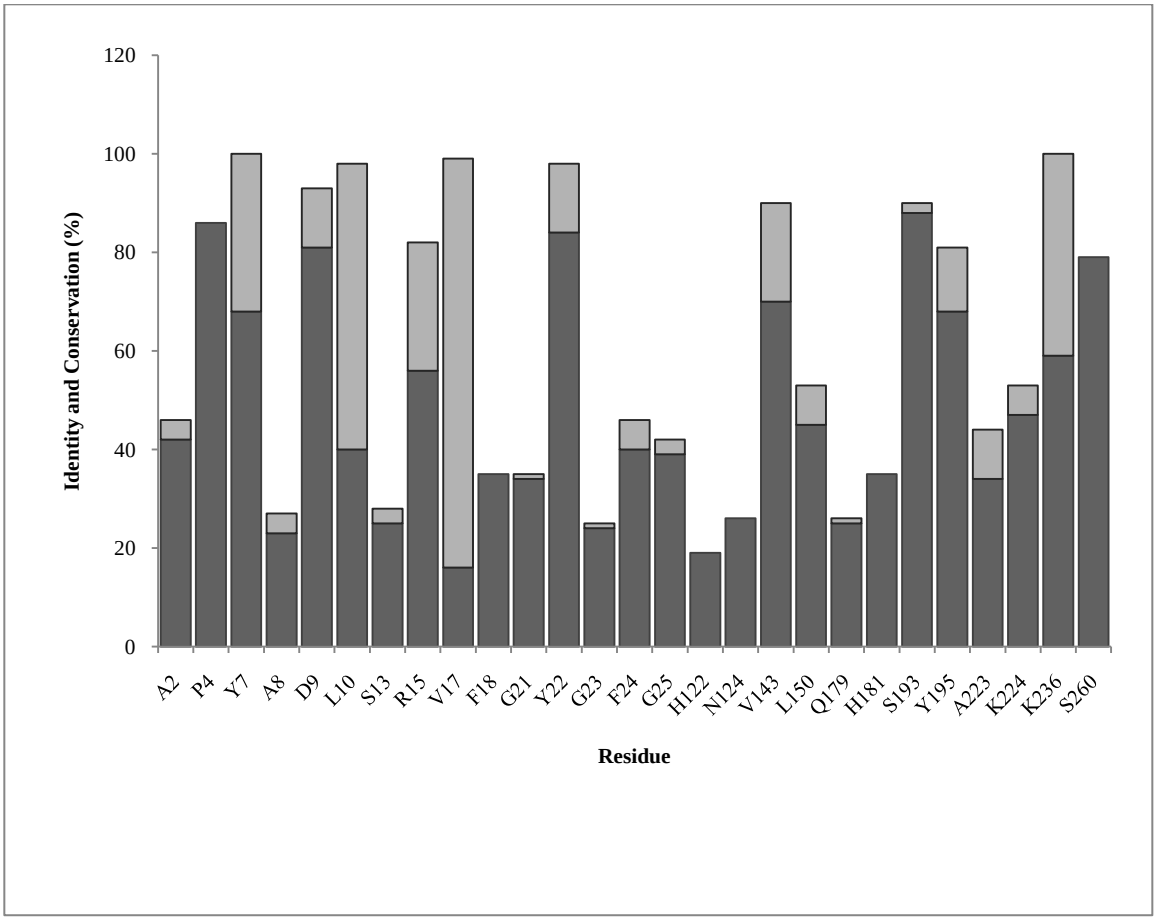
120
100
80
60
40
20
0
Identity and Conservation (%)
A2
P4
Y7
A8
D9
L10
S13
R15
V17
F18
G21
Y22
G23
F24
G25
H122
N124
V143
L150
Q179
H181
S193
Y195
A223
K224
K236
S260
Residue

(see Figure 1.1C). In this structure, residues A2 and P4 hydrogen bond with H122 and N124 in β8. Of these four residues, only P4 is highly conserved in all VDAC (Young et al., 2007; Figure 1.4), suggesting that it provides a structural component to the gating system. Residues 6-9 and 12-20 form two short helices that are bridged by a bidentate hydrogen bond between the carbonyl oxygens of A8 and L10 in the first helix and R15 in the second helix; of these, positions 10 and 15 are the best conserved with respect to chemically-similar residues. Under the conditions used in their experiments, the N-terminus is tightly fixed to the wall, through hydrogen bonds between S13 and Q179 (β12), F18 and K236 (β16), and G23 and S260 (β18). In the N-terminus, the residues corresponding to S13 and G23 were shown to be important for gating of fungal VDAC (Table 1.3), although neither is conserved in all VDAC (Figure 1.4). Of the β-strand residues, only K236 is chemically conserved. V17 and Y22 are hydrogen bonded to a water molecule interacting with A223 of β15. V17 and Y22 are well conserved, and A223 moderately conserved. The protein in these studies appears to be in an anion-selective state, but with larger lumen dimensions that the form studied by Bayrhuber et al., (2008).

1.3.4.7 *Proposed Models*

Based on the above structural data, and previous observations, several mechanisms of gating via the N-terminus can be envisioned: i) movement of the N-terminus into and out of the lumen, or ii) movement of the N-terminal domain within the lumen as a relatively static structure, or iii) transition of the N-terminus from an α-helical structure that aligns with the barrel wall to a less-structured element that interacts with the opposing barrel wall.

Electron microscopic analysis of two-dimensional VDAC arrays suggests a gating mechanism that involves movement of the N-terminus into and out of the lumen. In two-dimensional crystals of NcVDAC formed following phospholipase A2 treatment of MOM, the N-terminus of the protein is accessible to antibodies and in oblique arrays appears to extend laterally from the barrel, into the aqueous phase (Guo et al., 1995). It was suggested by the authors that partial closure of the pore could involve movement of the N-terminus into the lumen or along the barrel wall, via a flexible hinge. Such movement could lead to movement of the adjacent, flexible segments of the barrel (discussed above). If gating involves movement of the N-terminus in and out of the barrel, the conformations identified in the recent studies would represent different closed substates, in which the N-terminus resides in the lumen. However, the physiological relevance of structures analyzed in the two-dimensional arrays and in membrane mimetics remains to be determined.

A second mechanism of gating of mVDAC1 was suggested to involve movement of the N-terminus, facilitated by a molecular hinge consisting of G21-Y22-G23-F24-G25, and electrostatic interactions between the positively-charged residues in the α-helices and the negatively-charged residues on the opposing wall (β2, β3, β5, β6 and β8, Ujwal et al. 2008). The sequence of the hinge is highly conserved in mammalian porins (data not shown), but is not an absolute feature of VDAC (Figure 1.4). If the N-terminus moved about the hinge by 10^{o}, the lumen would become partially occluded, creating a closed state (Bayrhuber et al., 2008). This movement could be associated with, or require, some of the flexibility described above in the N-terminal six β-strands.

A third possible gating mechanism is suggested directly from the images presented in Figure 1.1. Assuming that the Hiller et al., (2008) structure represents a closed state, and the other two structures represent an open state, it is tempting to speculate that gating is simply a transition between the two structures (Figure 1.5). From the data discussed in this review, several functional regions could be envisioned in the porin molecule. β-strands 19 and 1 through 5 compose one of the two components of the voltage sensor, and have been shown to exhibit flexibility. The remaining component of the sensor is comprised of β10-β13. This includes one (L150) of the contacting residues presented within the Hiller et al., (2008) structure, with the second (V143) being in the adjacent β-strand. The N-terminal region would comprise the gate, and it could exist in a conformation rich in α-helix in the open state, and in a more unfolded form in the closed state. It has been shown previously that the N-terminus can adopt different conformations under different conditions (Guo et al., 1995; De Pinto et al., 2007). The molecular hinge (GYGFG in mammalian VDAC) that links the N-terminal "gate' to β1 could also exist in different states (Figure 1.5B), and pivot at a point near the N-terminus of β1. Starting with the putative open state, applied voltage could alter the sensor regions such that the interaction of the N-terminus with the barrel wall is destabilized. Unfolding of the helix, and the establishment of new interactions with the β10-β13 sensor region could lead to a closed state. This rearrangement could be accompanied by other minor changes to the barrel wall and loops in the hinge region. This process presumably would be energetically expensive, and hence be dependent on voltage-induced changes to VDAC. If it were to occur *in vivo*, it could be driven by processes such as protein binding to

Figure 1.5 *Comparisons of the hVDAC structures*.

A) Location of the voltage sensors. The NMR structure (PDB ID code 2K4T, yellow, Hiller et al., 2008) was aligned to the other hVDAC1 structure (2JK4, cyan, Bayrhuber et al., 2008) with APBS Tools in PyMOL with an RMSD of 1.792 Å. The two components of the sensor region, as identified from the data in Table 1.3, are indicated by a grey and a black crescent. The hinge region, as defined by Ujwal et al., (2008) is shown in red in all three panels. Voltage-induced movement is suggested by the arrows and lightning bolts in panel B. For ease of viewing, the N-termini and hinge regions of the two structures are shown alone in panels B and C, and the differences in the position of the β-strands near the pivot point are estimated by the positions of the two grey crescents in B as shown in the ribbon diagram in C.

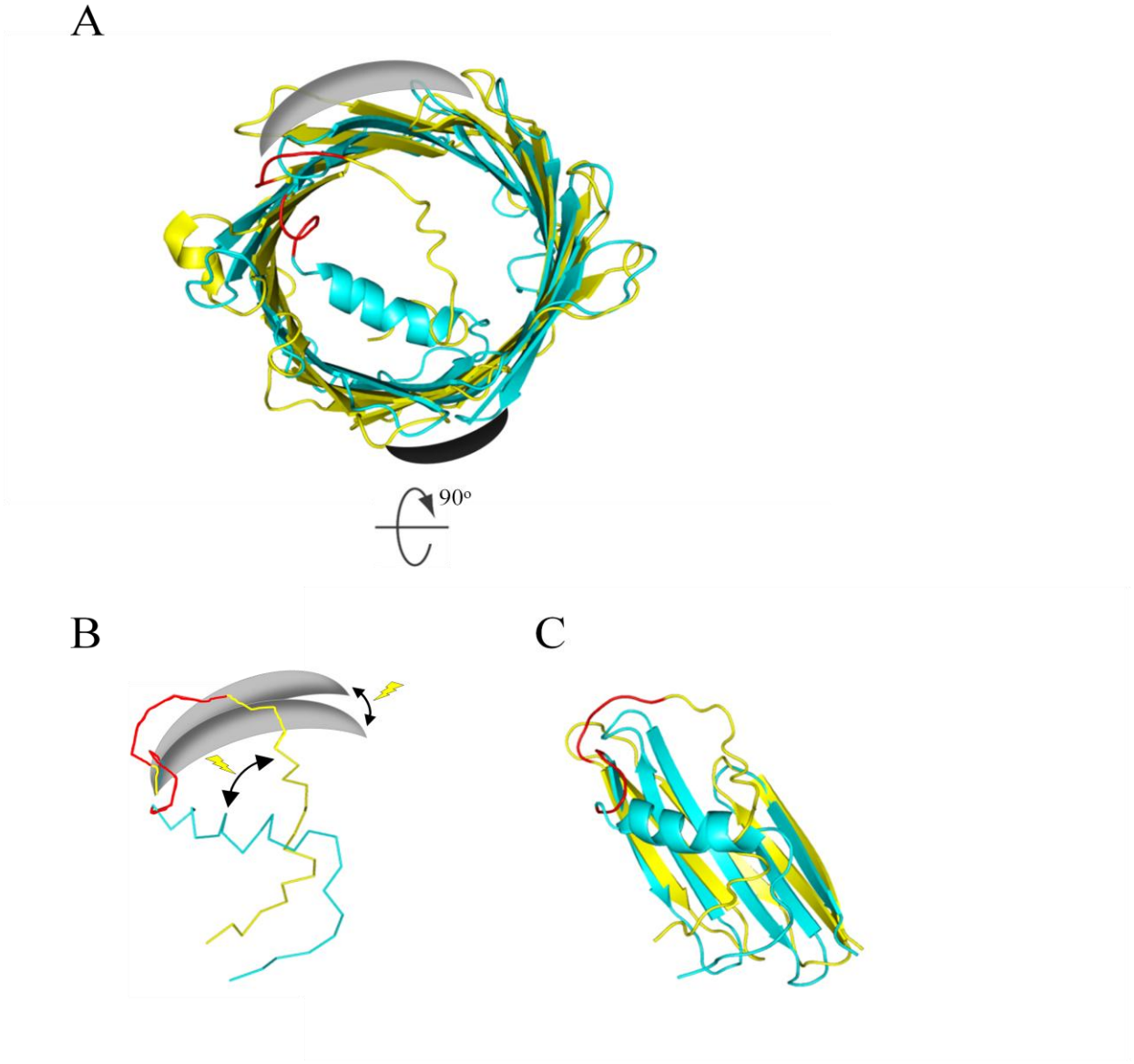
A
90º
B
C

VDAC, as it may be unlikely, but not impossible (Liu and Colombini, 1992; Lemeshko and Lemeshko, 2000), that a significant transmembrane potential exists across the outer membrane. VDAC is known to interact with many proteins (Roman et al., 2006), including potential regulators of apoptosis, although the exact role of these proteins in programmed cell death is currently under vigorous debate and investigation (Rostovtseva et al., 2004; Tsujimoto and Shimizu, 2007; Rostovtseva and Bezrukov, 2008 and references therein). Thus, protein-protein interactions may cause or mediate changes in VDAC that are mimicked in PLB experiments.

1.4 *Objectives of This Study*

The first goal of this study was to determine if mitochondrial porin is an essential constituent of the MOM in *Neurospora crassa*. The human mitochondrial porin (hVDAC1) is in high abundance in a bioptic specimen of healthy muscle tissue and completely absent from a bioptic specimen taken from the muscles of a patient suffering from severe myopathy (De Pinto et al., 2000). Deletion of the gene encoding mVDAC2 results in embryonic lethality in mice (Baines et al., 2007). Most of the research on mitochondrial porin completed at the time this study was begun had been performed in yeast and had demonstrated that both porin isoforms were dispensable for yeast grown in non-fermentable carbon sources (Blachly-Dyson et al., 1997). To determine the essentiality in the obligately aerobic *Neurospora crassa*, a null allele of the *por* gene was created and introduced into a *mus-51* mutant strain. This work demonstrated that porin is non-essential for the viability of *Neurospora crassa*.

The second goal was to characterise the phenotypic traits caused by the deletion of *por*. The disruption of *por1* in *Saccharomyces cerevisiae* resulted in the almost complete loss of respiration, but the strain required no additional amino acid supplements, suggesting that the biosynthesis of amino acids by mitochondrial matrix enzymes continued. The loss of porin resulted in reduced levels of all cytochromes and a reduced growth rate of about half of the wild-type rate when the cells were grown on glycerol-containing media after a 3 day adaption period (Dihanich et al., 1987). To determine the effect of porin loss in *Neurospora crassa* mitochondria, the macroscopic morphology, growth rate, cytochrome content, expression of alternative oxidase and ATP concentration of the knockout strains were compared to a control strain. This work revealed that strains lacking porin are hindered in cytochrome mediated respiration and express alternative oxidase to compensate.

The third goal of this work was to examine the mitochondrial proteome of the porin lacking mitochondria to identify constituents with alterations in expression in response to the lack of porin. Yeast deficient in porin and grown on glycerol-containing media for 10 days accumulate large amounts of an 86-kDa extramitochondrial protein not observed in the wild-type preparations (Dihanich et al., 1987). The results of the current study show that a *por* ¯ strain that exhibited altered mitochondrial morphology has several proteins that were identified as significantly up- and down-regulated in comparison to a control strain, which lend explanations to some of the observed phenotypic traits that were examined.

Chapter 2: Materials and Methods

2.1 *Bacterial, Yeast and Neurospora crassa Strains*

The yeast strain used in this study was *Saacharomyces cerevisiae* S150 (*ura3-53*, *his3-Δ1*, *trp1-289*, *leu2-3,112*, *MATα*) and *Neurospora crassa* strains used in this study are listed in Table 2.1.

E. coli strains DH5α (Hanahan, 1983), TOP10 (Invitrogen) and XL1-Blue (Bullock et al., 1987) were utilized in gene construction. The transformed *E. coli* strains were grown on Luria-Bertani (LB) media containing the appropriate antibiotics. Amplicillin (100 µg / ml), kanamycin (25 µg / ml) and tetracycline (10 µg / ml) were added to media that was inoculated with cultures of *E. coli* expressing amp^r, kan^r, *and* tet^r respectively.

General growth and handling of *Neurospora crassa* was as described (Davis and De Serres, 1970). Measurement of growth rate in race tubes was done in either 40-cm glass tubes or 100-cm glass tubes with the ends turned up on 45^o angles. 15 ml and 100 ml of Vogel's minimal (VM) media with appropriate supplements were used to fill the 40-cm tubes and 100-cm tubes respectively (Davis and De Serres, 1970). This is a convenient method for measuring the growth rate since it is a linear function of time, and typical rates obtained from wild type strains are measurable with a metre stick. Growth rate experiments at 22-23^{o}C were grown on the desktop, while the 30^{o}C experiments were incubated in an incubator with a beaker of water to add a little humidity to prevent premature dehydration of the race tubes.

Table 2.1 *Neurospora crassa strains created and used in this study.*

Homokaryotic Strains

Strain Name	Genotype	Mating type	Female Fertile[†]
74A[d]	unknown derivative of 74A OR23	A	+
FGSC 987	Wild-type	A	+
FGSC 7255	*cyh-2, lys-2, leu-5, mei-2*	a	n/d
FGSC 9717	Δ*mus-51*::*bar*$^+$, *his-3*	A	n/d
FGSC 9718	Δ*mus-51*::*bar*$^+$	a	+
FGSC 9719	Δ*mus-52*::*bar*$^+$	a	n/d
FGSC 9720	Δ*mus-52*::*bar*$^+$, *his-3*	A	+
FGSC 18892	Δ*por*::*hph*$^+$	A	+
WS001	FGSC 9720; *ad-3*A::*his-3*$^+$	A	n/d
WS002.1	WS001; Δ*lys-3*::*hph*$^+$	A	n/d
WS002.2	WS001; Δ*lys-3*::*hph*$^+$	A	n/d
WS002.3	WS001; Δ*lys-3*::*hph*$^+$	A	n/d
WS003.1	WS001; *trp-1*::*hph*$^+$	A	n/d
WS003.2	WS001; *trp-1*::*hph*$^+$	A	n/d
WS003.3	WS001; *trp-1*::*hph*$^+$	A	n/d
WS004	FGSC 9718; Δ*por*::*hph*$^+$	a	-
WS005	FGSC 9718; *hph*$^+$, *por*::*His*$_6$	a	n/d
WS007	FGSC 18892; *por*$^+$ [¥]	A	+
WS008	FGSC 18892; *por*$^+$ [¶]	A	n/d
WS009	FGSC 9719; *hph*$^+$, *His*$_6$::*por*	A	n/d
WS009.1	FGSC 9719; *hph*$^+$, *His*$_6$::*por*	A	n/d
WS010.1	WS001; *por*::*ad-3*A	A	n/d
WS010.2	WS001; *por*::*ad-3*A	A	n/d
WS010.3	WS001; *por*::*ad-3*A	A	n/d

Heterokaryotic Strains

Strain Name	Genotype	Mating type	Female Fertile
WS110	WS002.3 + WS003.1	A	n/d
WS110.1	WS002.3 + WS003.1	A	n/d
WS111.1	WS110; *por*::*ad-3*A	A	n/d
WS111.2	WS110; *por*::*ad-3*A	A	n/d
WS120	FGSC 9720 + WS001	A	n/d
WS122	WS120; *hph*$^+$, *eGFP*::*por*	A	n/d
WS123.1	WS120; Δ*por*::*hph*$^+$	A	n/d

WS123.2	WS120; Δ*por*::*hph*$^{+}$	A	n/d
WS123.3	WS120; Δ*por*::*hph*$^{+}$	A	n/d
WS123.4	WS120; Δ*por*::*hph*$^{+}$	A	n/d
WS123.5	WS120; Δ*por*::*hph*$^{+}$	A	n/d
WS124.1	WS120; *hph*$^{+}$, *por*::*His*$_{6}$	A	n/d
WS124.2	WS120; *hph*$^{+}$, *por*::*His*$_{6}$	A	n/d
WS124.3	WS120; *hph*$^{+}$, *por*::*His*$_{6}$	A	n/d
WS124.4	WS120; *hph*$^{+}$, *por*::*His*$_{6}$	A	n/d
WS124.5	WS120; *hph*$^{+}$, *por*::*His*$_{6}$	A	n/d
WS125.1	FGSC 9718; *hph*$^{+}$, *por*$^{+¥}$, Δ2-12 porin	a	n/d
WS125.2	FGSC 9718; *hph*$^{+}$, *por*$^{+¥}$, Δ2-12 porin	a	n/d
WS125.3	FGSC 9718; *hph*$^{+}$, *por*$^{+¥}$, Δ2-12 porin	a	n/d
WS125.4	FGSC 9718; *hph*$^{+}$, *por*$^{+¥}$, Δ2-12 porin	a	n/d
WS125.5	FGSC 9718; *hph*$^{+}$, *por*$^{+¥}$, Δ2-12 porin	a	n/d
WS125.6	FGSC 9718; *hph*$^{+}$, *por*$^{+¥}$, Δ2-12 porin	a	n/d
WS125.7	FGSC 9718; *hph*$^{+}$, *por*$^{+¥}$, Δ2-12 porin	a	n/d
WS125.8	FGSC 9718; *hph*$^{+}$, *por*$^{+¥}$, Δ2-12 porin	a	n/d
WS125.9	FGSC 9718; *hph*$^{+}$, *por*$^{+¥}$, Δ2-12 porin	a	n/d
WS125.10	FGSC 9718; *hph*$^{+}$, *por*$^{+¥}$, Δ2-12 porin	a	n/d
WS125.11	FGSC 9718; *hph*$^{+}$, *por*$^{+¥}$, Δ2-12 porin	a	n/d
WS125.12	FGSC 9718; *hph*$^{+}$, *por*$^{+¥}$, Δ2-12 porin	a	n/d
WS126.1	FGSC 9718; *hph*$^{+}$, *por*$^{+¥}$ Δ269-283 porin	a	n/d
WS126.2	FGSC 9718; *hph*$^{+}$, *por*$^{+¥}$ Δ269-283 porin	a	n/d
WS126.3	FGSC 9718; *hph*$^{+}$, *por*$^{+¥}$ Δ269-283 porin	a	n/d
WS126.4	FGSC 9718; *hph*$^{+}$, *por*$^{+¥}$ Δ269-283 porin	a	n/d
WS126.5	FGSC 9718; *hph*$^{+}$, *por*$^{+¥}$ Δ269-283 porin	a	n/d
WS126.6	FGSC 9718; *hph*$^{+}$, *por*$^{+¥}$ Δ269-283 porin	a	n/d
WS126.7	FGSC 9718; *hph*$^{+}$, *por*$^{+¥}$ Δ269-283 porin	a	n/d
WS126.8	FGSC 9718; *hph*$^{+}$, *por*$^{+¥}$ Δ269-283 porin	a	n/d
WS126.9	FGSC 9718; *hph*$^{+}$, *por*$^{+¥}$ Δ269-283 porin	a	n/d
WS126.10	FGSC 9718; *hph*$^{+}$, *por*$^{+¥}$ Δ269-283 porin	a	n/d

WS126.11	FGSC 9718; *hph*$^{+}$, *por*$^{+¥}$ Δ269-283 porin	a	n/d
WS126.12	FGSC 9718; *hph*$^{+}$, *por*$^{+¥}$ Δ269-283 porin	a	n/d
WS127.1	FGSC 9718; *hph*$^{+}$, *por*$^{+¥}$ ΔNDRGV porin	a	n/d
WS127.2	FGSC 9718; *hph*$^{+}$, *por*$^{+¥}$ ΔNDRGV porin	a	n/d
WS127.3	FGSC 9718; *hph*$^{+}$, *por*$^{+¥}$ ΔNDRGV porin	a	n/d
WS127.4	FGSC 9718; *hph*$^{+}$, *por*$^{+¥}$ ΔNDRGV porin	a	n/d
WS127.5	FGSC 9718; *hph*$^{+}$, *por*$^{+¥}$ ΔNDRGV porin	a	n/d
WS127.6	FGSC 9718; *hph*$^{+}$, *por*$^{+¥}$ ΔNDRGV porin	a	n/d
WS127.7	FGSC 9718; *hph*$^{+}$, *por*$^{+¥}$ ΔNDRGV porin	a	n/d
WS127.8	FGSC 9718; *hph*$^{+}$, *por*$^{+¥}$ ΔNDRGV porin	a	n/d
WS127.9	FGSC 9718; *hph*$^{+}$, *por*$^{+¥}$ ΔNDRGV porin	a	n/d
WS127.10	FGSC 9718; *hph*$^{+}$, *por*$^{+¥}$ ΔNDRGV porin	a	n/d
WS127.11	FGSC 9718; *hph*$^{+}$, *por*$^{+¥}$ ΔNDRGV porin	a	n/d
WS127.12	FGSC 9718; *hph*$^{+}$, *por*$^{+¥}$ ΔNDRGV porin	a	n/d

Cross Progeny

Strain Name	Female X Male	Phenotype	Female Fertile
WS1000	9718 X WS111.2	Trp^{+}	n/d
WS1001	9718 X WS111.2	Trp^{+}	n/d
WS1002	9718 X WS111.2	Lys^{+}	n/d
WS1003	9718 X WS111.2	Lys^{+}	n/d
WS1004	9718 X WS122	Ade^{+}	n/d
WS1005	9718 X WS122	His^{+}	n/d
WS1006	9717 X WS004	His?, Hyg^{r} §	n/d
WS1007	9717 X WS004	His?, Hyg^{r}	n/d
WS1008	WS123.4 X 9718	His?, Hyg^{r}	n/d
WS1009	WS123.4 X 9718	His?, Hyg^{r}	n/d
WS1010	WS123.4 X 9718	Ade?, Hyg^{r}	n/d

WS1011	WS123.4 X 9718	Ade?, Hyg^r	n/d
WS1012	WS123.5 X 9718	His?, Hyg^r	n/d
WS1013	WS123.5 X 9718	His?, Hyg^r	n/d
WS1014	WS123.5 X 9718	Ade?, Hyg^r	n/d
WS1015	WS123.5 X 9718	Ade?, Hyg^r	n/d
WS1016	WS124.4 X 9718	Ade^+, Hyg^r (His_6 confirmed with PCR)	n/d
WS1017	WS124.4 X 9718	Ade^+, Hyg^r (His_6 confirmed with PCR)	n/d
WS1018	WS124.4 X 9718	Ade^+, Hyg^r	n/d
WS1019	WS124.4 X 9718	Ade^+, Hyg^r	n/d
WS1020	WS124.4 X 9718	His^+, Hyg^r	n/d
WS1021	WS124.4 X 9718	His^+, Hyg^r	n/d
WS1022	WS124.5 X 9718	His^+, Hyg^r	n/d
WS1023	WS124.5 X 9718	His^+, Hyg^r	n/d
WS1024	WS124.5 X 9718	Ade^+, Hyg^r	n/d
WS1025	WS124.5 X 9718	Ade^+, Hyg^r	n/d
WS1036	$74A^d$ X WS004	Hyg^r, $Aer^{+Å}$, $Basta^s$ (confirmed with PCR)	-
WS1037	$74A^d$ X WS004	Hyg^r, Aer^+, $Basta^r$	-
WS1038	$74A^d$ X WS004	Hyg^r, Aer^-, $Basta^r$	-
WS1039	$74A^d$ X WS004	Hyg^r, Aer^+, $Basta^s$ (confirmed with PCR)	-
WS1040	$74A^d$ X WS004	Hyg^r, Aer^+, $Basta^s$ (confirmed with PCR)	-
WS1041	$74A^d$ X WS004	Hyg^r, $Basta^r$	-
WS1042	$74A^d$ X WS004	Hyg^r, $Basta^r$	-
WS1043	$74A^d$ X WS004	Hyg^r, Aer^-, $Basta^s$ (confirmed with PCR)	-
WS1044	$74A^d$ X WS004	Hyg^r, $Basta^r$	-
WS1045	$74A^d$ X WS004	Hyg^r, $Basta^r$	-
WS1046	18892 X 97-18	Hyg^r, $Basta^r$	-
WS1047	18892 X 97-18	Hyg^r, $Basta^r$	-

WS1048	18892 X 97-18	Hyg^r, Aer^+, $Basta^r$	-
WS1049	18892 X 97-18	Hyg^r, $Basta^r$	-
WS1050	18892 X 97-18	Hyg^r, $Basta^r$	-
WS1051	18892 X 97-18	Hyg^r, $Basta^r$	-
WS1052	18892 X 97-18	Hyg^r, $Basta^r$	-
WS1053	18892 X 97-18	Hyg^r, Aer^-, $Basta^r$	-
WS1054	18892 X 97-18	Hyg^r, $Basta^r$	-
WS1055	18892 X 97-18	Hyg^r, $Basta^r$	-
WS1056	$74A^d$ X WS004	$Basta^r$, Aer^+	+
WS1057	$74A^d$ X WS004	Aer^+	+
WS1058	$74A^d$ X WS004	$Basta^r$, Aer^+	+
WS1059	$74A^d$ X WS004	$Basta^r$, Aer^+	+
WS1060	$74A^d$ X WS004	$Basta^r$, Aer^+	+
WS1061	$74A^d$ X WS004	Aer^+	+
WS1062	$74A^d$ X WS004	Aer^+	+
WS1063	$74A^d$ X WS004	$Basta^r$, Aer^+	+
WS1064	$74A^d$ X WS004	Aer^+	+
WS1065	$74A^d$ X WS004	$Basta^r$, Aer^+	+
WS1066	$74A^d$ X WS004	Aer^+	+
WS1067	$74A^d$ X WS004	$Basta^r$, Aer^+	+
WS1068	$74A^d$ X WS004	Hyg^r, $Basta^r$, Aer^+	+
WS1069	$74A^d$ X WS004	$Basta^r$, Aer^+	+
WS1070	$74A^d$ X WS004	Aer^+	+
WS1071	$74A^d$ X WS004	Aer^+	+
WS1072	$74A^d$ X WS004	Aer^+	+
WS1073	$74A^d$ X WS004	Aer^+	+
WS1074	$74A^d$ X WS004	$Basta^r$, Aer^+	+
WS1075	$74A^d$ X WS004	Aer^+	+
WS1076	$74A^d$ X WS004	Aer^+	+
WS1077	$74A^d$ X WS004	Aer^+	+
WS1078	$74A^d$ X WS004	Aer^+	+
WS1079	$74A^d$ X WS004	Aer^+	+
WS1080	$74A^d$ X WS004	Aer^+	+
WS1081	$74A^d$ X WS004	$Basta^r$, Aer^+	+

WS1082	74A^{d} X WS004	Basta^{r}, Aer^{+}	+
WS1083	74A^{d} X WS004	Basta^{r}, Aer^{+}	+
WS1084	74A^{d} X WS004	Basta^{r}, Aer^{+}	+
WS1085	74A^{d} X WS004	Hyg^{r}, Basta^{r}, Aer^{+}	+
WS1086	74A^{d} X WS004	Basta^{r}, Aer^{+}	+
WS1087	74A^{d} X WS004	Aer^{+}	+
WS1088	74A^{d} X WS004	Basta^{r}, Aer^{+}	+
WS1089	74A^{d} X WS004	Aer^{+}	+
WS1090	74A^{d} X WS004	Aer^{+}	+
WS1091	74A^{d} X WS004	Aer^{+}	+
WS1092	74A^{d} X WS004	Basta^{r}, Aer^{+}	+
WS1093	74A^{d} X WS004	Aer^{+}	+
WS1094	74A^{d} X WS004	Aer^{+}	+
WS1095	74A^{d} X WS004	Aer^{+}	+

† Female fertile, defined by the observation of protoperithecia after 7-8 days of incuabation under continuous light

¥ *por*$^{+}$, cDNA version of *por* flanked by endogenous up- and down-stream UTRs

¶ *por*$^{+}$, cDNA version of *por* flanked by endogenous up- and down-stream UTRs and containing the first three intron present in the endogenous *por* gene.

§ Hyg, hygromycin

Ⱥ Aer^{+}, + = wild-type aerial hyphae production, - = no production of aerial hyphae

r = resistance, s = sensitive

2.2 *Oligonucleotides and Plasmids Used in This Study*

All of the oligonucleotides used in this study are listed in Table 2.2. All of the plasmids used in this study are listed in Table 2.3 and Table 2.4. The methods used to construct the plasmids are given in section 2.9.

2.3 *Plasmid DNA Isolation from Bacteria*

Plasmid DNA was isolated by the alkaline lysis method (Sambrook, 2001). DNA for subsequent restriction / ligation cloning and / or sequencing was produced in large quantity via the Qiagen Plasmid Midi Kit (Qiagen Inc., Mississauga, ON, Canada) according to the manufacture's protocol with the exception of using the "Maxi" volumes with the Midi kit. DNA specifically for sequencing, cloning in yeast or producing transformation fragments was prepared using the Qiagen QIAprep Spin Miniprep Kit (Qiagen Inc., Mississauga, ON, Canada) according to the manufacture's protocols with the exception of 10 000 rpm spins replacing all 13 000 rpm spins but the elution spin. Additionally, the column was left to stand at RT for 10 min instead of 1 min prior to collecting the elution. The DNA was eluted with 30-50 µl of sdH_2O in place of the provided Buffer EB.

2.4 *Purification of DNA from Agarose Gels*

The desired products of PCR reactions or resulting DNA fragments from digestion reactions were cut from either a 0.8% or 1.0% agarose gel and transferred to a 1.5 ml microfuge tube. Three volumes of buffer QC were added to the agarose fragment ($^{w}/_{v}$) and this was heated at 50^{o}C and mixed with periodic vortexing until the agarose was completely dissolved. 750 µl of this mixture was transferred to a mini-prep column

Table 2.2 *Oligonucleotides used in this study*

Primers Used in Plasmid Construction with Restriction Endonuclease / Ligation Method (See Table 2.3)

Primer name	Sequence	Colour Info.	Tm (C)
NcPprom 5'	AAAAGAGCTCCTTGGCATCGG	Green = *Sac*I; Red = *por* upstream UTR overlap	32
NcPprom 3'	AAAAACTAGTTGTGAAAGATG	Green = *Spe*I; Red = *por* upstream UTR overlap; Blue = overlap in both	30
NcPH6a5'	AAACTAGT**CAATGG**CTCACCACCACCACCACCACGCTGTTCCCGC	Green = *Spe*I; **Bold** = Kozak; Yellow = His_6; Red = *por* overlap	42
NcPH6b5'	AAACTAGTATGGCTCACCACCACCACCACCACGCTGTTCCCGCTT	Green = *Spe*I; Yellow = His_6; Red = *por* overlap	42
NcPH6 3'	AAAAGATATCATTACTCTAAGA	Green = *Eco*RV; Red = *por* overlap	30
ad3A-5’	AAAAGGATCCGGGCCCAGGGAATCTTCAAGGAATCG	Green = *Bam*HI; Red = *ad-3*A upstream UTR overlap	70
ad3A-3'	AAAAGATATCTGAACCTCCTGTCTGCACGCCC	Green = *Eco*RV; Red = *ad-3*A upstream UTR overlap; Blue = overlap in both	72
His3asc5'	AAGAATTCGGCGCGCCGGTTGTAAGGATTATATGACTTCCG	Green = *Asc*I; Red = *his-3* overlap	70
His3asc3'	AAGAATTCGGCGCGCCGGGTCTGAATGCTAAAAGACACC	Green = *Asc*I; Red = *his-3* overlap	68
Trp1 5' SPE I	AAAAACTAGTATGGT	Green = *Spe*I; Red = *trp-1*	62

	GGTGTTGTGTGCAGG	overlap	
Trp1 3' SPE I	AAAAACTAGTCGTTG TGTTATGTGGCTGGG	Green = *Spe*I; Red = *trp-1* overlap	62
hphFnarI	AAAAAGGCGCCCCGT CGACAGAAGATGATA TTGAAGGAGC	Green = *Nar*I; Red = *hph* overlap	86
hphRnarI	AAAAAGGCGCCAGCT GACATCGACACCAAC G	Green = *Nar*I; Red = *hph* overlap	62

Primers Used in Plasmid Construction with Yeast Recombination Method (See Table 2.4)

Primer name	Sequence	Colour Info.	Tm (C)
LYS3 5’ UTR F	GTAACGCCAGGGTTT TCCCAGTCACGACGT TGTAAAACGATTCCC ATCTTACCTAGCGTG	Black = pRS416 overlap; Red = *lys-3* upstream UTR overlap	60
LYS3 5’ UTR R	GACGAATCTGGATAT AAGATCGTTGGTGTC GATGTCAGCTTCCGA TCTGCGTTAGAAGCC	Black = *hph* overlap; Red = *lys-3* upstream UTR overlap	62
LYS3 3’ UTR F	GCCCAAAAAGTGCTC CTTCAATATCATCTTC TGTCGACGGGACAAC AGTCATGGTCAGGC	Black = *hph* overlap; Red = *lys-3* downstream UTR overlap	62
LYS3 3' UTR R	GCGGATAACAATTTC ACACAGGAAACAGCT ATGACCATGAACAGC TCTTCAGTACGAACC	Black = pRS416 overlap; Red = *lys-3* downstream UTR overlap	60
hphFnarI	AAAAAGGCGCCCCGT CGACAGAAGATGATA TTGAAGGAGC	Green = *Nar*I; Red = *hph* overlap	86

hphRnarI	AAAAAGGCGCCAGCT GACATCGACACCAAC G	Green = *Nar*I; Red = *hph* overlap	62
5' Prom::pRS416	GTAACGCCAGGGTTT TCCCAGTCACGACGT TGTAAAACGAATCGG GATTACAATGCAGGG	Black = pRS416 overlap; Red = -1000 *por* overlap	60
3' Prom::Hyg	GCCCAAAAAGTGCTC CTTCAATATCATCTTC TGTCGACGGTTAGAC GGAGTCGTGATTGG	Black = *hph* overlap; Red = -320 *por* upstream UTR overlap	60
por3'UTRF	GACGAATCTGGATAT AAGATCGTTGGTGTC GATGTCAGCTACATG TGAAGAAGCAGCGG C	Black = *hph* overlap; Red = *por* downstream UTR overlap	62
por3'UTRR	GCGGATAACAATTTC ACACAGGAAACAGCT ATGACCATGAGGCAC CTGACTTCAACAGCG	Black = pRS416 overlap; Red = *por* downstream UTR overlap	64
5' Porin::Hyg	GACGAATCTGGATAT AAGATCGTTGGTGTC GATGTCAGCTACATT GCACCTGGTCTTGGG	Black = *hph* overlap; Red = -320 *por* upstream UTR overlap	62
3' Porin::pRS416	GCGGATAACAATTTC ACACAGGAAACAGCT ATGACCATGAAGTTG CTCTGCTTGAAGTGG	Black = pRS416 overlap; Red = *por* upstream UTR overlap	60
porTAG_his6 5'	GTAACGCCAGGGTTT TCCCAGTCACGACGT TGTAAAACGGCGCGC CAAGGGTCTCAAGGC	Black = pRS416 overlap; Green = *Asc*I; Red = +1071 *por*; Blue = overlap in both	60

porTAG_his6 3'	CTTCACATGTGTCCT GCGATTACTTACGTA CTAGTGGTGGTGGTG GTGGTGGGCAGACTC GAAGGTGAAGCTGGT GCCG	Black = *por* downstream UTR overlap; Green = *Sna*BI; Yellow = His_6; Magenta = linker Alanine; Red = 3' *por*	80
porTerm 5'	CGGCACCAGCTTCAC CTTCGAGTCTGCCCA CCACCACCACCACCA CTAGTACGTAAGTAA TCGCAGGACACATGT GAAG	Red = 3' *por*; Magenta = linker Alanine; Yellow = His_6; Green = *Sna*BI; Black = *por* downstream UTR overlap	72
porTerm 3'	GCCCAAAAAGTGCTC CTTCAATATCATCTTC TGTCGACGGCTTCAC TTCATTGCACAGCC	Black = *hph* overlap; Red = *por* downstream UTR overlap	64
porTermUTR F	GACGAATCTGGATAT AAGATCGTTGGTGTC GATGTCAGCTTATTC AACGTGTTGTCCGC	Black = *hph* overlap; Red = +2234 *por* downstream UTR overlap	66
porTermUTR R	GCGGATAACAATTTC ACACAGGAAACAGCT ATGACCATGGCGCGC CGCCCAGCCTCTGGC	Black = pRS416 overlap; Green = *Asc*I; Blue = overlap in both; Red = *por* downstream UTR overlap	62
5'GFP:his6VDAC	ACCATCATACCCGTG TCGCCCTCACACAAC ATCTTTCACAATGTC TAAAGGTGAAGAATT	Black = pRS416 prom His_6 *hph* overlap; Red = *eGFP* from pKT128 overlap	52
3'GFP:his6VDAC	CAGAGAAAGCGGGA ACAGCGTGGTGGTGG TGGTGGTGAGCTTTG TACAATTCATCCATA C	Black = pRS416 prom His_6 *hph* overlap; Red = *eGFP* from pKT128 overlap	52

NcPprom:cDNA_3'	TGGCCGACTTGGCGA TGTCAGAGAAAGCGG GAACAGCCATTGTGA AAGATGTTGTGTGAG	Black = *por* cDNA overlap; Red = *por* upstream UTR overlap	56
5'_por_ATG	ATGGCTGTTCCCGCT TTCTC	Black = *por*	62
3'_cDNA:porTerm	GTTCGAAGGAATACT ATTACGCCGCTGCTT CTTCACATGTCTAAG ACTCGAAGGTGAAGC	Black = *por* downstream UTR; Red = *por*	60
NcPprom:cDNA_3'_deltaN	CGAGGTGGTAGAAGT CCTTGTTGAGGAGGT CGTTGGCCATTGTGA AAGATGTTGTGTGAG	Black = cDNA overlap starting +76 to 36; Green = ATG; Red = *por* upstream UTR overlap	56
5'_por_ATG_deltaN	GCCAACGACCTCCTC AACAAGG	Black = ΔN *por* cDNA	70
3'_cDNA:porTerm_deltaC	AGGAATACTATTACG CCGCTGCTTCTTCAC ATGTCTAATTAAGCT TCTGGGTATCGAAAG	Black = *por* downstream UTR overlap; Green = TAG; Magenta = N (Q in Runke et al.); Red = ΔC *por* cDNA	58

Other Primers Used in This Study

Primer name	Sequence	Colour Info.	Tm (C)
5'UTRF3Kb	GTAACGCCAGGGTTTTCCCAGTCACGACGACACTAGTACGGACACCC	Black = pRS416 overlap; Magenta = Incorrect with sequence; Red = *por* upstream UTR overlap	54
5'UTRF1Kb	GTAACGCCAGGGTTTTCCCAGTCACGACGAATGCAGGGCGTTATATGG	Black = pRS416 overlap; Red = *por* upstream UTR overlap	54
5'UTRR3Kb	ACCGGGATCCACTTAACGTTACTGAAATCAAGATGTTGTGTGAGGGC	Black = *hph* cassette overlap; Red = *por* upstream UTR overlap	54
3'UTRF3Kb	CGTTCTATAGTGTCACCTAAATCGTATGTACACATGTGAAGAAGCAGC	Black = *hph* cassette overlap; Red = *por* dowstream UTR overlap; NOTE : *hph* overlap has poor to no homology, primer NO GOOD see 3'UTRF2	56
3'UTRF2	GCTCCTTCAATATCATCTTCTGTCGACGGACACATGTGAAGAAGCAGCGGC	Black = *hph* cassette overlap; Red = *por* downstream UTR overlap	76
3'UTRR3Kb	GCGGATAACAATTTCACACAGGAAACAGCATACAGCAAGTCAGTGGTG	Black = pRS416 overlap; Red = *por* downstream UTR overlap	56
3'UTRR1Kb	GCGGATAACAATTTCACACAGGAAACAGCACCTGACTTCAACAGCG	Black = pRS416 overlap; Red = *por* downstream UTR overlap; Magenta = Incorrect with sequence	48
hphF(short)	CCGTCGACAGAAGAT		86

	GATATTGAAGGAGC		
hphR(short)	AGCTGACATCGACAC CAACG		62
hsm-f	AAAAAGCCTGAACTC ACCGCGACG		74
hsm-r	TCGCCTCGCTCCAGT CAATGACC		74
his3-5’	AAAAGAATTCGGGCC CGGTTGTAAGGATTA TATGACTTCCG	Green = *Eco*RI; Red = *his-3* downstream UTR overlap	68
his3-3’	AAAAAAGGGCCCCCC GGGTCTGAATGCTAA AAGACACC	Green = *Apa*I; Red = *his-3* downstream UTR overlap	68
Ad3Amid5’	ATGGTGTGCAACCAG TCTGC		62
Ad3Amid3'	TTCAGCAAGCTCCTG CGG		62
pRS416 MCS R	AAAAAGGGCCCGAT ATCAAGCTTATCGAT ACC		62
5' ad-his junc confirm	GTTCTGCACTAAGCG AACGG		62
3' ad-his junc confirm	TCCACTTCAGTTGCT GACGG		62
5' his-ad junc confirm	ATGCTGCATTGCATG AAGCG		60
3' his-ad junc confirm	GGTCAGTTTACATGA GACGC		60
pRS416 F	CTCTTCGCTATTACG CCAGC		62

pRS416 R	CACTTTATGCTTCCG GCTCC		62
URA5'	AAAACTAGTACATCG TCGACACATTATCC	Green = *Spe*I; Red = *pyr-4* overlap	58
Ura5'short	AAAACTAGTCACTGC ATCGAGAGTTCGG	Green = *Spe*I; Red = *pyr-4* overlap	60
URA3'	AAAACTAGTGATCAC TAACCACTTTGACG	Green = *Spe*I; Red = *pyr-4* overlap	58
hphF2	ACATACGATTTAGGT GACACTATAGAACGC		84
hphR2	GGAGCTGACATCGAC ACCAACG		70
dc3	CTTGAAGTGGAGGTT GAACTTGGC		72
dc22	CAAGGGTCTCGAGGC TGAGGGTATC	A-G to make GLE mutant	76
DBNC-8	CGGGGTACCCCGCTC AGCTTCAGTCTGTG	Green = *Kpn*I; Red = *por* upstream UTR overlap	52
DBNC-11	TCCCCCGGGGGATTC GTCATCTTCACTATC	Green = *Xma*I; Red = *por* downstream UTR overlap	50
por-ad3A 5'	CGAACGACAAGTGA AACAACC	porin - 216 bps downstream of DBNC-8	62
por-ad3A 3'	TATGACGGAAGGCAT GGAGG		62
ad3A-por 5'	GTAAGAACATCGAAG CAGCC		60
ad3A-por 3'	TTCACTTCATTGCAC AGCCC	porin - 269 bps upstream of DBNC-11	60

Tub-Lys5'UTR	AGCTGACATCGACAC CAACGATCTTATATC CAGATTCGTCCCTAC TACTGGGCTGCTTCC	Black = *hph* cassette overlap; Red = Tub(Bn r) overlap; NOTE: Reverse complement to *hph* overlap in primer Lys3 5 UTR F to replace *hph* with Tub	64
Tub-Lys3'UTR	CCGTCGACAGAAGAT GATATTGAAGGAGCA CTTTTTGGGCCGCCG AAAATGACCCAGAGC	Black = *hph* cassette overlap; Red = Tub(Bn r) overlap; NOTE: Reverse complement to *hph* overlap in primer Lys3 3 UTR R to replace *hph* with Tub	64
tubsm-F	GAACGTCTACTTCAA CGAGG		60
tubsm-R	TTGCGGAAGTCAGAA GCAGC		62
WS1a	CCGGCTCCAAGGCCG GTAACACCGTCGGC	Sequence to be deleted: ACCTGGAACTCCAAGAC C	
WS1b	GCCGACGGTGTTACC GGCCTTGGAGCCGG	Reverse complement of WS1a	
WS2a	CCAAGACCGGTAACA CCACCAAGTACCGCA TTGACC	Sequence to be deleted: GTCGGCCTCGAGGTCGCC	
WS2b	GGTCAATGCGGTACT TGGTGGTGTTACCGG TCTTGG	Reverse complement of WS2a	
WS3a	GCCTCGAGGTCGCC_ CCCGTCTCTTTCGTCA AGG	Sequence to be deleted: ACCAAGTACCGCATTGA C	50L 58R
WS3b	CCTTGACGAAAGAGA CGGGGGCGACCTCGA GGC	Reverse complement of WS3a	

EM1a	CTTACTACCACAAGGTC_TCCAAGGCCACCTGGAAC	sequence to be deleted: AACTCCCAGGTTGAGGCCGGC	50L 58R
EM1b	GTTCCAGGTGGCCTTGGAGACCTTGTGGTAGTAAG		
EM2a	CGCTGCCATTGCCTAC_GGCGTCACCCTCGGTG	sequence to be deleted: AATGTTCTCCTCCGTGAG	52L 56R
EM2b	CACCGAGGGTGACGCCGTAGGCAATGGCAGCG		
EM3a	CTCCGTGAGGGCGTC_TCTTTCGATACCCAGAAGC	sequence to be deleted: ACCCTCGGTGTTGGTGCC	52L 54R
EM3b	GCTTCTGGGTATCGAAAGAGACGCCCTCACGGAG		
EM4a	GGGTTTCCTCGCTGGT_GATGTCCAGAAGGCTGCC	sequence to be deleted: GCCTCCGCTGGCTAC	52L 58R
EM4b	GGCAGCCTTCTGGACATCACCAGCGAGGAAACCC		
EM5a	CCACCTCGCTGCCGGC_AACACCCCCAACAATGTCG	sequence to be deleted: ACCATCGAGGTCAAGTCC	58L 60R
EM5b	CGACATTGTTGGGGGTGTTGCCGGCAGCGAGGTGG		
EM6a	CAACACCCCCAACAATGTC_AAGTCCACACACGACAAGG	sequence to be deleted: GCCTTCAAGGTTACCGGC	58L 58R

EM6b	CCTTGTCGTGTGTGG ACTTGACATTGTTGG GGGTGTTG		
promoter region pQE9	CCCGAAAAGTGCCAC CTG		58
reverse sequencing pQE9	GTTCTGAGGTCATTA CTGG		
ad3A-5’ porKO	AGCTGACATCGACAC CAACGATCTTATATC CAGATTCGTCAGGGA ATCTTCAAGGAATCG		58
ad3A-3' porKO	CCGTCGACAGAAGAT GATATTGAAGGAGCA CTTTTTGGGCAACCT CCTGTCTGCACGCCC		66
pQE9_5'_Prom	CGCCAGGGTTTTCCC AGTCACGACGTTGTA AAACGAGGCGCGCCC GAAAAGTGCCACCTG		58
pQE9_3'_Term	GATAACAATTTCACA CAGGAAACAGCTATG ACCATGGCGCGCCTT TACGATGCCATTGGG		54
pRS416:CaUra3_5'	CGCATATGTAGTGTT GAAGAAACATGAAA TTGCCCAGTATCTGT TTAGCTTGCCTCGTC C	Black = pRS416 overlap at the URA locus; Red = Ca Ura3 5' end	62
pRS416:CaUra3_3'	TTTCTCCTTACGCATC TGTGCGGTATTTCAC ACCGCATAGCATCGA TGAATTCGAGCTCG	Black = pRS416 overlap at the URA locus; Red = Ca Ura3 3' end	60
mus51_F	ATTTCTTCGCACTGG TACTCGGACC	-1000 to mus51 ATG	76

mus51_R	CGTTGACATTGCCGTTGGCACCTCC	+1000 to mus51 TAG	80
mus52_F	TCAACGTCAGTAACGACACGATACC	-1000 to *mus-52* ATG	74
mus52_R	CTAGGTGTCTCTGCTACGATATTCC	+1000 to *mus-52* TAG	74

Table 2.3 *Plasmids created using a restriction endonuclease cleavage and ligation*

Plasmid name	**Starting Vector**	**Insert**	**Primers / Restriction Endonuclease**	**Source of Insert**
NcPprom#6	pCNS44	-1000 to -1 *N.c. por* ATG	NcPprom5' and NcPprom3'	FGSC 7255 (HV) genomic DNA
NcPprom#7	pCNS44	-1000 to -1 *N.c. por* ATG	NcPprom5' and NcPprom3'	FGSC 7255 genomic DNA
NcPprom + 1.7 kb *por*	NcPprom#7	*N.c. por* (Product of PCR 2)	(1) NcPH6b5' and NcPH6 3' (2) NcPH6a5' and NcPH6 3'	(1) pQE9 + *N.c. por cDNA* (Court lab) (2) PCR product of (1)
NcPprom + *por* cDNA#7	NcPprom#7	*N.c. por* cDNA (Product of PCR 2)	(1) NcPH6b5' and NcPH6 3' (2) NcPH6a5' and NcPH6 3'	(1) pQE9 + *N.c. por cDNA* (Court lab) (2) PCR product of (1)
pBSad3A#12	pBluescript	*N.c. ad*3A + flanks	ad3A-5’ and ad3A-3'	FGSC 9719 genomic DNA
pBSad3A#14	pBluescript	*N.c. ad*3A + flanks	ad3A-5’ and ad3A-3'	FGSC 9719 genomic DNA
Topohis3#9	TopoVector	*N.c. his*3 + flanks	His3asc5' and His3asc3'	FGSC 9719 genomic DNA
Topohis3#10	TopoVector	*N.c. his*3 + *flanks*	His3asc5' and His3asc3'	FGSC 9719 genomic DNA
pBSAD*	pBS*ad*3A#12	Converted *Nar*I to *Asc*I	N/A	N/A
pBSAD::His3	pBSAD*	*N.c. his*3 + flanks	*Asc*I	Topohis3#10
pBSTrpI#2	pBluescript	*N.c. trp*I + flanks	Trp1 5' SPE I and Trp1 3' SPE I	FGSC 9719 genomic DNA
pBSTrpI#3	pBluescript	*N.c. trp*I + flanks	Trp1 5'SpeI and Trp1 3'SpeI	FGSC 9719 genomic DNA

pBStrpI::Hyg#16	pBSTrpI#2	*hph*	hphFnarI and hphRnarI	pCNS44
puc18 + 2.5 kb por::ad3A	puc + 2.5 kb N.c. *por* (Court lab)	*N.c. ad*3A + flanks	*Apa*I	pBSad3A#12

Table 2.4 *Plasmids created using the method of homologous recombination*

Plasmid Name: lysko#17	**Starting Vector:**	pRS416
Insert	Primers	Source
*lys*3 upstream UTR (2.1 kb)	Lys3 5'UTRF and Lys3 5'UTRR	FGSC 9719 genomic DNA
*lys*3 downstream UTR (2.2 kb)	Lys3 3'UTRF and Lys3 3'UTRR	FGSC 9719 genomic DNA
hph	hphFnarI and hphRnarI	pCNS44

Plasmid Name: porko#1 & 2	**Starting Vector:**	pRS416
Insert	Primers	Source
-1000 to -320 *por* upstream UTR (715 bp)	5' Prom::pRS416 and 3' Prom::Hyg	NcPprom + 1.7 kb *por*
por downstream UTR (1.4 kb)	por3'UTRF and por3'UTRR	FGSC 9720 genomic DNA
hph	hphFnarI and hphRnarI	pCNS44

Plasmid Name: pRS416 + NcPprom::HygR ATG His6 porin	**Starting Vector:**	pRS416
Insert	Primers	Source
-1000 to -320 *por* upstream UTR (715 bp)	5' Prom::pRS416 and 3' Prom::Hyg	NcPprom + 1.7 kb *por*
-320 to + 1185 por (1.6 kb)	5' Porin::Hyg and 3' Porin::pRS416	NcPprom + 1.7 kb *por*
hph	hphFnarI and hphRnarI	pCNS44

Plasmid Name:	pRS416 C-terminal His6 VDAC	**Starting Vector:**	pRS416

Insert	Primers	Source
+1071 to +2151 *por* (1.3 kb product of cross-stitch PCR)	(1) porTAG_his6 5' and porTAG_his6 3' (2) porTerm 5' and porTerm 3' (3) porTAG_his6 5' and porTerm 3'	(1 & 2) FGSC 9720 genomic DNA (3) PCR Products of (1 & 2)
+2233 *por* downstream UTR (1.2 kb)	porTermUTR F and porTermUTR R	FGSC 9720 genomic DNA
hph	hphFnarI and hphRnarI	pCNS44

Plasmid Name:	pRS416 eGFP::VDAC #4	**Starting Vector:**	pRS416 + NcPprom::HygR ATG His6 porin (*Spe*I digested)

Insert	Primers	Source
eGFP	5'GFP:his6VDAC and 3'GFP:his6VDAC	pKT128

Plasmid Name:	pRS416 NcPprom cDNA porterm	**Starting Vector:**	pRS416

Insert	Primers	Source
por upstream UTR (1 kb)	5' Prom::pRS416 and NcPprom:cDNA 3'	FGSC 9720 genomic DNA
por downstream UTR (1.4 kb)	por3'UTRF and por3'UTRR	FGSC 9720 genomic DNA
por cDNA	5'_por_ATG and 3'_cDNA:porTerm	pQE9 + WTcDNA

Plasmid Name:	pRS416 NcPprom cDNA 3of4 porterm	**Starting Vector:**	pRS416 NcPprom cDNA porterm (*Nar*I digest)

Insert	Primers	Source
por upstream UTR + first 2/3 *por* (2.2 kb)	5' Prom::pRS416 and 3' Porin::pRS416	FGSC 9720 genomic DNA

Plasmid Name:	NcGR4-7; NcGR6; NcGR9-5; NcGR10; NcGR11; NcGR12; NcGR13-6; NcGR14-6	**Starting Vector:**	pRS416

Insert	Primers	Source
por upstream UTR (1 kb)	5' Prom::pRS416 and NcPprom:cDNA 3'	FGSC 9720 genomic DNA
por downstream UTR (1.4 kb)	por3'UTRF and por3'UTRR	FGSC 9720 genomic DNA
GR4, GR6, GR9, GR10, GR11, GR12, GR13, GR14 deletion variant *por* cDNA	5'_por_ATG and 3'_cDNA:porTerm	GR4, GR6, GR9, GR10, GR11, GR12, GR13, GR14 cDNA

Plasmid Name:	NcΔN-4	**Starting Vector:**	pRS416

Insert	Primers	Source
por upstream UTR (1 kb)	5' Prom::pRS416 and NcPprom:cDNA 3'_deltaN	FGSC 9720 genomic DNA
por downstream UTR (1.4 kb)	por3'UTRF and por3'UTRR	FGSC 9720 genomic DNA
ΔN *por* cDNA	5'_por_ATG_deltaN and 3'_cDNA:porTerm	pQE9ΔN_cDNA

Plasmid Name: NcΔC-2 **Starting Vector:** pRS416

Insert	Primers	Source
por upstream UTR (1 kb)	5' Prom::pRS416 and NcPprom:cDNA 3'	FGSC 9720 genomic DNA
por downstream UTR (1.4 kb)	por3'UTRF and por3'UTRR	FGSC 9720 genomic DNA
ΔC *por* cDNA	5'_por_ATG and 3'_cDNA:porTerm_deltaC	pQE9ΔC_cDNA

Plasmid Name: NcHygGR6; NcHygGR9; NcHygGR10; NcHygGR11 **Starting Vector:** pRS416

Insert	Primers	Source
por upstream UTR::HygR (2.5 kb)	5' Prom::pRS416 and NcPprom:cDNA 3'	pRS416 + NcPprom::HygR ATG His6 porin
por downstream UTR (1.4 kb)	por3'UTRF and por3'UTRR	FGSC 9720 genomic DNA
GR6, GR9, GR10, GR11 deletion variant *por* cDNA	5'_por_ATG and 3'_cDNA:porTerm	pQE9 +GR6, GR9, GR10, GR11 cDNA

Plasmid Name: NcHygΔN **Starting Vector:** NcΔN-4 (*Mlu*I digested)

Insert	Primers	Source
por upstream UTR::HygR (2.5 kb)	5' Prom::pRS416 and NcPprom:cDNA 3'	pRS416 + NcPprom::HygR ATG His6 porin

Plasmid Name: NcHygΔC		**Starting Vector:** NcΔC-2 (*Mlu*I digested)
Insert	Primers	Source
por upstream UTR::HygR (2.5 kb)	5' Prom::pRS416 and NcPprom:cDNA 3'	pRS416 + NcPprom::HygR ATG His6 porin

equipped with a DNA binding matrix at the bottom of the column (Qiagen, Mississauga, ON). The DNA was bound to the matrix by spinning the column in a desktop microcentrifuge at 10 000 rpm for 1 min and discarding the flow-through. When the volume of the buffer QC containing DNA solution exceeded the capacity of the column, this step was repeated until all the DNA was bound to the matrix. The column was then washed with 750 µl of buffer PE by spinning for 1 min at 10 000 rpm. All traces of buffer PE were removed from the column by spinning for 1 min at 10 000 rpm. 30 to 50 µl of sdH_2O was added to the column and incubated for 10 minutes at room temperature. DNA was eluted into a 1.5 ml mircofuge tube by spinning for 1 min at 13 000 rpm. For isolation of DNA fragments <500 bp and >4 000 bp, three volumes of isopropanol were added after solubilisation of the agarose gel fragment.

2.5 *Transformation of Saccharomyces cerevisiae S150*

1-2 ml of overnight culture of yeast strain S150 was used to inoculate 50 ml of YPD (1% yeast extract, 2% peptone, 0.1% dextrose) at an OD_{600} of 0.2 to 0.3. This was grown for about 5 hours to an OD_{600} of 1.0-1.2. Cells were collected by centrifugation at 5 000 rpm in an SS34 tube in a Sorvall RC6 Plus centrifuge for 5 min at 4^oC. Cells were resuspended with 16 ml of lithium acetate buffer (0.1M LiAc, 10 mM dithiolthreitol, 1 mM EDTA, 10 mM Tris-Cl pH 7.5) and left at room temperature for 1 hour. Cells were recollected and washed with 16 ml of cold sdH_2O. The cells were sequentially washed with decreasing amounts (16 ml and 6.5 ml) of 1M sorbitol. Finally, the cells were resuspended in 54 µl and aliquots of 40 µl were placed into 1.5 ml microfuge tubes. This process would usually yield 4-5 tubes of 1.6 x 10^8 cells per tube. Typically, 2-4 linear DNA fragments were added to each tube in a volume no larger than 8 µl with about 1 µg

of DNA in total. The mixture was then transferred to a disposable electroporation cuvette (0.2 mm gap) and electroporated with a BIO-RAD Micropulser electroporator using the Sc2 pre-programmed settings. Immediately following the pulse, 1 ml of cold 1M sorbitol was added to the cuvette, mixed and then transferred to a fresh tube. The tube was place in a 30^{o}C incubator for 30 min to allow the cells to recover. The cells were collected by spinning at 5 000 rpm in a desktop microcentrifuge for 4 min. The supernatant was removed and the cells were resuspended in 200 µl of 1M sorbitol and plated on two SC-Ura plates (0.167% yeast nitrogen base without amino acids; 0.5% ammonium sulphate; 4% dextrose; 0.083%, amino acid mixture -Ura mix; pH 5.6; Guthrie, 2002) and incubated at 30^{o}C for 2-3 days, until large colonies formed.

2.6 *Yeast "Smash & Grab"*

The DNA of yeast transformants, including the recently constructed plasmid, was collected using the "Smash and Grab" method (http://www.fgsc.net/neurosporaprotocols/How%20to%20create%20gene%20knockouts%20in%20Neurospora.pdf). Using a glass slide, colonies were resuspended from the transformation plates into 1-2 ml of YPD broth. 1 ml of YPD-yeast suspension was transferred to a screw-cap microfuge tube and the yeast cells were harvested with a 5 000 rpm spin at RT for 5 min. The supernatant and any cells in excess of 75 µl were removed. Yeast cells were lysed with 200 µl of Smash and Grab lysis buffer (2% Triton X-100, 1% SDS, 100 mM NaCl, 1 mM ethylenediaminetetraacetic acid), 200 µl phenol:chloroform:isoamyl (24:25:1) and 100 µl of acid washed glass beads and vigorous vortexing for 1-2 min. The mixture was separated with a 10 min, 13 000 rpm spin at 4^{o}C and 100 µl of the aqueous layer collected in a microfuge tube. The DNA was

precipitated with 10 µl of 3M NaOAc (pH 5.3) and 250 µl cold 95 % ethanol and a 5 min spin at 13 000 rpm at 4°C. The resulting pellet was washed with 500 µl of cold 70% ethanol and spun at 13 000 rpm for 5 min at 4°C. The supernatant was removed with aspiration and the DNA pellet dried next to a flame for 15 min. 30-50 µl of sdH_2O was used to resuspend the DNA. Individual plasmids were isolated by *E. coli* transformation (See section 2.7) since a variety of resulting plasmids existed.

2.7 *Transformation of E. coli*

Transformation of *E. coli* was performed using the method of $CaCl_2$ treatment or electroporation as previously described (Sambrook, 2001). Top10 cells transformed with any of the plasmids containing porin cDNA variant DNA took two days to grow at 37°C as opposed to the usual 16 hours. The plasmids were isolated from transformed *E. coli* as described in section 2.3.

2.8 *Isolation of Neurospora crassa Genomic DNA*

Neurospora crassa was grown in 20 ml of Vogel`s medium plus appropriate supplements at 30°C for 16-120 hours followed by vacuum filtration to harvest the hyphae. The resulting hyphal mat was then diced with an ethanol sterilized scalpel and transferred into four microcentrifuge tubes. The hyphal mat was then moistened with 50 µl of isolation buffer (1% N-lauroylsarcosine, 50 mM Tris-Cl pH8.0, 170 mM EDTA) and frozen at -60°C for at least 15 mins. The hyphal cell wall was disrupted with an additional 500 µl of isolation buffer, 100 µl of acid washed glass beads and vortexing for 3 min followed by 7 min in a 65°C water bath. 300 µl of 7.5 M NH_4Ac (pH 8.0) was added to each microcentrifuge tube and transferred to ice for 10 min. Cellular debris was pelleted with a 13 000 rpm spin in a desktop microcentrifuge for 10 min at 4°C. The

genomic DNA was precipitated from the resulting supernatant with 500 µl of cold isopropanol in a clean microcentrifuge tube left to stand on ice for 10 min and then a 13 000 rpm spin at 4^{o}C for 10 min was performed. The resulting pellets were resuspended with 200 µl of TE (10 mM Tris-Cl, pH 8.0, 5 mM EDTA) and 50 µl of 50 µg/ml RNase A in TE and incubated at 37^{o}C for 30-60 minutes. The 4 tubes were combined into 2 and extracted with an equal volume of phenol: chloroform: isoamyl alcohol (24:25:1). Briefly, the extraction process involved vortexing the mixture and centrifuging at 13 000 rpm for 10 min at 4^{o}C. The aqueous layer was collected and transferred to a clean microcentrifuge tube. The genomic DNA was again precipitated with 2 volumes of 95 % ethanol, 10 µl of 3 M NaAc (pH 5.3) and a 20 min spin at 13 000 rpm at 4^{o}C. The resulting DNA pellet was washed with 1 ml of 70 % ethanol and spun again at 13 000 rpm at 4^{o}C for an additional 10-20 min. The ethanol wash was removed by aspiration and the remaining pellet was dried next to a flame for 15 minutes. The genomic DNA was collected from both tubes with 10-100 µl of sdH_2O and quality and quantity assessed with agarose gel electrophoresis.

2.9 *Generation of Plasmids Used in This Study*

Plasmids constructed using the method of restriction endonuclease cleavage / ligation are listed in Table 2.3. Briefly, digests were performed using the manufacturer's (Invitrogen, Carlsbad, CA, USA; NEB, Pickering, ON, Canada) suggested protocols with 1-2 µg of DNA. Ligations were also performed as described by the manufacturer (Invitrogen) with a insert to vector ratio of 3:1. Plasmid constructs that required the insert to be PCR amplified, had both the vector and insert digested with the restriction endonucleases that corresponded to the restriction sites that were engineered into the

primers used to amplify the fragments (Table 2.2). Subcloned inserts were excised by restriction endonuclease digestion and ligated into an appropriately-digested vector as described above and listed in Table 2.3.

This classical method for creating plasmids relies on unique restriction sites for constructing complex plasmids with multiple inserts. Colot *et al.* (2006) solved this difficulty by utilizing the extremely efficient homologous recombination DNA repair system of *Saccharomyces cerevisiae* to build the plasmids. Their method requires PCR amplification of the insert using primers with 5' tails consisting of vector-specific sequence and 3' ends of gene-specific sequence. Thus, the creation of a plasmid with multiple inserts is possible by incorporating appropriate 5'tails into the primers used to amplify all DNA fragments (Figure 2.1A).

For the *por* knockout plasmid, the *por* upstream UTR was PCR amplified from plasmid NcPprom + 1.7 kbp por (Table 2.3) using the primer set 5' Prom::pRS416 and 3' Prom::Hyg and the downstream UTR was PCR amplified from genomic DNA isolated from FGSC 9720 as template using the primer set por3'UTRF and por3'UTRR. The hygromycin-resistance cassette was PCR amplified from the plasmid pCNS44 using the primer set hphFnarI and hphRnarI. The plasmid pRS416 was digested with *Xba*I and *Xho*I and gel extracted (see section 2.4) to minimize the amount of uncut plasmid being used in subsequent yeast transformations. The yeast strain S150 was then transformed (see section 2.5) with about 200-300 ng of each PCR product and 100 ng of the purified, linearized pRS416 (Figure 2.1B). The constructed plasmid was recovered from yeast transformants using a "smash and grab" (see section 2.6) and *E. coli* transformation (see

Figure 2.1 *Neurospora crassa gene knockout strategy*.

(A) The *por* knockout construct was made from four fragments of DNA including the plasmid pRS416. The linear fragments of DNA that were generated by PCR are depicted as the three rectangular boxes on the left. The two untranslated regions (UTR) up- and downstream of *por* have homology to both the hygromycin resistance cassette (green boxes) and the plasmid multiple cloning sites (MCS, red and blue boxes) utilized for directional assembly in yeast. (B) pRS416 was linearized, and along with the three other linear fragments in panel A were transformed into yeast strain S150 where recombination of the fragments occurs (top) to make the knockout construct plasmid (bottom). The linear fragment to be transformed into *Neurospora crassa* to generate the disruption was excised from this plasmid via the pair of *Pvu*II flanking the UTRs. (C) The nuclear gene encoding mitochondrial porin (*por*, purple arrow) and flanking genomic DNA sequence is represented by a black line. *N. crassa* conidia were transformed with the linear fragment described in panel B. Homologous recombination resulted in the replacement of the target gene sequence with the hygromycin resistance cassette (green box).

A

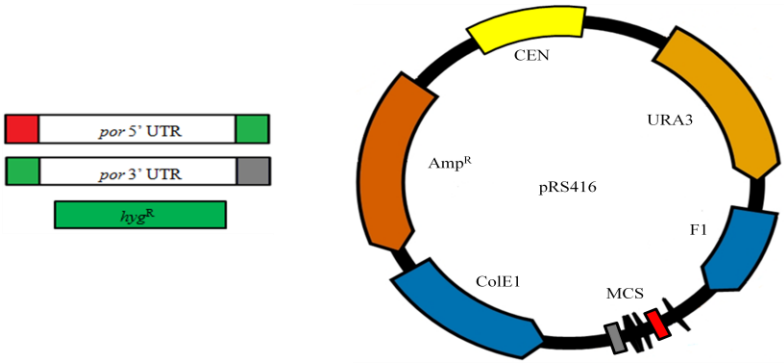
por 5' UTR
por 3' UTR
hygR
CEN
URA3
AmpR
pRS416
F1
ColE1
MCS

B

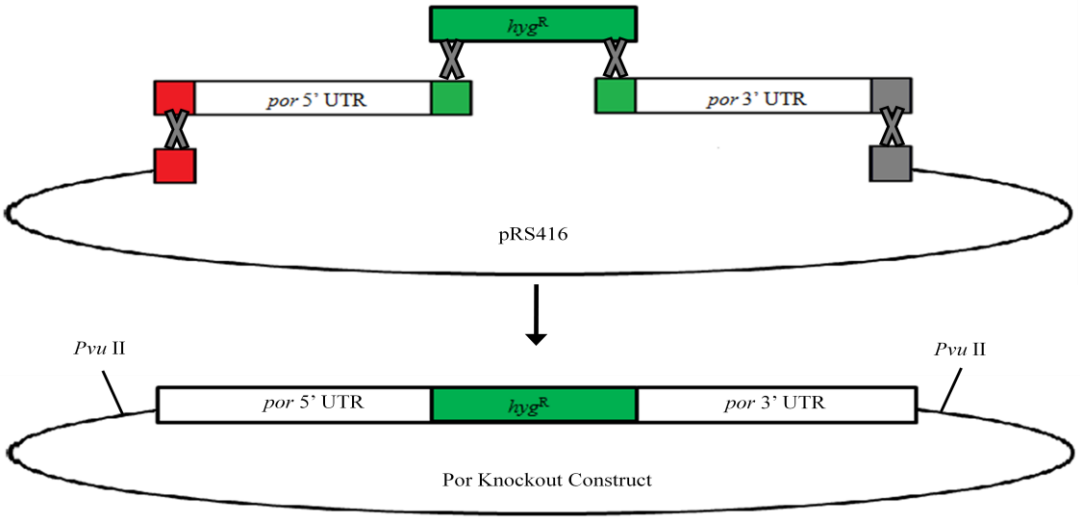
hygR
por 5' UTR
por 3' UTR
pRS416
Pvu II
Pvu II
por 5' UTR
hygR
por 3' UTR
Por Knockout Construct

C

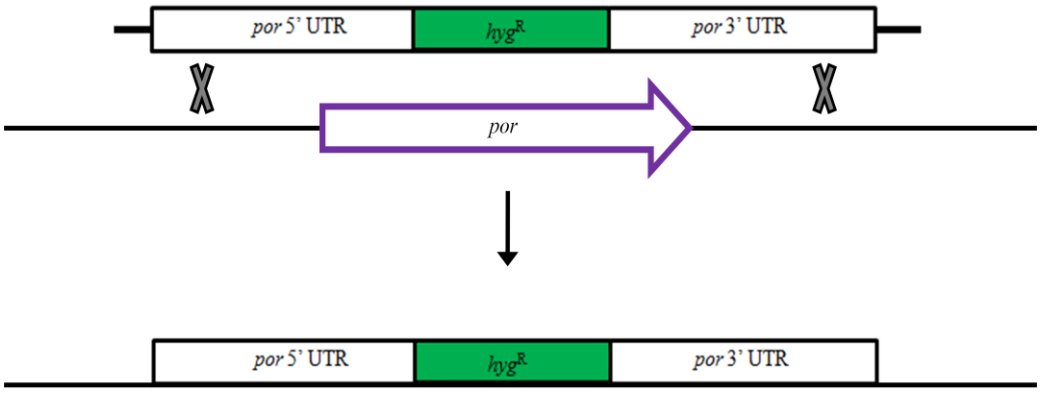
por 5' UTR
hygR
por 3' UTR
por
por 5' UTR
hygR
por 3' UTR

section 2.7). All other plasmids created using this method of yeast recombination assembly were constructed as described above using the components listed in Table 2.4.

2.10 *Transformation of Neurospora crassa Conidia*

Neurospora crassa was cultivated in 50 ml flasks containing VM media as previously described. The conidia were harvested from these conidia flasks using 50 ml sdH_2O with agitation for several minutes. The mixture was passed through a fine mesh screen to remove any hyphal fragments and increase the ratio of micro- to macro-conidia in the filtrate. Transformation of macro-conidia can lead to the production of un-intentional heterokaryons, which contain a wild-type untransformed nucleus in addition to the transformed nucleus. The conidial suspension was then centrifuged at 3800 rpm at 4^{o}C using a desktop conical centrifuge to collect the conidia. The conidia were washed three times with cold 1M sorbitol. The conidia were then resuspended in 1 ml of cold 1M sorbitol and counted using a haemocytometer. The volume of the conidia suspension was then adjusted to correct the number of conidia to 2.5 x 10^9 conidia per ml of sorbitol. 50 µl of conidia and 1 µg of DNA (1-8 µl) were transferred to a microcentrifuge tube and set on ice for 15-30 minutes before transferring to a pre-chilled 0.2 mm gapped electroporation cuvette. The mixture was electroporated using the SHS program of a BIO-RAD Micropulser (BIO-RAD, Mississauga, ON, Canada) and 1 ml of cold 1M sorbitol added to the cuvette immediately after the pulse. The 1 ml of conidia and 1M sorbitol was mixed with 9 ml of prewarmed VM medium with appropriate supplements and incubated at 30^{o}C with gentle shaking for 30-60 minutes to allow the cells to recover. When the transformational selection was hygromycin resistance, 1 ml of recovered conidia was mixed with 9 ml of top agar (VM + 1M sorbitol) + 0.4 µl / ml hygromycin

and overlaid onto a VM + sorbose + 0.4 µl / ml hygromycin plate. For transformation that used auxotrophic markers as selection (transformations which created WS001, WS111.1 and WS111.2; Table 2.1), 1 ml of recovered conidia was mixed with 99 ml of topagar + supplements and poured over 10 VM + sorbose + supplements plates. This dilution was done to minimize the possibility of germinating conidia fusing to neighbouring conidia. All of the transformation plates were incubated at 30^{o}C with the exception of the transformation plates for the complementation assay experiments (see section 2.19), which were incubated at 22^{o}C. Colonies were picked to selective VM medium slants after 5-10 days of incubation. In all cases, transformed strains were reisolated as a single colony off of a second selective VM medium plate and picked to a slant prior to further analysis. This process was repeated for as many times required to isolate a homokaryotic transformant.

2.11 *Isolation of Neurospora crassa Mitochondria*

Mitochondria were collected from cultures of *Neurospora crassa* grown in 1 l VM medium. The hyphae were filtered through a course filter paper (Fisherbrand P8 Cat no. 09-795E) with vacuum and dried under continued vacuum for 5 min. The dry weight of the culture was determined. The hyphae were removed from the filter paper and ground with a mortar and pestle on ice, with 2 ml of cold SEM buffer (250 mM sucrose, 1 mM EDTA, 9 mM 3-**[**N-Morpholino**]**-propanesulfonic acid, pH 7.5) per gram of hyphae, 6 µl of 35.5 mg/ml PMSF (phenylmethanesulfonylfluoride) per ml of SEM buffer and 1.5 grams of cold quartz sand per gram of hyphae. The hyphae were ground until no clumps remained. In cases where the weight of the hyphal mat was less than 5 grams, SEM buffer and PMSF were added to a final volume of 10 ml and 60 µl

respectively, after the grinding was completed. The mixture was then transferred to a pre-chilled SS-34 tube and spun at 4 000 rpm for 4 min at 4°C. The supernatant was transferred to a second SS-34 tube and mitochondria were pelleted with a 12 000 rpm spin at 4°C for 12 min. When mitochondria were being isolated with the intent of assaying for ATP concentrations, the supernatant was collected and kept on ice, otherwise it was just discarded. The mitochondrial pellet was washed with 10 ml of cold SEM buffer and processed with the same differential centrifugation described above. The mitochondrial pellet of the second high speed centrifugation was resuspended with 300-700 µl of SEM buffer depending on the size of the pellet and the mitochondrial protein concentration was determined using a Bradford assay (Sigma, St. Louis, MO, USA).

2.12 *in situ Fluorescent Staining of Mitochondria*

Neurospora crassa cultures were grown in 20 ml of Vogel's medium at either 22°C or 30°C. 1 ml of medium plus hyphae were transferred to a microcentrifuge tube and incubated at growth temperature with 0.5 µl of Mitotracker Green FM (Invitrogen, 1 µg/ml in DMSO) for 30 minutes. MitoTracker Green FM has negligible fluorescence in aqueous environments, requiring its accumulation in the membrane to activate its bright green fluorescence. This should allow for immediate visualization of the stained cells with minimal background fluorescence. To optimise the contrast however, the stained hyphae collected by centrifugation at 6 000 rpm for 2 min and washed with 1 ml sdH_2O. The mycelia were again harvested and resuspended in 1 ml 1% low temperature gelling agarose (Nusieve GTG agarose, Courtesy of Dr. Hausner). 5 x 10 µl of this mixture was applied to 5 microscope slides and covered with coverslips. The coverslips were sealed on all four edges to prevent dehydration of the agarose during viewing. Images of hyphal

tips and distal hyphal tubes were taken using differential phase contrast (DIC) and fluorescence microscopy using a Ziess Axio Imager Z1 at a magnification of 1000 X with the appropriate filters.

2.13 *Collecting Cytochrome Spectra of Isolated Mitochondria*

Isolated mitochondria were diluted in SEM to a concentration of 4.5-6 mg / ml and equilibrated to room temperature. 500 µl of each mitochondrial sample was transferred to a fresh microcentrifuge tube and solubilised with 10 ±0.3 mg of deoxycholic acid (DOC, final concentration 2% ($^{w}/_{v}$)) and centrifuged at 13 000 rpm for 5 minutes to remove any insoluble debris. The supernatant was collected in a fresh microcentrifuge tube ready for spectra collection. One large grain of potassium ferricyanide was added and mixed by inverting 5 or 6 times to oxidise all the cytochromes. The absorbance was collected from 500-650 nm using a 500 µl quartz cuvette with a 1-cm path length, and used as a baseline for calculations. The cytochromes were then completely reduced with the addition of a spatula tip full of sodium dithionite, mixed within the microcentrifuge tube prior to being returned to the quartz cuvette. The absorbance again was collected from 500-650 nm and subtracted from the baseline. This spectrum is the equivalent to the difference spectrum, which is simply the reduced spectrum minus the oxidised spectrum, reported elsewhere (Bertrand and Pittenger, 1969).

2.14 *Analysis of ATP Levels of Isolated Mitochondria and Neurospora crassa Cytoplasm*

The concentration of ATP present within isolated mitochondria and the cytoplasm of the *Neurospora crassa* in which the mitochondria were isolated from was deteremined

using the Bac Titer-Glo assay kit (Promega, Madison, WI, USA) adapted for mitochondria. Briefly, the assay generates light by the mono-oxygenation of luciferine by luciferase in an ATP dependent manner. The kit's single reagent contains the required Mg^{2+} and a proprietary formulation for extracting ATP from bacteria, in addition to the beetle luciferine and firefly luciferase. It was assumed that at the concentration of mitochondria tested, the reagent would extract the ATP from the mitochondria similarly to bacteria.

The mycelium of 74A and FGSC 9718 were cultivated in 1 l of VM media at both 22^{o}C for 16-17 hrs and 30^{o}C for 24 hrs. FGSC18892 and WS004 were cultivated in 1 l of VM media at both 22^{o}C for 40 hrs and 30^{o}C for 120-144 hrs. The mitochondria from these cultures were isolated using the method given in section 2.11. The isolated mitochondria and cytoplasmic fractions were diluted to 0.23-0.4 mg / ml with sterile SEM buffer lacking EDTA. Two aliquots of 100 µl from both mitochondria and cytoplasmic fractions were placed in microcentrifuge tubes and frozen at -60^{o}C for >2 hr and < 24 hr before measuring the ATP concentrations. A third aliquot was used to determine the exact concentration using the Bradford method, after the dilutions were aliquoted and frozen. Each aliquot was measured twice and the average of the two values used in the calculations of the ATP concentration. The frozen aliquots were mixed with 100 µl of Bac Titer-Glo reagent and mixed by vortex. An ATP standard curve was made using ATP diluted in sterile SEM buffer lacking EDTA at concentrations of 1 nM, 10 nM, 50 nM, 75 nM, 100 nM and 500 nM. 100 µl of each standard was also combined with 100 µl of Bac Titer-Glo reagent and mixed by vortex. From each microcentrifuge

tube, 185 µl was transferred to an opaque walled 96 well plate with transparent bottom. Luminescence was measured using a Biotek Synergy 2 microplate reader.

2.15 *Assay for the Expression of an Alternative Oxidase*

Alternative oxidase is not usually observed in wild-type *Neurospora*, but is induced in strains with mitochondrial defects (Lambowitz and Slayman, 1971). To test for the expression of an alternative oxidase in the porin knockout strains (WS004 and FGSC 18892) which is not usually observed in wild type strains, 20 ml of VM media were inoculated with conidia of each strain. 74A, FGSC 987 and FGSC 9718 were grown for 14 hours at 30^{o}C and for 18 hours at 22^{o}C. WS004 and FGSC 18892 were grown for 24 hours at 30^{o}C and 72 hours at 22^{o}C. 1.8 ml of sample was transferred to the O_2 chamber and aerated with atmospheric air using a disposable Pasteur pipette for 2 minute before taking all measurements of rate of O_2 consumption. The oxygen electrode chamber was warmed to the growth temperature used to cultivate the mycelium being examined to prevent any changes in respiration before measurements could be taken. The measured rate of oxygen consumption is relative to both the efficiency of respiration and the amount of biomass used during the assay. Therefore, the absolute rate of oxygen consumption was not considered. Measurements were taken for at least 5 min allowing for the production of a constant slope before the monitoring of the rate was paused. The sample was re-aerated as above and O_2 consumption monitoring was continued. Once the rate of consumption was again constant for about 1 min, 50 µl of KCN solution (10 mM Tris-Cl pH 7.2, 5 mM EDTA; 0.1 M KCN added immediately before use) was added. Any samples which showed no change in slope with the addition of KCN after an additional 30 seconds, had 50 µl of SHAM (0.25 M salicylhydroxamic acid in 95%

ethanol, made immediately before use) added and measurements were collected for an additional 2-3 minutes.

2.16 *Sucrose Gradient Purification of Mitochondria for iTRAQ Labelling*

Mitochondria preparations for iTRAQ labelling experiments were isolated as in section 2.7 with the exception of the final pellet having been resuspended in 100-200 µl. The mitochondria were further purified using a discontinuous sucrose gradient centrifugation. A sucrose gradient of 65%, 55%, and 45% was layered into a 3.5 ml ultracentrifuge tube. 2-3 ml of 65% sucrose was mixed with the 100-200 µl and divided into 2 ultracentrifuge tubes. 1.5 ml of 55% sucrose was carefully layered over the 65% sucrose + mitochondria. The remaining volume of the tube was filled with 45% sucrose. The sucrose gradient was centrifuged at 47 000 rpm at 4^{o}C for 1 hr. During this spin the mitochondria would float up the sucrose gradient and settle at the 45-55 % interface. A 500 µl aliquot from each ultracentrifuge tube was collected and mixed with 1 ml of SEM buffer lacking EDTA. The mitochondria were recollected with a 20 min spin at 13 000 rpm at 4^{o}C. The resulting pellet was solubilised with 700-1500 µl of mitochondrial solubilisation buffer (10 mM Tris-Cl, pH 7.4, 3 mM $CaCl_2$, 2 mM $MgCl_2$; on the day used, NP40 was added to a final concentration of 0.1% ($^{v}/_{v}$)) and subjected to 1 min of sonication with a GE Sonicator, set to 30% and on ice. The solution was put on ice for 30 min and mixed by vortex every 10 min (5 repeats in total). Any insolubles were removed with a 30 min spin at 13 000 rpm at 4^{o}C. The supernatant was collected, quantitated with a Bradford assay, and stored at -60^{o}C. iTRAQ analysis was carried out at the Manitoba Centre for Proteomics and Systems Biology.

2.17 *Expression of an N- or C-terminal His_6- tagged Porin in Neurospora crassa*

The DNA constructs used to create both, the N- or C- terminal His_6-tagged porin mutants, contained the endogenous *por* up and downstream UTRs and the modified gene for porin, and were constructed using the components listed in Table 2.4 as described in section 2.9.

The N-terminal His_6-porin mutant strains were created using the 3380-bp fragment resulting from a *Pvu*II digest of pRS416 + NcPprom::HygR ATG His6 porin. Strain FGSC 9719 was transformed with 1 µg of this gel extracted DNA using the method given in section 2.10, with both the plates and top agar containing 0.4 µl / ml hygromycin. Transformed colonies were picked to VM + Hyg slants. Two isolates, WS009 and WS009.1, were analysed for the expression of the His_6-tagged porin. Western blot analysis, using a Ni-NTA conjugated HRP probe (Pierce, USA), was used to confirm the His_6-tag on the porin molecule within isolated mitochondria (see section 2.11). The blotting procedure was done in accordance with the manufacturer's suggested protocol with the exception of using 5% skim-milk in place of 1% BSA in the blocking buffer. The genomic DNA from these strains were isolated and screened by PCR to confirm the incorporation of the His_6 encoding DNA within the promoter region using the primer set NcPprom 5' and NcPprom 3'. The resulting PCT product was further confirmed by sequencing. 300 µg of isolated mitochondria from both WS009 and WS009.1 were solubilised with 1 ml Buffer B (100 mM NaH_2PO_4, 10 mM Tris-Cl pH 8.0, 8 M urea, Qiagen Qiaexpressionist, March 2001) in a microcentrifuge tube. The insoluble debris was removed by centrifugation at 13 000 rpm for 20 min. The supernatant was combined with 50 µl of a Ni-NTA superflow slurry (Qiagen,

Mississauga, ON, Canada) in a fresh tube and mixed on an orbital shaker at RT for 1 hour. The resin was pelleted by centrifugation at 13 000 rpm for 1 min and the supernatant removed. The resin was washed 4 times with 1 ml of Buffer C (100 mM NaH_2PO_4, 10 mM Tris-Cl pH 6.3, 8 M urea). The histidine rich proteins bound to the Ni-NTA resin were eluted with 25 µl Buffer C + 0.1 M EDTA. The elutions were analysis by SDS-PAGE. WS009 and WS009.1 were subcultured through three rounds of VM + Hyg plates and slants.

The C-terminal His_6-porin mutant strains were created as described above for the N-terminal strains with the exception that conidia from FGSC 9718 and WS120 were transformed instead of that of FGSC 9719. One isolate from the transformation of FGSC 9718 conidia (WS005) was screened by PCR with isolated genomic DNA and primer set 5' Prom::pRS416 and porTerm 3'. 7 µl of the PCR reaction was digested with *Sna*BI and 7 µl was digested with *Spe*I to confirm the successful integration of the His_6-tag . 30 µl of this PCR reaction was precipitated with 2.5 volumes of 95% EtOH and 5 µl of 3 M NaAc, pH 5.3 in a -20^{o}C freezer overnight. The DNA was then precipitated with a 20 min 13 000 rpm spin at 4^{o}C and washed with 100 µl of 70% EtOH. The DNA pellet was resuspended in 5 µl of sdH_2O and 1 µl was used in each sequencing reaction (see section 2.22). The growth rate of WS005 was measured using the race tube method (see section 2.1). His_6-tagged porin was purified from isolated mitochondria using 8 M urea and Ni-NTA superflow (Qiagen) as described above. The purified protein was analysed by SDS-PAGE and Western blotting using the Ni-NTA HRP conjugate probe described above. Initial attempts were made to extract His_6-tagged porin from WS005 using non-denaturing conditions. Mitochondria were isolated as described in section 2.11. The

mitochondria were collected by centrifugation at 13 000 rpm at 4^{o}C for 20 minutes in a microcentrifuge tube and the supernatant removed by aspiration. The mitochondria were solubilised with 1 ml of 2% digitonin containing lysis buffer (20 mM Tris-Cl pH 7.4, 10% glycerol, 50 mM NaCl, 1 mM PMSF) and mixed by vortex. The insoluble debris was removed by centrifugation at 13 000 rpm for 20 minutes. The resulting supernatant was applied to a 1.5 ml Ni-NTA superflow (Qiagen) in a 5 ml column and mixed by orbital shaker for 1 hour at RT. The column flow through was collected for analysis and then the column was washed with 0.1 % digitonin wash buffer (20 mM Tris-Cl pH 7.4, 10% glycerol, 50 mM NaCl, 1 mM PMSF) with increasing concentrations of imidazole (10 mM and 30 mM). Aliquots of every wash flow through were also collected for subsequent analysis. Finally, the column was eluted with 0.1 % digitonin wash buffer with 250 mM imidazole. The samples collected were analysed by SDS-PAGE and quantified using absorbance with a 1 cm quartz cuvette and Beers Law ($A = \varepsilon cl$; where A = absorbance at 280 nm, ε = extinction coefficient of 22900 cm^{-1} M^{-1}, c = concentration in moles / litre, l = pathlength in cm). The concentration was determined to be 16.5 µM or 0.5 mg / ml using the molecular weight of 30894 g / mol. The extinction coefficients and molecular weight were calculated using an online calculator (http://www.basic.northwestern.edu/biotools/proteincalc.html).

Two isolates from the transformation of the heterokaryon WS120 with the gene for C-terminally-tagged porin, namely WS124.4 and WS124.5, were crossed as females with FGSC 9718 as previously described (Davis and De Serres, 1970), to generate homokaryotic progeny. The ascospores were plated on both VM + Hyg + Ade and VM + Hyg + His, and colonies were picked to VM media slants with the same supplements

combinations. These cultures were subcultured to VM slants lacking the supplement they were initially plated on to test for prototrophs. The incorporation of the His_6 coding sequence onto the 3' end of *por* was screened with PCR. The primer set 5' Prom::pRS416 and porTerm 3' was used to generate a 3190 bp DNA fragment. 3 µl of this PCR reaction was used in a digestion reaction with *Sna*BI according to manufacturer's instructions to confirm the His_6 coding sequence was present.

2.18 *Expression of an N- terminal eGFP:Porin fusion in Neurospora crassa*

An N-terminal eGFP:porin fusion protein was created by the expression of the contents of plasmid pRS416 + eGFP::VDAC in *Neurospora crassa*. Plasmid pRS416 + eGFP::VDAC was created using the components listed in Table 2.4 and assembled as described in section 2.9. The linear fragment used for the transformation was removed from the plasmid with a double digest using both *Pvu*II and *Eco*RV. The 4583-bp fragment was gel extracted. Conidia of FGSC 9718 and WS120 were transformed with 1 µg of DNA as described in section 2.10. The plates and top agar used were VM + Hyg medium and incubated at 30^{o}C. 10 isolates of the WS 120 transformation were grown in 20 ml VM medium and analysed for green fluorescence as described in section 2.12 without the addition of MitoTracker Green FM.

2.19 *Complementation of the por $^{-}$ Phenotype*

The lack of porin causes a cold temperature sensitive phenotype which resulted in a 3 or 7 fold decrease in growth rate for FGSC 18892 and WS004 respectively (see Chapter 3.2.1). To clearly demonstrate this phenotype was in fact due to the loss of porin, a complementation experiment was performed. To complement the *por* $^{-}$ knockout, the wild type *por* locus was PCR amplified from genomic DNA isolated from

FGSC 9718. The primer set 5' prom::pRS416 and porterm 3' were used to amplify not only the gene encoding porin, but also the up and downstream UTRs. The up and downstream UTR were thought to be sufficient in size enough to ensure all regulatory factors required for efficient expression of the *por* gene were present. This DNA fragment was extracted from an agarose gel as per section 2.4. Conidia of FGSC 18892 were transformed by electroporation with 500-1000 ng of this purified DNA fragment as in section 2.10. Transformed conidia were plated on VM medium plates and incubated at 22^{o}C in the absence of any light for 3-5 days. Several colonies were picked to VM medium slants. In addition, two VM medium slants were also inoculated with FGSC 9718 and FGSC 18892 for use as positive and negative controls respectively.

Complementation with a cDNA copy of the gene was done with a similar strategy as above. The cDNA plasmid, pRS416 NcPprom cDNA porter, was created using the components listed in Table 2.4 and as described in section 2.9. The DNA fragment used for transformation was cut from this plasmid using *Pvu* II and purified as in section 2.4. Transformation of FGSC 18892 conidia was done as previously described and strong growth following incubation at 22^{o}C was used as selection. Isolates picked from the transformation plates were screen with PCR using isolated genomic DNA from each strain as described in section 2.8, and the primer set 5' prom::pRS416 and porterm 3'.

A chimera of genomic DNA and cDNA was created and also used to test for complementation. The plasmid was constructed of genomic DNA *por* sequence containing the first 3 intron and then joined to cDNA sequence, resulting in the loss of the fourth intron. The components used to construct pRS416 NcPprom cDNA 3of4 porterm are also listed in Table 2.4 and assembled as described in section 2.9. This plasmid was

double digested with both *Pvu*II and *Eco*RV and electrophoresed in a 0.8% agarose gel. The resulting 4188-bp fragment was gel extracted and then used to transform FGSC 18892 as described above.

2.20 *Complementation Assay with Porin Deletion Variants Using Hygromycin as Selection*

Isolation of *Neurospora crassa* strains expressing cDNA deletion variants tested with the complementation assay described in section 2.19 was done using hygromycin resistance as a transformation selection. The plasmid constructs for the cDNA variants for expression in *N. crassa* with hygromycin resistance added into the 5' UTR were constructed according to the method described in section 2.9. The components of the plasmids: NcHygGR6, NcHygGR9, NcHygGR10, NcHygGR11, NcHygΔN and NcHygΔC are listed in Table 2.4. The transformation of FGSC 9718 conidia was done using 1 µg of linear DNA resulting from a *Pvu*II digest and gel extraction. Both the plates and top agar contained 0.4 µl / ml hygromycin.

2.21 *Neurospora crassa Female Sterility Assay*

Female sterility of *Neurospora crassa* strains was assessed on the strains ability to produce protoperithecia when inoculated onto Westergaards slants and grown at 23-24^{o}C under continual light (Davis and De Serres, 1970). The slants of the mutant strains were compared to a wild type control slant after 7-8 days of incubation and again after 3 weeks. In some cases, the hyphae on the slants were gently wiped over with a cotton tipped applicator dipped in a conidia / sdH_2O suspension to confirm either the presence or lack of protoperithecia by looking for evidence of fertilization. The conidia used to make the sdH_2O suspension were of the opposite mating type.

2.22 *DNA Sequencing*

DNA sequencing was either performed here at the University of Manitoba or at the University of Calgary. DNA template for in house sequencing was prepared as described in section 2.3 for plasmid template or 2.4 for PCR amplified fragments. Cycle sequencing was performed using the BigDye Terminator version 3.1 (Applied Biosystems, Foster City, California) with modifications. The reaction mixture contained, 560 ng of template DNA, 0.75 µl of a sequencing primer at 3.2 pmol / µl, 2.25 µl of the Big-Dye buffer, 1.5 µl of Big-Dye, and filled to 15 µl with sdH_2O. The cycle sequencing reaction was carried out in a Thermocycler using the program suggested by the manufacturer. The reaction was stopped with 5 µl of sdH_2O, 5.6 µl of 125 mM EDTA, 71 µl of 95% ethanol. This was mixed and left at RT for 10 min. The DNA was precipitated with a 15 min spin of 13 000 rpm at 4^{o}C. The supernatant was removed by aspiration and the DNA washed with 70% ethanol, and spun again for 15 min at 13 000 rpm at 4^{o}C. The supernatant was again removed by aspiration and the pellet dried next to a flame. The dried DNA pellets were either stored at -20^{o}C to be processed at a later time or immediately resuspended with 15 µl of formamide. The DNA was denatured by heating to 95^{o}C for 5 min, and snap cooled on ice to maintain single-stranded DNA fragments. Sequences were collected in house using an ABI Prism® 3130 Genetic Analyzer (Applied Biosystems, Foster City, California).

2.23 *Standard Lab Techniques*

Agarose gel electrophoresis, western blotting, SDS-PAGE, PCR, mini-plasmid preparations, and other general molecular biology procedures were carried out essentially as described by Sambrook (2001).

Chapter 3: Results

3.1 *Construction of Porin Knock-out strain of Neurospora crassa*

3.1.1 *Investigation of the Function of the N. crassa Mitochondrial Porin*

The understanding of the role of porin in the outer membrane remains incomplete. The most agreed upon function for porin is the translocation of mitochondrial substrates and products across the MOM. Additional functions have been reported to include: interactions with other proteins such as hexokinase (Abu-Hamad et al., 2008), anti- and proapoptotic protein family members (Roman et al., 2006) and cytochrome c oxidase (Roman et al., 2005) and enzymatic functions such as NADH:ferricyanide reductase activity for porin found in the cytoplasmic membrane (Baker et al., 2004). Studies of mitochondrial porin have been performed both *in vitro* and *in vivo*. The *in vitro* studies offer evidence for pore-forming ability, pore size, voltage-dependant gating and ion selectivity. Many different structural models for porin have been devised from such works. However, *in situ* testing of the models, which included the high resolution structures presented in 2008, has created some controversy (see section 1.3; Colombini 2009). Most notably, the question of whether or not the high resolution structure accurately represents a physiologically relevant structure remains. In spite of these issues, to further understand the role of porin in the outer membrane of mitochondria, *in vivo* studies are of the utmost importance.

3.1.2 *Site-directed Disruption of por with the ad-3A Gene*

Site-directed mutations of the *Neurospora crassa* genome is a relatively new development in the arsenal of genetic techniques available for working with this fungus. A protocol developed by Colot et al., (2006) makes use of the increased frequency of homologous recombination (HR) in strains deficient in either *mus-51 or mus-52*; these strains are a relatively recent discovery of Ninomiya et al., (2004). The products of *mus-51* and *mus-52* show homology to KU70 and KU80 which are responsible for non-homologous end-joining (NHEJ) of DNA in humans (Ninomiya et al., 2004). NHEJ is the normal mechanism of DNA repair in *Neurospora crassa*. By making disruptions of either *mus-51* or *mus-52*, Colot et al., (2006) created four different strains with increased frequency of homologous recombination, which were submitted to the Fungal Genetic Stock Center (FGSC, Kansas City, Missouri). They were utilized in this study and are listed in Table 2.1 as FGSC 9717, FGSC 9718, FGSC 9719 and FGSC 9720. The increased frequency of HR allows for the integration of a linear DNA construct consisting of a drug resistance or auxotrophic marker flanked by target DNA sequence, similar to the techniques used in yeast transformations (Guthrie, 2002). Amazingly, the yeast HR repair system requires only 30 bp for homologous integration. In contrast, Ninomiya et al., (2004) showed that using 500 basepairs (bp) of homologous sequence was required for homologous integration 91% and 93% of the time when *mus-51* or *mus-52* strains respectively, were transformed. This percentage could be increased to 100% when either strain was transformed with DNA containing flanking sequences of 1000 bp.

The first approach to creating a por knockout was attempted by an insertion of an *ad-3*A gene into the porin locus. For site-directed mutations using the *ad-3*A gene,

Neurospora crassa strain FGSC 9720 (*mus-51*::*bar*$^{+}$; *his-3*) was utilized (Table 2.1). The strategy for the disruption of *por* was set up to be a two-step process. Due to technical errors in the strategy design, the *por* disruption resulted in a possible chimera of porin and translated *ad-3*A sequence. Complete details of the attempts are described in Appendix 5.1. First, WS001 was created by transforming conidia of FGSC 9720 into an adenine auxotroph using a cassette for histidine biosynthesis flanked with *ad-3*A sequence (Table 2.1). A mutation in the adenine biosynthetic pathway at *ad-3*A results in a build up of the intermediate, 5'-phosphoribosyl-4-carboxy-5-aminoimidazole (CAIR). Accumulation of CAIR results in the usual orange pigmentation observed during conidiation being replaced with purple. Secondly, a *por* disruption was created by transformation with a linear DNA fragment containing the *ad-3*A locus flanked with *por* sequence (*por* disruption cassette). Restoration of the strain's ability to produce adenine results in the pigmentation returning from purple to its original orange color during conidiation. Therefore, transformational selection was both growth on adenine free media and orange color. No ade^{+} transformants were recovered either due to a failed transformation experiment or the fact that *por* is an essential gene. Therefore the strategy was modified taking into account the possibility that porin is essential.

A heterokaryon can be employed to shelter a lethal gene disruption, and is created by allowing hyphal anastomosis to occur between two different strains. Therefore, two double mutants of *ad-3*A / *lys-3* (WS002.3) and *ad-3*A / *trp-1* (WS003.1) were constructed (Table 2.1). Subsequently, both strains were inoculated into a single slant lacking lysine and tryptophan and growth was the result of the fusion of hyphal tips of neighbouring germinating conidia, producing the desired heterokaryon (WS110). The

heterokaryon was transformed with the *por* disruption cassette described above. From this transformation, ade^{+} colonies were isolated. Western blot analysis of isolated mitochondria from one isolate with an antibody for the N-terminus of porin not only identified porin, but also several peptides of smaller size. These peptides could be porin / *ad-3*A sequence chimeras because the *por*::*ad-3*A disruption resulted in an open reading frame that could encode a chimera of porin and translated *ad-3*A sequence (see appendix 5.1 for complete details). Because the expression of this chimera could be toxic, a strategy to generate a complete knockout of *por* was devised.

3.1.3 *Construction of the por Knockout Neurospora crassa strain WS004*

To ensure no expression of porin from the *por* locus, both the promoter and the gene were targeted for replacement with a Hygromycin B resistance cassette. A detailed description of the protocol is given in section 2.9 and diagrammed in Figure 2.1. Briefly, the linear fragment of DNA used to transform conidia was engineered to contain the hygromycin-resistance cassette from pCNS44 (Staben et al., 1989), flanked by up-and downstream *por* sequence. The upstream fragment consisted of the sequence from position -320 to -1020 relative to the translation start site, to include any putative promoter for *por* in the replacement. The downstream DNA consisted of 1407 bp starting 6 bp after the stop codon for *por*. The Hygromycin B resistance cassette consisted of the *hph* gene from *E. coli*, which confers the resistance; its expression in *Neurospora crassa* is driven by the *trp*C promoter and terminator from *Aspergillus nidulans* present in the construct.

Given that the results described above maybe suggest that porin is essential, both a homokaryotic strain, FGSC 9718 (transformation 1), and a heterokaryotic strain WS120

(transformation 2; Table 2.1) were transformed with the knockout construct. Transformants of WS120 were picked as colonies that grew on VM medium + hygromycin plates after 3 days of incubation at 30^{o}C and were designated WS120porko 1-10. The transformation of FGSC 9718 however, produced smaller, slower growing colonies that were also picked to VM medium + hygromycin slants after 3 days of incubation at 30^{o}C, and labelled porko 1-10. They took 3 days longer than the WS120porko 1-10 strains to reach the top of the slants. The first five isolates of transformation 1 were replated onto VM + hyg plates to ensure hygromycin-resistance. After 7 days of incubation, plate 1 had 2 colonies, plate 2 had 7 colonies and the other three plates were empty. One isolate from each plate was picked for further analysis. Isolates were screened for the successful replacement of *por* by PCR using the primer set 5'_prom::pRS416 and porTermUTR R to amplify the porin locus. As a control, genomic DNA of FGSC 9718 was used as PCR template with the above mentioned primers; a 4371-bp fragment of DNA consisting of the wild-type *por* gene flanked by UTR sequence was produced. One transformational isolate grew particularly slowly and was screened for the replacement of *por* with *hph* by PCR; a 3796-bp fragment was produced, which corresponded to the expected size for a successful replacement (Figure 3.1). The lack of a wild-type sized fragment in addition to the *hph* replacement product indicated the isolate was a homokaryon. This strain was named WS004 and served as evidence that porin is non-essential. Nothing further was done with the isolates of transformation 2, which were stored for future analysis.

A *por* knockout was also independently constructed through the efforts of the *Neurospora crassa* genome knockout project around the same time WS004 was created

Figure 3.1 *PCR screening of the por locus in the por ⁻ strains.*

The *por* locus was PCR amplified from isolated genomic DNA of FGSC 9718 (lane 2), WS004 (lane 4) and FGSC 18892 (lane 5). Amplification of the wild-type locus results in a 4371-bp fragment. Amplification of the *por* locus containing the *hph* cassette is expected to be 3796-bp and 3391-bp for WS004 and FGSC 18892 respectively. The 2.5 kb fragment indicated by the arrow, is a non-specific priming product.

A

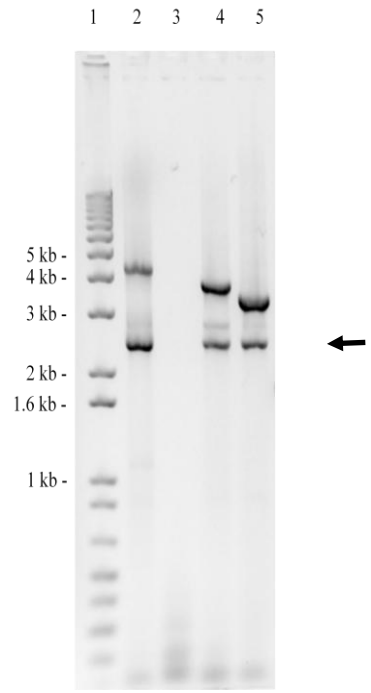

(http://www.dartmouth.edu/~neurosporagenome/index.html). This strain (FGSC 18892; Table 2.1) was obtained from the Fungal Genetic Stock Center and analysed in parallel to WS004. The endogenous porin locus of FGSC 18892 was also screened with PCR using the same primer set as was used for WS004 (Figure 3.1). FGSC 18892 differed somewhat from WS004 in its construction. WS004 is isogenic to its parent strain FGSC 9718 whereas FGSC 18892 was isolated as a hygromycin-resistant isolate from a transformation of a *mus-51/52*::*bar*$^{+}$ (*bar* confers resistance to basta) parent. This isolate was then sexually crossed with a wild-type strain and a hygromycin-resistant, basta-sensitive progeny was picked as FGSC 18892.

3.1.4 *Southern hybridization analysis of the por ˉ strains.*

The successful replacement of *por* with *hph* was analysed by Southern hybridization analysis. Genomic DNA was isolated from FGSC 9718, FGSC 18892 and WS004 and separately digested with *Pst*I to produce a 3.0-kb fragment of endogenous *por* sequence (Figure 3.2A). The genomic DNA of the three strains was also digested with *Apa*I to produce a 912-bp fragment which is internal to the *por* gene (Figure 3.2A). This was done to identify any *por* sequence that might be elsewhere in the genome not flanked by the endogenous *por* flanking UTRs. Samples of each digest were hybridized with a probe for *por* and only the genomic DNA of FGSC 9718 showed evidence of *por*, confirming the successful knockout of both *por* ˉ strains (Figure 3.2B). Un-digested genomic DNA was also hybridized with the *por* probe to assay for the existence of any extranuclear DNA elements possibly harbouring a *por* gene (Figure 3.2B, Lanes 13-15). To ensure equal amounts of genomic DNA were used, a sample of the *Apa*I digest was

Figure 3.2 *Southern hybridization analysis of the gene knockout of FGSC 18892 and WS004.*

(A) Diagram of the relevant region of the endogenous *por* gene and the homologously integrated *hph* gene. The thick lines show the up-and downstream UTRs attached to the *hph* cassette. The knockout cassette was introduced into FGSC 9718 and hygromycin-resistant transformants were isolated. (B) Results of Southern hybridization analysis. Lanes 1 and 9 contain a DNA standard and Lane 5 is empty. Lanes 1-8 and 13-15 were all hybridized with the *por* probe. Lane 2 and 6 contains a non-transformant, showing the 3 kb *Pst*I fragment (lane 2) and the 912 bp *Apa*I fragment (lane 6) of *por* respectively. Lanes 3 and 8 contain genomic DNA from WS004 digested with *Pst*I and *Apa*I respectively and Lanes 4 and 7 contain similarly digested FGSC 18892 genomic DNA. Lanes 13-15 contain un-digested DNA from FGSC 9718, FGSC 18892 and WS004 respectively. Lanes 9-12 were all hybridized with a probe for the *lys-3* upstream UTR. Lanes 10-12 contain *Apa*I digested DNA from FGSC 9718, FGSC 18892 and WS004 respectively.

A

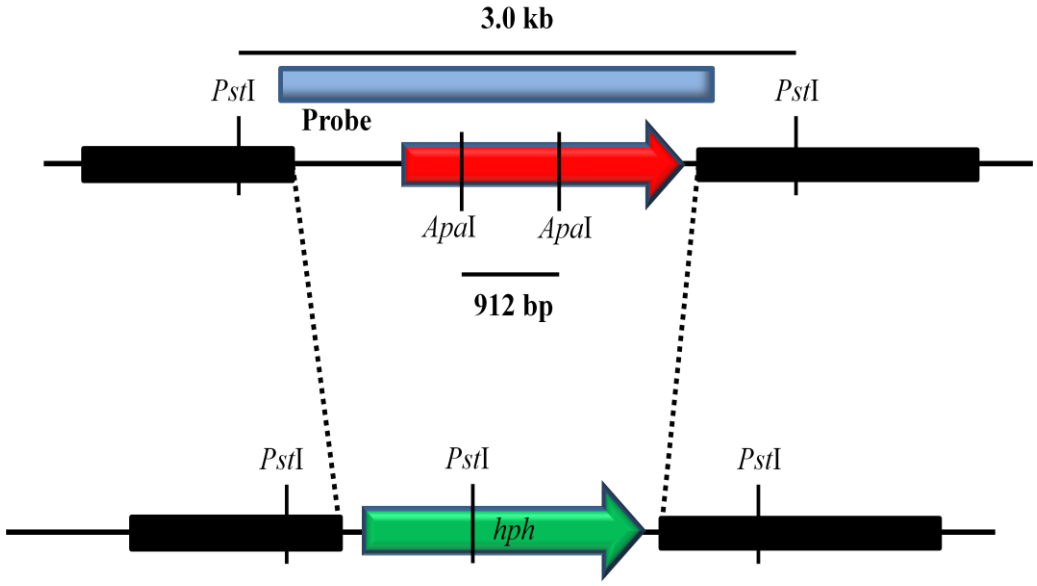
3.0 kb
PstI
Probe
PstI
ApaI
ApaI
912 bp
PstI
PstI
PstI
hph

B

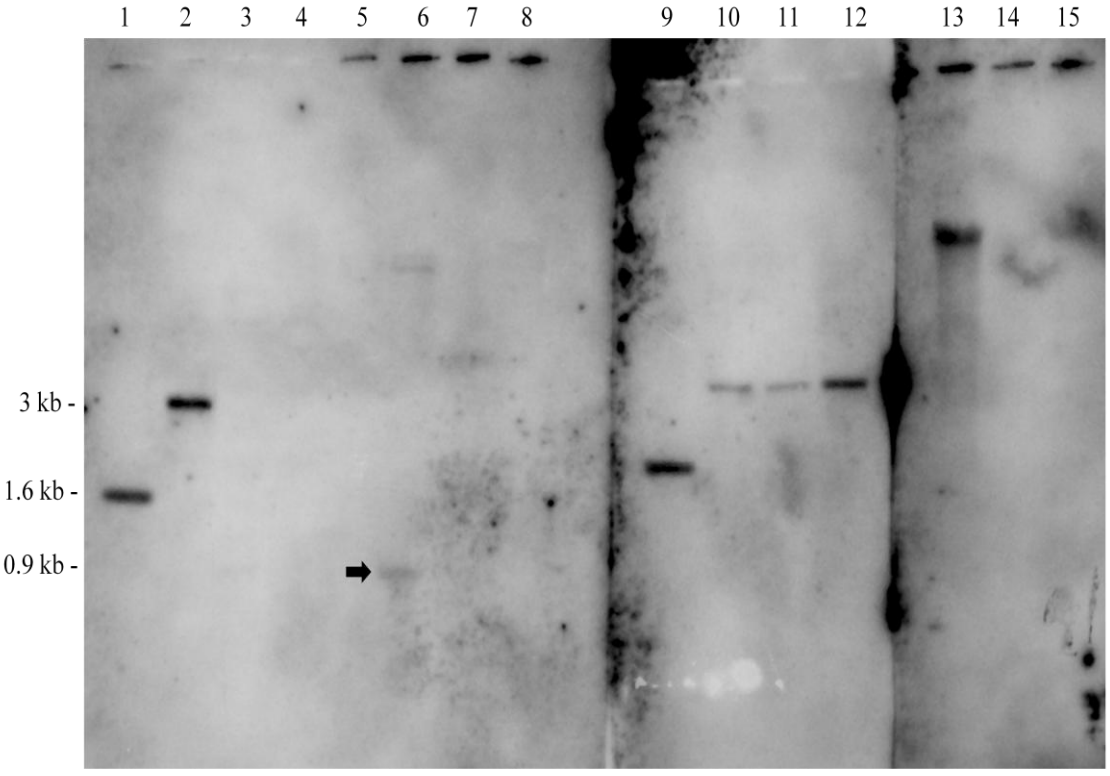
1 2 3 4 5 6 7 8 9 10 11 12 13 14 15
3 kb -
1.6 kb -
0.9 kb -

hybridized with a probe constructed of *lys-3* upstream UTR sequence. Both FGSC 18892 and WS004 DNA were used in equal (or slightly higher) amounts compared to FGSC 9718 (Figure 3.2B, Lanes 10-12).

3.2 *Characterisation of the por knock-out strains WS004 and FGSC 18892*

3.2.1 *Lack of Porin Causes Temperature Dependant Reduction in Growth Rate*

Porin is a non-essential constituent of the mitochondrial outer membrane. However, its absence is not without consequence. The growth rate for the two knock-out strains used was determined as mycelial elongation per day in glass race tubes (Figure 3.3). Race tubes of both wild type and mutant strains were incubated at $30^{o}C \pm 2^{o}C$. The growth rate of FGSC 9718 was determined to be 11.7 cm ± 0.1 cm per day (Table 3.1). The rate is reduced by approximately 65 % for the isogenic knockout strain WS004 and only 26% for FGSC 18892. This difference in growth rate was larger when the rate was measured at a reduced temperature. The growth rate of FGSC 9718 at $22^{o}C \pm 2^{o}C$ was 7.7 cm ± 0.1 cm per day, whereas the growth rate of WS004 however, was 1.1 cm ± 0.1 cm per day. This indicates a reduction in growth rate with respect to temperature of approximately 73%, whereas FGSC 9718 growth was only reduced by 34%. FGSC 18892 however, showed less dependence on temperature with a reduction in growth rate of only 62%. To confirm the wild-type nature of the parent FGSC 9718, its growth rate was compared to a standard lab strain of $74A^{d}$ later determined to have a spontaneous mutation which had altered its mitochondria`s morphology, cytochrome content and

Figure 3.3 *The apical extension growth rate of Neurospora crassa strains, FGSC 9718, WS004 and FGSC 18892*.

The apical extension growth rate of the indicated *Neurospora crassa* strains was determined using 100 cm race tubes incubated at $22^{o}C \pm 2^{o}C$ (A) and $30^{o}C \pm 2^{o}C$ (B) subjected to regular daylight cycles. Each graph is showing only one representative curve for each strain used to calculate the average growth rates seen in Table 3.1.

A

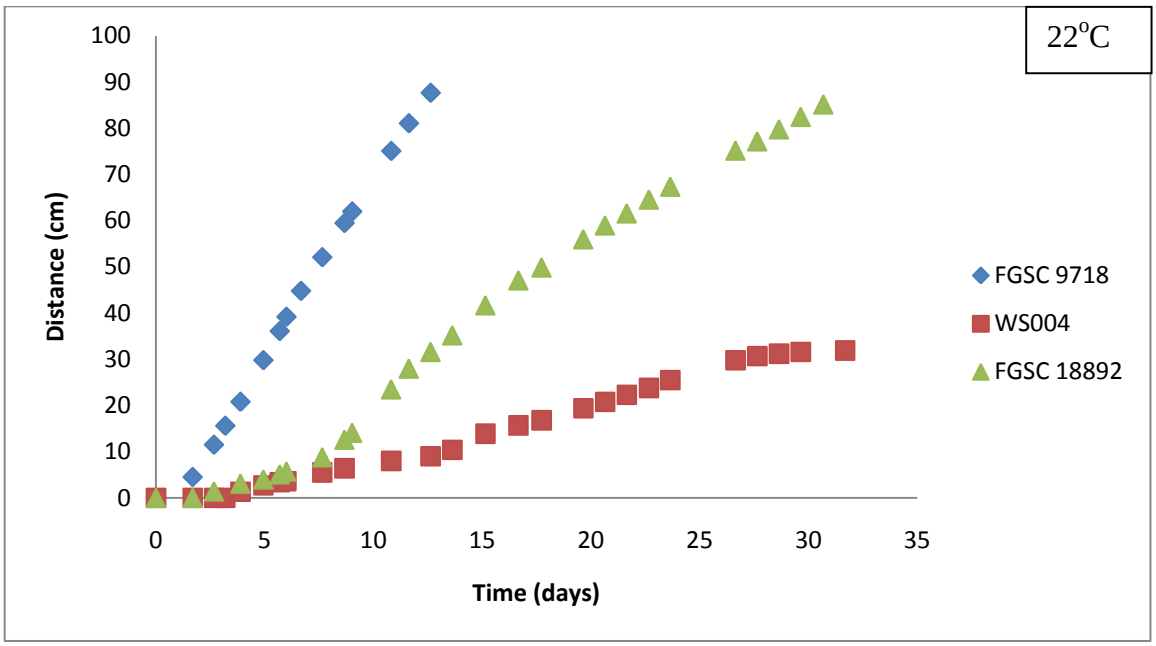
22°C
Distance (cm)
Time (days)
FGSC 9718
WS004
FGSC 18892

B

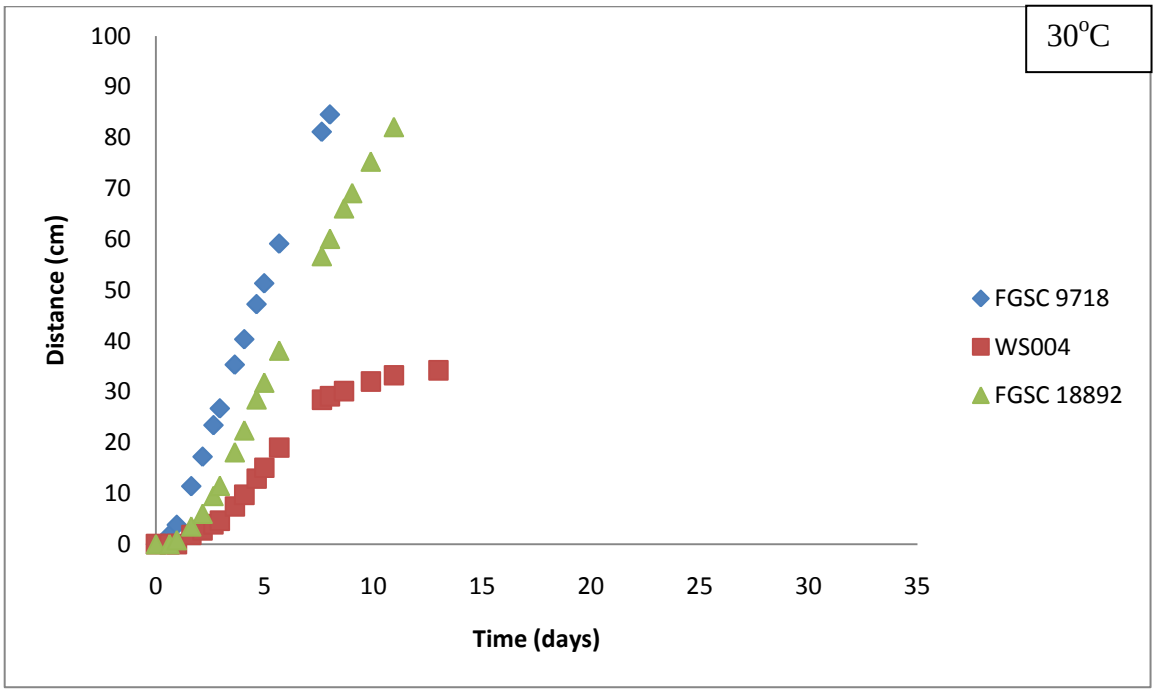
30°C
Distance (cm)
Time (days)
FGSC 9718
WS004
FGSC 18892

Table 3.1 *The average apical growth rate of Neurospora crassa strains FGSC 9718,74A[d] WS004 and FGSC 18892.*

Incubation Temperature	22 °C ± 2 °C		23.5 °C ± 2 °C		30 °C ± 2 °C	
	Average* cm / Day	% of FGSC 9718 Rate	Average cm / Day	% of FGSC 9718 Rate	Average cm / Day	% of FGSC 9718 Rate
Strain						
FGSC 9718	7.7 ± 0.1	n/a	8.6 ± 0.3	n/a	11.7 ± 0.1	n/a
74A[d]	n/d		8.5[†]			
WS004	1.1 ± 0.1	15	1.2 ± 0.8	14	4.1 ± 0.7	35
FGSC 18892	3.3 ± 0.3	42	n/d	n/d	8.7 ± 0.8	74

* Average growth rate is calculated as the average growth rate of three race tubes.

[†] Value given is from a single race tube and therefore not an average.

alternative oxidase expression (discussed further in sections 3.2.3 and 3.2.4). Interestingly, the resulting growth rates for $74A^{d}$ were essentially no different from the FGSC 9718 rate (Table 3.1). The standard growth temperature for cultivating *Neurospora crassa* cultures is $30^{o}C$ so growth was not measured at temperatures above that with race tubes, but was examined in test tube slants. VM medium slants were inoculated with conidial suspensions in sdH_2O of FGSC 9718 and FGSC 18892 and incubated at $25^{o}C$, $27^{o}C$, $30^{o}C$ and $37^{o}C$ in the dark for two days (Figure 3.4). Slants were then moved to room temperature to allow conidiation and photographed on the fourth day. The distance grown by each strain increased with increasing temperatures further suggesting a dependence on temperature. Due to the limited size of the slant, the difference in growth rates at $30^{o}C$ and $37^{o}C$ could not be quantified.

3.2.2 *Characterization of the por Knockout Strains, WS004 and FGSC 18892*

3.2.2.1 *Lack of Porin Can Cause Reduction in Aerial Hyphae Production*

The lack of porin caused many observable differences between porin-lacking and porin-containing strains. Macroscopically, aerial hyphae of wild-type strains can be observed in slants, conidia flasks and in race tubes and takes on the appearance of cotton candy. The *por* ¯strains WS004 and FGSC 18892 differed in their ability to grow vertically off of the surface of the media, with only FGSC 18892 exhibiting ability similar to wild types (Figure 3.5A). WS004 fails to grow any significant amount off the surface of the medium when any of the previously mentioned vessels are used for cultivation. This difference was most clearly observed in conidia flasks containing VM medium resulting in a lawn of growth across the surface when inoculated with WS004. It

Figure 3.4 *The loss of porin causes a temperature dependant growth defect.*
VM media slants were inoculated with conidia from FGSC 9718 (*por* $^{+}$) and FGSC 18892 (*por* $^{-}$) and incubated at the indicated temperature for 4 days in the absence of light. The growth fronts of tubes 2 and 4 are drawn with a black line and indicated by an asterisk.

A

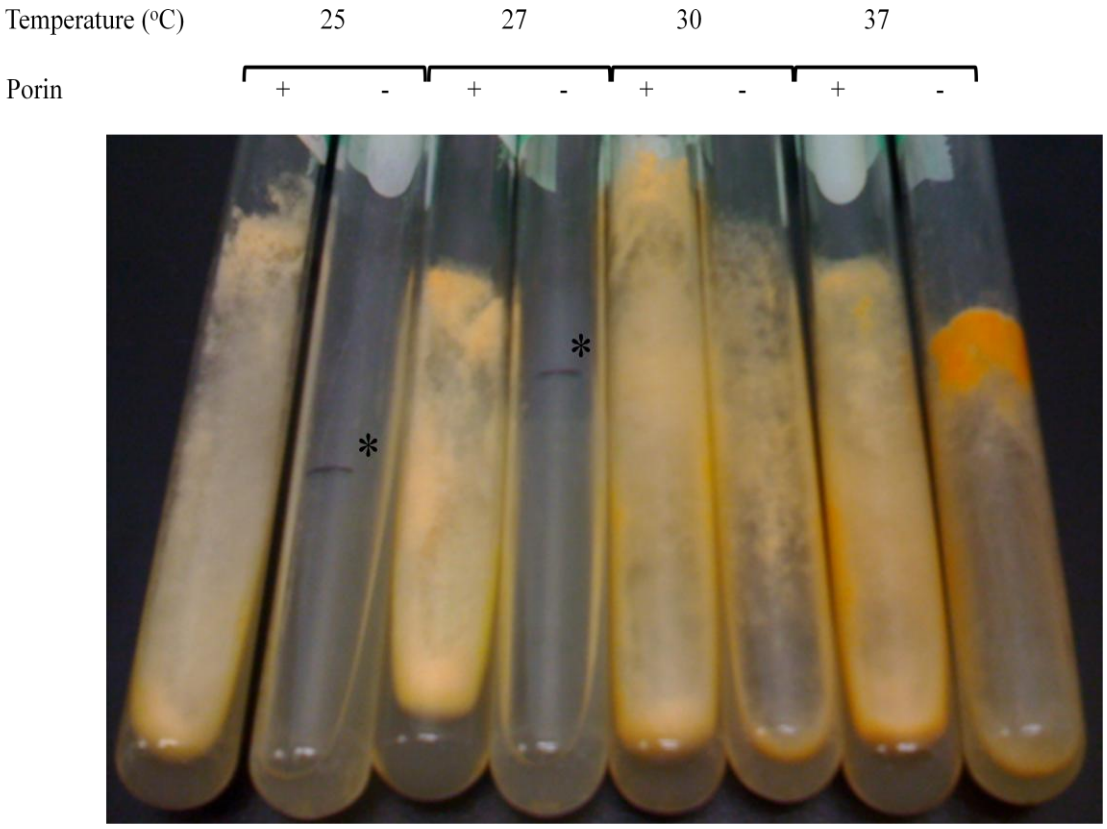

is noteworthy, that the amount of aerial growth decreases as the distance from the inoculation site increases. Thus, when a suspension of conidia was used to inoculate the conidia flask, the site of inoculation grew elevated in comparison to the rest of the lawn (Figure 3.5B). This inability to produce aerial hyphae was predicted to be in part due to a reduction in hyphal branching, since branching seemed necessary to support the weight of the culture. This was examined by inoculating the center of a VM medium + sucrose plate with a drop of water-conidia suspension of 74A^{d}, WS004 and FGSC 18892. The plates were incubated at 23^{o}C for 18 hours for 74A^{d} and 36 hours for WS004 and FGSC 18892 before photographing the growth front (Figure 3.6). The degree in branching for WS004 was reduced when compared to 74A^{d} (Figure 3.6B) and even further reduced if the growth fronts were compared after 18 hours for both strains (data not shown). This difference observed at 18 hours was believed to be a result of the reduced growth rate rather than because of the loss in development ability due to the lack of porin and therefore not considered. When FGSC 18892 grown for 30 hours was compared to 74A^{d} grown for 18 hours the amount of branching is similar (Figure 3.6C).

3.2.2.2 *Lack of Porin Can Cause a Reduction in Conidia Production*

The ability of the *por* $^{-}$ strains to produce conidia was also examined. *Neurospora crassa* produced conidia by budding of hyphal tips during nutrient limiting conditions or desiccation (Davis and De Serres, 1970) or in response to blue light (discussed in Lee et al., 2006). Therefore, the potential for conidia production is directly related to the amount of hyphal tips present at the time of conidiation. Cultivation of FGSC 18892 on VM medium resulted in the production of aerial hyphae similar to that of wild type. Consequently, the ability of FGSC 18892 to produce conidia was only slightly reduced

Figure 3.5 *Aerial hyphae production ability of the por knockout strains.*
(A) 50 ml VM media conidia flasks were inoculated with FGSC 9718, $74A^{d}$, WS004 and FGSC 18892 and incubated in the dark at 30^{o}C for 3, 3, 5 and 7 days respectively to allow for aerial hyphae production. A positive for aerial hyphae production was scored as the presence of hyphae grown up off the surface of the agar medium. (B) 50 ml VM media conidia flask inoculated with a liquid suspension of conidia showing increased growth at the site of inoculation.

A

WS004 FGSC 9718 FGSC 18892 74A^{d}

B

Figure 3.6 *Hyphal branching of Neurospora crassa strains.*

VM + sucrose plates were inoculated with $74A^{d}$ (A), WS004 (B) and FGSC 18892 (C) and incubated at $23^{o}C$ for 18 hours for $74A^{d}$ and 36 hours for WS004 and FGSC 18892. The magnification of all three images is the same.

A

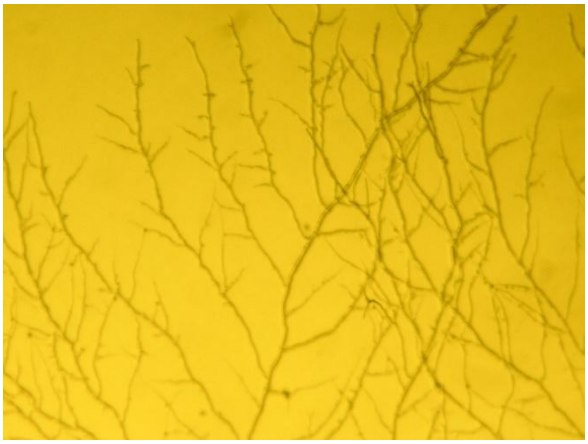

B

C

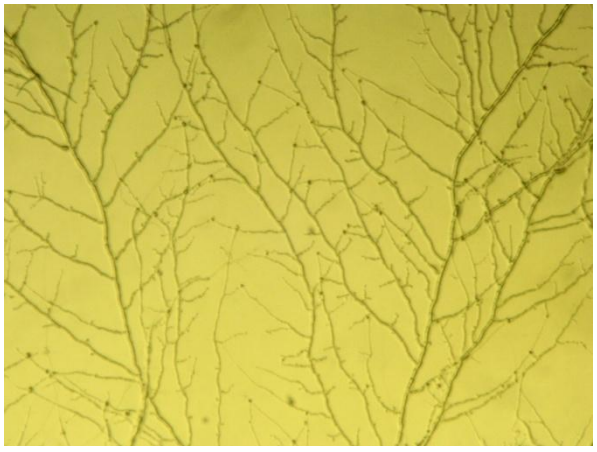

when cultivated at 30^{o}C compared to a control strain and increased when grown at 37^{o}C (Figure 3.4). FGSC 18892 was able to grow off the surface of the media, but the degree of fluffiness was less, which was expected because of reduced branching. Therefore, the reduction in fluffiness is more likely due to the advancement after 7 days to the conidiation stage of the life cycle, in spite of less hyphal growth compared to wild-type . Thus, longer incubation times did not allow for additional branching to occur with the final result appearing as a lack or reduction in aerial hyphae for WS004 and FGSC 18892 respectively. In contrast, WS004 showed a deficiency in aerial hyphae production and similarly, conidia production was also extremely reduced. Like FGSC 18892, it was observed that conidia production could be increased if the culture was incubated at 37^{o}C (data not shown). WS004 was regularly incubated at 37^{o}C to increase the yield of conidia decreasing the number of conidia flasks required for subsequent experimentation.

3.2.2.3 *Lack of Porin Alters Culture Pigmentation and Causes Hyphal Lysis*

Cultivation of FGSC 18892 resulted in the production of a colour pigmentation differing from that of wild type. Hyphae grown on solid medium appeared yellow instead of the usual orange colour once the culture was taken out of the incubator and set at room temperature to conidiate. After about 2-3 weeks, the yellowish colouring turned to a dark brown / black colour also not seen in wild type cultures grown in similar conditions (Figure 3.7A). *Neurospora crassa* is known to lyse in nutrient-deprived environments resulting in a dark discolouring of the mycelium. The lysis of FGSC 18892 then, suggests an unhealthy culture irrespective of the nutrient rich media in which it was cultivated. A discolouration was also observed when FGSC 18892 was grown in liquid VM media (Figure 3.7B). A similar result was seen for WS004 (data not shown).

Figure 3.7 *Pigmentation and lysis of the por ¯ strain FGSC 18892.*
(A) VM slants were inoculated with the indicated strains. FGSC 9718 and FGSC 987 were incubated at 30^{o}C for 3 days before being moved to room temperature to allow for conidiation. WS004 and FGSC 18892 were incubated at 37^{o}C and 30^{o}C respectively for 7 days before being moved to room temperature. The lysis of FGSC 18892 is indicated by the arrow. (B) Liquid VM media was inoculated with FGSC 9718 (Left) and FGSC 18892 (Right) and incubated at 30^{o}C for 16 and 24 hours respectively before being photographed. (C) The mitochondria from FGSC 9718 (Left) and FGSC 18892 (Right) were isolated using a differential centrifugation purification method.

A

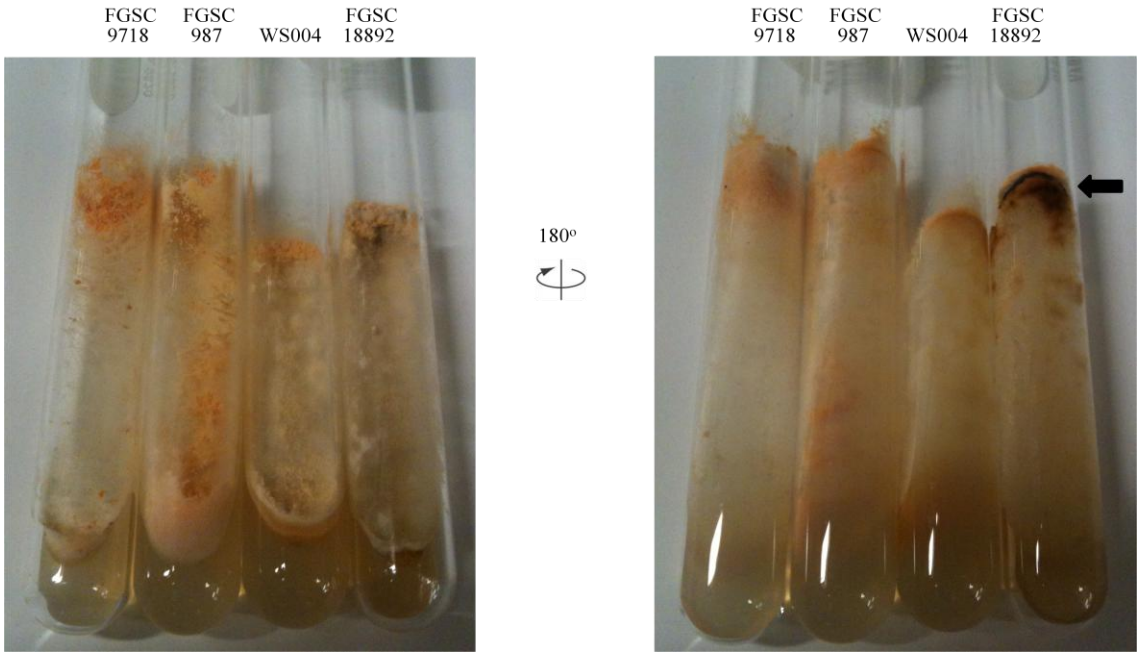
FGSC 9718
FGSC 987
WS004
FGSC 18892
180º
FGSC 9718
FGSC 987
WS004
FGSC 18892

B

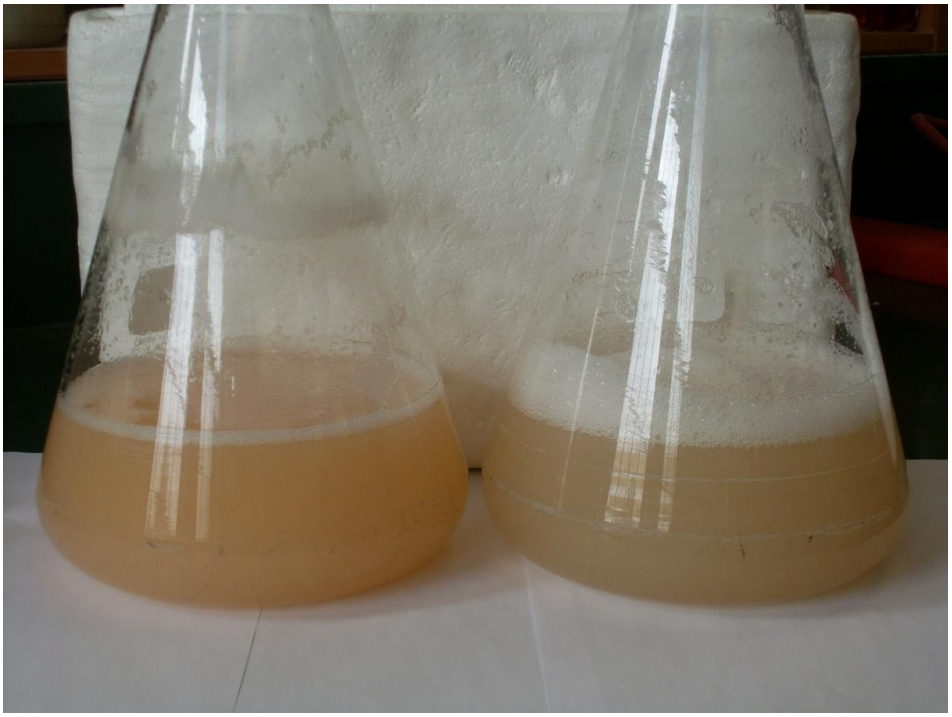

C

Wild-type strains grown in liquid media appear peach in colour while the porin-lacking strains appear darker. This same difference in colouring was also observed with mitochondria isolated from both porin-containing and porin-lacking strains (Figure 3.7C). One possible explanation for the discolouration of the mitochondria could be a difference in the cytochrome content between the strains.

3.2.3 *Mitochondria lacking porin have altered cytochrome content*

Defects in respiratory complexes have been observed in nuclear and extranuclear mutants. The most extensively studied example known as [poky], is characterised by its slow growth rate, reduced levels of cytochromes *b* and aa_3 and increased levels of cytochrome *c*; the mutation is maternally-inherited (discussed in Bertrand and Kohout, 1977). Nuclear mutations have also been identified in respiratory-defective strains, which affected the expression of the mitochondrial encoded subunit 1 of cytochrome *c* oxidase (Nargang et al., 1978).

Since the *por* ⁻ strains exhibited slow growth similar to [poky] and contained discoloured mitochondria, the cytochrome content of WS004 and FGSC 18892 was determined. The mitochondria of FGSC 9718, $74A^d$, FGSC 18892 and WS004 were isolated from mycelium cultivated at both 22°C and 30°C as described in section 2.11. The difference spectrum from each strain was collected and used to determine the absolute concentration of the three different cytochromes as described by Lambowitz and Slayman, (1978). To demonstrate that FGSC 9718 has wild-type cytochrome content, the difference spectra was compared with $74A^d$, but in fact showed some difference offering evidence for $74A^d$ no longer being a wild-type strain (data not shown). Therefore the cytochrome content of FGSC 9718 was compared with FGSC 987 wild-type strain and

showed almost no difference between them (data not shown). Demonstrating the wild-type characteristic of FGSC 9718 was of importance since FGSC 9718 is the parent to the porin knockout mutant and was used for comparison with WS004. WS004 and FGSC 18892 had similar cytochrome spectra when grown at 22^{o}C (Figure 3.8A) and some variation when grown at 30^{o}C (Figure 3.8C). FGSC 18892 is unique as it showed a temperature-dependent decrease in cytochrome *c*. A comparison of WS004 and FGSC 18892 with FGSC 9718 showed significant decreases in both cytochromes *b* and aa_3 and an increase in cytochrome *c* at both tested temperatures (Figure 3.8B and D). In contrast to the lack of temperature dependence observed in the wild-type strains, both WS004 and FGSC 18892 showed a small temperature dependence with regards to the level of cytochrome aa_3 as evident by a further decrease in its concentration (Figure 3.8B). The extreme reduction in cytochromes *b* and aa_3 concentrations presumably translates to reduced levels of complex III and IV of the ETC. This in turn could cause a reduced proton gradient resulting in decreased ATP production and offer a possible explanation for the reduced growth rate of the porin-lacking strains.

3.2.4 *Porin Knockout Strains Express High Levels of Alternative Oxidase*

The extremely low levels of cytochrome aa_3 present in the mitochondria of the porin-lacking strains suggest very low levels of ETC complex IV. It has been shown previously that for *Neurospora crassa* strains with mutations, or exposure to inhibitors resulting in a blocking of electron flow through the cytochrome-mediated ETC, survive by inducing the expression of *aod*1 (Figure 3.9; Lambowitz and Slayman, 1971). The result is the expression of a KCN-insensitive alternative oxidase that transfers electrons directly from the ubiquinone pool to oxygen.

Figure 3.8 *The cytochrome content of mitochondria isolated from Neurospora crassa strains FGSC 9718, WS004 and FGSC 18892*.

Isolated mitochondria were solubilised with 2% DOC and the resulting supernatant from a clarifying spin was oxidized with potassium ferricyanide. The absorbance was measured as a wavescan from 500 nm to 650 nm. The solution was then reduced using sodium dithionite and the wavescan repeated. Presented, is the difference spectra (reduced-oxidized) for mitochondria isolated from FGSC 9718, WS004 and FGSC 18892 cultivated at 22^{o}C (A) and 30^{o}C (C). FGSC 9718 was confirmed to have a wild type spectra by comparison with a spectra collected using isolated mitochondria from FGSC 987 (data not shown). The quantitation of the cytochrome levels is shown as an average of at least three biological replicates in (B) and (D) for the indicated cultures grown at 22^{o}C and 30^{o}C respectively. The error bars represent the standard deviation.

A

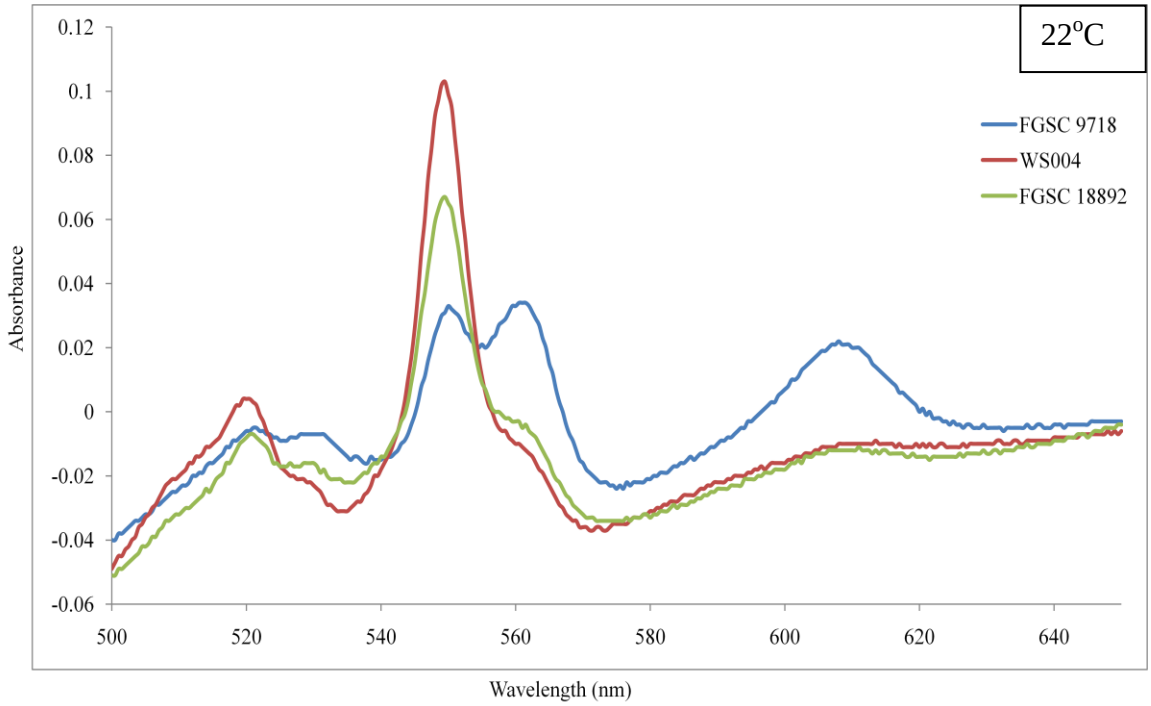
22°C
FGSC 9718
WS004
FGSC 18892
Absorbance
0.12
0.1
0.08
0.06
0.04
0.02
0
-0.02
-0.04
-0.06
500
520
540
560
580
600
620
640
Wavelength (nm)

B

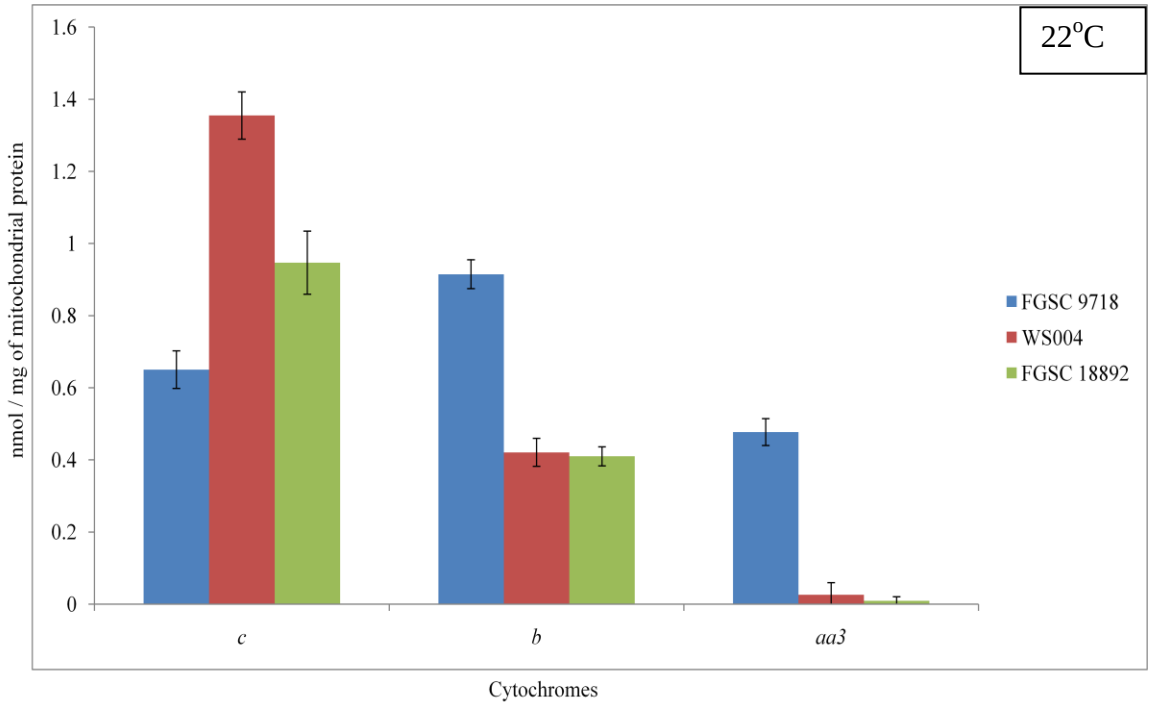
22°C
FGSC 9718
WS004
FGSC 18892
nmol / mg of mitochondrial protein
1.6
1.4
1.2
1
0.8
0.6
0.4
0.2
0
c
b
aa3
Cytochromes

C

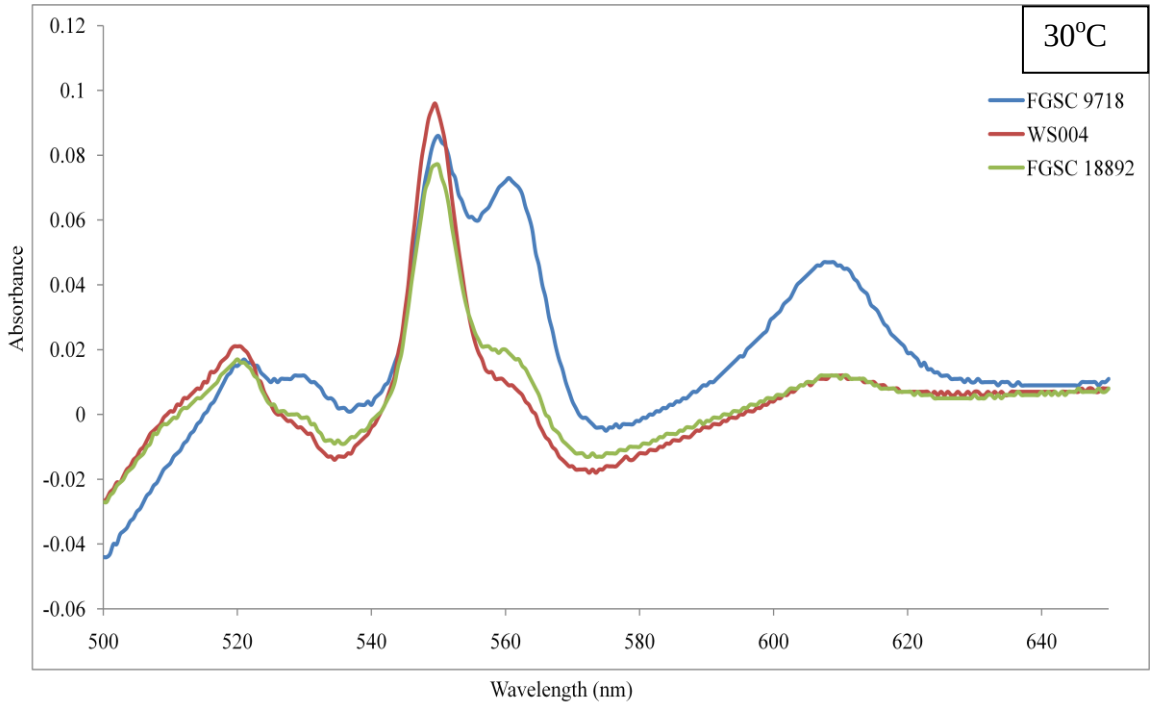
30°C
FGSC 9718
WS004
FGSC 18892
Absorbance
0.12
0.1
0.08
0.06
0.04
0.02
0
-0.02
-0.04
-0.06
500
520
540
560
580
600
620
640
Wavelength (nm)

D

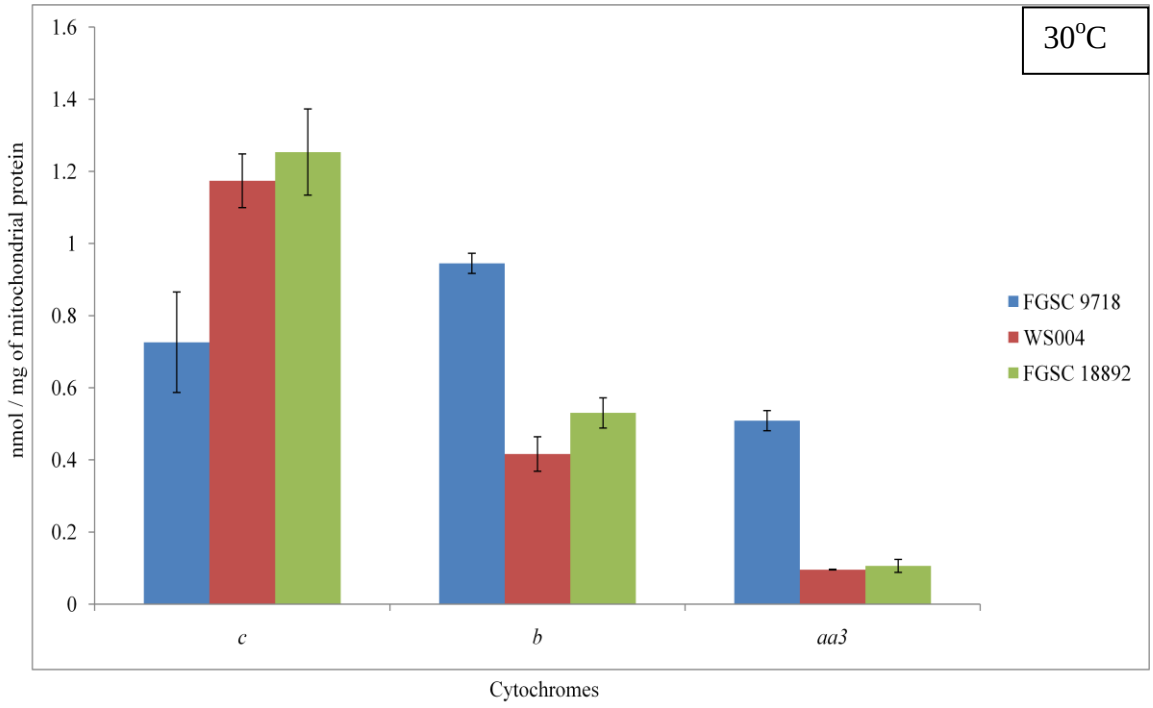
30°C
FGSC 9718
WS004
FGSC 18892
nmol / mg of mitochondrial protein
1.6
1.4
1.2
1
0.8
0.6
0.4
0.2
0
c
b
aa3
Cytochromes

Figure 3.9 *Cytochrome mediated and alternative oxidase pathways of respiration.* Schematic diagram of the cytochrome mediated pathway (upper pathway) and the alternative oxidase pathway (lower pathway). Black arrows indicate flow of electrons. Red arrows indicate cytochromes with reduced levels in WS004 and FGSC 18892. FP_D, and FP_S, flavoproteins; Q, ubiquinone; COX, cytochrome *c* oxidase.

A

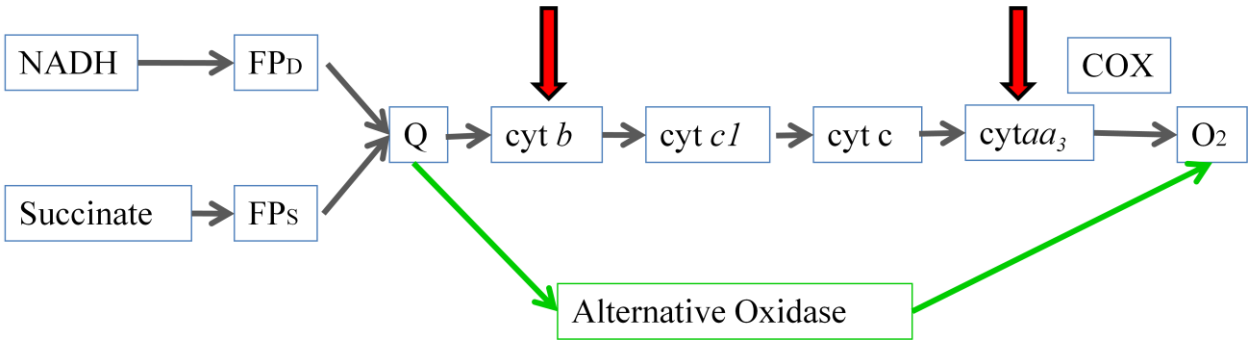
NADH
FPD
Succinate
FPS
Q
cyt b
cyt c1
cyt c
cytaa3
COX
O2
Alternative Oxidase

To assay for increased expression levels of alternative oxidase mycelium of FGSC 9718, WS004 and FGSC 18892 were grown to early exponential phase in VM medium at both 22^{o}C and 30^{o}C and oxygen consumption was assayed at the same temperatures. The oxygen consumption for all strains tested was monitored for at least 2 minutes allowing for a convincing constant slope and to demonstrate that oxygen consumption could be detected at low levels (data not shown). The samples were then re-oxygenated and treated with potassium cyanide. Oxygen consumption of FGSC 9718 grown at 22^{o}C was completely inhibited by the addition of KCN as indicated by the change in slope of the trace (Figure 3.10A). A similar result was observed when the culture was grown at 30^{o}C (Figure 3.10B). This indicated a normally functioning ETC similar to the results obtained for wild-type strain FGSC 987 (data not shown; Tanton et al., 2003). This was not the case for the presumed wild-type strain 74A^{d}, which showed an elevated level of alternative oxidase. Since the growth of 74A^{d} was not completely KCN sensitive, it was deemed a non-wild type and no longer used for comparison. Oxygen consumption by both *por* $^{-}$ strains however, was completely cyanide-insensitive, as evidenced by no change in the slopes of the traces with the addition of KCN (Figure 3.10). This result is indicative of the expression of the alternative oxidase. Furthermore, cyanide resistant respiration was inhibited by the subsequent addition of salicyl hydroxamic acid (SHAM), an inhibitor of alternative oxidase (Lambowitz and Slayman, 1971), thus confirming its expression.

3.2.5 *The ATP Levels of por $^{-}$ strains are similar to FGSC 9718*

The slower growth rate of the *por* $^{-}$ strains might possibly be explained by a reduction in the levels of available ATP. Evidence for reduced levels of ETC complex III

Figure 3.10 *The loss of porin causes an increase in alternative oxidase expression.* The *por* knockout strains WS004 and FGSC 18892 were examined for the expression of alternative oxidase. VM media cultures were incubated at 22^{o}C (A) or 30^{o}C (B) and the respiration of each strain is shown. The tracings show oxygen consumption over time with the moment inhibitors of the cytochrome pathway (KCN) or the alternative oxidase pathway (SHAM) were added.

A

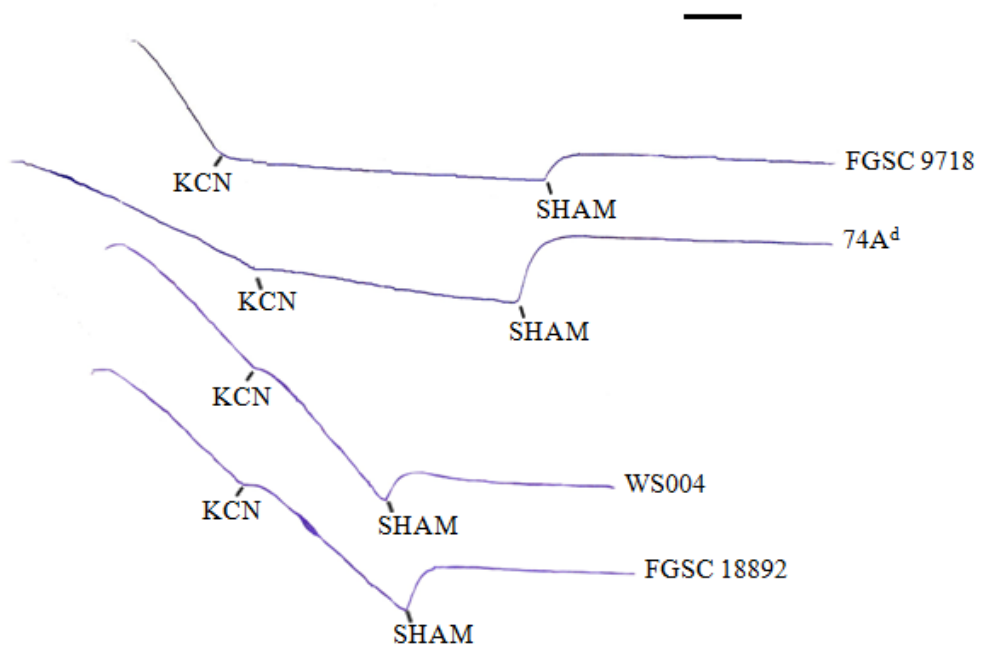
KCN
SHAM
FGSC 9718
KCN
SHAM
74A[d]
KCN
KCN
SHAM
WS004
FGSC 18892
SHAM

B

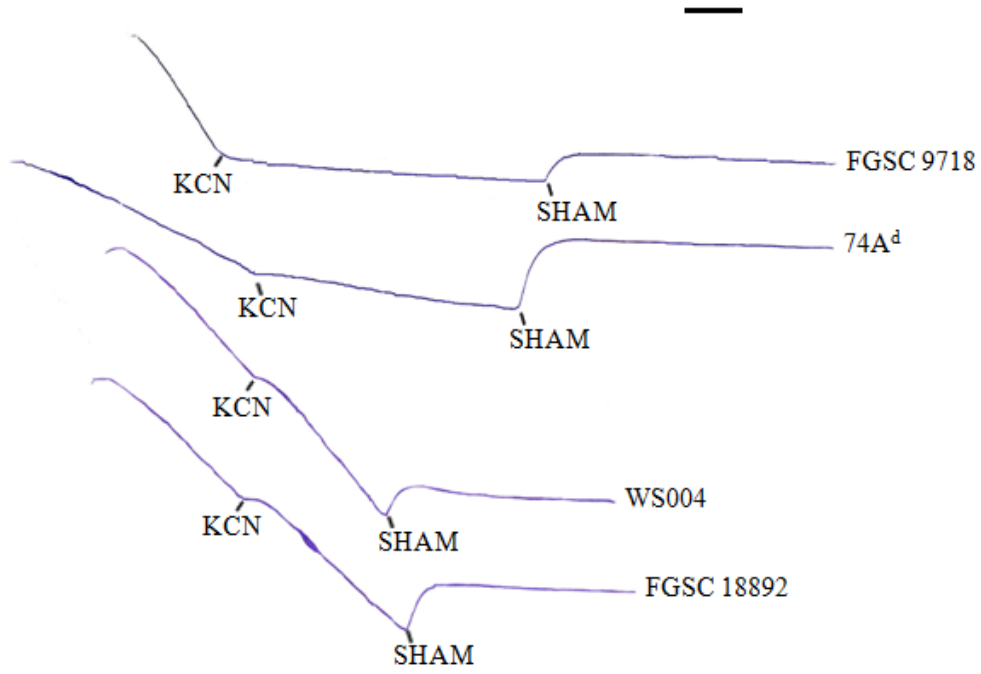
KCN
SHAM
FGSC 9718
KCN
SHAM
74A[d]
KCN
KCN
SHAM
WS004
FGSC 18892
SHAM

and IV, as well as the expression of alternative oxidase, would infer a reduction in the levels of ATP. Therefore, the concentration of available ATP was determined using a Bac Titer-Glo™ microbial cell viability assay kit (Promega) adapted for use with isolated mitochondria. 22-32 µg of isolated mitochondrial protein or isolation buffer containing cytoplasmic contents from FGSC 9718, WS004 and FGSC 18892, grown at either 22^{o}C or 30^{o}C, were combined in equal volumes with Bac Titer-Glo reagent and the luminescence measured with a plate reader. An ATP standard curve was generated to determine the absolute concentration of available ATP. The concentration of ATP present in the cytoplasm of the *por* $^{-}$ strains grown at 22^{o}C showed a slight difference when compared to FGSC 9718 (Figure 3.11A). This difference was less significant when assayed at the elevated temperature (Figure 3.11B). Interestingly, the steady state concentration of ATP determined from the mitochondria of the *por* $^{-}$ strains was not significantly different from the concentration observed for FGSC 9718 at either temperature tested (Figure 3.11). This may have been due to the rapid decay of or consumption of ATP by enzymes still functioning during the isolation process, until a constant minimum level was reached since substrate was not added to continue ATP production. A likely more physiologically relevant measure of available ATP during the growth of the different strains might be to measure the ATP production potential of the isolated mitochondria. The potential for wild-type yeast mitochondria to produce ATP has been demonstrated previously with reported values being in the mM / mg of mitochondrial protein range as opposed to the µM/mg of mitochondrial protein amounts shown here (Stuart *et al.*, 1994). Therefore, limited amounts of available ATP to the *por* $^{-}$ strains as an explanation for the reduction in growth rate remains a conceivable

Figure 3.11 *Determination of the concentrations of ATP available to por¯strains.* Mitochondria from FGSC 9718, WS004 and FGSC 18892 grown at either 22^{o}C (A) or 30^{o}C (B) were isolated using a differential centrifugation purification. The supernatant from the initial spin containing the cytoplasmic contents was collected for analysis of ATP concentration. An ATP standard curve was used to determine the concentration of ATP present from 22-32 µg of either mitochondrial or cytoplasmic protein mix with Bac Titer-Glo reagent by the relative amount of luminescence produced. The average of at least three biological replicates is presented. The error bars represent standard deviation.

A

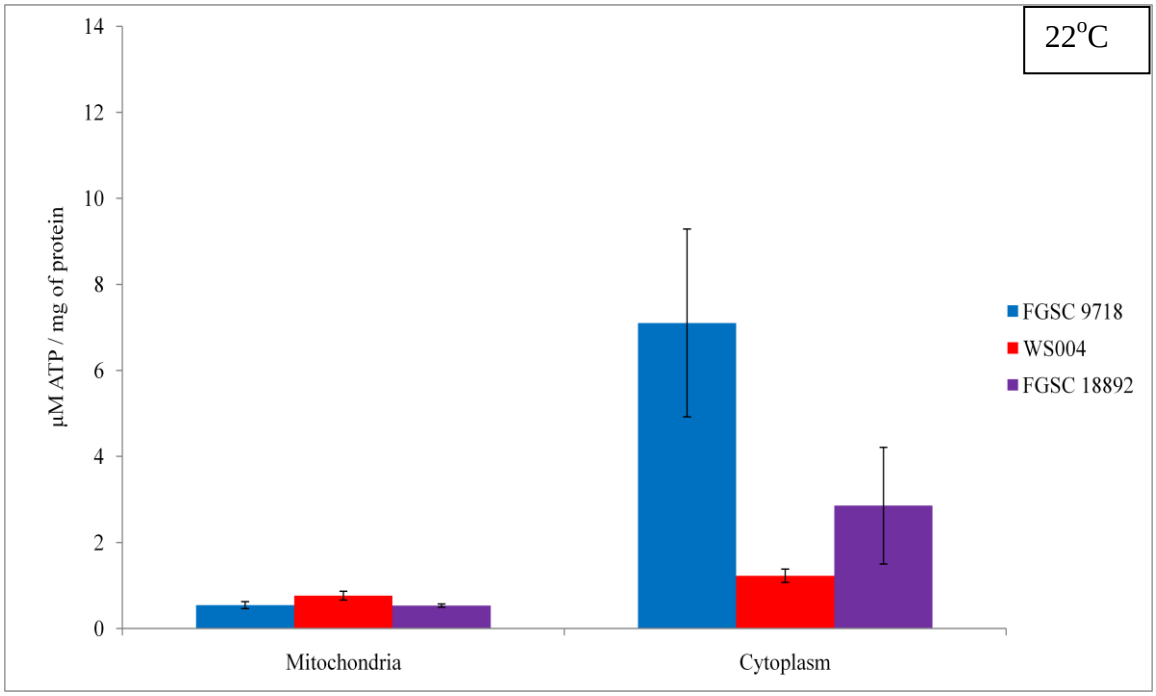
22°C
14
12
10
8
6
4
2
0
µM ATP / mg of protein
FGSC 9718
WS004
FGSC 18892
Mitochondria
Cytoplasm

B

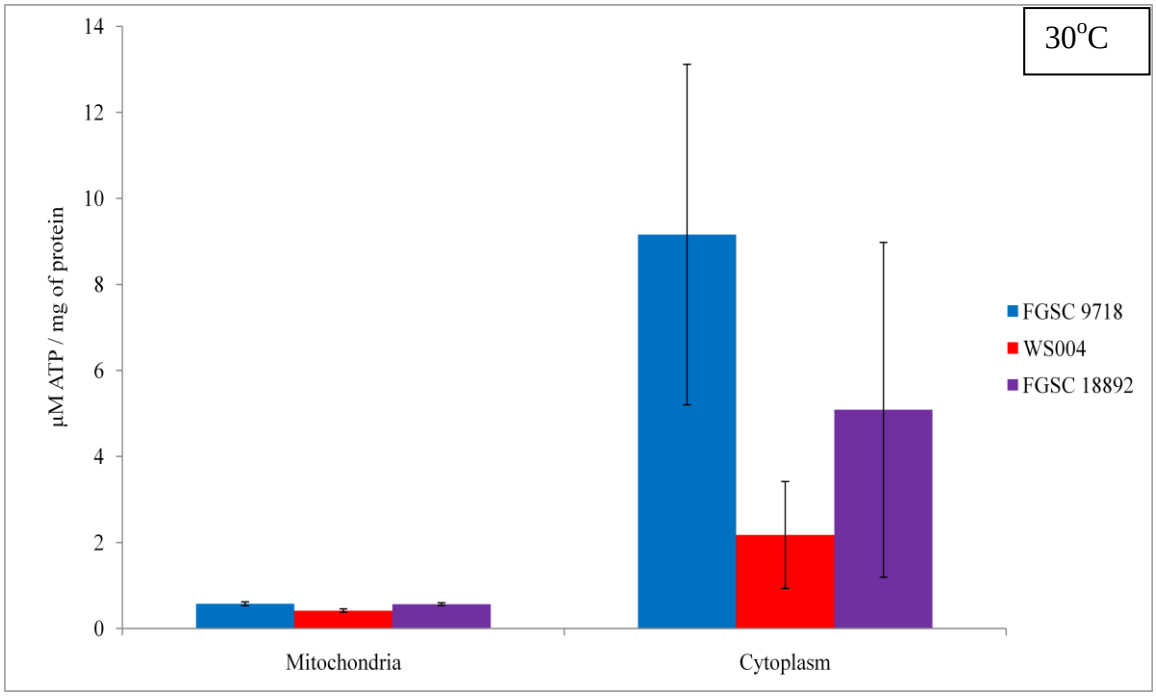
30°C
14
12
10
8
6
4
2
0
µM ATP / mg of protein
FGSC 9718
WS004
FGSC 18892
Mitochondria
Cytoplasm

possibility.

3.3 *Comparison of the Genetic Backgrounds of Different por⁻ Strains*

Genetic background can be influential on the expression and function of many different proteins as a result of synergistic or antagonistic effects. For example, two different alleles of the *Saccharomyces* mitochondrial DNA polymerase gene (*MIP*)*1* confer differing degrees of error-prone replication when in the presence of an *ade2* allele (Young and Court, 2008). The phenotypic differences observed between *por*⁻ strains WS004 and FGSC 18892, must be due to their unique genomes. Therefore, an analysis of the genetic backgrounds was attempted to shed some light on the factors influencing the effects of porin loss.

3.3.1 *Comparison of the Methods Used to Create the por⁻ Strains*

The construction of both *por*⁻ strains was done by the replacement of *por* with *hph* driven by the *trp*C promoter and terminator. Both mutations were constructed such that about 320 bp of sequence upstream of the translation start site were removed. The two strains differ however in the amount of DNA removed after the translational stop site. In FGSC 18892, 274 bp were removed after the stop codon, but they remained in the genome of WS004. The neighbouring genes on the chromosome are located over 850 bp upstream (asparagine synthetase 2) and over 700 bps downstream (annotated as a conserved hypothetical protein), so the deletion of *por* plus some flanking sequences should have no effect on their expression.

Both WS004 and FGSC 18892 were created in a *mus*51 or *mus*52 mutant, deficient in non-homologous end-joining. The four *mus* mutants were constructed using FGSC 4200 for transformation, which was then sexually crossed with FGSC 6103 to isolate pure homokaryons, resulting in the creation of FGSC 9717, FGSC 9718, FGSC 9719 and FGSC 9720 (Table 2.1). These knockout strains were all created with a cassette that conferred resistance to basta. WS004 was constructed using FGSC 9718 (*mus-51*::*bar*$^{+}$) and is isogenic to FGSC 9718 for all genes except *por*. FGSC 18892 has no isogenic strain for comparison. An isolate resulting from the transformation of one of these four mutant *mus* strains was then sexually crossed with one of two strains, FGSC 2489 (wild-type) or FGSC 6103 (*his*3) to create FGSC 18892. The sexual crossing of the transformational isolate with the wild-type strain, resulted in the exchange of the mutant *mus* allele for a wild-type allele. Therefore, while the only known genetic difference between the two *por* $^{-}$ strains is the double mutation of *por* and *mus-51* in WS004, many other subtle differences may exist, including mitochondrial DNA.

3.3.2 *The Double Mutation of por and mus-51 is not the Cause of the Phenotypic Differences Between the por* $^{-}$ *Strains*

To determine if the phenotypic differences observed between WS004 and FGSC 18892, specifically the ability to produce aerial hyphae, were due to the combined mutations of *mus-51* and *por*, sexual crosses between WS004 and 74A^{d} (cross 1) and FGSC 18892 and FGSC 9718 (cross 2) were performed. The idea was to replace the mutant *mus-51* allele in WS004 with the wild-type allele from 74A^{d} and conversely, introduce the mutant *mus-51* allele into FGSC 18892. WS004 was unable to produce protoperithecia when cultured on Westergaard's medium (Davis and deSerres, 1970) at

23°C under constant light for 7 days, a standard procedure used to determining female fertility. Therefore, the cross was performed using 74A^{d} as the female which was fertilized with conidia from WS004. FGSC 18892 was able to produce protoperithecia and therefore was used as the female for cross 2. Both crosses resulted in the production of ascospores after 3.5 weeks of incubation at 23°C.

3.3.2.1 *The Aerial Hyphae Phenotype is Caused by an Epistatic Relationship with an Unknown Allele*

The ascospores of cross 1 were plated on VM + hyg medium plates, at low dilution, to permit growth of well separated colonies of only *por* $^{-}$ progeny. A 50:50 mixture of *mus-51* mutant and wild-type alleles was predicted. From these plates, 10 isolates were labelled WS1036-WS1045 (Table 2.1) and picked to VM medium slants and labelled WS1036-WS1045 (Table 2.1), where they exhibited varied ability to produce aerial hyphae (data not shown). WS1037 and WS1038 were selected as representatives and inoculated into VM medium conidia flasks to more clearly demonstrate the two classes of aerial hyphae production exhibited by the cross progeny (Figure 3.12). Interestingly, WS1037 and WS1038 were both *por* $^{-}$ and *mus-51* $^{-}$ suggesting that the aerial hyphae phenotype was not due to the double mutation and therefore must be influenced by another unknown genetic factor. The ten cross 1 progeny were subcultured to VM + basta medium plates to screen for basta resistance. Six of the ten isolates were basta resistant; the other four were confirmed to contain the wild-type *mus-51* allele by PCR (data not shown). These four were WS1036, WS1039, WS1040 and WS1043 with only WS1043 lacking the ability to produce wild-type like aerial hyphae (data not shown). Together, these results suggest a putative third allele, which for

Figure 3.12 *The progeny of wild type and por ¯ strains varied ability to produce aerial hyphae.*

50 ml conidia flasks were inoculated with indicated *Neurospora crassa* strains and incubated at 30^{o}C until hyphae were half way up the side of the flask, to a maximum of 7 days. The ability to produce aerial hyphae was scored as growth up off the surface of the media. The progeny from cross 1 (74A^{d} X WS004) are shown bottom left and the progeny of cross 2 (FGSC 18892 X FGSC 9718) are shown bottom right.

A

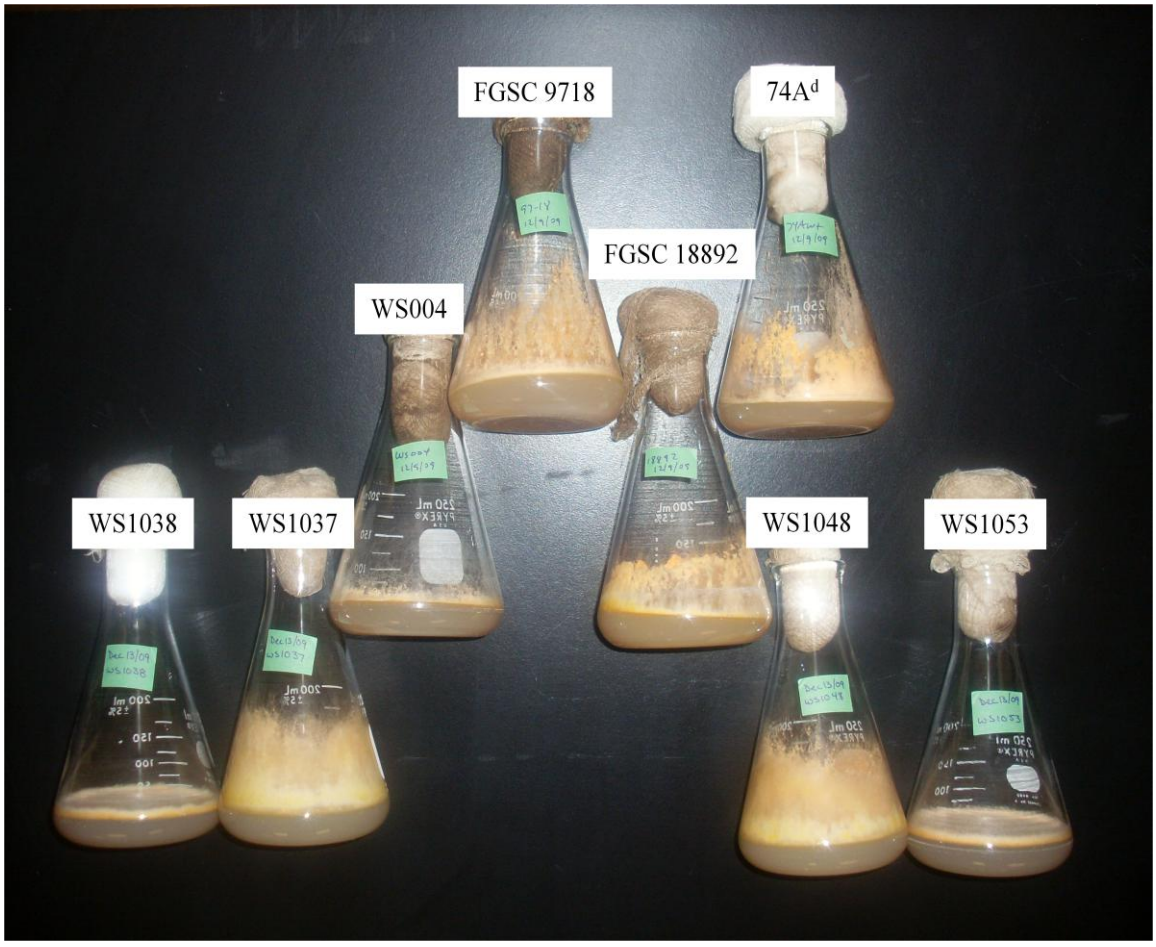
FGSC 9718
74A^{d}
FGSC 18892
WS004
WS1038
WS1037
WS1048
WS1053

discussion purposes will be referred to as *aer*, which in combination with the *por*$^{-}$ allele results in the inhibition of aerial hyphae production. Additionally, all of these strains contain mtDNA from 74A^{d} and not WS004, so the aerial hyphae phenotype observed in WS004 must not be due to mitochondrial DNA.

The ascospores of cross 2 were plated on VM + hyg + basta, at low dilutions, to permit formation of well separated colonies and selection of double mutants. Similar to cross 1, 10 isolates were picked to VM medium slants, which yielded a mixture of the two classes with respect to aerial hyphae production. WS1048 and WS1053 were inoculated into conidia flasks for comparison (Figure 3.12). This result further supports the proposed *aer* allele and its synergistic affect with the lack of porin.

To obtain further support for the hypothesis that the aerial hyphae phenotype was due to a double mutation of *por* and *aer*, additional ascospores from cross 1 were germinated, without selection for either mutation, allowing the isolation of more genetic combinations for analysis. In total, forty more isolates were recovered and labelled WS1056-WS1095. The *por* and *mus-51* alleles were determined using VM + hygromycin and VM + basta media respectively (Table 3.2). Interestingly, out of the 40 isolates picked only WS1068 and WS1085 were hygromycin-resistant, indicative of *por*$^{-}$ strains. However, PCR screening of the *por* locus revealed WS1068 was a heterokaryon, containing both wild-type and mutant alleles for both *por* and *mus-51*, and presumably derived from hyphal fusion on the germination plate, or picking of two overlapping colonies. WS1085 contained only wild-type alleles and the location of the hygromycin- and basta-resistance genes is unknown. The remaining 38 isolates harboured a wild-type

Table 3.2 *Phenotyping, aerial hyphae production ability and female sterility of cross 1 progeny.*

	VM Media		VM + Basta Media	VM + Hyg Media	Female Sterility[¥]
Strain	Growth[†]	Aerial Hyphae[††]	Growth	Growth	
FGSC 987	+	+	–	–	+++
FGSC 9718	+	+	+	–	+++
WS004	+	–	+	+	–
FGSC 18892	+	+	–	+	++
WS1056	+	+	+	–	+++
WS1057	+	+	–	–	++
WS1058	+	+	+	–	++
WS1059	+	+	+	–	++
WS1060	+	+	+	–	++
WS1061	+	+	–	–	+
WS1062	+	+	–	–	+++
WS1063	+	+	+	–	+
WS1064	+	+	–	–	+
WS1065	+	+	+	–	+
WS1066	+	+	–	–	+
WS1067	+	+	+	–	+++
WS1068	+	+	+	+	++
WS1069	+	+	+	–	+
WS1070	+	+	–	–	+++[¶]
WS1071	+	+	–	–	+++
WS1072	+	+	–	–	+++[¶]
WS1073	+	+	–	–	+[§]
WS1074	+	+	+	–	+++[¶]
WS1075	+	+	–	–	+
WS1076	+	+	–	–	+++[¶]
WS1077	+	+	–	–	+++[¶]
WS1078	+	+	–	–	+
WS1079	+	+	–	–	+[§]
WS1080	+	+	–	–	++[¶]
WS1081	+	+	+	–	+
WS1082	+	+	+	–	++

WS1083	+	+	+	–	++
WS1084	+	+	+	–	+
WS1085	+	+	+	+	+++
WS1086	+	+	+	–	+++
WS1087	+	+	–	–	+[§ ¶]
WS1088	+	+	+	–	++[§ ¶]
WS1089	+	+	–	–	++
WS1090	+	+	–	–	++
WS1091	+	+	–	–	++
WS1092	+	+	+*	–	+++[§ ¶]
WS1093	+	+	–	–	+
WS1094	+	+	–	–	+
WS1095	+	+	–	–	+

[†] + growth;-no growth

[††] + produced aerial hyphae;-no aerial hyphae

[¥] +++, wild-type; ++, < 50% wildtype; +, very few

[§] abnormally large

[¶] abnormally tiny

[§ ☥] mixture of abnormally large and abnormally tiny

* strain grew in VM + basta media but failed to produce aerial hyphae

allele of *por* and a mixture of *mus-51* alleles. The ability to produce aerial hyphae was scored as growth off the surface of 1 ml of VM liquid media in a 10 ml test tube and compared to FGSC 987 (wild-type), FGSC 9718, FGSC 18892 and WS004 (Table 3.2). WS1056-WS1095 all produced aerial hyphae in VM media as well as in the VM + basta media and VM + hyg media where growth was observed with the exception of WS1092, which grew in VM + basta media but did not make aerial hyphae in VM + basta media. Given that all forty strains tested wild-type for *por* and produced aerial hyphae, it was concluded that the lack of aerial hyphae, observed in WS004 and various other cross progeny that were *por* ⁻ strains also, was the result of an epistatic connection between the *por* ⁻ allele and an unknown *aer* allele.

3.3.2.2 *Protoperithecia Production is Affected by Unknown Genetic Factors*

WS004 was unable to produce protoperithecia when cultured on Westergaard's medium under continuous light for 7 days at 25^{o}C , making WS004 female sterile (data not shown). However, FGSC 18892 was able to produce protoperithecia under standard conditions and therefore is female fertile. The possibility of the double mutation of *por* and *mus-51* causing the female sterility in WS004 was investigated using the same cross progeny used to investigate the aerial hyphae deficiency phenotype. The *por* ⁻ progeny of cross 1 (WS1036-WS1045) were tested for female fertility and under standard conditions, all 10 were sterile. The same result was obtained from the 10 progeny of cross 2 (WS1046-WS1055). It was noted that given 2.5 weeks, some of the progeny showed varied ability to produce what appeared to be protoperithecia. WS1041 is an example of one of the strains that remained sterile even after the extended incubation period (Figure 3.13A). In contrast, WS1045 appeared fertile, producing wild-type like protoperithecia

Figure 3.13 ***Ascospore production by cross progeny*****.**

Westergaard's slants (Davis & deSerres, 1970) were inoculated with the progeny of cross 1 and cross 2 and incubated for 2.5 weeks at 25^{o}C in continual light before being photographed. (A) Representative of strains that remained sterile, shown is WS1041. (B) Representative of strains that produced wild type like protoperithecia, shown is WS1045. (C) Strains that produced abnormally small structures are exemplified by WS1040. (D) Representative of strains that produced abnormally large structures, shown is WS1048. Examples of the described structures are indicated with the red arrow.

A

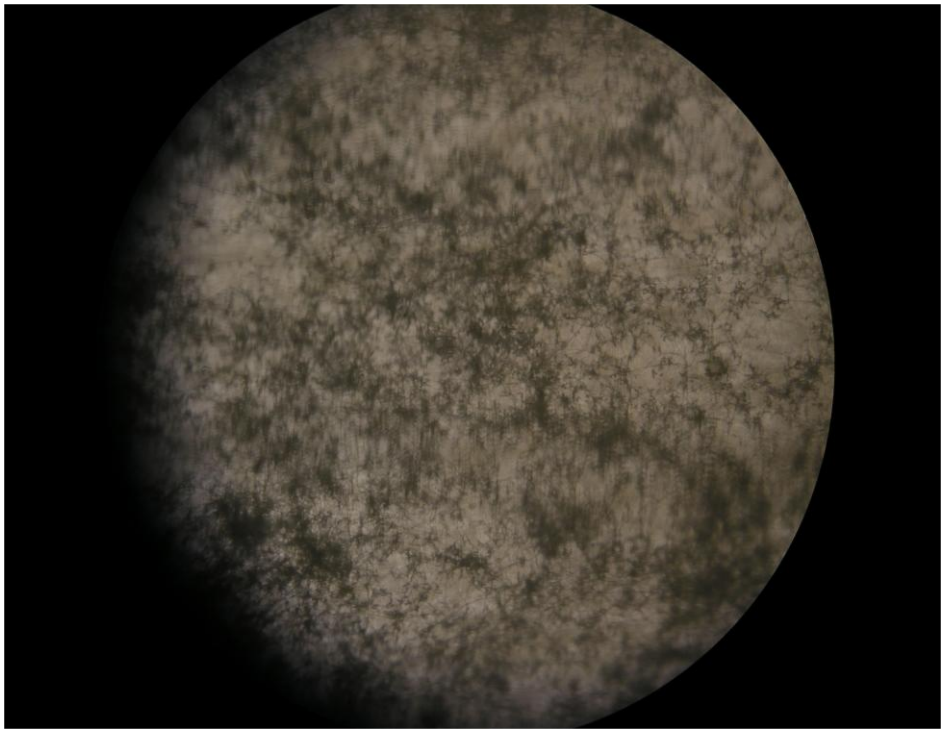

B

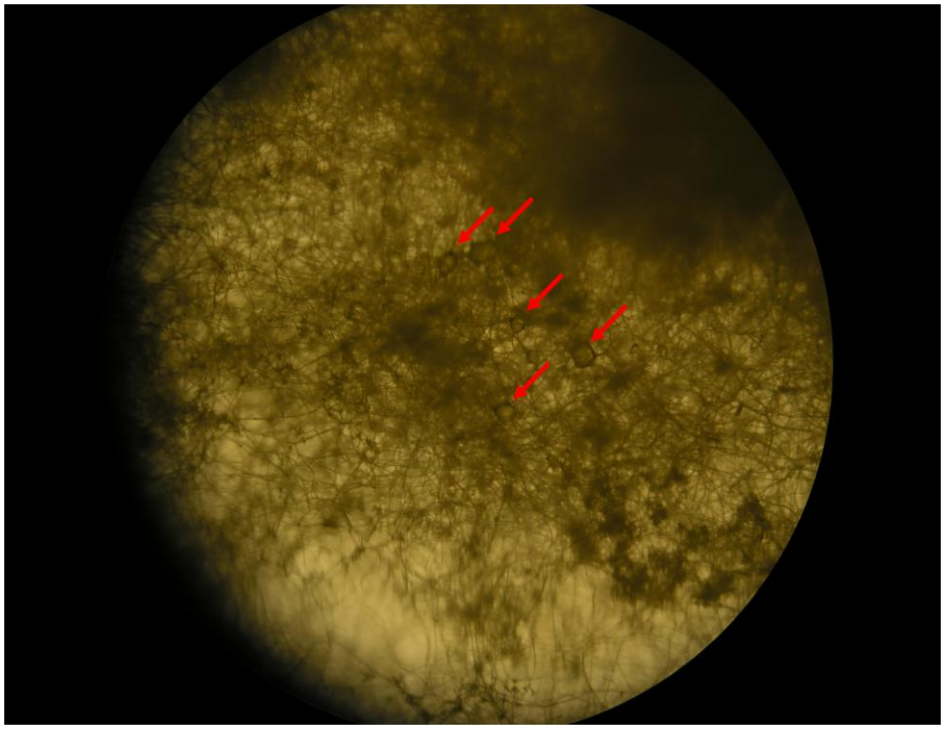

C

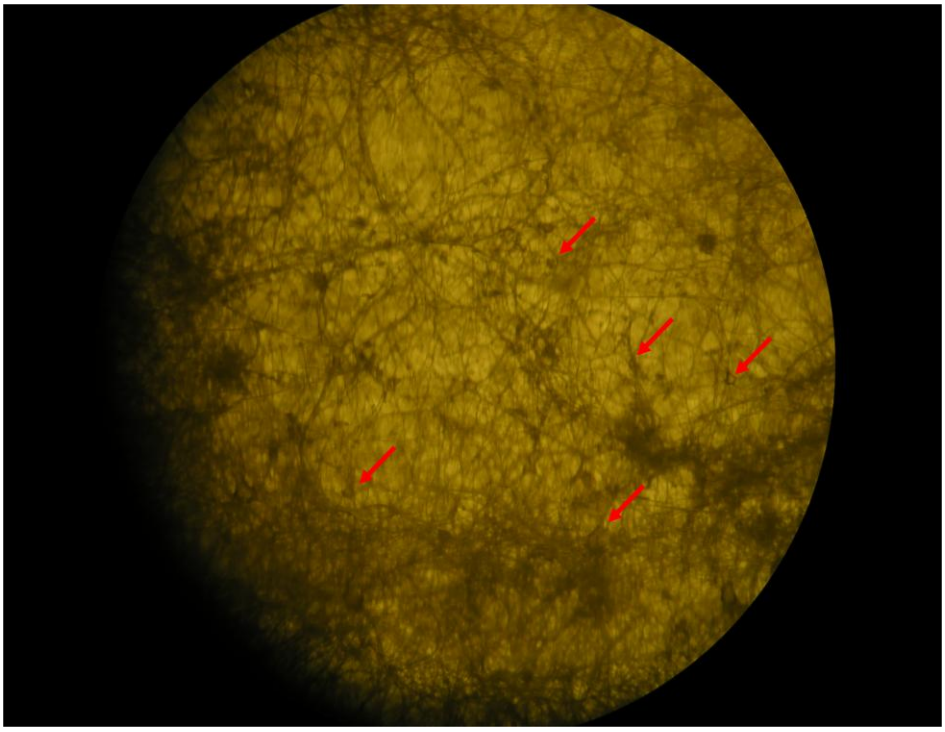

D

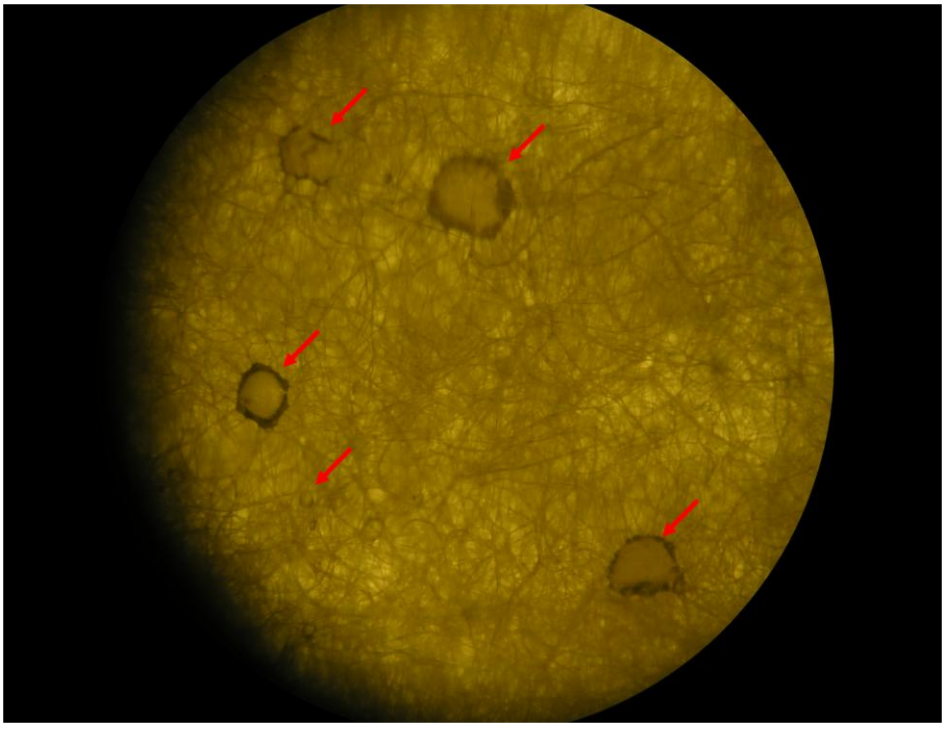

(Figure 3.13B). Several isolates including WS1040, produced tiny structures, which may or may not have been protoperithecia (Figure 3.13C). Most interesting were the strains that produced abnormally large structures, like WS1048 (Figure 3.13D) and WS1051 (data not shown). WS1051 is an example of a strain that produces abnormally large protoperithecia comparable to WS1048, which could be fertilized and produced ascospores (data not shown). Whether or not any of the ascospores resulting from this strain will be viable remains to be shown. Since the progeny from both crosses were sterile when considered with standard procedure, the female sterility of WS004 was considered not to be due to the double mutation, since WS1036, WS1039, WS1040 and WS1043 are single mutants of just the *por* gene. Instead it was thought to be derived from a second epistatic allele inherent to FGSC 9718. To confirm this hypothesis, the progeny of cross 1 with the wild-type allele for *por* (WS1056-WS1095) were tested for female fertility as described above and scored after 8 days of incubation (Table 3.2). The ability to produce protoperithecia varied amoung all forty isolates, but they all did produce some protoperithecia. Several strains produced protoperithecia in numbers comparable to wild-type, and other strains produced so few putative protoperithecia that they would need to be fertilized to confirm that they are in fact protoperithecia. Surprisingly, several progeny produced abnormally large protoperithecia similar to the *por* ¯ progeny. This suggests that the sterility phenotype observed may not be as simple as a single allele's epistatic effect with the *por* allele. Rather, several genetic factors may be involved to produce the observed phenotype, with the mutant *por* allele synergistically contributing. However, the progeny of cross 1 and cross 2 contain different

mitochondrial DNA, supporting the idea that it is not the mitochondrial DNA influencing female fertility of these strains.

The effect of porin loss was examined in two independently constructed strains, each of which had a unique combination of the described phenotypes. Attempts to explain some of the different phenotypes with the differences in genotype identified further differences and increased the variations of the observed phenotypes. Taken together, this work strongly supports examining the effects of the loss of porin, or any other protein, by comparison of isogenic strains.

3.4 *Comparison of Mitochondria containing and lacking Porin*

The mitochondrion relies on the function of many complexes to maintain its structure and function either directly or indirectly, as most of the proteins that compose the mitochondrion are produced on cytosolic ribosomes. The import of most proteins across the outer membrane is an ATP dependant process and requires the translocase of the outer membrane (TOM) complex to do so (Pon et al., 1989). Strains lacking MOM19 (TOM20) showed reduced import of most proteins and lacked inner membrane cristae when examined by electron microscopy (Harkness et al., 1994). It seemed reasonable then, that mitochondria lacking porin, which is responsible for the translocation of ATP / ADP + Pi, may exhibit alterations in mitochondrial morphology due to an impediment on protein import.

3.4.1 *Mitochondria Lacking Porin Exhibit Morphological Defects*

To examine this possibility, mycelium of FGSC 9718 and WS004 from liquid VM media cultures grown to early exponential phase at either 22^{o}C or 30^{o}C were stained with MitoTracker Green FM to visualize the mitochondria. MitoTracker Green FM has negligible fluorescence in aqueous environments, requiring accumulation in the membrane to activate its bright green fluorescence. The mitochondria of FGSC 9718 appear as mostly long discrete tubular structures present within the tips of elongating hyphae (Figure 3.14A). The mitochondria observed further from the tips appeared to have smaller oval shapes. This morphology was observed at both 23^{o}C and 30^{o}C and was so well defined it could be observed using only differential interference contrast (DIC) microscopy (Figure 3.14C). The mitochondria of the *por* $^{-}$ strain WS004, however, showed few to no discrete structures with the mitochondria appearing much more punctate (Figure 3.14). There also appeared to be an increase in the number of individual mitochondria when compared with the mitochondria from FGSC 9718 at either temperature. Given that WS004 requires almost twice the time to accumulate the same amount of biomass as FGSC 9718, it is difficult to say whether the variation in mitochondrial morphology is due to protein composition of the membranes or simply the reduced growth rate. However, it remains to be shown whether the variations in mitochondrial morphology caused by the loss of porin is due to a loss of porin function, or rather the lack of the porin molecule itself in the MOM.

3.4.2 *Comparison of the Mitochondrial Proteomes of FGSC 9718 and WS004*

The mitochondrion is comprised of approximately 1150 different proteins that give the mitochondria its shape and function (Scharfe et al., 2000). The gross alteration

Figure 3.14 *The morphology of mitochondria in wild-type and por ˉ strains*. Conidia were germinated and grown in liquid cultures for approximately 24 hours for FGSC 9718 and 48 hours for WS004 in VM media incubated at 22^{o}C (A and B) and 16 hr and 24 hr for FGSC 9718 and WS004 respectively at 30^{o}C (C). Mycelium of each strain was stained with MitoTracker® Green FM at the same temperature as they were grown at. The hyphae were observed at 1000X magnification using differential interference contrast microscopy (grey images) with the mitochondria visualized with fluorescence microscopy (green images). Scale bar represents 10 μm.

A

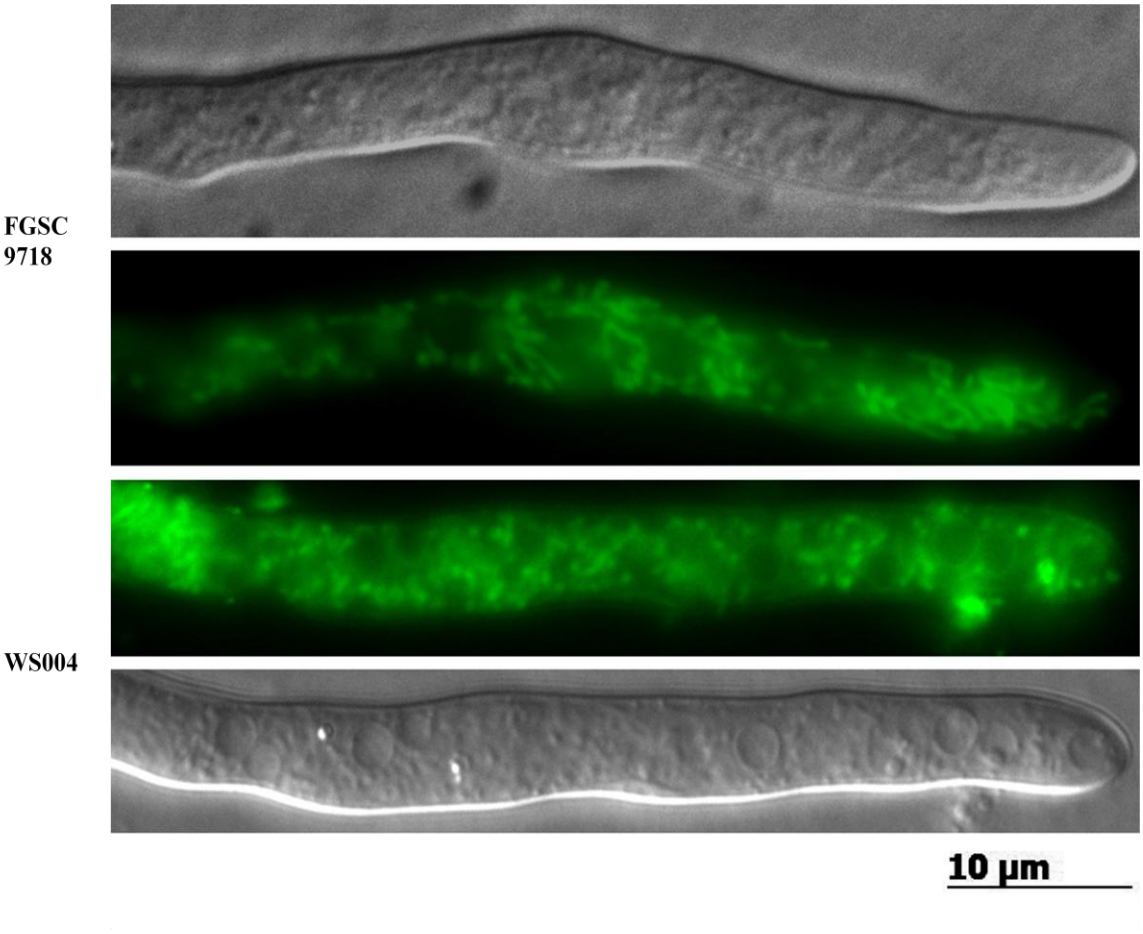

B

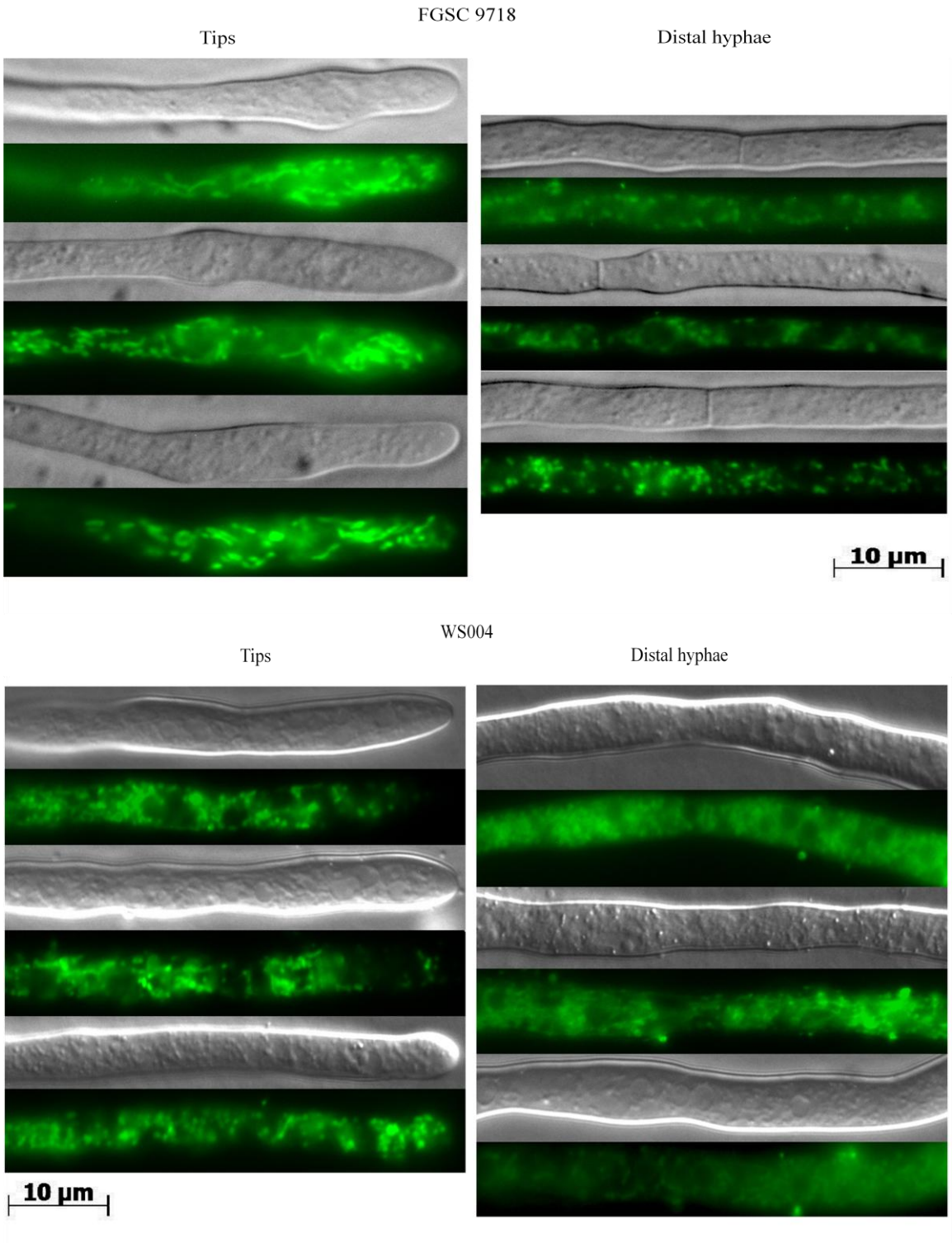
FGSC 9718
Tips
Distal hyphae
10 µm
WS004
Tips
Distal hyphae
10 µm

C

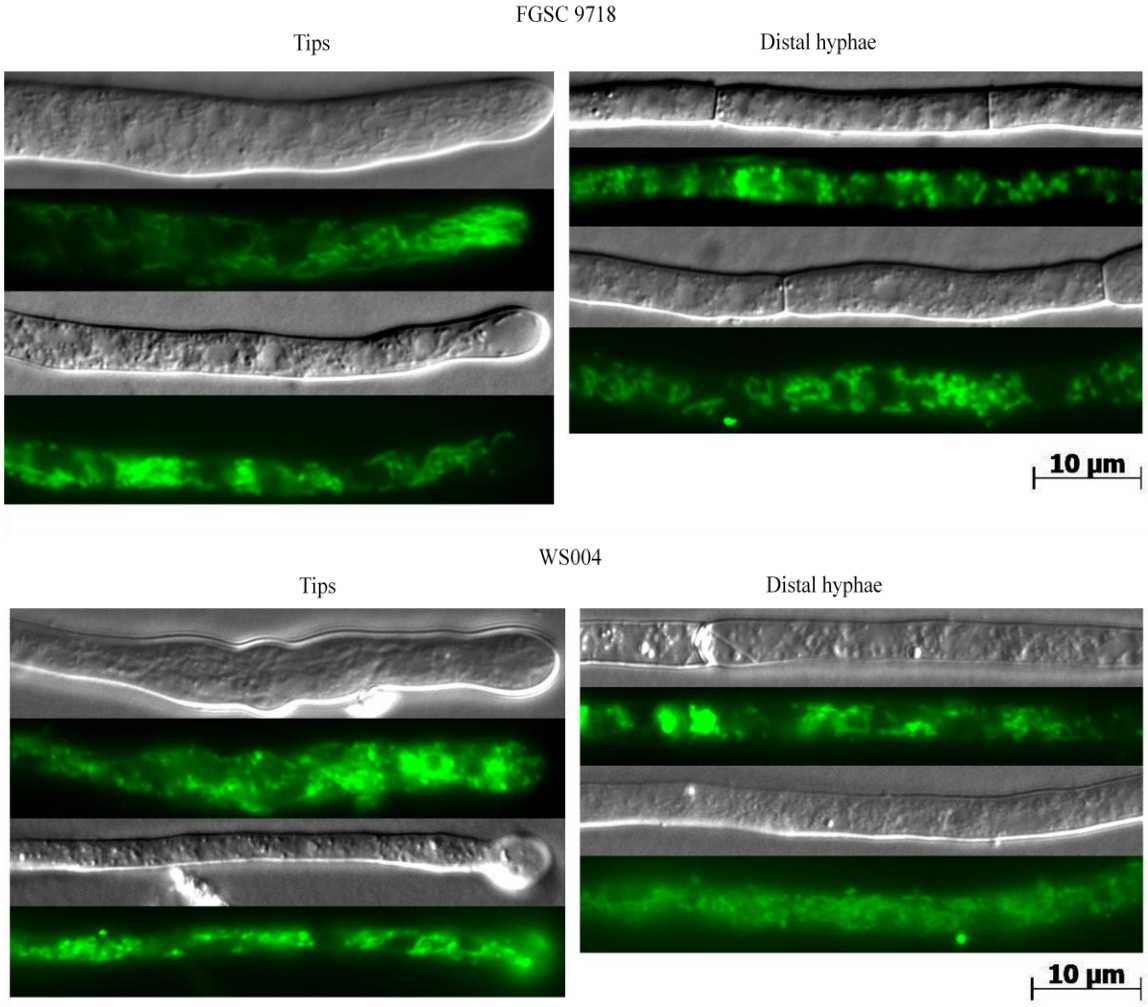
FGSC 9718
Tips
Distal hyphae
10 µm
WS004
Tips
Distal hyphae
10 µm

in mitochondrial morphology observed in the *por*⁻ strain WS004 is most likely due to a number of factors in response to the loss of porin. Therefore, an initial comparison of the mitochondrial proteomes of FGSC 9718 and WS004 was performed by SDS-PAGE. The mitochondria of FGSC 9718 and WS004 were harvested from cultures incubated at 22^{o}C using a differential centrifugation technique. The mitochondria were then further purified using a discontinuous sucrose gradient. The reisolated mitochondria were solubilised in NP40 with sonication. These protein samples were used in the analysis presented in sections 3.3.2, 3.3.3 and 3.3.4. The mitochondrial proteomes were separated with 4-12 % SDS-PAGE allowing for higher resolution of both high and low molecular weight proteins (Figure 3.15). There were noticeable differences in the expression levels of various proteins at several different molecular weights. The mitochondria of WS004 produced fewer proteins at apparent molecular weights of 25 kDa, 32kDa, 40 kDa and 130 kDa, with the reduction at 32 kDa presumably being, but not limited to, the loss of porin. Possible constituents of these sizes could be: members of the translocase of the outer membrane (TOM) complex, TOM20, TOM22 and TOM40; or the inner membrane counterpart, the translocase of the inner membrane (TIM) complex, TIM22, TIM23 and TIM44. The reduced expression of the 40 kDa proteins are of particular interest since TOM40, like porin, is a pore-forming outer membrane protein. There were also proteins noticed to have an increase in expression levels, including 22 kDa, 28 kDa, 35 kDa, 50 kDa, 72 kDa and 105 kDa species. Again, some of the sizes could be members of either the TOM or TIM complexes. Thus, the loss of porin is reconciled by a reorganization of the expression of several different proteins and most likely responsible for the altered mitochondrial morphology discussed in section 3.3.1. Attempts to identify these proteins

Figure 3.15 *Comparison of the mitochondrial proteomes of FGSC 9718 and WS004.* Mitochondria were isolated from two biological replicates of FGSC 9718 (lane 2 and 3) and WS004 (lanes 4 and 5) grown at 22^{o}C and purified on a sucrose gradient. The mitochondria were then solubilized with NP40 and equal amounts of protein (10 µg per lane) were separated with 4-12 % SDS-PAGE. The four different samples gave quantitatively similar bands of proteins. However, some differences were observed; the increased level of protein expression in the *por* $^{-}$ strain is indicated by the column of asterisks to the left and the decreased level of protein expression is indicated by the column of asterisks to the right. Lane 1, molecular weight markers.

A

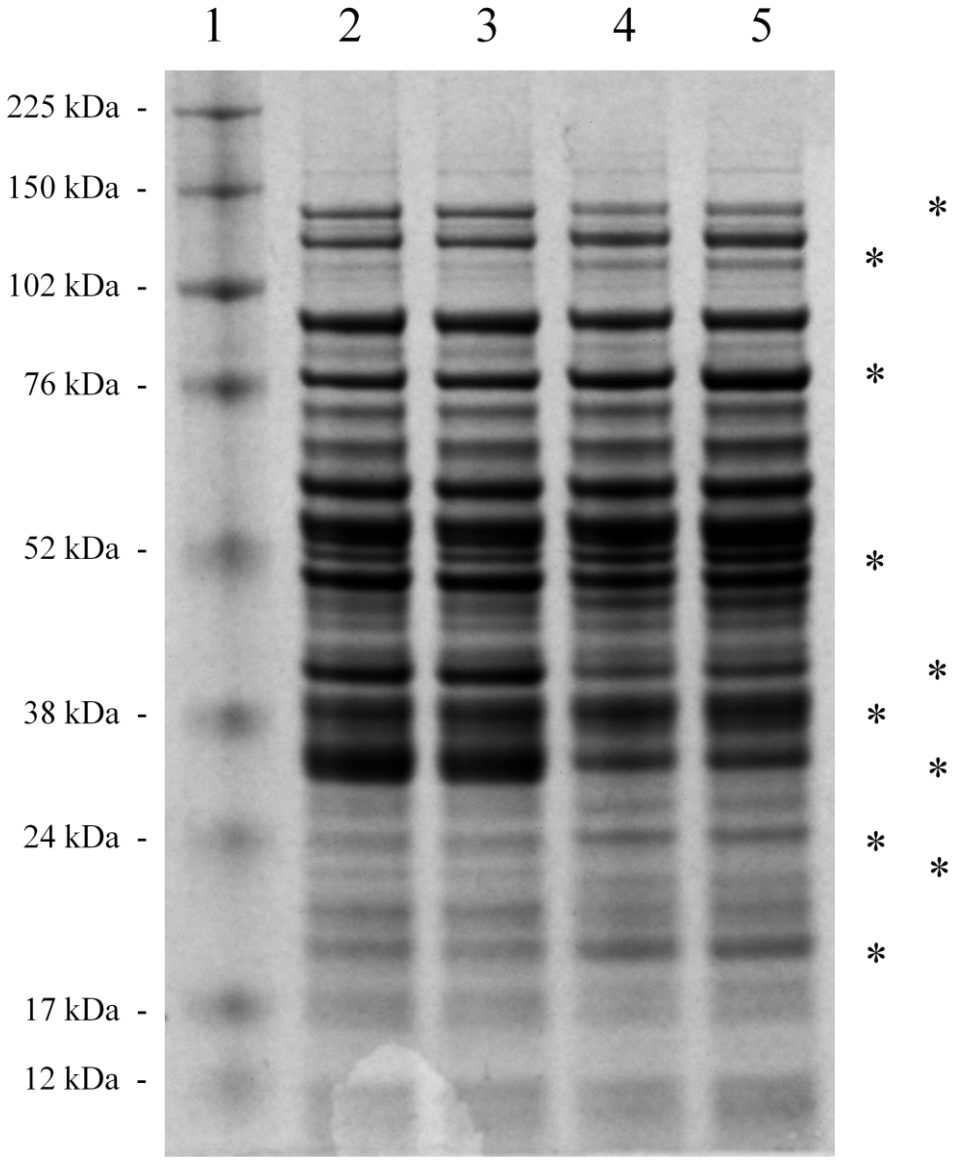
1
2
3
4
5
225 kDa -
150 kDa -
102 kDa -
76 kDa -
52 kDa -
38 kDa -
24 kDa -
17 kDa -
12 kDa -
*
*
*
*
*
*
*
*
*

are described in the next two sections.

3.4.3 *Western Blot Analysis Reveals Differential Expression of TOM40 and TOM70*

Several of the differentially expressed protein bands identified by 4-12% SDS-PAGE described above were analysed by Western blotting. NP40-solubilised mitochondria from FGSC 9718 and WS004 grown at 22^{o}C were separated in triplicate (per gel) with 12% SDS-PAGE and transferred to a nitrocellulose membrane. Western blot analysis confirmed a complete lack of porin in WS004 (Figure 3.16A and B). The loss of porin in the mitochondrial sample from WS004 is in agreement with the reduction of 32 kDa species by SDS-PAGE analysis, but as suggested above, does not rule out the possibility of any other changes in expression of other 32 kDa proteins. A down regulation of 2.1 fold was observed for TOM70. The reduction in the level of TOM70 in mitochondria from WS004 is in contrast with the observed difference at 72 kDa by 4-12% SDS-PAGE analysis, suggesting the expression of other 72 kDa proteins are also affected by the loss of porin. It should be noted that while the apparent molecular weight of the TOM70 protein identified by immunodetection appears closer to 80 kDa, it was still believed to be TOM70. This discrepancy was most likely the result of interacting detergent molecules (NP40), which were not added to the molecular weight markers.

Western blot analysis also showed an up-regulation of 1.9 fold for TOM40 and no change in the expression level of TOM22 (Figure 3.16C). Band intensity in the portions of the gel including TOM40 and TOM 22 (Figure 3.15) does not correlate with these changes, further suggesting that WS004 altered expression levels in several different mitochondrial proteins in order to overcome the loss of porin.

Figure 3.16 *Western blot analysis of isolated mitochondria from FGSC 9718 and WS004.* Mitochondria from FGSC 9718 and WS004 grown at 22^{o}C were isolated and purified using a sucrose gradient followed by solubilised with NP40. Equal amounts of mitochondrial protein (25 µg per lane) from FGSC 9718 (lanes 2, 3 and 4) and WS004 (lanes 6, 7 and 8) were loaded in triplicate and separated with 12% SDS-PAGE. Western blot analysis was performed using antibodies for TOM70 and Porin (A and C) and TOM40 and TOM22 (D). Chemiluminescence was detected using a FluoroChem Imager and the captured images used for densitometry analysis. The TOM70 and porin (B) and TOM40 and TOM22 (E) blots were Ponceau stained and were then scanned for comparison of protein loading. An over-exposure of the blot in (A) is shown in (C). Lanes 1 and 9, molecular weight markers.

A

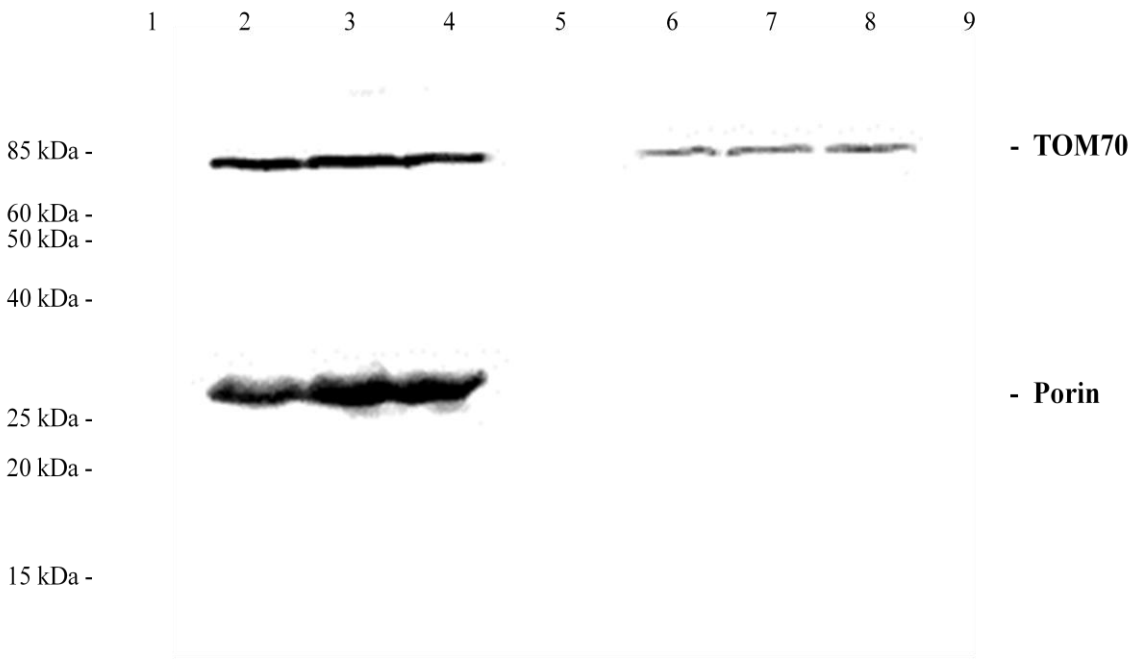
1 2 3 4 5 6 7 8 9
85 kDa -
60 kDa -
50 kDa -
40 kDa -
25 kDa -
20 kDa -
15 kDa -
- TOM70
- Porin

B

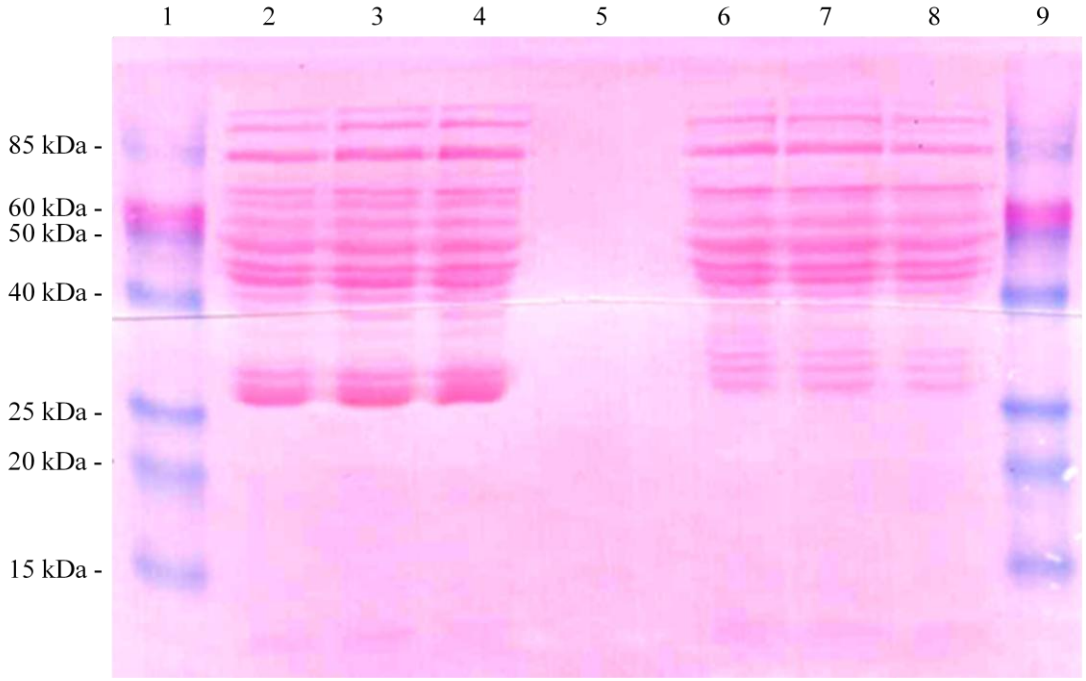
1 2 3 4 5 6 7 8 9
85 kDa -
60 kDa -
50 kDa -
40 kDa -
25 kDa -
20 kDa -
15 kDa -

C

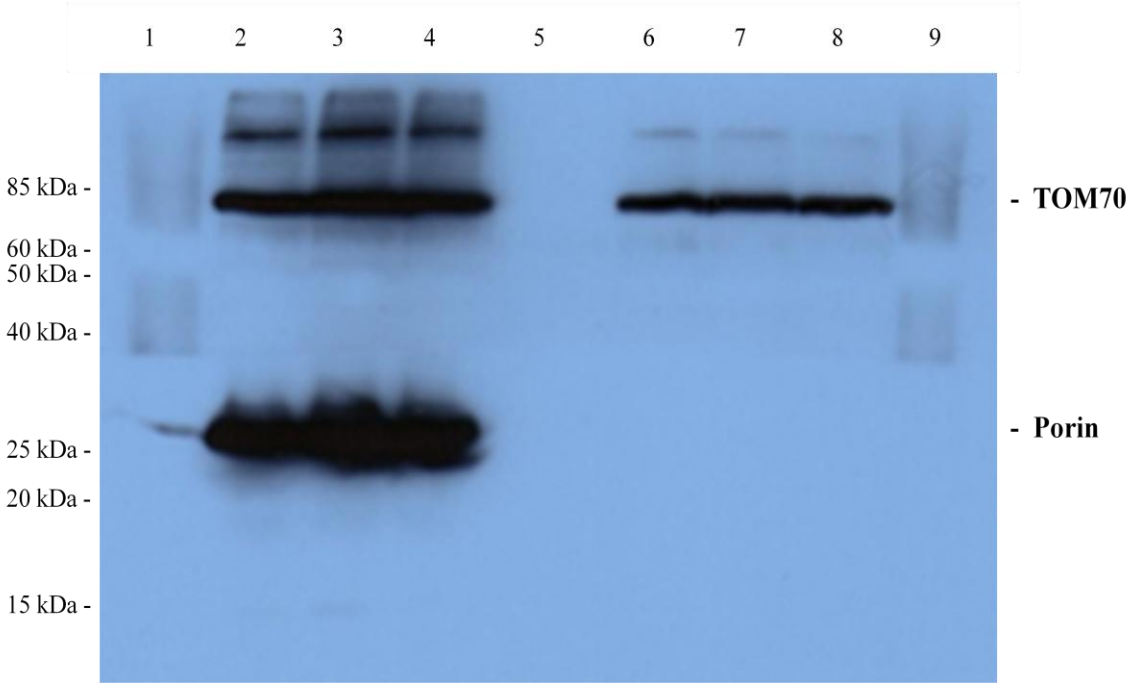
1
2
3
4
5
6
7
8
9
85 kDa -
60 kDa -
50 kDa -
40 kDa -
25 kDa -
20 kDa -
15 kDa -
- TOM70
- Porin

D

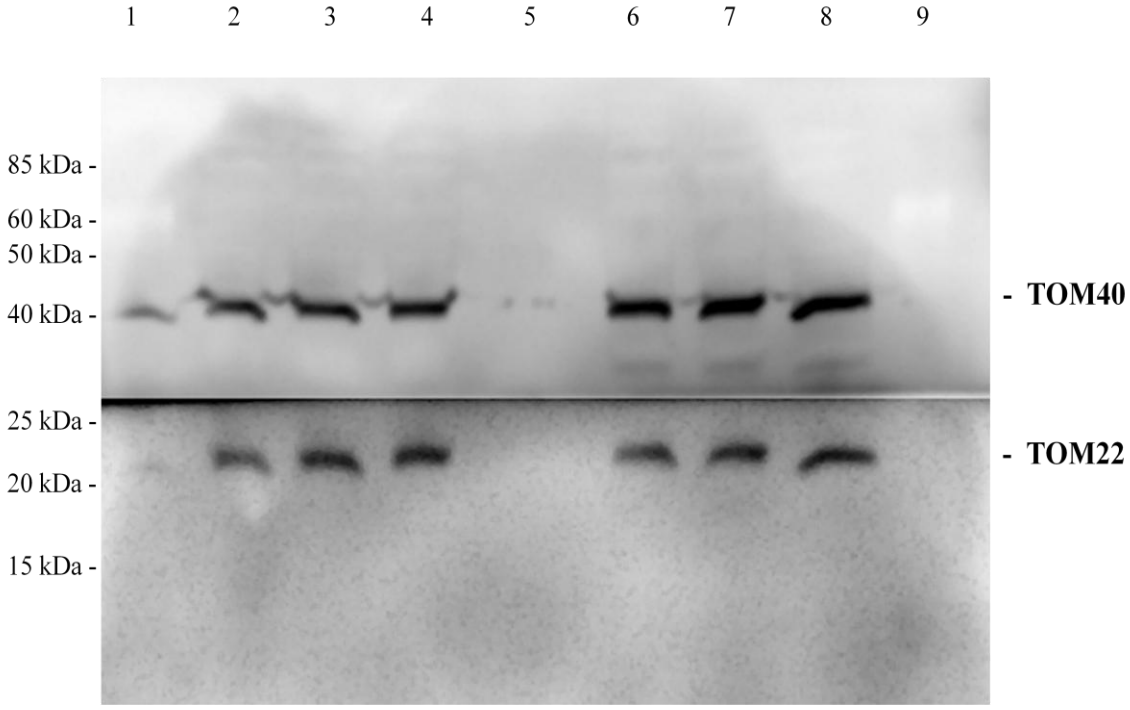
1 2 3 4 5 6 7 8 9
85 kDa -
60 kDa -
50 kDa -
40 kDa -
25 kDa -
20 kDa -
15 kDa -
- TOM40
- TOM22

E

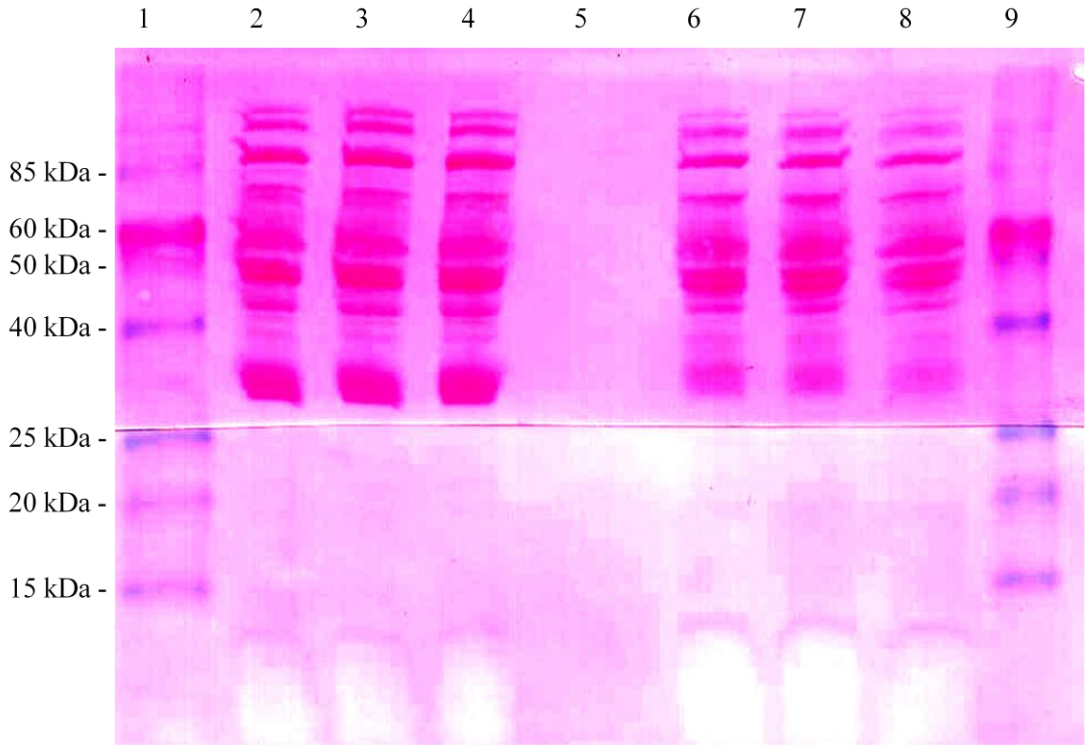
1 2 3 4 5 6 7 8 9
85 kDa -
60 kDa -
50 kDa -
40 kDa -
25 kDa -
20 kDa -
15 kDa -

3.4.4 Results of *iTRAQ Analysis Support a Lack of Complex IV*

In order to carry out a more thorough analysis of the mitochondrial proteome in WS004, iTRAQ analysis was carried out. In short, the protein samples for comparison are each labelled with one of a series of isobaric tags, and mixed together. The tags allow copurification of each peptide and further mass spectrometry allows protein identification and the relative levels of the protein from each sample. The NP40-solubilised mitochondria from two biological replicates of FGSC 9718 and WS004 (described in section 3.3.2.) were separately trypsin treated and labelled with different species of iTRAQ reagents (reporters with masses of 114 and 115 were used to label the biological replicates of FGSC 9718 and 116 and 117 were used for WS004 replicates) and then combined in equal amounts based on protein concentration. LC-MS / MS was performed on the two trials to obtain quantitative protein profiles of the two mitochondrial proteomes. If the identified proteins were expressed in equal quantities within both strains, the iTRAQ ratio would be 1. Therefore, the identified proteins of interests for this study are those for which the iTRAQ ratio deviated from 1. Values are usually presented as log2(ratio), such that proteins for which there is no difference in levels are represented by a value of zero, and negative and positive values reflect ratios less than or greater than 1.

A total of 651 and 652 proteins were identified from Trial 1 (116 over 114) and Trial 2 (117 over 115) respectively, with the single additional protein identified in Trial 2 being the only difference in identities. To make the analysis statistically relevant for a biological system, the $\log_2$ of the iTRAQ ratios was used in the calculation of the standard score (z). The cut off for statistically significant up or down regulation was set

to 95%. Since the samples originated from a dynamic biological system, the ratios obtained from Trial 1 and Trial 2 for a single protein were not always in agreement. The z-score of the $\log_2$ ratios obtained for Trial 1 was used to arrange the identified proteins from most up-regulated to most down-regulated (Figure 3.17). The ratio of each protein obtained for Trial 2 was placed onto the distribution curve at the location of the same protein in Trial 1 in order to show the difference in a single protein's expression between the two trials. At the 95% confidence level, the iTRAQ ratios suggest that the vast majority of proteins were not up or down regulated significantly. From the common 651 proteins identified, only the 19 proteins that were significantly up-or down- regulated in both trials were considered further.

Amongst the 12 proteins up-regulated in both biological trials, two were identified as conserved hypothetical proteins and four were predicted to be non-mitochondrial using MITOPRED (http://bioapps.rit.albany.edu/MITOPRED/; Table 3.3). Three others were identified as known domain containing or family proteins in which little is known about the protein and its exact function. An example is accession number NCU09403, predicted to be a mitochondrial protein and described as a NmrA family protein. Post-translational modification of the transcription factor AreA, which forms part of a system controlling nitrogen metabolite repression is done with the involvement of NmrA. Interestingly, the structure of NmrA shows evidence for a nucleotide binding site, but no dehydrogenase activity has been shown (Stammers et al., 2001). A clustering of identities however, all belong to or contribute to components of the electron transport chain. NADH-cytochrome b5 reductase 2 serves as an electron donor for cytochrome b5 and contains a FAD-binding domain

Figure 3.17 *Distribution of ratios of protein levels as measured by iTRAQ.*
The mutant : wild-type iTRAQ ratios obtained for Trial 1 were ordered according to their $\log_2$ values, largest to smallest along the x-axis. The iTRAQ ratios obtained for Trial 2 were graphed to position the data for same proteins in the same positions along the x-axis as for Trial 1. The solid blue (Trial 1) and red (Trial 2) lines represent the ratios ($\log_2$) for which the *z* score was at least 1.96 (95% confidence level). The enlarged data points indicate proteins reproducibly present in significantly different levels in the mutant strain. They are discussed and described in detail in Table 3.3 and Table 3.4.

A

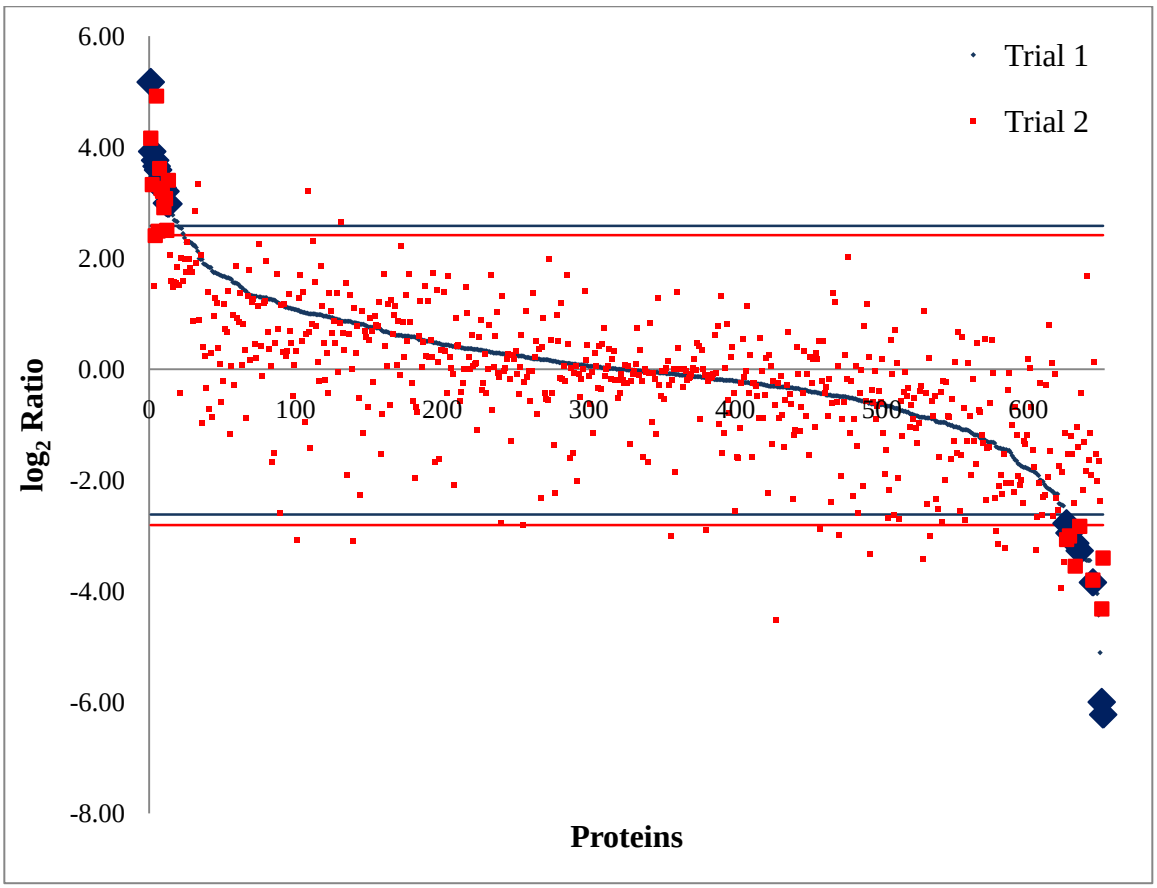
6.00
4.00
2.00
0.00
-2.00
-4.00
-6.00
-8.00
log2 Ratio
0
100
200
300
400
500
600
Proteins
Trial 1
Trial 2

Table 3.3 *Protein identities for significantly up regulated proteins in WS004 as determined by iTRAQ analysis.*

Accession Number and Description	Trial 1		Trial 2		Localization Prediction[¶] (Prediction Confidence)
	log_2 ratio	z score[§]	log_2 ratio	z score[§]	
| NCU05005 | HHE domain-containing protein (233 aa)	5.17	3.91	4.16	3.27	Mitochondrial (99.0%)
| NCU06518 | NADH-cytochrome b5 reductase 2 (327 aa)	3.92	2.97	3.32	2.64	Mitochondrial (92.3%)
| NCU05633 | stomatin family protein (432 aa)	3.76	2.85	2.41	1.96	Mitochondrial (99.0%)
| NCU06550 | pyridoxine 1 (309 aa)	3.65	2.77	4.92	3.84	Non-Mitochondrial (N/A)
| NCU09403 | NmrA family protein (305 aa)	3.59	2.72	2.48	2.02	Mitochondrial (99.0%)
| NCU09285 | zinc-containing alcohol dehydrogenase (347 aa)	3.40	2.58	3.61	2.86	Non-Mitochondrial (N/A)
| NCU09536 | conserved hypothetical protein (892 aa)	3.35	2.54	3.26	2.59	Non-Mitochondrial (N/A)
| NCU08476 | conserved hypothetical protein (372 aa)	3.27	2.48	3.20	2.55	Mitochondrial (92.3%)
| NCU02157 | COQ4 (348 aa)	3.22	2.44	2.91	2.33	Mitochondrial (100.0%)
| NCU08998 | 4-aminobutyrate aminotransferase (516 aa)	3.20	2.43	3.07	2.45	Non-Mitochondrial (N/A)

| NCU05850 | rubredoxin-NAD(+) reductase (612 aa)	2.99	2.27	2.50	2.03	Mitochondrial (92.3%)
| NCU07953 | alternative oxidase-1 (363 aa)	2.98	2.26	3.40	2.70	Mitochondrial (100.0%)

[¶] prediction of mitochondrial or non mitochondrial done with MITOPRED (http://bioapps.rit.albany.edu/MITOPRED/)

[†] n/a, not applicable

[§] z score for each $\log_2$ ratio is calculated as ($\log_2$ ratio - mean of all $\log_2$ ratios) / standard deviation of all $\log_2$ ratios. z scores of greater than 1.96 or less than -1.96 indicate significant at the 95% confidence level.

(http://www.ebi.ac.uk/interpro/IEntry?ac=IPR001834) making it possible, that it is functioning to remove electrons from complex II of the ETC. One of the predicted non-mitochondrial proteins was a zinc-containing alcohol dehydrogenase, which is capable of producing or assimilating alcohol. The zinc-containing ADH1 in *Neurospora crassa* preferentially assimilates primary alcohols consuming NAD+ as a preferred cofactor (Park et al., 2007). Similarly, Rubredoxin-NAD^+ reductase helps to generate NADH from electron donating iron-sulfur proteins, and therefore provides a substrate for the ETC. However COQ4 in *Saccharomyces*, is required for ubiquinone biosynthesis (Belogrudov et al., 2001) and this molecule provides the entry point for electrons into the conventional ETC, or the alternative oxidase pathway. Finally, alternative oxidase-1 catalysis the transfer of electrons from the Q pool to oxygen. The strong induction of the alternative oxidase pathway, and up-regulation of components leading to the alternative oxidase, together suggests a dysfunction in either complex III or IV of the ETC.

Only seven proteins were identified in both trials as being significantly down-regulated (Table 3.4). Similar to the up-regulated group, two of these were conserved hypothetical proteins. Translocase of inner mitochondrial membrane, subunit 13 (TIM13), which forms a hexameric complex with TIM8, was down-regulated 8 fold in WS004 mitochondria. Together the TIM8-TIM13 complex transports a subset of hydrophobic proteins through the aqueous IMS, including mitochondrial carriers and import components TIM17, TIM22 and TIM23 to be inserted into the inner membrane (discussed in Beverly et al., 2008). A second subset of proteins chaperoned by the TIM8-TIM13 complex are OM bound β - barrel proteins. It has been shown that the import of both TOM40 and porin is reduced in mitochondria lacking TIM13

Table 3.4 *Protein identities for significantly down regulated proteins in WS004 as determined by iTRAQ analysis.*

Accession Number and Description	Trial 1		Trial 2		Localization Prediction[¶] (Prediction Confidence)
	log_2 ratio	z score[§]	log_2 ratio	z score[§]	
| NCU03608 | ketol-acid reductoisomerase (403 aa)	-2.78	-2.08	-3.07	-2.15	Mitochondrial (100.0%)
| NCU06244 | translocase of inner mitochondrial membrane, subunit 13 (87 aa)	-2.95	-2.21	-3.00	-2.10	Mitochondrial (100.0%)
| NCU04202 | nucleoside diphosphate kinase-1 (153 aa)	-3.14	-2.35	-3.55	-2.51	Mitochondrial (61.5%)
| NCU05989 | conserved hypothetical protein (142 aa)	-3.27	-2.45	-2.83	-1.98	Mitochondrial (92.3%)
| NCU01550 | adenylate kinase cytosolic (279 aa)	-3.84	-2.88	-3.80	-2.70	Non-Mitochondrial (N/A)
| NCU11655 | outer mitochondrial membrane protein porin (284 aa)	-5.99	-4.50	-4.32	-3.09	Mitochondrial (100.0%)
| NCU05989 | conserved hypothetical protein (142 aa)	-6.22	-4.67	-3.40	-2.40	Mitochondrial (100.0%)

[¶] prediction of mitochondrial of non mitochondrial done with MITOPRED (http://bioapps.rit.albany.edu/MITOPRED/)

[†] n/a, not applicable

[§] z score for each log_2 ratio is calculated as (log_2 ratio - mean of all log_2 ratios) / standard deviation of all log_2 ratios.

(Hoppins and Nargang, 2004). This suggests that β-barrel import into WS004 mitochondria is reduced. This was surprising since it was thought that other β-barrel proteins may have been up regulated to compensate for the loss of porin. However, the results of the iTRAQ analysis revealed porin as the only β - barrel protein that was significantly down - regulated. Ketol-acid reductoisomerase is an enzyme that catalyses the reversible alkyl migration and NADPH dependent reduction in the second common step in branched-chain amino acid synthesis (Liu et al., 2007). NADPH is used in protection from toxicity of reactive oxygen species (ROS) and in anabolic pathways, such as sterol production. It has been reported that inhibition of ETC complex III during the oxidation of complex I substrates results in an increase in ROS production by complex I (Chen et al., 2003). Both nucleoside diphosphate kinase-1 (NDK) and adenylate kinase cytosolic participate in nucleoside homeostasis. Specifically, NDK catalyzes the conversion of NTP + NDP ↔ NDP + NTP, and therefore would be able to convert the GTP from the Kreb cycle into ATP to compensate for the lack of ATP production by oxidative phosphorylation. The *Neurospora crassa* NDK1 has been implicated in regulating the production of thick walled hyphae by controlling the expression of the *cat*3 gene, which codes for a catalase enzyme (Lee et al., 2009). A $ndk1^{RIP}$ mutant of *Neurospora crassa* is characterised by slow growth and is defective in aerial hyphae and conidia production similar to WS004, and only the growth rate can be restored with a disruption of *cat*3 (Lee et al., 2009). Adenylate kinase cytosolic (ADK) catalyzes the reversible interconversion of adenine nucleotides (2 ADP ↔ ATP + AMP) thereby playing an important role in cellular energy homeostasis, since the rate of oxidative phosphorylation is controlled by the levels of ADP. Interestingly, MITOPRED predicts

NDK to be a mitochondrial protein with only 61.5% confidence and ADK to be non-mitochondrial. Considering the extreme defect observed in growth rate by the *por* $^{-}$ strains, especially at cold temperatures, it seems contradictory for the latter two enzymes to be down-regulated. Lastly, outer mitochondrial membrane protein porin was identified as being down-regulated by 50 and 20 fold for Trial 1 and Trial 2 respectively. Given that WS004 is a genetic knockout for *por*, the expected ratio should have been infinitely large. Because of the convincing Western blot analysis and screen with PCR, contamination during sample processing after mitochondrial isolation is the likely explanation. However, had the knockout mitochondria not contained some wild-type mitochondria, the observed trends in ratios would be similar but with larger values. Therefore, the results obtained by the iTRAQ labelling of the wild-type and knockout mitochondria remain valid and offer evidence for: a dysfunction of the electron transport chain, possibly explaining the lack of energy required for wild-type like growth, and insight into a possible regulator of the proposed *aer* gene, ultimately responsible for the reduction in aerial hyphae and conidia production.

3.5 *Expression of Porin Variants in vivo*

3.5.1 *N-Terminal Modification to Porin*

Since the recent publications of the structure of mammalian porin, there has been some debate as to whether or not the crystal structure represents a physiologically relevant structure (Colombini 2010). Because the proteins used were produced using recombinant techniques and not isolated from membranes using a non-denaturing approach, it remains to be demonstrated that the fold is accurate. Porin can be isolated

from the MOM and purified using hydroxyapatite but the yield is low and the method is limited by its detergent selection (Freitag et al., 1982). Since different detergents can have subtle effects on the tertiary structure of porin (Bay et al., 2008) screening many different detergents may be required before suitable crystals for x-ray diffraction analysis can be produced. The use of a His_6 tag on a protein makes purification relatively simple without the limitations on detergent selection and should increase yield. It may also prove useful in co-purifying interacting protein or protein complexes.

3.5.1.1 *An N-Terminal His_6-tag interferes with Porin's Function*

In an attempt at making porin more accessible in folded form, a His_6-tagged porin variant was constructed. The purification tag was engineered into the 5' end of the gene encoding porin. The isolates collected from a transformation of *Neurospora crassa* strain FGSC 9719 were determined to be un-intentional heterokaryons, consisting of both a transformed nucleus and an un-transformed nucleus. Attempts at purifying a homokaryon only produced strains enriched for the transformed nuclei, which showed reduced growth rate and aerial hyphae production when compared to a wild-type strain (data not shown). This reduction in growth rate was interpreted as a reduction in functional porin molecules. This suggests the N-terminal His_6-tagged porin protein is non-functional. One possible explanation for the loss of function may be that the N-terminus is involved in gating of the pore (see Introduction for review), and the addition of the His_6-tag disrupts the mechanism. This however, made the protein insufficient for use in determining a physiological structure. For further details see appendix 5.2.

3.5.1.2 *A N-Terminal eGFP::Porin Fusion Impedes Import*

An eGFP::porin fusion was expressed in *Neurospora crassa* to allow the visualization of the mitochondrial morphology using fluorescent microscopy. In anticipation of all other N-terminal modifications to porin producing non-functional proteins, a heterokaryotic strain of *Neurospora crassa* was used to shelter the expression of an eGFP::porin fusion protein. *N. crassa* strain WS122 produces both wild-type porin and the eGFP::porin fusion protein from two different nuclei. Preliminary examination of this strain using fluorescent microscopy shows the eGFP:porin fusion protein predominantly in large circular structures, possibly nuclei or vacuoles. The lack of long tubular green fluorescing mitochondria within the hyphae of WS122 may be due to an impediment on the importability of the fusion protein. For further details see appendix 5.3.

3.5.2 *A C-Terminal His_6-Tagged Porin Variant functions in vivo*

A second attempt to add a purification tag was done by engineering the His_6-tag into the C-terminus of the gene encoding porin. Briefly, homologous replacement of the *por* gene with the His_6-tag version flanked with a hygromycin-resistance marker lead to the generation of strain WS005 (Figure 3.18A). WS005 was screened with PCR to confirm the successful integration and that it was a homokaryon. The primer set 5' Prom::pRS416 and porTerm 3' was used to amplify the *por* locus, which produced a 3217 bp fragment that included the integrated His_6-tag, *Sna*BI and *Spe*I restriction sites (Figure 3.18B). Digestion of the PCR product with the endonuclease *Sna*BI and *Spe*I showed a complete digestion, which confirmed the successful integration (Figure 3.18C) and lack of a wild-type *por* locus consisting of a 3190-bp fragment with no

Figure 3.18 *Confirmation of the C-terminal His_6-tagged porin variant.*

(A) Cartoon depiction of a successful integration of the C-terminal His_6-*por* gene within the endogenous *por* locus and the hygromycin resistance marker (*hph*), not to scale. The straight black arrows represent the primers used to amplify the locus, the yellow box represents the CACCACCACCACCACCAC sequence used to code the His_6-tag and the green lines correspond to the introduced endonuclease restriction sites not present in the wild-type *por* locus. (B) 5 µl of each of the products of the PCR reaction with primer set 5' Prom::pRS416 and porTerm 3' using isolated genomic DNA as template from FGSC 9720 (lane 2) and WS005 (lane 3). Lane 1 contains 2 µl of a 1 kb plus DNA ladder (Invitrogen). (C) 7 µl of the PCR product produced using WS005 genomic DNA as template was digested with *Sna*BI (lane 2) and *Spe*I (lane 3). Lane 1 contains 2 µl of a 1 kb plus DNA ladder (Invitrogen).

A

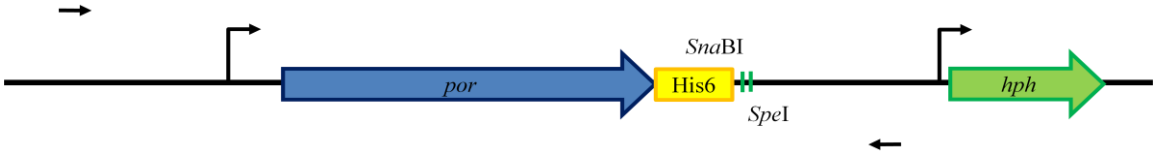
SnaBI
por
His6
hph
SpeI

B

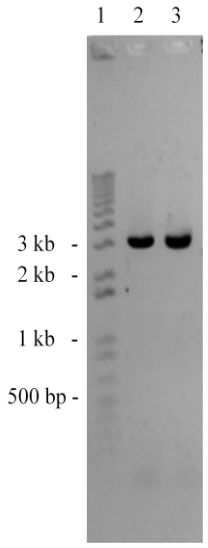
1 2 3
3 kb -
2 kb -
1 kb -
500 bp -

C

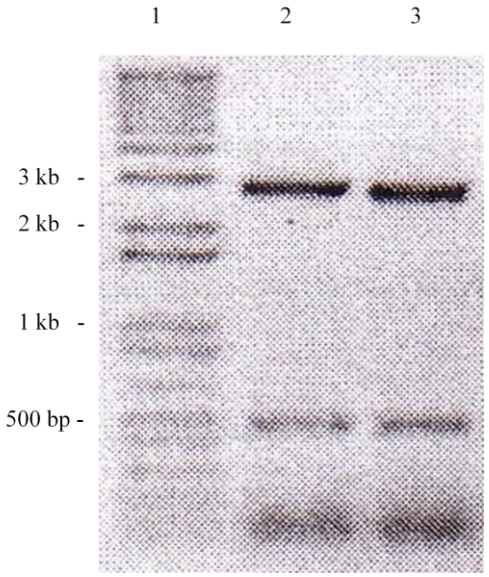
1 2 3
3 kb -
2 kb -
1 kb -
500 bp -

*Sna*BI and *Spe*I restriction sites. The entire *por* locus was then amplified and sequenced (data not shown).

The ability of the C-terminal His_6-tagged porin to complement the loss of wild-type porin was assessed using the race tube method (Figure 3.19). When grown at 23.5^{o}C ± 1^{o}C the WS005 strain grew about 82% of the rate of the control strain, FGSC 9718 (Table 3.5). However, when tested at 30^{o}C, the complementation ability of the porin variant was only about 60%, suggesting an elevated temperature phenotype, opposite to the cold sensitive phenotype of the porin minus strains. The reason for this remains unclear.

The C-terminal His_6-tagged porin proteins are successfully targeted to and imported into the mitochondrion. Mitochondria isolated from WS005 were analysed for the presence of His_6-tagged porin using Ni-NTA affinity chromatography. When the mitochondria were solubilised using 8 M urea as a denaturant and purified using a Ni-NTA resin, a protein of 30 kDa was concentrated and identified by Western blot analysis using a Ni-HRP conjugate probe as containing a His_6-tag (data not shown). Furthermore, His_6-tagged porin was purified using a non-denaturing method of solubilising mitochondria isolated from WS005 with 1% digitonin. Using the non-denaturing method, His_6-tagged porin was purified to homogeneity when visualized by SDS-PAGE and stained with Coomassie Blue R-250 (Figure 3.20). The concentration obtained was estimated to be 16 µM. In spite of the functional complementation, it does however remain to be shown that the C-terminal His_6-tagged porin variant is actually within the MOM and not just contained within the intermembrane space.

Figure 3.19 *Growth rate curve of WS005*.

(A) Graphical depiction of a representative growth rate of FGSC 9718 and WS005 growth in 40 cm race tubes at 23.5^{o}C ± 1 ^{o}C. (B) Graphical depiction of a representative growth rate of FGSC 9718 and WS005 growth in 100 cm race tubes at 30^{o}C ± 1 ^{o}C.

A

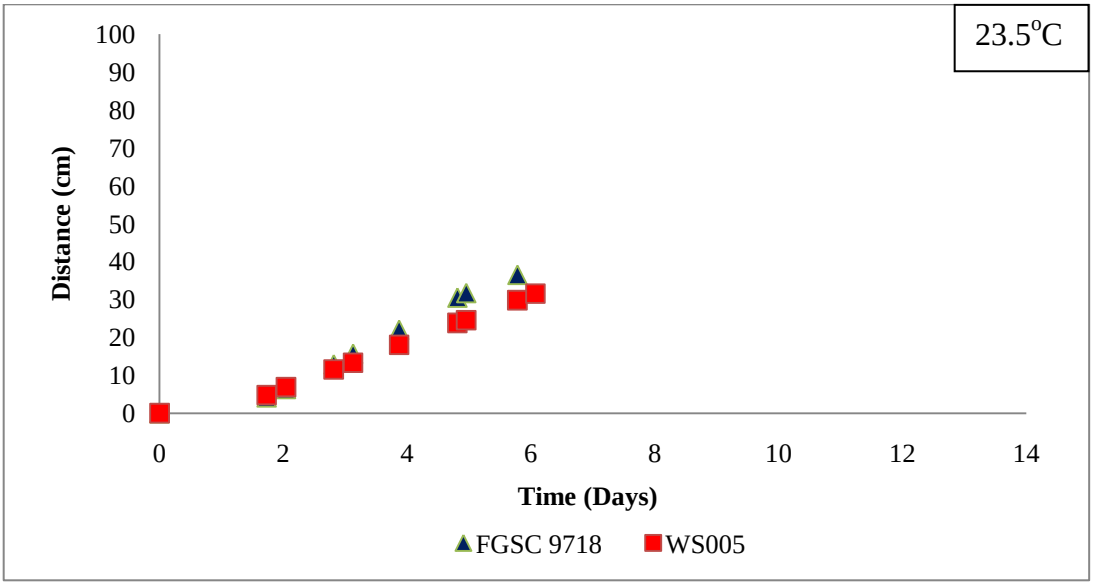
23.5°C
Distance (cm)
100
90
80
70
60
50
40
30
20
10
0
0
2
4
6
8
10
12
14
Time (Days)
FGSC 9718
WS005

B

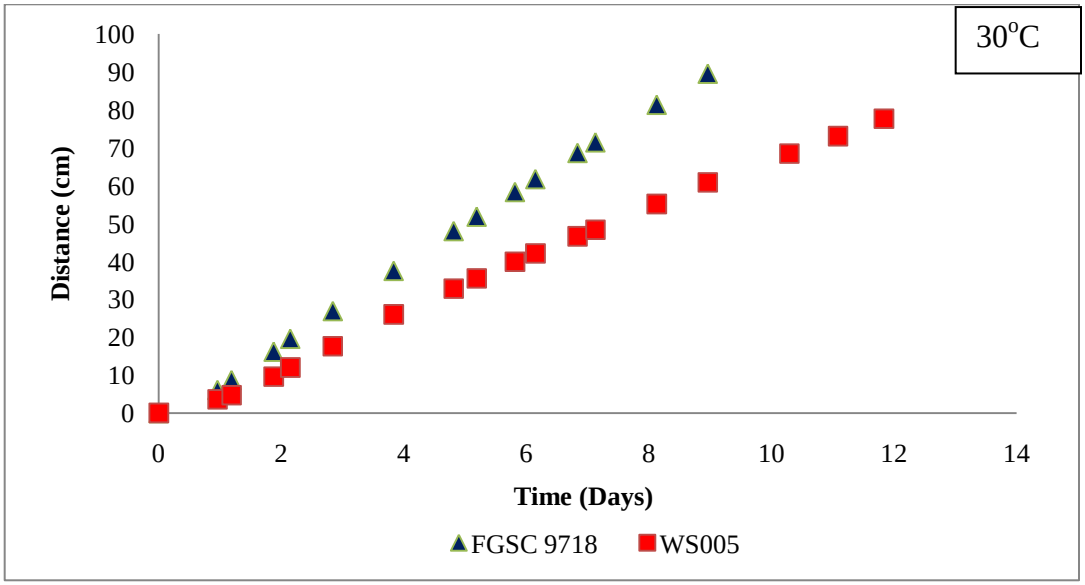
30°C
Distance (cm)
100
90
80
70
60
50
40
30
20
10
0
0
2
4
6
8
10
12
14
Time (Days)
FGSC 9718
WS005

Table 3.5 *The average growth rate of porin variants strains.*

Incubation Temperature	22 °C ± 2 °C		23.5 °C ± 2 °C		30 °C ± 2 °C	
	Average* cm / Day	% of FGSC 9718 Rate	Average cm / Day	% of FGSC 9718 Rate	Average cm / Day	% of FGSC 9718 Rate
Strain						
FGSC 9718	7.5 ± 0.5	n/a†	8.6 ± 0.3	n/a	10.6 ± 0.6	n/a
WS005	n/d†	n/a	7.0 ± 0.9	82	6.4 ± 0.7	60
WS125.5	1.1 ± 0.5	15				
WS126.1	6.3 ± 0.0	85	n/d	n/a	n/d	n/a
WS127.8	3.3 ± 0.3	90	n/d	n/a	n/d	n/a

* Average growth rate is calculated as the average growth rate of at least three race tubes.

† n/a, not applicable.

† n/d, not determined.

Figure 3.20 *Purification of porin by non-denaturing method.*
Isolated mitochondria from WS005 were solubilized with1% digitonin followed by a clarification spin. An aliquot from the resulting pellet is shown in lane 2. The supernatant was mixed with Ni-NTA superflow resin in a polypropylene column for 1 hour. The flow through was collected and an aliquot loaded into lane 3. The column was washed with wash buffer containing 0.5% digitonin and 10 mM and 30 mM imidazole with aliquots loaded into Lane 4 and Lane 5 respectively. Four sequential elutions were taken with elution buffer containing 250 mM imidazole (lanes 6-9). Lanes 1 and 10, molecular weight markers.

A

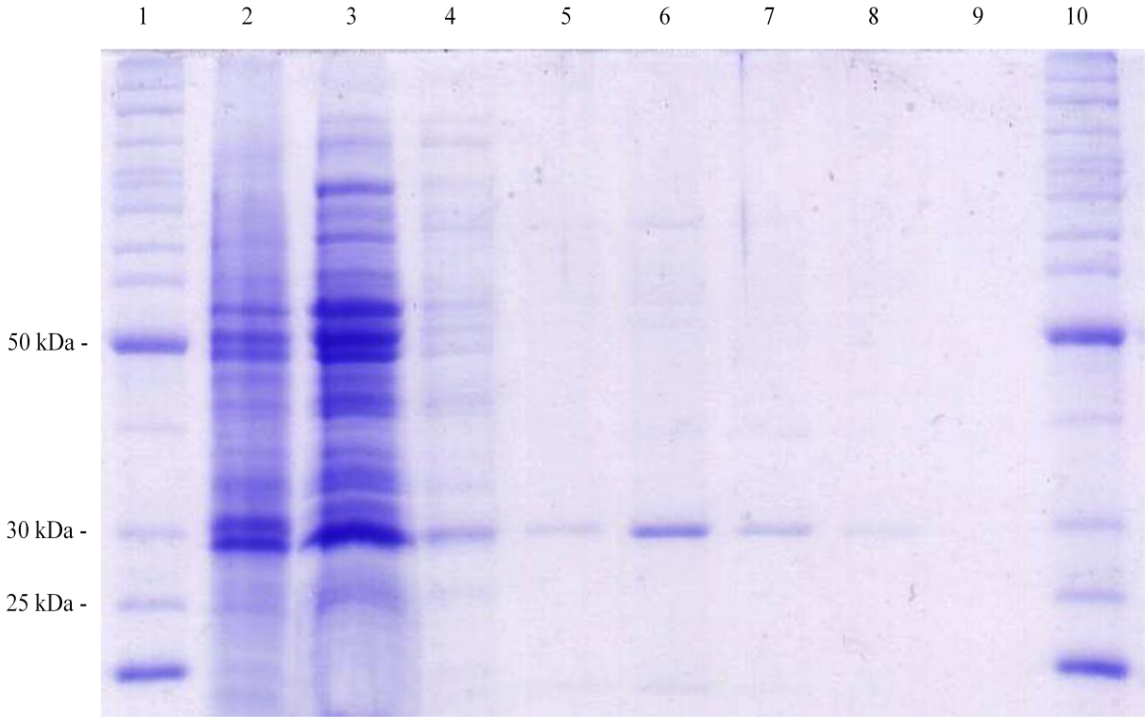

3.5.3 *The por⁻ Phenotype can be Complemented with a cDNA Variant*

Neurospora crassa has only one known isoform of porin encoded by the gene *por*, which like most eukaryotic genes, contains four introns disrupting the coding sequence. This can complicate the creation of small deletion variants if the sequence intended for deletion is bisected by an intron. It has been shown previously that some transcripts require an intron present for efficient translation (Le Hir et al., 2000). To determine if porin could be produced from a cDNA copy of the *por* gene, thus complementing the *por*⁻ phenotype, FGSC 18892 was transformed with the inserts in plasmid pRS416 NcPprom cDNA 3of4 porterm and pRS416 NcPprom cDNA porterm. The first case (transformation-1) was done with a gene for porin engineered to contain the first three introns, flanked by the endogenous upstream and downstream UTRs that presumably contained the required regions for efficient transcription. Transformation-2 was done using intron-free cDNA for porin flanked with the same UTRs. FGSC 18892 was selected for transformation because of its cold-sensitive temperature phenotype and an ectopic integration was the most likely event due to the fact that it is *mus*$^{+}$. From transformation plates incubated at 22^{o}C, four large colonies and one small colony from both transformations were picked to VM media slants, which were also incubated at 22^{o}C. From transformation-1, three out of the four large colonies picked showed growth rates similar to the control strain FGSC 9718 (data not shown). The small colony picked showed reduced growth rate when compared to FGSC 9718 as expected for a non-complemented isolate. The fourth large colony isolate, however, was unique in that it showed a growth rate similar to FGSC 9718 but reduced aerial hyphae production (data not shown). Similar results were seen from transformation-2. Three of the four large

colonies picked had growth rates comparable to the control strain FGSC 9718 (Figure 3.21). The small colony isolate, as well as the fourth large colony isolate, grew at a much slower rate compared to FGSC 9718. Since similar results were seen from both transformations, one isolate from transformation with intron-free cDNA, namely WS007, was chosen for further analysis. WS007 was confirmed to contain the hygromycin-resistance cassette within the *por* locus and the cDNA *por* insert elsewhere in the genome using PCR with a single primer set. This was done to demonstrate complementation, since a conventional complementation assay is not possible as no system of plasmid maintenance is developed for *Neurospora crassa*. The PCR reaction produced both, the 2203-bp fragment expected for the *por* locus containing *hph* and the 2304-bp fragment expected for the cDNA version (Figure 3.22A). To differentiate the two fragments from each other, the products were digested with an endonuclease specific for each fragment and a third endonuclease for which there are restriction sites found in both fragments (Figure 3.22B). The digestion with *Eco*RI cut the 2203-bp fragment into two fragments, an 832 bp and a 1371 bp; the 2304-bp fragment remained uncut. The digestion with *Hin*dIII was specific for only the 2304-bp fragment, and was cleaved into three fragments of 506 bp, 595 bp and 1203 bp, and left the 2203-bp fragment uncut. The third digest was aimed at cutting both fragments, and did so to completion. Digestion with *Xho*I therefore, cleaved the 2304-bp fragment into 4 pieces of 414 bp, 486 bp, 650 bp and 754 bp. The 2204-bp fragment was cleaved into a common fragment of 414 bp and the remaining 1790-bp fragment. Though it remains to be shown that the product of the cDNA *por* gene was indeed imported into the MOM, it would appear as though the *por*$^-$ phenotype was successfully complemented by a cDNA variant. Since the cDNA *por*

Figure 3.21 *Complementation of the por ˉ phenptype with a cDNA version of por*. Large colonies (lanes 1, 2, 3 and 4) and one small colony (lane 5) resulting from the transformation of FGSC 18892 conidia with a cDNA version of *por* were picked on to VM media slants and incubated at 22^{o}C for 3 days in complete darkness. Positive complementation was scored as comparable growth to the control strain FGSC 9718 (lane 7). A *por* ˉ control was also inoculated for comparison (lane 6).

A

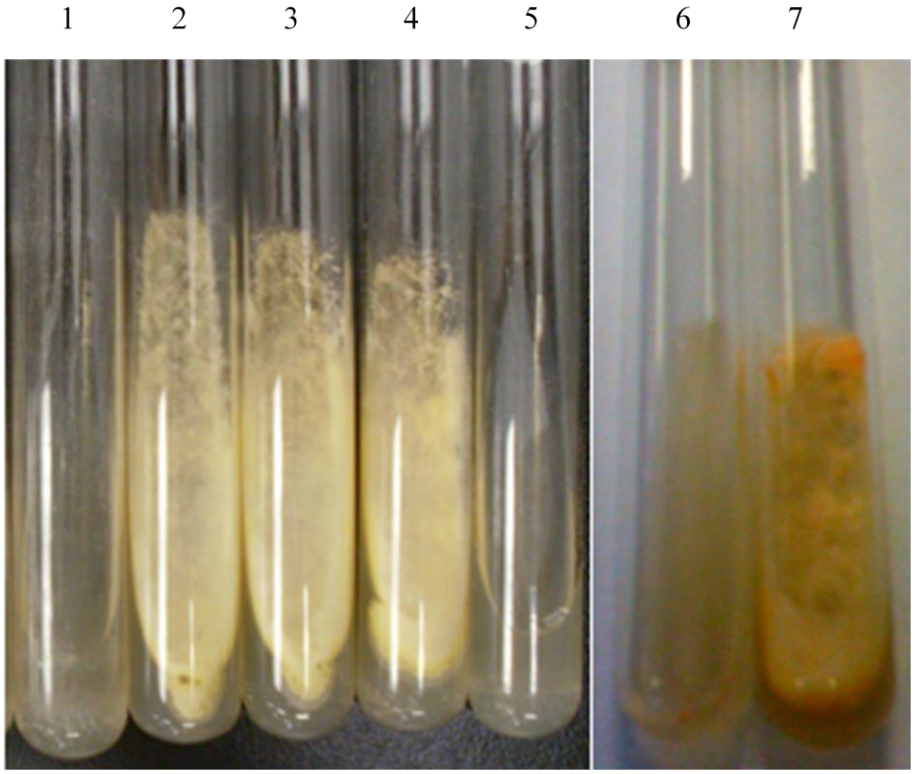

Figure 3.22 *PCR confirmation of the ectopic integration of the cDNA por gene within the WS007 genome*.

(A) PCR amplification of the *por* locus and the ectopically integrated cDNA *por* gene from isolated genomic DNA of WS007 using the primer set 5' Prom::pRS416 and porTerm 3' (lane 2). Lane 1 contains 2 µl of a 1 kb+ DNA ladder (Invitrogen). (B) Restriction endonuclease digestion of the PCR products in (A). The products of *Eco*RI digestion are shown in lane 3; the 2204-bp fragment was cut into the 832-bp and 1371-bp fragments shown. The 2304-bp band is the uncut cDNA *por* gene fragment. Lane 4 was digested with *Hin*dIII, which cut the 2304-bp fragment into the 506 bp, 595 bp and 1203 bp segments shown. The 2204 bp band is the uncut *por* locus fragment. In lane 5 are the products following digestion of the *por* locus with *Xho*I, which cut the 2304-bp fragment into 4 pieces of 414 bp, 486 bp, 650 bp and 754 bp. The 2204-bp product was cleaved into a 1790-bp fragment and a fragment of 414 bp. Lane 1 contains 2 µl of a 1 kb+ DNA ladder (Invitrogen) and Lane 2 is empty.

.

A

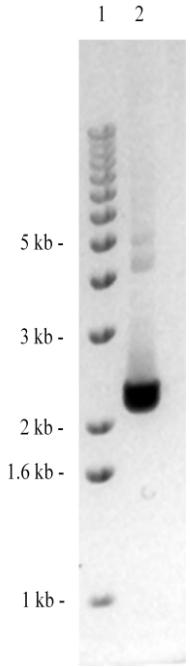
1
2
5 kb -
3 kb -
2 kb -
1.6 kb -
1 kb -

B

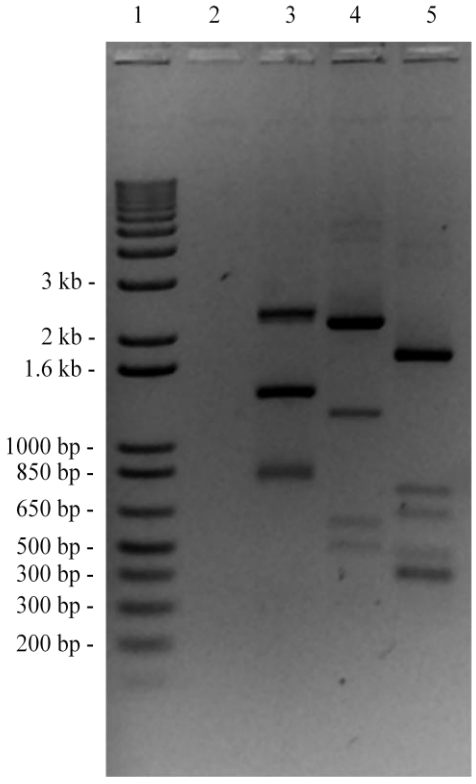
1
2
3
4
5
3 kb -
2 kb -
1.6 kb -
1000 bp -
850 bp -
650 bp -
500 bp -
300 bp -
300 bp -
200 bp -

gene appeared to complement the *por* ⁻ mutation, no further analysis of the isolates from transformation-1 was performed.

3.5.4 *Small Deletion Variants of Porin Failed the Complementation Test?*

The cold temperature sensitive phenotype of the *por* ⁻ strains is convenient for use as a selection for transformation with DNA that produces functional porin. Therefore, the use of complementation at a cold temperature was used to investigate the functionality of several small deletion variants of porin. The construct used for transformation was similar to the cDNA *por* gene used to prove complementation as in section 3.4.2 with the exception of small deletions encompassing either the N- or C-terminus or a short internal segment of 15-21 nucleotides. The plasmid constructs used are listed in Table 2.4 and described in section 2.9. Transformation of FGSC 18892 conidia with the variant cDNA from NcGR6, NcGR10, NcGR11, NcGR12, NcΔN-4 and NcΔC-2 resulted in transformation plates with only a lawn of germinating conidia present. The absence of any large colonies was taken to mean that none of the deletion variants tested produced functional porin within the MOM. However, it should be noted, that the amount of conidia plated without a drug for selection is less, making it more difficult to encounter a successful transformation product. The possibility of an unsuccessful transformation cannot be entirely ruled out either. In addition, should the deletion variant not function, there is no way to isolate a transformed colony for further analysis. Therefore, the strategy was revised to include a drug selection.

3.5.5 *Generation of Small Deletion Variants of Porin Strains*

The generation of the *Neurospora crassa* strains expressing porin molecules containing one of several small deletions was done so by using hygromycin resistance as

a transformation selection. The plasmids used are listed in Table 2.4. Isolates were screened with PCR using the primer set 5' Prom::pRS416 and porTerm 3' and the products were sequenced to confirm the successful integration of the mutant cDNA. A description of the further examination of individual deletion variants will follow. During the screening of isolates from the different variant *por* cDNA transformations, a common unexpected recombination event was observed. Instead of the recombination event occurring within the given 1400 bp of downstream UTR, recombination occurred within the fourth exon of *por* so as to incorporate the hygromycin resistance marker and the cDNA up to the end of the fourth exon (Figure 3.23). This resulted in the incorporated variant *por* cDNA containing the last intron.

3.5.5.1 *The N-Terminus of Porin is Required for its Function*

FGSC 9718 was transformed with a linear fragment of DNA as previously described consisting of the endogenous *por* locus upstream and downstream UTRs flanking a cDNA *por* gene that codes for a porin molecule with a deletion of amino acids 2-12 ($\Delta N_{2\text{-}12}$ porin). Isolate WS125.5 was identified by a PCR screen and sequencing of the *por* locus PCR product (Figure 3.24) to show that it contained the ΔN deletion. However, this also revealed that WS125.5 had incorporated the last intron as described above. Since the intron does not interfere with the intended deletion, WS125.5 was considered sufficient for further analysis. Race tubes were inoculated with WS125.5 to determine the growth rate (Figure 3.25). For reasons that remain unclear, the inoculations showed little to no growth, with sporadic growth spurts throughout the duration of the experiment. The average rate of this growth, however, is comparable to the rate obtained for WS004 (Table 3.5). Also, the ability of WS125.5 to produce aerial

Figure 3.23 *The homologous recombination integration of deletion variant cDNA.* (A) Cartoon representation of the expected homologous recombination event during the transformation of FGSC 9718 conidia with a deletion variant cDNA fragment. The numbered red boxes indicate three separate deletion variants cDNAs that code for $\Delta N_{2\text{-}12}$ porin, $\Delta_{238\text{-}243}$ porin and $\Delta C_{269\text{-}283}$ porin respectively and were transformed independently of each other. The thin purple lines separating the purple boxes represent the introns in the genomic DNA sequence. (B) Cartoon representation of the results obtained from the actual recombination event which occurred during the transformation. The grey X's represent the expected (A) and proposed (B) sites at which strand invasion and subsequent resolution of the Holliday intermediate occurred.

A

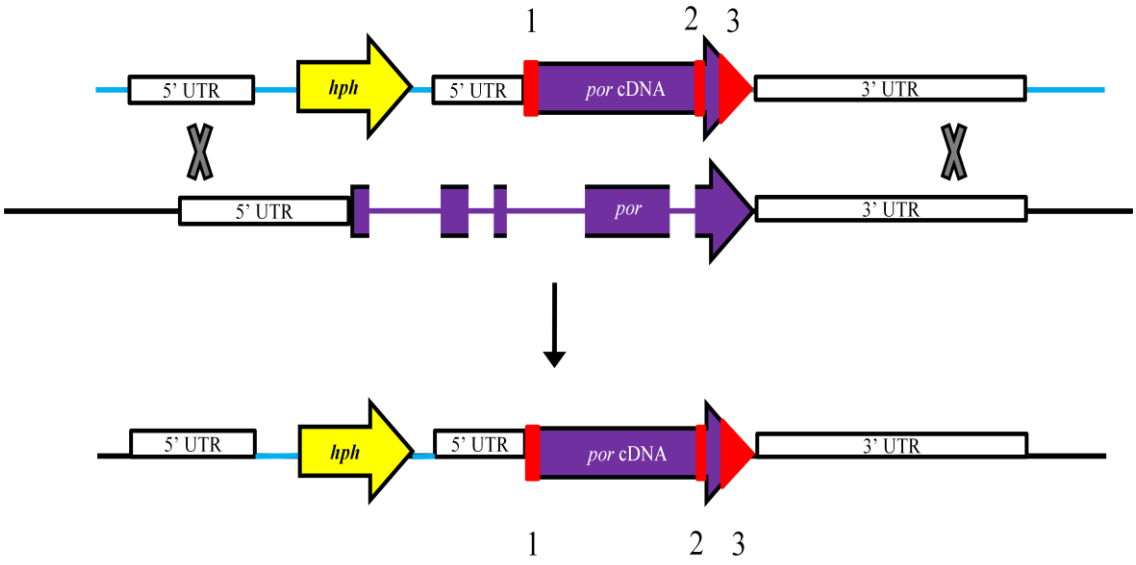
1
2
3
5' UTR
hph
5' UTR
por cDNA
3' UTR
5' UTR
por
3' UTR
5' UTR
hph
5' UTR
por cDNA
3' UTR
1
2
3

B

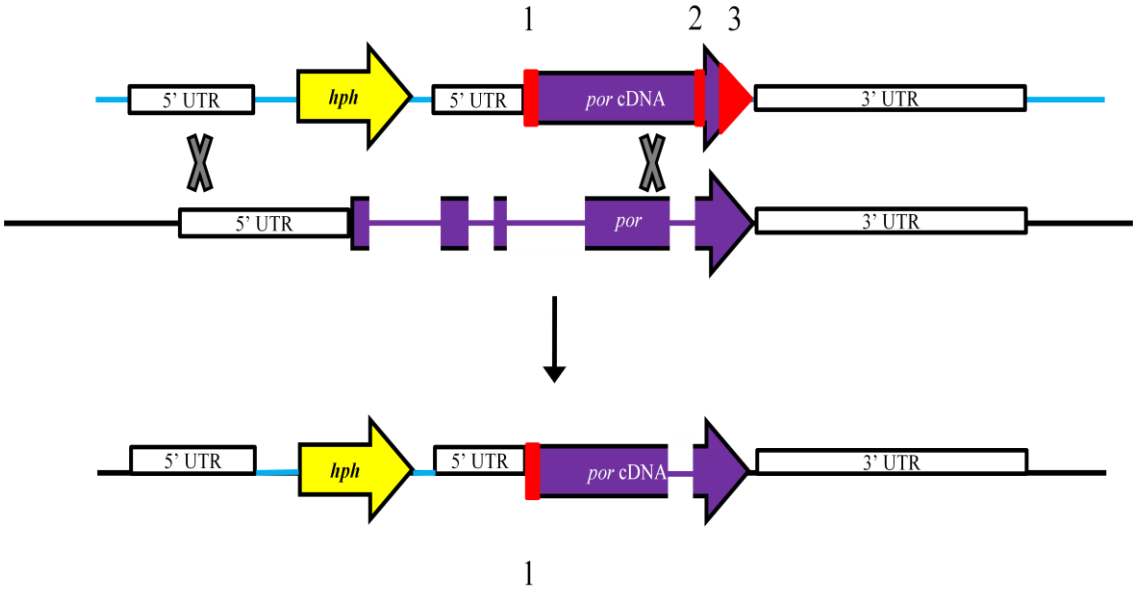
1
2
3
5' UTR
hph
5' UTR
por cDNA
3' UTR
5' UTR
por
3' UTR
5' UTR
hph
5' UTR
por cDNA
3' UTR
1

Figure 3.24 *PCR confirmation of integrated deletion variant cDNA.*
(A) The *por* locus was PCR amplified from isolated genomic DNA of FGSC 9718 (lane 2), WS126.1 (lane5), WS127.8 (lane 6) and WS125.5 (lane 8). Amplification of the wild-type locus results in a 3190 bp fragment. Amplification of the variant DNA is expected to be 3739 bp, 3766 bp and 3751 bp for WS126.1, WS127.8 and WS125.5 respectively. Bands indicated by the asterisks were gel extracted and sequence to confirm the integration of the variant DNA. Lanes 1, 4 and 7, 1 kb^{+} ladder. (B) Amplification of the por locus using genomic DNA from the initial isolate of WS127.8 produced both, the wild-type and variant expected fragment sizes indicated by the arrows.

A

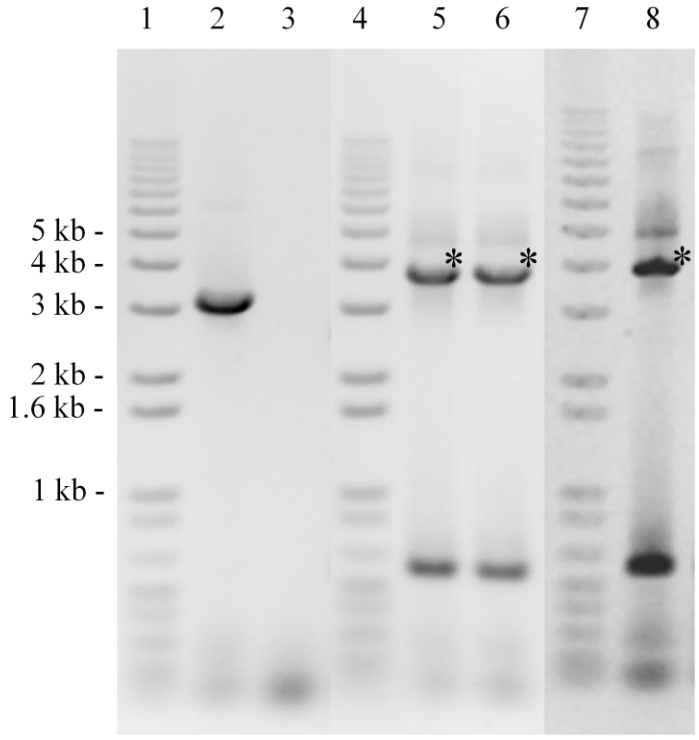

B

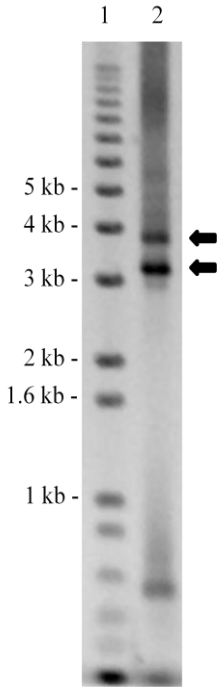

Figure 3.25 *Comparison of the growth rates of the deletion variant strains.*

Conidia from deletion variants WS125.5, WS126.1 and WS127.8 and the control strain FGSC 9718 were used to inoculate 100 cm race tubes. The tubes were incubated at 22^{o}C ± 2^{o}C with regular day light cycles. The growth fronts were mark once or twice daily. The graph shows only one representative growth curve from each strain.

A

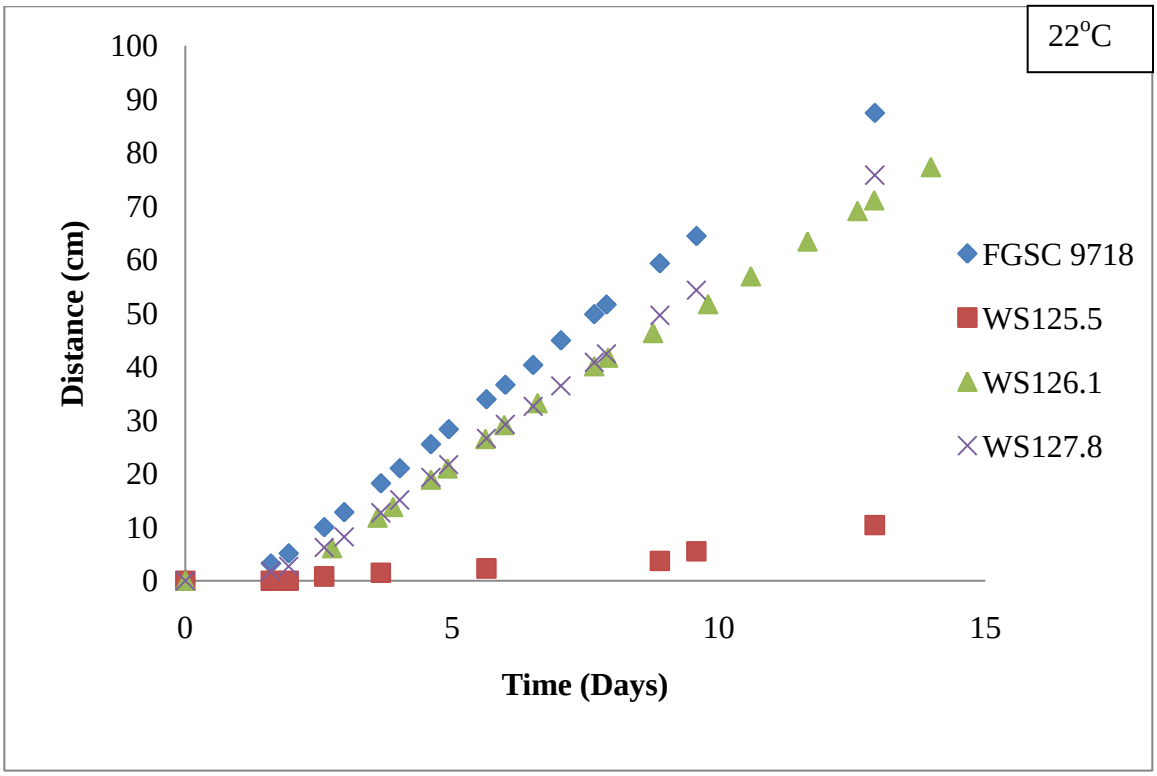
22°C
100
90
80
70
60
50
40
30
20
10
0
Distance (cm)
0
5
10
15
Time (Days)
FGSC 9718
WS125.5
WS126.1
WS127.8

hyphae was reduced, similar to strain WS004 (Figure 3.25). This would suggest that the $\Delta N_{2\text{-}12}$ porin cannot work as a replacement for wild-type porin either due to a loss in function or failure to import into the MOM. Both possibilities however, remain to be examined.

3.5.5.2 *The C-Terminus is Not Required for Porin Function*

FGSC 9718 was transformed with a linear fragment of DNA consisting of the endogenous *por* locus upstream and downstream UTRs flanking a cDNA *por* gene that codes for a porin with a deletion of amino acids 269-283 ($\Delta C_{269\text{-}283}$ porin). Isolates were screened with PCR using the primer set 5' Prom::pRS416 and porTerm 3' and the product was sequenced to confirm the successful integration of the mutant cDNA (Figure 3.24). Isolate WS126.1 was selected for further analysis. When grown in conidia flasks, WS126.1 exhibited a similar phenotype to WS004 with regards to both aerial hyphae and conidia production (Figure 3.26). However, the growth rate of WS126.1, determined using the race tube method, differed from the rate of WS004 (Figure 3.25). Interestingly, when WS126.1 was grown at $22^{o}C \pm 2^{o}C$, it grew at 85% of the rate of the control strain FGSC 9718 (Table 3.5). The vast improvement in growth over the porin-lacking strains, would suggest that WS126.1 is producing a feasible replacement for wild-type porin. This would also suggest that the last 14 amino acids are not necessary for mitochondrial targeting or assembly into the MOM. Recently, it was determined that the last 14 amino acids of porin contain a β-sorting signal, conserved in the terminal β-strand of all β-barrel proteins destined for the MOM, and required for the recognition by SAM35 of the SAM complex (Sorting and Assembly complex) and subsequent assembly of β-barrel proteins into the MOM of isolated mitochondria (Kutik et al., 2008). To determine whether or not

Figure 3.26 *Aerial hyphae production by the porin deletion variant strains.* Conidia flasks were inoculated with FGSC 9718, WS125.5 and WS126.1 and incubated at 30^{o}C for 4, 7 and 7 days respectively. Aerial hyphae production was scored by the existence of hyphae up off of the media surface.

A

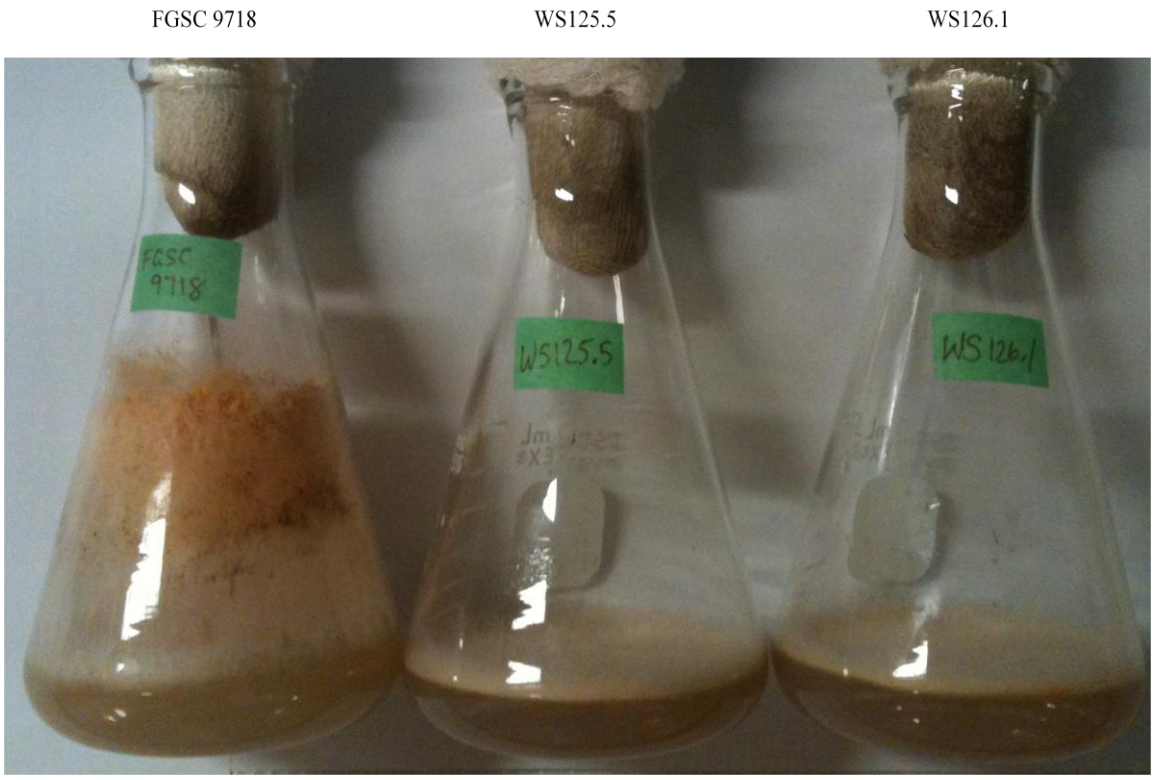

this was the case, mitochondria from FGSC 9718 and WS126.1 grown at 30^{o}C were isolated using a differential centrifugation purification method and subjected to 12% SDS-PAGE and Western blot analysis (Figure 3.27). The supernatant from the initial spin, which contains the cytoplasmic contents, was also collected and subjected to the same treatments as the mitochondria. Immunodetection with an antibody for porin revealed the majority of the $\Delta C_{269\text{-}283}$ porin was in fact in the mitochondria as opposed to the cytoplasm. However, densitometry analysis used to quantitate the chemiluminescence of the blot showed a 3.4-fold reduction in the signal representing the amount of porin present in the WS126.1 mitochondria compared to the FGSC 9718 mitochondria. This result was surprising, since it was expected that without the β-sorting signal, porin assembly into the MOM would be far more reduced than observed, if not absent entirely. Sequence analysis of the newly created terminal β-strand of the $\Delta C_{269\text{-}283}$ porin (β-strand 18 in the wild-type sequence) revealed a putative β-signal which could possibly provide the function of the signal lost in the deletion of β-strand 19 (Figure 3.28). Together, this suggests that the proposed β-sorting signal by Kutik *et al.*, (2008) may indeed be required for the import and assembly of porin into the MOM. Although, it remains to be shown that the reduction in porin concentrations observed is not in fact due to reduced transcription of the variant gene.

The increased growth rate of WS126.1 over the rate of WS004 suggests an increase in energy output by the mitochondria. Therefore the cytochrome content of WS126.1 was determined as previously described. The mitochondria of WS126.1 cultivated at 30^{o}C, produced a cytochrome spectrum similar to WS004 at first glance (Figure 3.29A). Analysis of the difference spectrum for WS126.1 showed similar

Figure 3.27 *Immunodetection of porin in WS126.1 mitochondria.*
Mitochondria from FGSC 9718 and WS126.1 grown at 30^{o}C were isolated and purified using differential centrifugation purification. The supernatant of the first centrifugation set contains the cytoplasmic contents of the mycelium and was collected for analysis. Equal amounts of cytosolic proteins (25 µg per lane) were loaded in Lanes 2-4 and Lanes 8-10 for WS126.1 and FGSC 9718 respectively. Equal amounts of mitochondrial protein (25 µg per lane) from WS126.1 (lanes 5-7) and FGSC 9718 (lanes 11-13) were loaded in triplicate and separated with 12% SDS-PAGE. Western blot analysis was performed using antibodies for TOM70 and Porin. Chemiluminescence was detected using a FluoroChem Imager and the captured images used for densitometry analysis. (B) The TOM70 and porin blot was Ponceau stained and then scanned for comparison of protein loading. Lanes 1 and 9, molecular weight markers.

A

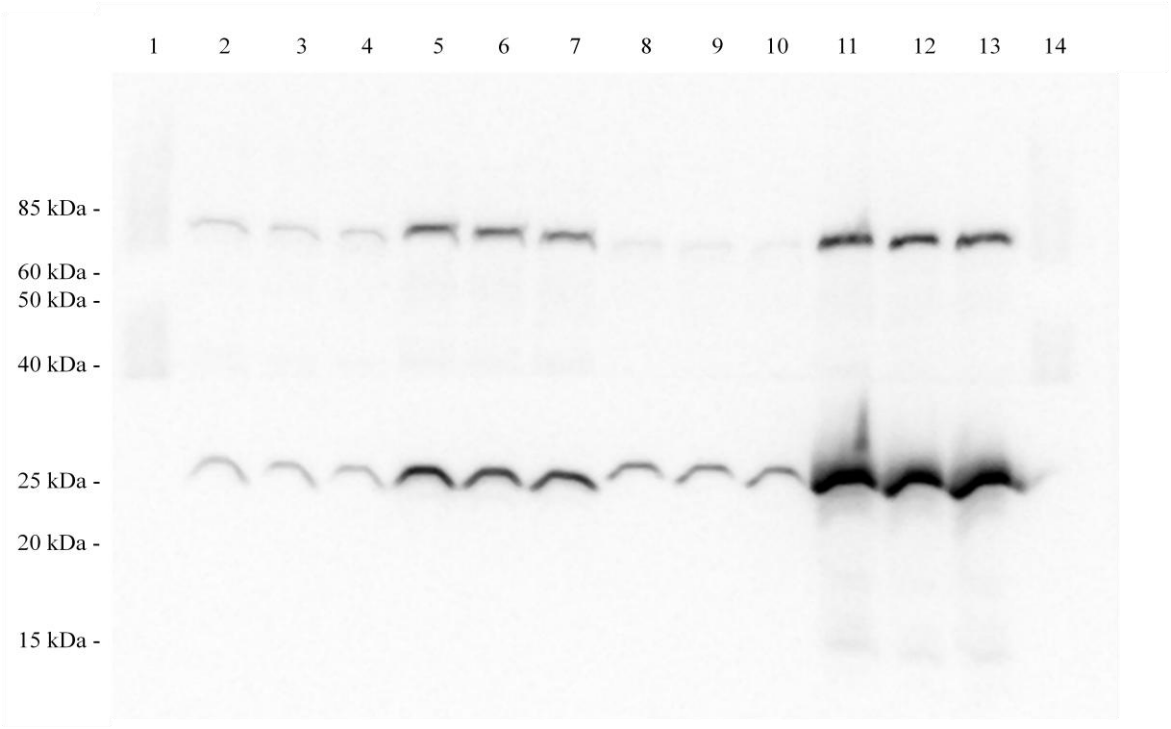
1 2 3 4 5 6 7 8 9 10 11 12 13 14
85 kDa -
60 kDa -
50 kDa -
40 kDa -
25 kDa -
20 kDa -
15 kDa -

B

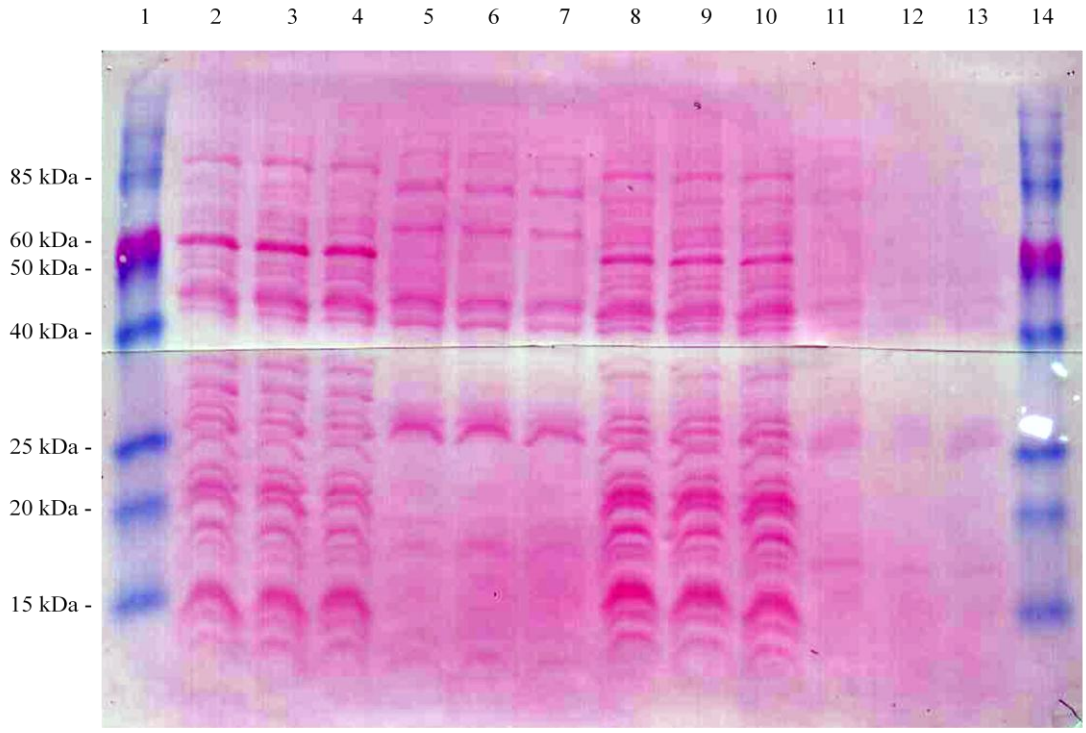
1 2 3 4 5 6 7 8 9 10 11 12 13 14
85 kDa -
60 kDa -
50 kDa -
40 kDa -
25 kDa -
20 kDa -
15 kDa -

Figure 3.28 *$\Delta C_{269\text{-}283}$ porin contains a putative β-sorting signal within its last β-strand.* The sequence criteria for the β-sorting signal is given (top row; Kutik et al., 2008) . X = any residue, **π** = polar residue, **ϕ** = hydrophobic residue, n = 1-28. The C-terminal sequence of wild-type porin (middle row) and $\Delta C_{269\text{-}283}$ porin (bottom row) are shown with the residues corresponding to the β-sorting signal in bold. It should be noted that the putative β-sorting signal found within $\Delta C_{269\text{-}283}$ porin would also be present in wild-type porin within β-strand18. The subscripted number at the end of the porin sequences represents the amino acid position within the sequence. Underlining depicts the predicted nineteenth β-strand of wild-type porin and the eighteenth β-strand in $\Delta C_{269\text{-}283}$ porin. Amino acid residues are depicted using the single letter code.

A

β-signal	X	X	**π**	X	**G**	X	X	**ϕ**	X	**ϕ**	$X_{(n)}$

Wild-type porin	T_{272}	H	**K**	V	**G**	T	S	**F**	T	**F**	E S_{283}
$\Delta C_{269\text{-}283}$ porin	G_{253}	V	**T**	L	**G**	V	G	**A**	S	**F**	$DTQKLN_{268}$

Figure 3.29 *Cytochrome content of WS126.1*.

Isolated mitochondria were solubilised with 2% DOC and the resulting supernatant from a clarifying spin was oxidized with potassium ferricyanide. The absorbance was measured as a wavescan from 500 nm to 650 nm. The solution was then reduced using sodium dithionite and the wavescan repeated. (A) Presented, is the difference spectra (reduced-oxidized) for mitochondria isolated from FGSC 9718, WS004 and WS126.1 cultivated at 30^{o}C. FGSC 9718 was confirmed to have a wild type spectra by comparison with a spectra collected using isolated mitochondria from FGSC 987 (data not shown). (B) The quantitation of the cytochrome levels is shown as an average of at least three biological replicates in for the indicated cultures grown at 30^{o}C. The error bars represent the standard deviation.

A

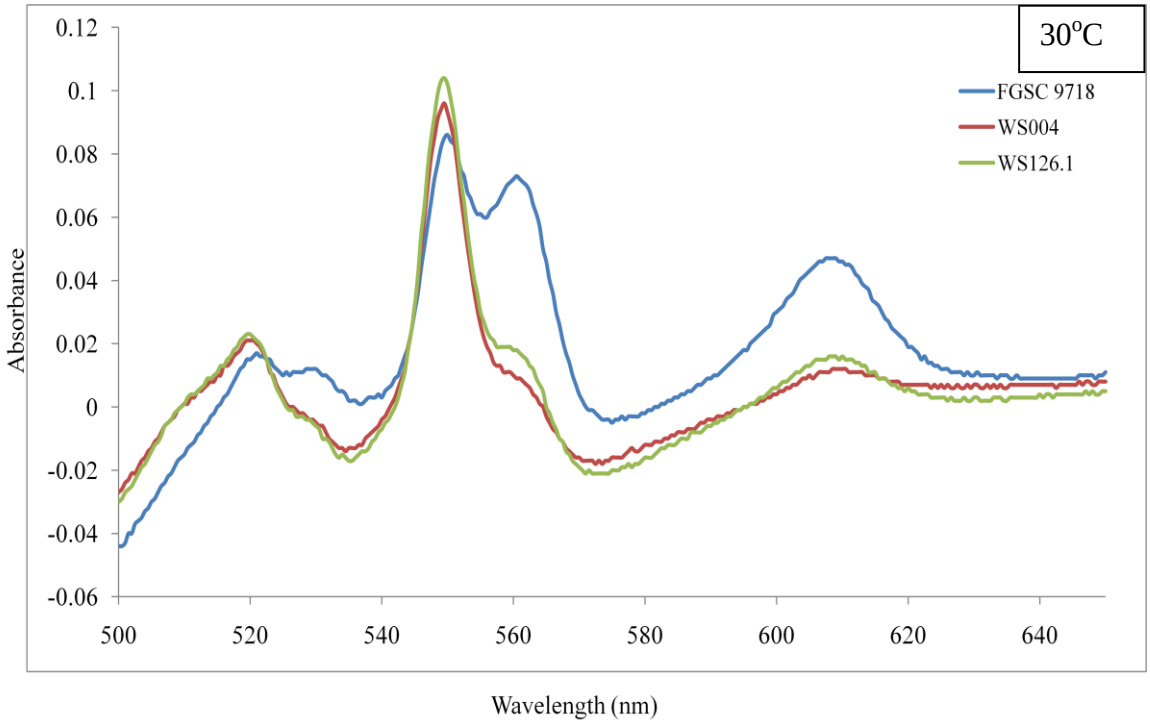
30°C
FGSC 9718
WS004
WS126.1
Absorbance
0.12
0.1
0.08
0.06
0.04
0.02
0
-0.02
-0.04
-0.06
500
520
540
560
580
600
620
640
Wavelength (nm)

B

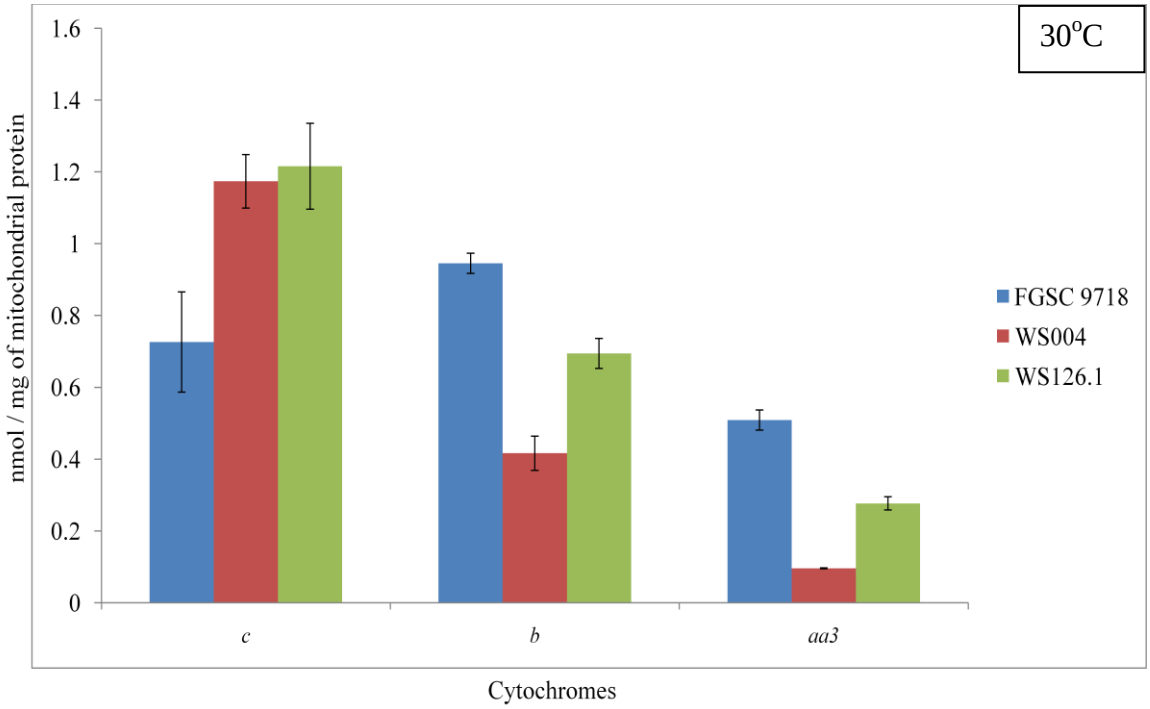
30°C
FGSC 9718
WS004
WS126.1
nmol / mg of mitochondrial protein
1.6
1.4
1.2
1
0.8
0.6
0.4
0.2
0
c
b
aa3
Cytochromes

amounts of cytochrome *c* when compared to WS004, which for both strains was significantly higher than the levels observed for FGSC 9718 (Figure 3.29 B). Interestingly, the levels of cytochrome *b* and aa_3 were centred between the levels in WS004 and FGSC 9718. The increase in cytochromes *b* and aa_3 levels is likely responsible for the near wild-type growth rate of WS126.1 by increasing the functionality of the ETC. The mechanism by which porin affects the level of cytochromes remains to be determined. Given that the level of $\Delta C_{269\text{-}283}$ porin in the MOM is less than half of the normal level, and the restoration of cytochrome *b* and aa_3 levels are nearly half, one possibility is the cytochrome levels are somehow influenced by the level of porin in the MOM.

3.5.5.3 *The Expression* of *ΔNDRGV Porin can Complement the por⁻ Growth Rate*

FGSC 9718 was transformed with a linear fragment of DNA consisting of the endogenous *por* locus upstream and downstream UTRs flanking a cDNA *por* gene that codes for a porin with a deletion of amino acids 238-242. Isolates were screened with PCR using the primer set 5' Prom::pRS416 and porTerm 3' and the product was sequenced to confirm the successful integration of the mutant cDNA. The sequence of WS127.4 showed an unintentional recombination incorporating the fourth intron as described above. The intended deletion is within the last exon of the gene and therefore was not incorporated into isolate WS127.4; no further analysis was considered. The sequence of WS127.8 showed evidence of both a wild-type locus and a variant *por* gene, making this strain an unintentional heterokaryon (Figure 3.24B). This isolate was purified to a homokaryon by spreadplating a few conidia onto VM + hygromycin plates. After 3 days of incubation at 30^{o}C a single colony was picked to a VM + hygromycin

slant. This process was repeated through 5 rounds before genomic DNA was isolated and rescreened with PCR. This process successfully purified WS127.8 to a homokaryon with only a variant *por* locus (Figure 3.24A). The growth rate of WS127.8 was determined using the race tube method (Figure 3.25). WS127.8 grew 90% of the control strain FGSC 9718 suggesting successful import and assembly of the ΔNDRGV porin (Table 3.5). No further analysis has been done to confirm this.

Chapter 4: Discussion

4.1 *Neurospora crassa por Knockout Strains*

Mitochondrial porin was originally characterized as a non-essential protein in yeast. The yeast genome contains two paralogues of the gene which codes for porin (Blachly-Dyson et al., 1997). Interestingly, the product of the second yeast isoform is also a non-essential protein (Blachly-Dyson et al., 1997). Given that porin is considered to provide the primary pathway for the movement of metabolic substrates across the MOM, it was expected that cells lacking porin would be respiratory deficient. Annotation of the *Neurospora crassa* genome predicts only a single isoform. In this study, the *Neurospora crassa* homologue was determined to be non-essential, but its absence is not without consequence.

The increased frequency of homologous recombination of the *mus-51* mutant strain FGSC 9718, was exploited to replace the *por* gene with a cassette that confers resistance to hygromycin. PCR analysis of the endogenous *por* locus confirmed the successful replacement and that there was no wild-type locus present either as a second copy located elsewhere in the genome, or from the presence of a second nucleus (a heterokaryon). The Southern blot of *Neurospora crassa* genomic DNA probed with the *por* gene revealed only the expected fragments for that gene, suggesting that porin is encoded by a single gene. Consistent with this conclusion, two independently constructed deletions of *por* resulted in two strains which produced no immunologically detectable porin with a polyclonal antibody raised against amino acids 7-20 of porin. Although the mounting evidence suggests only one porin isoform, a similar criteria was

used to analyze the yeast Δ*por1* strain prior to the identification of a suppressor to the yeast temperature sensitive phenotype (discussed in Blachly-Dyson et al., 1997). Therefore, the possibility of a second isoform for porin in *Neurospora crassa* cannot be ruled out entirely.

The lack of porin causes a reduction in growth rate. As made evident by the two independently constructed *por*$^{-}$ strains, the amount by which the growth rate is reduced can vary with other genetic factors (discussed further below). Nevertheless, the observed difference in growth rate for either mutant strain was considerable. The most obvious explanation for the reduction in growth rate is merely the lack of metabolite translocation, resulting in reduced energy output by the mitochondria, irrespective of the results from the ATP concentration analysis (section 3.3.2.5). This would suggest that the other β-barrel proteins within the MOM, namely TOM40 and TOB55, cannot completely complement the lack of porin. The possibility of these protein channels being able to contribute any compensatory translocase function however remains to be shown.

As in yeast, the growth rate deficiency caused by the lack of porin in *Neurospora crassa* is a temperature sensitive phenotype. Interestingly though, the yeast deficiency in growth was observed at elevated temperatures (37^{o}C) whereas the *Neurospora crassa* phenotype was a cold temperature sensitivity, observable at 30^{o}C and increased in severity at even lower temperatures (22^{o}C). One possible explanation for this observation could be the membrane composition of the mitochondria. *Neurospora crassa* produces sterols, ergosterol being the most predominant in the outer membrane, which function similarly to cholesterol in mammalian cells, but with stronger activity in promoting ordered lipid domains (Czub and Baginski, 2006). The lack of porin in the MOM of the

por ⁻ strains means diffusion of water, ions and other metabolites must be by means of an alternative aqueous channel or by passive diffusion across the MOM. While other membrane channels may provide some substituted function for porin, their action might not be expected to differ with temperature. Rather, the temperature dependence may be in part due to insufficient sterols within the MOM to maintain membrane fluidity, thereby reducing the amount of passive diffusion occurring at lower temperatures. Sterols also influence protein behaviour, such as the requirement of ergosterol for wild-type like function of VDAC examined in PLB (Popp et al., 1996) and therefore may affect the behaviour of other proteins as well. In addition the lack of sterols may affect the behaviour of MOM proteins indirectly by the changes in membrane fluidity. The anabolic pathways which produce the sterols require NADPH, which may be in low concentration given the down-regulation of ketol-acid reductoisomerase in strain WS004. The effect of even a small reduction in sterol amounts may be exaggerated by the loss of porin itself. The lack of porin, being the most abundant protein in the MOM, may reduce membrane fluidity because there is less integral membrane protein to disrupt lipid packing. This hypothesis of alterations in membrane fluidity can be examined using the fluorescent probe 6-dodecanoyl-2-dimethylamino-naphtalene (laurdan) and calculating the ratio of fluorescence at 440 nm versus 490 nm (F_{440}/F_{490}). Values could be determined for wild-type and porin-lacking mitochondria and then compared: the higher the ratio the lower the membrane fluidity.

The cytochrome content of both *por* ⁻ strains was determined and showed evidence of a temperature dependent expression of cytochrome aa_3 and possibly cytochrome *c* in strain FGSC 18892. The extremely low levels of cytochrome aa_3

measured at either the permissive or non-permissive temperature imply reduced levels of functional complex IV of the ETC. The reason for the loss of porin to cause these alterations in cytochrome levels remains unclear. It is possible that the deletion of *por* has indirectly affected a regulatory element required for COX assembly. Although subunit 1 of cytochrome *c* oxidase (COX) is encoded by mitochondrial DNA, and synthesised on mitochondrial ribosomes, it has been shown previously that nuclear mutations also can result in the absence of subunit 1 (Nargang et al., 1978). This strain of *Neurospora crassa* was characterized by slow growth and contained no spectrally detectable cytochrome aa_3 similar to the *por* $^-$ strains. However, the deletions made in constructing the *por* $^-$ strains include a relatively short flanking region of untranslated DNA not spanning neighbouring annotated genes. If the deletion removed a regulatory element, the proposed element would have to be porin itself.

The notion of porin acting as a regulatory element at the level of COX assembly may be reasonable because a physical interaction between porin and COX has been detected (Roman et al., 2005). The interaction between porin and COX would require their assembly at sites of contact between the inner and outer membrane. Although, it remains to be determined if this interaction supports the formation of the contact sites thus playing a role in maintaining the cristae structures formed by the inner membrane. The rate of oxidation of cytochrome *c* by COX has been previously shown to be enhanced when porin is added during an *in vitro* assay demonstrating a physical interaction between the two proteins (Roman et al., 2005). It can be postulated then, that the reduced activity of COX in the absence of porin may signal the down regulation of the pathway to prevent wasteful production of dysfunctional ETC components in an

already energy-deprived system, assuming the translocation of ADP is reduced in response to porin loss. The shutdown of the ETC then makes necessary the existence of an alternate pathway to ensure viability and this is found in the alternative oxidase pathway.

To test the hypothesis that induction of the alternative oxidase pathway was occurring in the *por* ⁻ strains, their response to potassium cyanide was determined. Normal cytochrome-mediated respiration is KCN sensitive at complex IV, resulting in the termination of oxygen consumption. Oxygen consumption in both WS004 and FGSC 18892 continued in the presence of KCN, suggesting that oxygen was being reduced by some other pathway. The alternative oxidase pathway is suggested by the sensitivity of both to salicylhydroxamic acid (SHAM), a known inhibitor of the alternative oxidase (Lambowitz and Slayman, 1971). This was not that surprising given that the levels of cytochrome aa_3 were almost undetectable at 22^{o}C but the organism remained viable. What was interesting was the high degree of induction of the alternative oxidase pathway at 30^{o}C, particularly in FGSC 18892 given that the growth rate of FGSC 18892 compared to FGSC 9718 at the same temperature, was only reduced by 26%. In comparison, the response of 74A^{d} to KCN was only a partial inhibition of oxygen consumption with the complete shutdown in respiration occurring only after the addition of SHAM. This suggests both pathways are functioning to some degree in 74A^{d} but not in either FGSC 18892 or WS004. It has been shown, that the alternative oxidase pathway can be induced by heat shock (Michea-Hamzehpour and Turian, 1987), inhibitors that indirectly affect the level of ETC components (discussed in Chae and Nargang, 2009) and its activity stimulated when in the presence of nucleoside 5'-monophosphates (Vanderleyden et al.,

1980). Therefore, the induction of the alternative oxidase pathway is most likely in response to the defective state of the ETC.

An attempt to explain the variation in growth rate of the porin lacking strains by a lack of energy was undertaken by quantifying the ATP concentration within the cytoplasm and isolated mitochondria. However, the results showed no discernable difference in ATP concentrations among the mitochondria of FGSC 9718 and the porin-lacking strains. It may be, having not provided the mitochondria with a metabolic substrate from which to continue producing ATP, that the levels observed in all mitochondria are at a rather minimally sustainable concentration. The results obtained from the cytoplasmic fractions may provide some evidence to support the idea that intramitochondrial levels are not the limiting factor for growth. If the level of ATP in the cytoplasm was high enough and the rate of decay was constant for all strains, then the minimum concentration may not have been attained in the cytoplasm. Thus, the concentrations obtained may not be the absolute concentration available during the growth of the fungus, but rather the remaining concentrations may be relevant for comparison. FGSC 9718 grown at 22^{o}C contained 7.1 µM ATP / mg of protein, while FGSC 18892 contained 2.9 µM ATP / mg or 41% of the ATP available to FGSC 9718. Interestingly, the growth rate of FGSC 18892 when grown at 22^{o}C is 42% that of FGSC 9718, suggesting the available ATP level may in fact be controlling the rate of growth. The same trend was observed with WS004 grown at 22^{o}C, with the ATP concentrations within the cytoplasm being 17% of that of FGSC 9718. The growth rate of WS004 was determined to be 15% of the rate attained for FGSC 9718, which is also in agreement with the hypothesis that limiting cellular ATP is the cause of the reduced growth rate. To

obtain a more accurate measurement of physiologically relevant levels of available ATP, all metabolic activity would need to be stopped to prevent ATP decay. However, the isolation of intact mitochondria limits the available means of ceasing metabolic activity, such as the damage to membrane which occurs during flash freezing. Therefore, all samples were treated identically and in a timely manner to determine the ratio of available ATP between the control strain and the porin lacking strains.

4.2 *Genetics Underlining the Different Phenotypes*

The method of creating the two independently constructed *por* ⁻ strains examined in this study differs at the stage of purification of a homokaryon. WS004 was isolated through repeat streak-plating of conidia until a colony resulting from a homokaryotic conidium was picked and identified with a PCR screen. In contrast, FGSC 18892 was purified to a homokaryon by exploiting the fact that a sexual cross between two strains of opposite mating types results in the production of four pairs of genetically different, but homokaryotic, ascospores. The sexual cross method is a convenient way of isolating a homokaryon, but results in a random assortment of the parent strains' alleles. Therefore, WS004 is isogenic to FGSC 9718 and represents the most logical comparison for characterising the effects of the loss of porin. Unfortunately, as is the case with almost any biological system, the function of a single protein is rarely dependent upon that protein alone. Similarly, the expression of a single gene often is influenced by some other factor. Together, the result is the possibility of different phenotypes observed in different genetic backgrounds for a single mutation. This is the explanation put forward to rationalize the differing phenotypes observed in the two different *por* ⁻ strains, given

that there is known to be one locus different between WS004 and FGSC 18892, which is *mus-51*.

A comparison of the growth rates of the two knockout strains showed a difference of 4.6 cm per day when incubated at 30^{o}C and 2.2 cm per day when incubated at 22^{o}C. In addition to growth rate, the ability of WS004 to produce aerial hyphae was reduced, whereas for FGSC 18892, this ability was not affected. Finally, the two strains also differed in their ability to produce protoperithecia. This implies that the loss of porin has less of an impact in the genetic background of FGSC 18892. To determine if the double mutation of *por* and *mus-51* was the cause of the aerial hyphae phenotype and female sterility, the *mus* mutation was reintroduced into FGSC 18892 and it was replaced with a wild-type allele in WS004 through sexual crosses. However, both of these changes in the genomes of WS004 and FGSC 18892 again resulted in the random assortment of parental phenotypes making a logical explanation somewhat convoluted.

The aerial hyphae deficiency phenotype of WS004 was not correlated to the presence of the double mutations. Progeny resulting from the cross of 74A^{d} with WS004 showed a mixed population of single and double mutants. The subpopulation of strains isolated that were single *por* $^{-}$ mutants also consisted of a mixed population of strains that could or could not produce wild-type like aerial hyphae, indicating that the double mutation was not the cause. However, it should be noted that 74A^{d}, which albeit was able to produce protoperithecia, was later determined to not be completely wild type. Thus, the unknown mutations within the genome of 74A^{d} may have contributed to the expression of the observed phenotype and therefore this cross would need to be repeated with a "real" wild-type strain to confirm the results. The progeny of the cross of FGSC

18892 with FGSC 9718 were all isolated as double mutants, but were a mixed population with regards to their ability to produce aerial hyphae. The results from both crosses suggest that the aerial hyphae phenotype is a product of a particular allele as opposed to a lack of energy due to the loss of porin, since the phenotype is exhibited by both porin-containing and porin-lacking strains. The results also suggest that the *aer* allele present within FGSC 9718 and by inheritance, within WS004 is partially defective in comparison with the allele present within the genomes of FGSC 18892 and $74A^{d}$. One plausible suspect could be one of the genes required for hyphal fusion, such as the *so* locus. The production of aerial hyphae requires the development of an anastomosis in order to support the weight of the hyphae. A strain of *Neurospora crassa* with a mutation in the *so* locus is unable to fuse together two contacting hyphae and is characterised by a lack of aerial hyphae production similar to WS004 (Fleissner et al., 2005). However, the parent strain FGSC 9718 produces aerial hyphae, so epistasis is required to detect the defective *aer* allele.

The ability to produce protoperithecia was another difference observed between FGSC 18892 and WS004. Progeny from both crosses that were *por* $^{-}$ were female sterile similar to WS004, regardless of whether or not they contained the wild-type allele or mutant allele for *mus-51*. The progeny that contained the wild-type *por* allele were able to produce protoperithecia, but with some morphological and quantity differences compared to wild-type protoperithecia for some strains. The complete lack of protoperithecia after 8 days by the *por* $^{-}$ progeny from both crosses may be due to a combination of a lack of energy required to produce the structure and some combination of genetic factors, given that FGSC 18892 was female fertile. A *ndk*1^{RIP} (nucleotide

diphosphate kinase 1) strain of *Neurospora crassa* displays a defect in photomorphogenic characteristics, namely conidia production and protoperithecia development, similar to WS004 (Lee et al., 2006). In addition, the growth rate of the *ndk*1^{RIP} strain is only 17% of the wild type growth rate when cultivated at 30^{o}C and the strain lacks the ability to produce aerial hyphae and conidia (Lee et al., 2006). The observation of either tiny or abnormally large protoperithecia produced by the porin containing cross progeny suggests that there are other genetic factors aside from the *por* allele that can affect the protoperithecia production.

The cross of FGSC 9718 with WS004 was performed using FGSC 9718 as the female. Some of the progeny from this cross exhibited characteristics similar to WS004, suggesting that these characteristic were not maternally-inherited and therefore the cause is not associated with the mitochondrial DNA. Conversely, FGSC 18892 was crossed with FGSC 9718 with FGSC 18892 producing the female structure and again the progeny showed characteristics similar to WS004. This is further support that the genetic factors influencing the aerial hyphae and female sterility phenotypes are not mitochondrial DNA related and all originated as alleles present in FGSC 9718 prior to the construction of WS004.

4.3 *Mitochondrial Proteomes of FGSC 9718 and WS004*

The absence of porin in the mitochondria of WS004 caused alterations in mitochondrial morphology presumably due to alterations in the mitochondrial proteome. A comparison of the fluorescent images of mitochondria from FGSC 9718 and WS004 clearly shows a difference in mitochondrial morphology of actively growing hyphal tips.

This supports the idea of mitochondrial dysfunction as a source of reduced growth rate. There was no discernable difference between the morphologies observed at either temperature tested for either FGSC 9718 or WS004. Therefore, the temperature dependent growth rate of WS004 is not correlated to alterations in mitochondrial morphology at different temperatures. The precise cause of the alterations in mitochondrial morphology is not known. It has been previously shown that *Neurospora crassa* strains lacking MMM1have mitochondria with altered morphologies similar to what was observed for WS004 (Prokisch et al., 2000). Unfortunately MMM1 was not detected in the current iTRAQ study, precluding discussion of its potential role in WS004. It has been reported that mitochondria attach to microtubules, which provide transport throughout the hyphae and contribute to the elongated appearance seen for wild-type strains (Fuchs et al., 2002). Interestingly, these interactions were demonstrated to be ATP-sensitive and dependent on peripherally associated mitochondrial proteins suggesting that limiting ATP in WS004 may contribute to the observed mitochondrial morphology. While the iTRAQ analysis did detect some mitochondrially-associated proteins, the experimental conditions were not designed to quantitatively collect these proteins.

The mitochondrial proteomes of FGSC 9718 and WS004 have several notable differences when examined with SDS-PAGE. The lack of porin resulted in a the significant up- and down-regulation of several proteins ranging from low to high molecular weights, as visualized by SDS-PAGE analysis. The loss of other β-barrel proteins from the MOM has been previously demonstrated to alter the protein composition of the MOM. A TOM40 deficient strain of *Neurospora crassa* showed

reduced levels of TOM6 and TOM22 by immunoblotting and smaller mitochondria with virtually no cristae as determined by examination with electron microscopy (Taylor et al., 2003). Mitochondria with reduced levels of TOB55 were observed to contain reduced levels of TOM40 and porin, as well as TOM22 (Hoppins et al., 2007). Given that either of these β-barrel proteins, TOM40 and TOB55, function in the import or assembly of proteins respectively into the MOM, the alterations in MOM protein composition is not surprising. Therefore, the reduced amounts of proteins observed by SDS-PAGE analysis may be the result of a reduction in protein import. The up-regulated proteins are presumably due to an effort to compensate for the loss of porin. Therefore, identifying the mitochondrial proteins that were either, up- or down-regulated in WS004 mitochondria is key to understanding the effect of the loss of porin has had on the mitochondria morphology and function.

Western blot analysis was performed on isolated mitochondria from both FGSC 9718 and WS004 to determine the relative levels of TOM22, TOM40 and TOM70 (Figure 3.16). A TOM22 deficient strain of *Neurospora crassa* contains mitochondria with morphological defects and reduced levels of TOM20 and TOM70 (Nargang et al., 1995). There was no discernable difference in the level of TOM22 between mitochondria of FGSC 9718 or WS004 indicating that TOM22 was not involved in the observed morphology defect of WS004 mitochondria. The level of TOM40 was increased in WS004 mitochondria by 1.9 fold. Given that TOM40 is a β-barrel protein, it is plausible that the up-regulation of TOM40 may be to provide additional metabolite translocation function. Yeast mitochondria deficient for Por1p have been shown to have increased levels of both TOM40 and TOM70, and imported external NADH through the TOM

complex (Kmita and Budzinska, 2000). In contrast with the observations made with yeast mitochondria, the level of TOM70 in WS004 mitochondria was about half of what was observed in the mitochondria of FGSC 9718. TOM70 functions as a receptor within the TOM complex but is a non-essential protein. Slight morphology defects in mitochondria lacking TOM70 were observed (Grad et al., 1999), but these defects were not similar to the morphology of the WS004 mitochondria report by this study. Taken together, the Western blot analysis of the mitochondrial proteome dictates the necessity of a proteome wide analysis to identify all possible proteins contributing to the differences observed with SDS-PAGE analysis and the alterations in mitochondrial morphology.

The proteomic profiles of the mitochondria from FGSC 9718 and WS004 were determined using LC-MS / MS. The use of an iTRAQ labelling technique allowed for the relative quantitation of the proteins identified by MS / MS analysis. The results of this analysis suggested that the vast majority of the proteins identified were not significantly up- or down-regulated in the mitochondria of WS004. Even though 95% of the proteins identified were not significantly up- or down-regulated, the analysis did identify proteins that had subtle changes in expression that may be pursued by other means to demonstrate association with a given phenotype. However, the variation in expression of individual proteins identified by the two trials suggests that during the regular growth of the organism, the expression level of most proteins is subject to a rather large degree of flux.

The small cluster of proteins that were significantly up-regulated in both trials contained proteins involved in cellular respiration prior to complex III and IV of the

electron transport chain and via the alternative oxidase pathway. These data correlated well with the biochemical determination of the expression of alternative oxidase (see section 3.2.4). The increased expression of enzymes that generate NADH such as rubredoxin-NAD^+ reductase and a zinc-containing alcohol dehydrogenase, suggest a possible increase in the level of complex I. The reduced levels of complex III and IV as determined by cytochrome *b* and aa_3 levels would have complex I in the inner membrane as the primary H^+ pump generating the proton gradient required for ATP synthesis. However, none of the subunits of NADH:ubiquinone oxidoreductase were identified by iTRAQ analysis as being significantly up-regulated. Complex I is suspected as being a site of electron leakage directly to oxygen, which contributes to the generation of reactive oxygen species, such as H_2O_2, by complex I. Thus the cell may not overexpress complex I in order to prevent ROS accumulation. In support of the prediction of increased generation of ROS in WS004, catalase 3 was noted to be up-regulated in WS004 mitochondria from both trials, although significantly so in only one of the trials.

Fewer proteins were identified as significantly down-regulated. Nucleoside diphosphate kinase-1 (NDK1) was identified as significantly down - regulated in both trials. A growth rate deficiency was reported for a strain with a mutation in *ndk-1*, which could be restored by the deletion of *cat*3 (Lee et al., 2009). Therefore, the reduction of NDK1 combined with the increase of catalase 3 in WS004 may be contributing to the slow growth rate of WS004. The cyanide-resistant respiration of WS004 may allow for the use of cyanide as a catalase inhibitor to block its activity to examine this theory.

The iTRAQ analysis didn't support any simple, direct explanations for the observed alterations in mitochondrial morphology, given that proteins involved in

maintaining mitochondrial morphology such as MMM1 or MDM10 were not identified. However TIM13 was identified as significantly down-regulated, which could translate to a reduction in β-barrel assembly into the MOM (Hoppins and Nargang, 2004). The lack of both TOM40 and SAM50 in yeast result in aberrant mitochondrial morphology (Meisinger et al., 2004).

The most surprising protein identified as down-regulated was porin, which can only be explained by contamination. The mitochondria used for this analysis were prepared from cultures grown at 22^{o}C, at which WS004 grows about 6.5 times slower than the FGSC 9718 strain used for comparison. Therefore, if the source of contamination was from the culturing stage, the turbidity of the culture would have thickened prior to the expected 5-6 days commonly needed for WS004 growth. In addition, the Western blot analysis described in section 3.4.3 was performed using the same protein sample preparation used to perform the iTRAQ analysis. This suggests the source of contamination was introduced during the processing of the samples for LC-MS / MS.

This study was the first mitochondrial proteomic analysis of a respiratory deficient strain of *Neurospora crassa* and has provided evidence for an elaborate anastomosis of biochemical pathways required for mitochondrial morphology, respiration and energy generation. This also provides insight which will aid in future planning of more precisely directed experimentation to identify possible protein involved in phenotypic differences.

4.4 *The In vivo Expression of Porin Variants*

The structure and function of porin have been examined by characterizing the pore forming and gating ability of deletion variants in artificial membranes (Runke et al., 2006). Some deletions resulted in a loss of voltage-dependent gating and others produce channels with smaller diameters. It was also determined that the recombinant N-terminal His_6-tagged porin was indistinguishable from native porin in the artificial membrane assays (Popp et al., 1996). However the *in vivo* implications of these deletions may not mimic the results obtained from the *in vitro* assays and therefore require investigation.

During the course of this study, several N-terminal modifications to porin were expressed in *Neurospora crassa* to determine the effect of the modification *in vivo* and the function of the N-terminus. An enhancement of hVDAC3 function was previously shown in yeast cells by substituting its N-terminal sequence with the N-terminal sequence from hVDAC1 (Reina et al., 2010), suggesting the sequence of the N-terminus is important for porin function. The addition of a His_6-tag to the N-terminus of porin resulted in a slow growing strain of *Neurospora crassa* presumably due to an interference on the gating properties of the channel involving the N-terminus (see introduction and appendix 5.3 for details). Similarly, WS125.5 expressed a porin molecule with a deletion of the first 11 amino acids ($\Delta N_{2\text{-}12}$ porin) and was functionally similar to a strain having no porin at all. This strain had a growth rate comparable to WS004 which implied either that the deletion of the N-terminus prevents the import and assembly of porin, or once assembled into the MOM, the $\Delta N_{2\text{-}12}$ porin fails to function. Both possibilities remain to be examined; however, the latter is more likely since $\Delta N_{2\text{-}12}$ porin was previously shown to import into isolated mitochondria (Court et al., 1996) and a porin molecule with a

deletion of the first 20 amino acids was determined to import and assemble into mitochondria of Cos-7 cells but cause a depolarization of the mitochondrial inner membrane (De Pinto et al., 2007). Consistent with the hypothesis of the ΔN_{2-12} porin not functioning, is the lack of aerial hyphae production by WS125.5 presumably resulting from the epistatic relationship of the *aer* gene and a lack of porin as described for WS004. Given that the N-terminus is presumably not required for porin import in *Neurospora crassa*, mutation within the N-terminus may be used to elucidate a more detailed model of gating via the N-terminus. However, as evident from this study, the mutations will need to be relatively small, since the deletion of 11 consecutive amino acids was sufficient to diminish porin function.

A C-terminal deletion variant of porin was expressed *in vivo*. WS126.1 expressed the $\Delta C_{269-283}$ porin and grew at 85% of the growth rate of the control strain; this observation was taken to mean that the protein was successfully imported and assembled into the membrane. The slight reduction in growth rate may be in part due to a reduction of the pore's diameter. The loss of the terminal β-strand resulted in the reduction of channel conductance of $\Delta C_{269-283}$ porin when examined in artificial membranes (Popp et al., 1996). The deleted part of the C-terminus also coincides with a portion of the proposed voltage-sensor domain required for voltage-dependent gating of porin (see section 1.3.4.7). Given that the deletion does not encompass the entire domain, the function of the voltage-sensor may only be partially hindered thus resulting in only a slight reduction in growth rate. Another possibility may be due to the fact that there is less $\Delta C_{269-283}$ porin present in the MOM of WS126.1 as compared to the level of native porin in the mitochondria isolated from FGSC 9718. Densitometry analysis of the

detected fluorescence from the Western blot revealed the mitochondria of WS126.1 contained only 30% of the porin molecules present in the mitochondria of FGSC 9718. Therefore, either the level of porin present in mitochondria of FGSC 9718 is far in excess of what is needed for wild-type growth rate or the 30% reduction in porin molecules in the MOM of WS126.1 results in the 15% reduction in growth rate observed for WS126.1 when compared to FGSC 9718.

The higher growth rate of WS126.1 compared to the growth rate of WS004 is well correlated with the increase in the levels of cytochromes *b* and aa_3. The increase in cytochrome levels in mitochondria expressing the $\Delta C_{269\text{-}283}$ porin may be due to the restored contact between porin and cytochrome *c* oxidase (COX). This implies that the contact site required for this interaction of porin and COX is not within the last 14 amino acids. This is not that surprising considering that most of these amino acids comprise the last β-strand and therefore would not be accessible for contacting an integral membrane protein within the IM. The levels of cytochromes *b* and aa_3 in WS126.1 are however still less than the levels present in FGSC 9718 mitochondria. Consistent with the porin-COX interaction theory of regulation, this may be explained by the reduced concentration of $\Delta C_{269\text{-}283}$ porin in comparison to FGSC 9718 mitochondria. The increased levels of cytochromes in WS126.1, in comparison to the levels present in mitochondria of WS004, also supports the theory that ATP is a limiting factor on the growth rate of WS004. The increase in cytochromes *b* and aa_3 suggests that there is an increase in complex III and complex IV which in turn would provide an increase in membrane potential required for ATP generation by the F_oF_1 ATPase.

WS126.1 is isogenic to FGSC 9718 yet unlike FGSC 9718, WS126.1 is unable to produce wild-type like aerial hyphae. The lack of aerial hyphae production by WS126.1 is interesting given the analysis of the cross progeny (section 3.3) suggested an epistatic relationship between the *por* allele and a proposed *aer* allele. The observed lack of aerial hyphae by WS126.1 either indicates that the aerial hyphae phenotype is more complicated than the epistatic relationship proposed or that some moiety within the deleted segment of $\Delta C_{269\text{-}283}$ porin is required, directly or indirectly, for the production of aerial hyphae.

The terminal β-strand is predicted to contain the β-sorting signal required for the recognition and assembly into the MOM of the porin protein by the sorting and assembly (SAM) complex (Kutik et al., 2008). The protein expressed by WS126.1 is lacking this β-strand yet there is evidence provided by the relatively fast growth rate of WS126.1 and Western blot analysis of isolated mitochondria that the $\Delta C_{269\text{-}283}$ porin is in the MOM. The assembly of $\Delta C_{269\text{-}283}$ porin into the MOM may be facilitated by the putative β-sorting signal described in section 3.5.5.2. The putative β-sorting signal has a perfect match to the required criteria and therefore the deletion of the terminal β-strand may not be used to prove or disprove the essentiality of the β-sorting signal in *Neurospora crassa*.

WS127.8 was constructed to express a porin protein with a deletion of the loop between β-strand 16 and β-strand 17 (ΔNDRGV porin). Analysis of ΔNDRGV porin in artificial membranes showed wild-type conductance suggesting the formation of a pore was not inhibited by the deletion (Runke et al., 2006). The growth rate of WS127.8 was determined to be 90% of the rate determined for FGSC 9718, which suggests that the ΔNDRGV porin protein forms a pore in the MOM. WS127.8 is isogenic to FGSC 9718

indicating that the deletion in ΔNDRGV porin must be directly responsible for the 10% loss in growth rate. Precisely how the deletion could account for the 10% reduction in growth rate is not known. One possibility is a reduced level of ΔNDRGV porin import suggesting the region deleted contains some portion of the import targeting signal.

4.5 *The Project Summary*

The question of whether or not porin is essential for the life of *Neurospora crassa* was answered in this study: it is non-essential. The characterisation of the *por* ⁻ strain WS004 has placed porin in a central role in the regulation of mitochondrial function and cellular respiration. Porin is required for the normal expression of several components of the electron transport chain presumably through its direct contact with cytochrome *c* oxidase. The down regulation of the cytochrome mediated pathway of respiration resulted in the induction of the alternative oxidase pathway as a compensatory solution. In addition, the lack of porin resulted in morphological alterations to the mitochondria, which are most likely due to changes in membrane protein composition of both membranes, in particular the lack of ETC complexes within the inner membrane. The dysfunction of the ETC would imply a reduction in ATP concentrations, ultimately resulting in slow growth and poor development of the organism, but also a hindrance on ATP dependent protein import in general, further contributing to changes in membrane protein composition. Additionally, this study has shown the importance of using isogenic strains for comparison in characterising any mutation within a biological system since rarely does a protein function independently of any other protein within the cell.

4.6 *Future Works*

The continued advancements in the understanding of mitochondrial porin function require further experimentation. In addition to the other experiments suggested in this discussion, a follow up to this study would be to confirm the results of the iTRAQ experiments using quantitative reverse transcriptase PCR (qRTPCR), with particular interest in confirming the lack of porin mRNA in WS004. A complete characterisation of import of WS127.8 into mitochondria needs to be performed to determine if the deletion variant contains targeting information, as the targeting signal for β-barrel proteins destined to the MOM is still unknown. The function of porin gating can be addressed using differences observed between WS125.5 and control strains and WS004. It remains to be shown that the porin of WS125.5 is within the MOM and therefore the lack of complementation is atleast in part because of a loss of function. With this information, specific mutations can be introduced which make it possible to crosslink or covalently bind the N-terminus to the barrel to address the question of movement as a mechanism of gating using either *in vitro* or *in vivo* techniques. Along these lines, small deletion variants should be introduced *in vivo* and the resulting strains characterised similarly to WS004. Finally, given the differences observed between WS004 and FGSC 18892, transposon mutagenesis of FGSC 18892 could be used to identify any possible suppressors of the *por* ⁻ phenotype or conversely, transform WS004 with a genomic library and identify coding sequences that "rescue" the *por* ⁻ phenotype.

The results of this study contribute to the understanding of the function of porin, showing how the loss of porin could result in cellular dysfunction similar to the myopathy of muscle tissue lacking mitochondrial porin. Thus, the central role of porin in

regulating both mitochondrial and cellular processes has been confirmed. This work also exposes the potential of *Neurospora crassa* to be used as a model organism to study the function of porin, given that non-functional variants can be expressed and used to determine functional moieties within the protein since porin is non-essential.

Chapter 5: Appendix

5.1 *Construction of por Disruption with ad-3A Gene*

The first approach to creating a *por* knockout strain of *Neurospora crassa* was designed to exploit the phenotypic result of an *ad-3*A gene mutation. A mutation in the adenine biosynthetic pathway at *ad-3*A results in the build up of the intermediate, 5'-phosphoribosyl-4-carboxy-5-aminoimidazole (CAIR), which causes the usual orange pigmentation observed during conidiation to be replaced with purple. Next, by disrupting the *por* gene with a cassette of wild-type *ad-3*A gene, the parent strain and the resulting *por* disruption strain could be differentiated based on the observed colour of the strains, allowing for better control over possible cross contamination. Strain WS001 (*mus-51*::*bar*$^{+}$, *ad-3*A::*his-3*; Table 2.1) was created from FGSC 9720 (*mus-51*::*bar*$^{+}$; *his-3*) by integrating a DNA cassette of wild-type *his-3* locus flanked by *ad-3*A sequence from plasmid pBSAD::His3 (Table 2.3) by homologous recombination. The successful integration was purified to a homokaryon by repeated subculturing of single conidia, which maintained the isogeneity of WS001 to parent strain FGSC 9720, and was confirmed by Southern blot analysis (Figure 5.1). The growth rate of WS001 grown on VM + ade media was comparable to the control strain FGSC 9720 and the strain was capable of producing wild-type like aerial hyphae and conidia, with the exception of pigmentation (data not shown). Strain WS001 was therefore considered suitable for investigating the porin's essentiality. WS001 was transformed with a DNA cassette of *ad-3*A sequence flanked by *por* sequence from plasmid pUC18+2.5kb *por::ad-3*A (Table 2.3) to disrupt *por*. No ade^{+} transformants were recovered either due to a failed

Figure 5.1 *Southern hybridization analysis of WS001, WS002.3 and WS003.1*.
(A) Results of Southern hybridization analysis of genomic DNA isolated from FGSC 9720 (lane 1) and WS001 (lane 2) digested with *Xba*I and hybridised with the *ad-3*A locus DIG-labelled probe. The expected fragment sizes resulting from the digests were 2503 bp for the wild-type *ad-3*A locus and 5208 bp and 1288 bp for the disruption of *ad-3*A with *his-3* (asterisks). In both cases the *ad-3*A probe will also hybridise to sequence flanking the digestion sites resulting in two fragments for each larger than 10 000 bp. Lane 3 is empty. Genomic DNA isolated from FGSC 9720 (lane 4) and WS002.3 (lane 5) digested with *Sca*II and hybridised with the *lys-3* upstream UTR DIG-labelled probe. The expected fragment sizes resulting from the digests were 5278 bp for the wild-type *lys-3* locus and 2970 bp for the *hph* replacement of *lys-3*. (B) Results of Southern hybridization analysis of genomic DNA isolated from FGSC 9720 (lane 1) and WS03.1 (lane 2) digested with *Pst*I and hybridised with the *trp-1* locus DIG-labelled probe. The expected fragment sizes resulting from the digests were 4104 bp for the wild-type *trp-1* locus (arrow) and 2704 bp and 1733 bp for the *trp-1* locus with the *hph* insertion (asterisks).

A

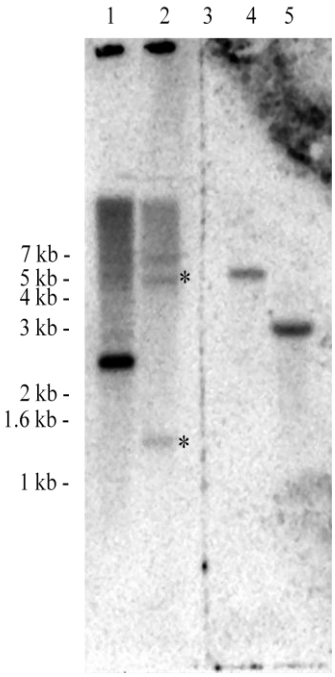
1
2
3
4
5
7 kb -
5 kb -
4 kb -
3 kb -
2 kb -
1.6 kb -
1 kb -
*
*

B

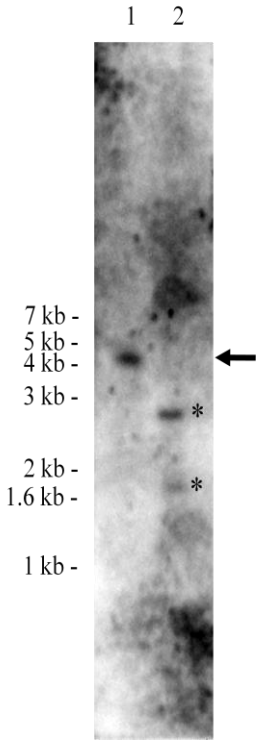
1
2
7 kb -
5 kb -
4 kb -
3 kb -
2 kb -
1.6 kb -
1 kb -
*
*

transformation experiment or the fact that *por* is an essential gene. Therefore the strategy was modified taking into account the possibility that porin is essential.

A heterokaryon can be employed to shelter a lethal gene disruption, and is created by allowing hyphal anastomosis to occur between two different strains. Therefore, two double mutants of *ad-3*A / *lys-3* (WS002.3) and *ad-3*A / *trp-1* (WS003.1) were constructed (Table 2.1). WS002.3 was constructed by transforming WS001 conidia with a DNA fragment consisting of *hph* sequence flanked by *lys-3* up- and downstream UTRs, excised from plasmid lysko#17 (Table 2.4). WS003.1 was constructed by transforming WS001 conidia with a DNA fragment consisting of *hph* sequence flanked by *trp-1* sequence, excised from plasmid pBStrpI::Hyg#16 (Table 2.3). The growth rates of WS002.3 and WS003.1 grown on VM + lys and VM + trp media respectively, were comparable to FGSC 9720 and produced both aerial hyphae and conidia similar to WS001 (data not shown). Genomic DNA isolated from WS002.3 and WS003.1 was subjected to Southern blot analysis (Figure 5.1), which confirmed the successful disruption of the *lys-3* locus and *trp-1* locus respectively. Subsequently, both strains were inoculated into a single VM + ade media slant lacking lysine and tryptophan and growth was the result of the fusion of the germ tubes of neighbouring conidia, producing the desired heterokaryon (WS110; Table 2.1). Parallel transformations of WS001 and WS110 conidia with the *por* disruption cassette described above were carried out and ade^+ colonies were isolated. Three isolates from the transformation of WS001, labelled as WS010.1, WS010.2 and WS010.3, and two isolates from the transformation of WS110, labelled WS111.1 and WS111.2, were characterised further. The growth rates of WS111.1 and WS111.2 were examined using the race tube method with two separate race

tubes filled with VM + lys media in one and VM + trp media in the other. By supplementing with only one amino acid, the nucleus containing the *por* disruption could be enriched for on one of the two media types. Assuming the disruption of *por* results in a growth rate phenotype (assumed by the lack of ade$^+$ colonies in the first three transformations described above) and that the disruption occurred in the *por*::*ad-3*A, Δ*lys-3*::*hph*, trp$^+$ nucleus, then this nucleus would be enriched for in the VM + lys media race tube. This was the case for WS111.2 when it was grown in both VM + lys media and VM + trp media (Figure 5.2). Culturing of WS111.2 on VM + lys media resulted in an erratic growth rate after 50 cm of apical extension, assumed to be due to an enrichment of the *por* disrupted nucleus, and suggesting that the lack of porin results in a growth rate deficiency. A similar result was obtained from race tubes inoculated with WS111.1 (data not shown). The mitochondria from WS010.1, WS010.2, WS010.3 and WS111.1 enriched for the *por*::*ad-3*A, Δ*lys-3*::*hph*, trp$^+$ nucleus, were isolated and examined by Western blot analysis with an antibody raised against the N-terminus of porin (amino acids 7-20; Figure 5.3). Oddly, the mitochondria from WS010.1, WS010.2, WS010.3 showed evidence of wild-type porin in addition to two peptides of smaller size not observed in the parent strain sample (mitochondria isolated from WS001). These peptides could be porin / *ad-3*A sequence chimeras because the *por*::*ad-3*A disruption resulted in an open reading frame that could encode a chimera of porin and translated *ad-3*A sequence. The existence of wild-type porin in mitochondria isolated from WS111.1 was not surprising given that this strain is a heterokaryon, but it also contained the two smaller sized peptides. Because the expression of this chimera could be toxic to the strains expressing it, this disruption construct was determined not suitable for further

Figure 5.2 *Growth rate of the por::ad3A disruption strain WS111.2.*
Race tubes filled with VM + lys media and VM + trp media were inoculated with WS111.2. The control strain FGSC 9719 was inoculated in race tubes filled with VM media. Race tubes were incubated at 23.5^{o}C with regular day light cycles. The horizontal shift observed at about 30 cm was due to the subculturing of the cultures at the end of one race tube into a second race tube of the same media.

A

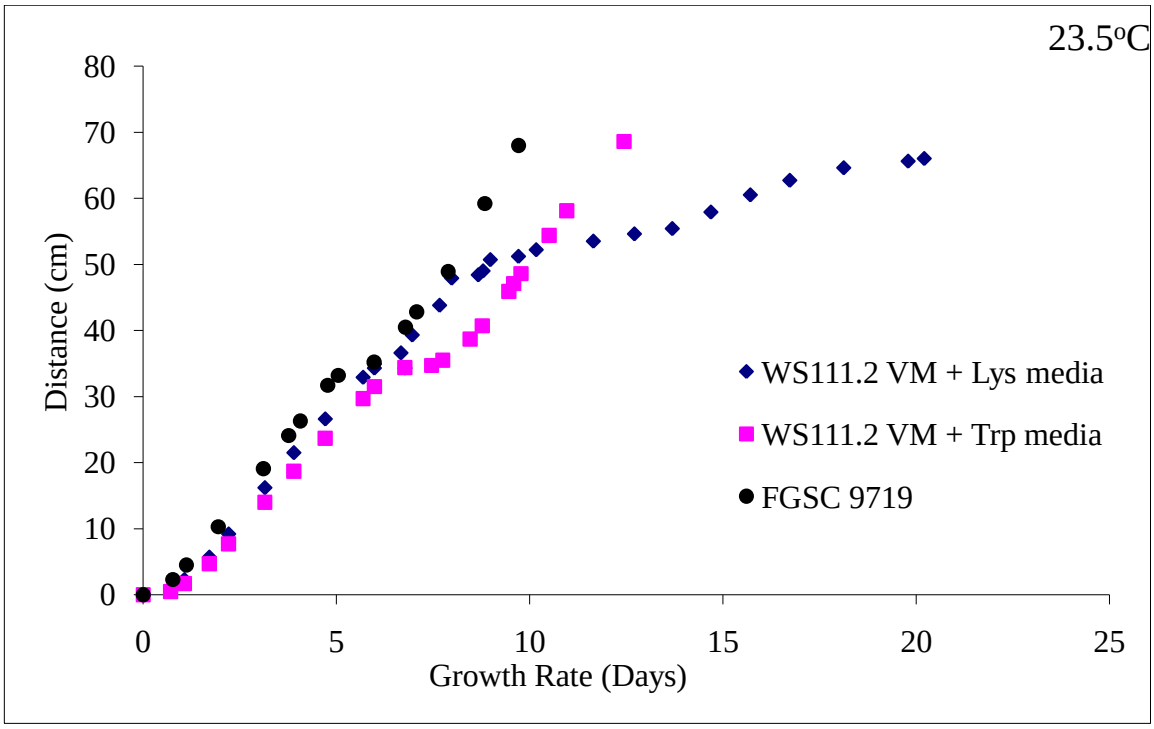
23.5°C
80
70
60
50
40
30
20
10
0
Distance (cm)
0
5
10
15
20
25
Growth Rate (Days)
WS111.2 VM + Lys media
WS111.2 VM + Trp media
FGSC 9719

Figure 5.3 *Western blot analysis of mitochondria from por disrupted strains*. Mitochondria were isolated from WS001 (*por*$^{+}$, lane 2) and *por*::*ad-3*A disruption mutants WS010.1 (lane 3), WS010.2 (lane 4), WS010.3 (lane 5), WS110.1 (lane 6) and separated with SDS-PAGE and transferred to a nitrocellulose membrane. (A) Immunodection of the blot with a polyclonal antibody for the N-terminus of porin (amino acids 7-20). Lane 7 was recombinant His_6-tagged porin and is indicated by the asterisk. The two black arrows indicate the proposed porin chimera. (B) Ponceau staining of the blot to visualize the protein loading of each sample. Lane 1, molecular weight standards.

A

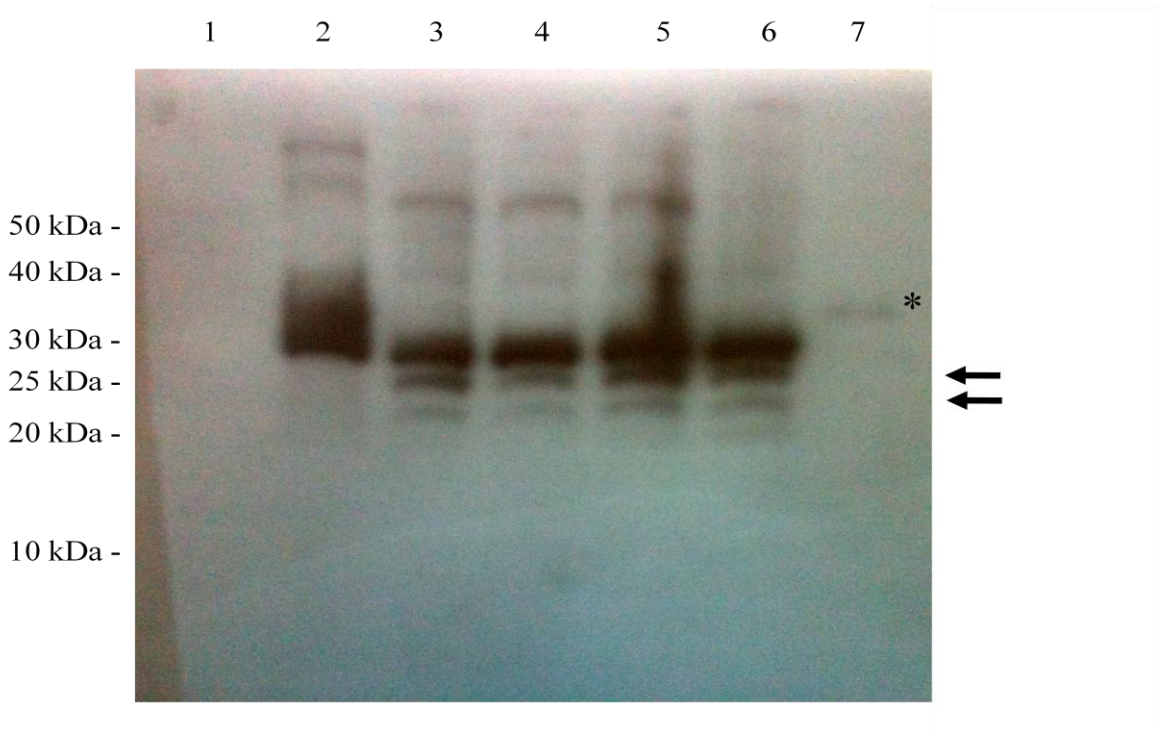
1
2
3
4
5
6
7
50 kDa -
40 kDa -
30 kDa -
25 kDa -
20 kDa -
10 kDa -
*

B

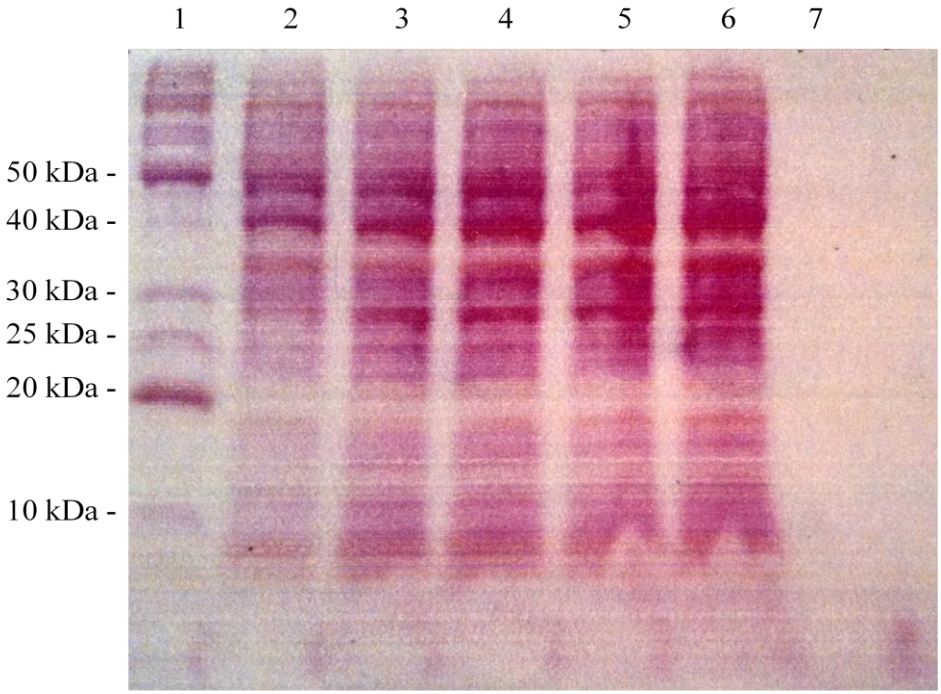
1
2
3
4
5
6
7
50 kDa -
40 kDa -
30 kDa -
25 kDa -
20 kDa -
10 kDa -

analysis. The wild-type porin, identified by Western blot analysis of mitochondria from WS010.1, WS010.2, WS010.3, was explained by PCR analysis of genomic DNA, which identified both a wild-type *por* locus and a disrupted *por*::*ad-3*A locus (data not shown). This was interpreted as an un-intentional heterokaryon produced by the transformation of a macroconidium (containing 2-3 nuclei) and the disruption of the *por* locus in one nuclei introduced selection for the wild-type *por* locus of one of the un-transformed nuclei. Since it appeared as though there was selection for the wild-type locus, no attempt to purify a homokaryon was made and therefore, no further analysis was performed. However, the studies of these strains together suggested that porin, whether essential or not, would most likely result in a growth rate deficiency which would be useful for examination of the function of porin.

5.2 *N-terminal His_6-tagged Porin*

In an attempt at making porin more accessible in folded form, a His_6-tagged porin variant was expressed in *Neurospora crassa*. The purification tag was engineered into the 5' end of the gene encoding porin immediately after the start codon. The DNA cassette within the multicloning site of plasmid pRS416 + NcPprom::HygR ATG His6 porin (Table 2.4) was used to transform conidia from FGSC 9719, with hygromycin as selection. The hygromycin-resistant isolates collected from a transformation of strain FGSC 9719 were analysed for the expression of the His_6-tagged porin variant by Western blotting with a Ni-HRP conjugate probe (Figure 5.4). Two isolates, labelled WS009 and WS009.1 were found to express the His_6-tagged porin, but in differing amounts. The difference in expression levels was interpreted as an indication that WS009 and WS009.1

Figure 5.4 *Western blot analysis of isolated mitochondria fromWS009 and WS009.1*. (A) Mitochondria isolated from FGSC 9719 (5 µg, lane 2; 15 µg, lane 3), WS009 (5 µg, lane 4; 10 µg, lane 5; 15 µg, lane 6) and WS009.1 (5 µg, lane 7; 10 µg, lane 8; 15 µg, lane 9) were separated by SDS-PAGE and analysed by Western blotting with a Ni-HRP conjugate probe. The His_6-tagged porin is indicated by the arrow. Non-specific binding of the probe in control sample (lane 3) is indicated with the asterisks. (B) The Ponceau stained blot for protein loading comparison. Lane 10, recombinant His_6-tagged porin. Lane 1, molecular weight standards.

A

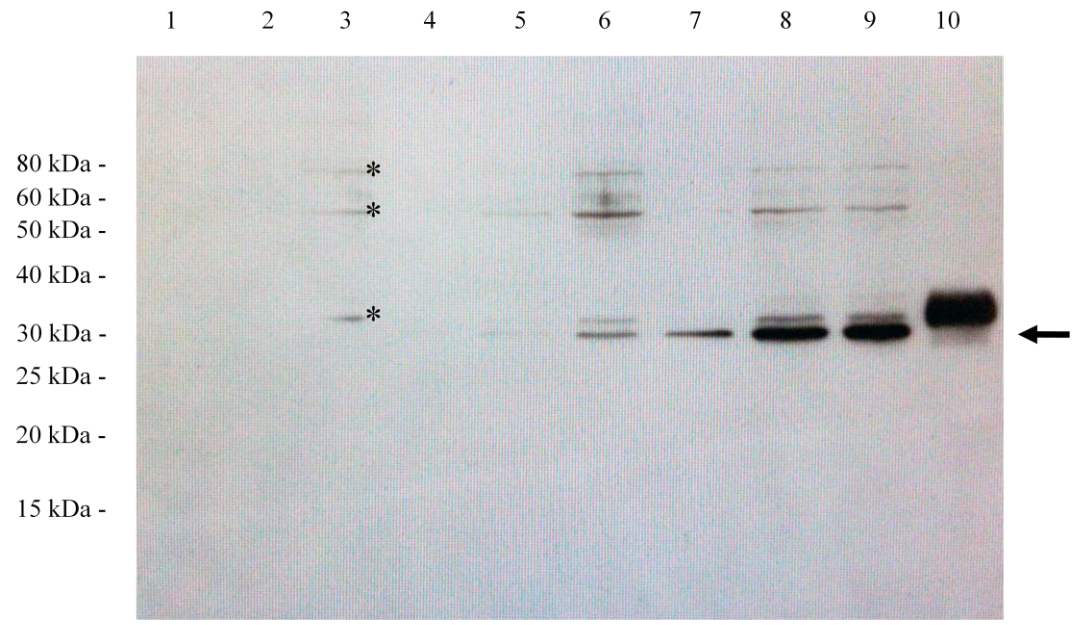
1 2 3 4 5 6 7 8 9 10
80 kDa -
60 kDa -
50 kDa -
40 kDa -
30 kDa -
25 kDa -
20 kDa -
15 kDa -
*
*
*

B

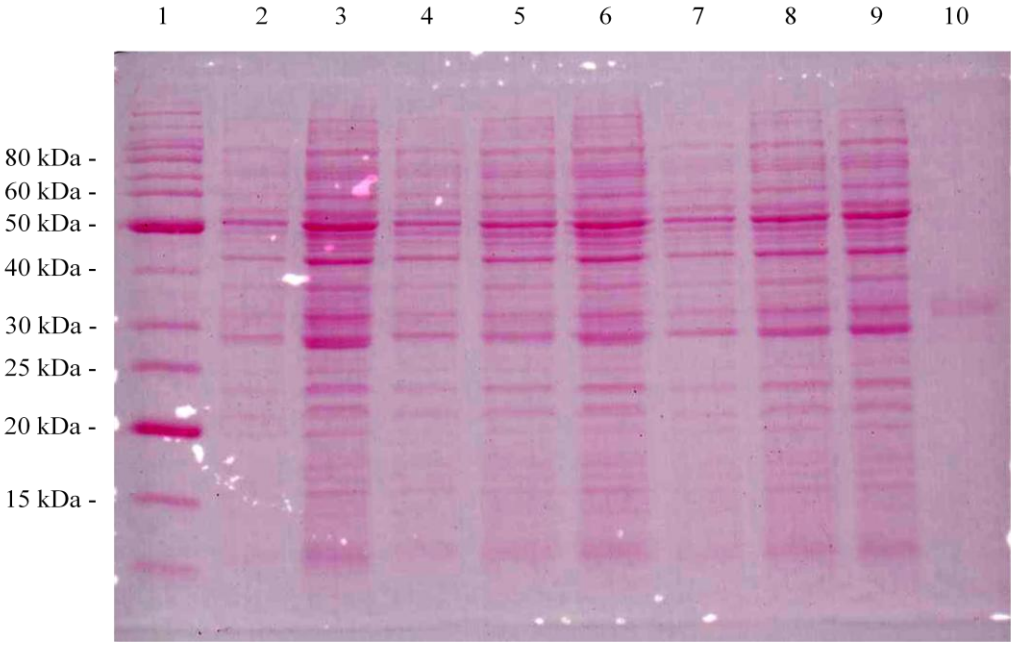
1 2 3 4 5 6 7 8 9 10
80 kDa -
60 kDa -
50 kDa -
40 kDa -
30 kDa -
25 kDa -
20 kDa -
15 kDa -

were un-intentional heterokaryons, consisting of both a transformed nucleus and an un-transformed nucleus. Attempts at purifying a homokaryon only produced strains enriched for the transformed nuclei, which grew at a reduced rate compared to FGSC 9719 and lacked the ability to produce wild-type like aerial hyphae (data not shown). This reduction in growth rate was interpreted as a reduction in functional porin molecules as the His_6-tagged porin's expression increased due to the enrichment of the transformed nuclei. This suggests the N-terminal His_6-tagged porin protein is non-functional. One possible explanation for the loss of function may be that the N-terminus is involved in gating of the pore (see section 1.3.4), and the addition of the His_6-tag disrupts the mechanism. This however, made the protein insufficient for use in determining a physiological structure and therefore it was not analysed further. This work did however, provide evidence that the 320 bp of upstream sequence relative to the *por* translational start site is sufficiently large enough to contain the genetic elements required for the transcription of the *por* locus. In addition, the Western blot analysis performed using isolated mitochondria suggests that the His_6-tagged porin was able to be imported into the mitochondria. Whether the His_6-tagged porin variant is assembled into the MOM remains to be determined.

5.3 *Expression of a N-terminal eGFP::Porin Fusion Protein*

An eGFP::porin fusion was expressed in *Neurospora crassa* to allow the visualization of the mitochondrial morphology using fluorescent microscopy and to assay the importability of various porin deletion variants in conjunction with the eGFP fusion. In anticipation of all other N-terminal modifications to porin producing non-functional

proteins, a heterokaryotic strain of *Neurospora crassa* was used to shelter the expression of an eGFP::porin fusion protein. Conidia from WS120 (Table 2.1) were transformed with the DNA cassette within the multicloning site of plasmid pRS416 eGFP::VDAC #4 (Table 2.4). Hygromycin-resistant isolates were screened for green fluorescence. Preliminary examination of this strain using fluorescent microscopy shows the eGFP::porin fusion protein predominantly in circular structures, some were large and possibly vacuoles, while others were smaller circles that were presumably nuclei (Figure 5.5A). The lack of long tubular green fluorescing mitochondria within the hyphae of WS122 may be due to an impediment on the importability of the fusion protein and therefore it accumulates in the nucleus during production. WS122 produces both wild-type porin and the eGFP::porin fusion protein from two different nuclei, being that it is a heterokaryon. Interestingly, the segregation of nuclei during lateral branching, which is one explanation for the erratic growth rates of the *por*::*ad-3*A disruptions strains described above, was observed as green fluorescence throughout one branch and no green fluorescence in the other branch (Figure 5.5B). While the N-terminal eGFP::Porin fusion construct may not be useful for observing mitochondrial morphology or assaying for porin deletion variant importability, this work has shown further evidence that the 320 bp upstream of the *por* translational start site is sufficient for transcription of the *por* locus. Additionally, this work suggests that the addition of a large peptide to the N-terminus of porin, in contrast to the relatively small His_6-tag, may hinder its importability.

5.4 *Complete iTRAQ Analysis Protein Profiles*

The complete protein profiles of trial 1 and trail 2 are listed in Table 5.1.

Figure 5.5 *Fluorescence microscopy images of WS006 hyphae.*
Conidia from WS006 were germinated and grown in shaking liquid cultures for approximately 18 hours and were observed at 1000X magnification using differential interference contrast microscopy (DIC; grey images) and fluorescence microscopy (green images) to determine the localization of the eGFP::Porin fusion protein. (A) The eGFP::Porin fusion protein presumably localized to nuclei (white arrow) and vacuoles, which were also visible in the DIC image (red arrows). (B) DIC image and corresponding fluorescence image of a lateral branching of a hyphal tip. Scale bar represents 10 μm.

A

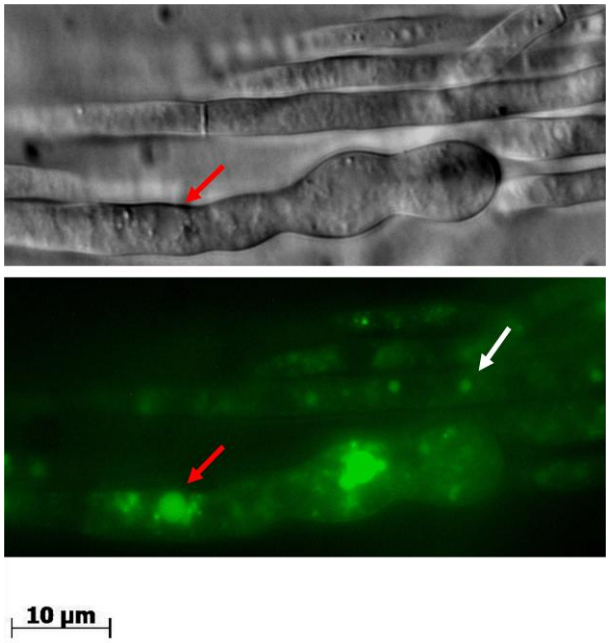

B

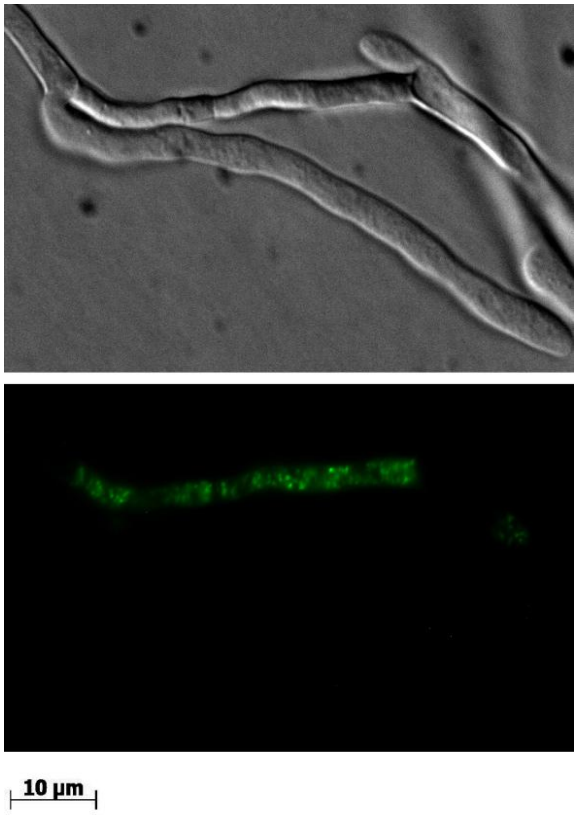

Table 5.1 *The differential expression ratios of proteins labelled with different iTRAQ species and identified by LC-MS/MS for trial 1 and trial 2*

	Trial 1		Trial 2	
Protein accession # and description	log_2 of the iTRAQ ratio	z score of the log_2 ratio	log_2 of the iTRAQ ratio	z score of the log_2 ratio
| NCU05005 | HHE domain-containing protein (233 aa)	5.17	3.91	4.16	3.27
| NCU06518 | NADH-cytochrome b5 reductase 2 (327 aa)	3.92	2.97	3.32	2.64
| NCU07267 | blue light-induced-3 (210 aa)	3.81	2.89	1.50	1.28
| NCU05633 | stomatin family protein (432 aa)	3.76	2.85	2.41	1.96
| NCU06550 | pyridoxine 1 (309 aa)	3.65	2.77	4.92	3.84
| NCU09403 | NmrA family protein (305 aa)	3.59	2.72	2.48	2.02
| NCU09285 | zinc-containing alcohol dehydrogenase (347 aa)	3.40	2.58	3.61	2.86
| NCU09536 | conserved hypothetical protein (892 aa)	3.35	2.54	3.26	2.59
| NCU08476 | conserved hypothetical protein (372 aa)	3.27	2.48	3.20	2.55
| NCU02157 | COQ4 (348 aa)	3.22	2.44	2.91	2.33
| NCU08998 | 4-aminobutyrate aminotransferase (516 aa)	3.20	2.43	3.07	2.45
| NCU05850 | rubredoxin-NAD(+) reductase (612 aa)	2.99	2.27	2.50	2.03
| NCU07953 | alternative oxidase-1 (363 aa)	2.98	2.26	3.40	2.70
| NCU06220 | conserved hypothetical protein (501 aa)	2.91	2.21	2.05	1.69
| NCU01320 | glutathione S-transferase (149 aa)	2.84	2.16	1.59	1.35

| NCU02271 | YagE family protein (467 aa)	2.78	2.11	1.49	1.27
| NCU05844 | conserved hypothetical protein (124 aa)	2.68	2.04	1.57	1.33
| NCU05196 | mitochondrial DnaJ chaperone (532 aa)	2.67	2.03	1.55	1.32
| NCU08092 | nipsnap family protein (332 aa)	2.66	2.02	1.83	1.53
| NCU05419 | hydroxymethylglutaryl-CoA lyase (400 aa)	2.56	1.95	1.51	1.29
| NCU01092 | 3-oxoacyl-(acyl-carrier-protein) reductase (315 aa)	2.55	1.94	-0.44	-0.18
| NCU00466 | glutamyl-tRNA synthetase (657 aa)	2.54	1.93	2.01	1.66
| NCU02124 | dienelactone hydrolase (256 aa)	2.44	1.86	1.59	1.35
| NCU07962 | conserved hypothetical protein (235 aa)	2.37	1.80	1.99	1.65
| NCU06120 | conserved hypothetical protein (167 aa)	2.29	1.74	1.75	1.47
| NCU08936 | clock-controlled gene-15 (412 aa)	2.29	1.74	2.29	1.87
| NCU08946 | hypothetical protein (277 aa)	2.29	1.74	1.98	1.64
| NCU11292 | conserved hypothetical protein (147 aa)	2.29	1.74	1.82	1.52
| NCU02906 | NAD-dependent malic enzyme 1 (612 aa)	2.27	1.73	1.74	1.46
| NCU05261 | ATP-dependent protease La (1108 aa)	2.23	1.70	0.86	0.80
| NCU06536 | conserved hypothetical protein (1050 aa)	2.23	1.70	2.86	2.30
| NCU08095 | conserved hypothetical protein (246 aa)	2.19	1.67	1.91	1.59

| NCU07287 | conserved hypothetical protein (227 aa)	2.13	1.62	3.34	2.65
| NCU01233 | aldose reductase (290 aa)	1.99	1.52	0.89	0.82
| NCU02513 | YjeF domain-containing protein (354 aa)	1.98	1.51	2.06	1.70
| NCU06978 | conserved hypothetical protein (372 aa)	1.98	1.51	-0.97	-0.58
| NCU09560 | superoxide dismutase (229 aa)	1.90	1.45	0.40	0.45
| NCU07232 | heat shock protein 30 (233 aa)	1.89	1.44	0.24	0.33
| NCU02482 | 2-methylcitrate synthase (471 aa)	1.87	1.43	-0.35	-0.11
| NCU03823 | ABC1 protein (775 aa)	1.85	1.41	1.38	1.19
| NCU04605 | conserved hypothetical protein (136 aa)	1.83	1.40	-0.72	-0.39
| NCU12151 | conserved hypothetical protein (162 aa)	1.83	1.40	0.29	0.37
| NCU02695 | conserved hypothetical protein (325 aa)	1.77	1.35	-0.86	-0.50
| NCU03310 | prohibitin-2 (311 aa)	1.74	1.33	0.96	0.87
| NCU11484 | conserved hypothetical protein (104 aa)	1.74	1.33	1.29	1.12
| NCU02630 | heat shock protein 78 (811 aa)	1.73	1.32	1.20	1.05
| NCU12046 | gamma-butyrobetaine dioxygenase (756 aa)	1.71	1.31	0.39	0.44
| NCU08291 | ferrochelatase (422 aa)	1.70	1.30	0.09	0.22
| NCU02887 | voltage-gated potassium channel beta-2 subunit (400 aa)	1.69	1.29	-0.60	-0.30
| NCU01479 | matrix AAA protease MAP-1 (929 aa)	1.67	1.28	-0.21	-0.01

| NCU04181 | translocase of outer mitochondrial membrane 7 (54 aa)	1.67	1.28	1.17	1.03
| NCU03749 | hydroxyacylglutathione hydrolase (283 aa)	1.66	1.27	0.73	0.70
| NCU05287 | 50S ribosomal protein L4 (264 aa)	1.65	1.26	0.66	0.65
| NCU07921 | conserved hypothetical protein (106 aa)	1.65	1.26	1.41	1.21
| NCU02595 | conserved hypothetical protein (136 aa)	1.63	1.25	-1.17	-0.73
| NCU01555 | conserved hypothetical protein (102 aa)	1.62	1.24	0.07	0.20
| NCU05667 | anchored cell wall protein-3 (220 aa)	1.57	1.20	0.97	0.88
| NCU05805 | serine hydroxymethyltransferase (547 aa)	1.55	1.19	-0.28	-0.06
| NCU10042 | enolase (439 aa)	1.55	1.19	1.86	1.55
| NCU05838 | conserved hypothetical protein (409 aa)	1.54	1.18	0.92	0.84
| NCU03076 | delta-1-pyrroline-5-carboxylate dehydrogenase (602 aa)	1.53	1.17	0.85	0.79
| NCU00655 | mitochondrial enoyl reductase (434 aa)	1.49	1.14	1.37	1.18
| NCU01169 | NADH:ubiquinone oxidoreductase 24 (264 aa)	1.47	1.13	0.08	0.21
| NCU07281 | glucose-6-phosphate isomerase (562 aa)	1.45	1.11	0.81	0.76
| NCU09754 | mitochondrial chaperone Frataxin (207 aa)	1.42	1.09	0.35	0.41
| NCU02943 | mitochondrial import inner membrane translocase subunit tim-50 (541 aa)	1.41	1.08	-0.88	-0.51

| NCU08005 | NADPH-adrenodoxin reductase Arh1 (529 aa)	1.37	1.05	1.32	1.14
| NCU08146 | conserved hypothetical protein (330 aa)	1.36	1.04	1.78	1.49
| NCU06086 | regulatory protein suaprga1 (275 aa)	1.33	1.02	0.16	0.27
| NCU07021 | peptide chain release factor 3 (853 aa)	1.33	1.02	1.21	1.06
| NCU06265 | conserved hypothetical protein (888 aa)	1.32	1.01	1.26	1.10
| NCU08699 | bli-4 protein (413 aa)	1.32	1.01	0.45	0.49
| NCU09255 | acetate non-utilizing protein 9 (149 aa)	1.32	1.01	0.20	0.30
| NCU00904 | D-lactate dehydrogenase (596 aa)	1.30	1.00	2.26	1.85
| NCU07061 | conserved hypothetical protein (178 aa)	1.30	1.00	0.41	0.46
| NCU02549 | processing enhancing protein (477 aa)	1.29	0.99	-0.12	0.06
| NCU03957 | COQ7 (257 aa)	1.29	0.99	1.18	1.04
| NCU07858 | DUF498 domain-containing protein (169 aa)	1.29	0.99	1.24	1.08
| NCU09596 | phytanoyl-CoA dioxygenase (337 aa)	1.29	0.99	1.95	1.62
| NCU00635 | nascent polypeptide-associated complex subunit alpha (201 aa)	1.26	0.97	0.66	0.65
| NCU02291 | glutaryl-CoA dehydrogenase (437 aa)	1.26	0.97	0.37	0.43
| NCU06270 | mitochondrial processing peptidase (578 aa)	1.26	0.97	0.05	0.19
| NCU01606 | ATP synthase subunit 5 (221 aa)	1.25	0.96	-1.67	-1.11
| NCU02807 | hypothetical protein (96 aa)	1.25	0.96	-1.51	-0.99

| NCU07434 | short-chain dehydrogenase/reductase SDR (349 aa)	1.24	0.95	0.47	0.50
| NCU04368 | glutathione S-transferase Gst3 (420 aa)	1.21	0.93	1.71	1.44
| NCU02267 | mitochondrial protein Fmp25 (607 aa)	1.20	0.92	0.73	0.70
| NCU00502 | ATP synthase subunit 4 (242 aa)	1.18	0.91	-2.59	-1.80
| NCU03814 | leucine-5 (995 aa)	1.17	0.90	1.16	1.02
| NCU11745 | conserved hypothetical protein (72 aa)	1.16	0.89	0.31	0.38
| NCU02220 | conserved hypothetical protein (234 aa)	1.13	0.87	1.17	1.03
| NCU03777 | mitochondrial 3-hydroxyisobutyryl-CoA hydrolase (509 aa)	1.12	0.86	0.24	0.33
| NCU08380 | plasma membrane phosphatase required for sodium stress response (449 aa)	1.12	0.86	0.32	0.39
| NCU02305 | decaprenyl-diphosphate synthase subunit 1 (450 aa)	1.10	0.85	1.36	1.17
| NCU05558 | 3-ketoacyl-CoA thiolase (421 aa)	1.10	0.85	0.68	0.66
| NCU02596 | conserved hypothetical protein (144 aa)	1.09	0.84	0.47	0.50
| NCU03297 | cytochrome c peroxidase (359 aa)	1.09	0.84	-0.48	-0.21
| NCU04098 | monothiol glutaredoxin-5 (166 aa)	1.08	0.83	0.08	0.21
| NCU08296 | 30S ribosomal subunit S4 (454 aa)	1.08	0.83	0.32	0.39
| NCU08693 | heat shock protein 70-5 (669 aa)	1.06	0.82	-3.07	-2.15
| NCU09266 | methylmalonate-semialdehyde dehydrogenase (584 aa)	1.06	0.82	1.29	1.12

| NCU02027 | acyl-protein thioesterase 1 (246 aa)	1.04	0.80	1.70	1.43
| NCU02806 | 14-3-3 family protein 7 (263 aa)	1.04	0.80	0.50	0.53
| NCU04192 | vacuolar aspartyl aminopeptidase Lap4 (536 aa)	1.02	0.79	1.40	1.20
| NCU06441 | D-lactate dehydrogenase 2 (552 aa)	1.02	0.79	-0.96	-0.57
| NCU00360 | NAD dependent epimerase/dehydratase (289 aa)	1.01	0.78	0.64	0.63
| NCU04591 | pentachlorophenol monooxygenase (680 aa)	1.01	0.78	3.20	2.55
| NCU00236 | flavoprotein oxygenase (367 aa)	1.00	0.77	0.66	0.65
| NCU00951 | inorganic pyrophosphatase (445 aa)	1.00	0.77	-1.42	-0.92
| NCU02177 | conserved hypothetical protein (237 aa)	1.00	0.77	0.81	0.76
| NCU06246 | ATP-dependent RNA helicase mrh-4 (626 aa)	1.00	0.77	2.31	1.89
| NCU08166 | conserved hypothetical protein (494 aa)	1.00	0.77	1.57	1.33
| NCU00414 | adenosine kinase (455 aa)	0.98	0.76	0.77	0.73
| NCU04946 | conserved hypothetical protein (185 aa)	0.98	0.76	0.13	0.25
| NCU06448 | enoyl-CoA hydratase (300 aa)	0.98	0.76	-0.21	-0.01
| NCU10732 | mitochondrial dicarboxylate transporter (332 aa)	0.98	0.76	1.86	1.55
| NCU00183 | DUF185 domain-containing protein (569 aa)	0.97	0.75	1.14	1.01
| NCU00920 | isoleucyl-tRNA synthetase (963 aa)	0.96	0.74	0.47	0.50

| NCU01474 | 60S ribosomal protein L4 (350 aa)	0.96	0.74	-0.20	0.00
| NCU09553 | 3-hydroxybutyryl CoA dehydrogenase (317 aa)	0.96	0.74	0.29	0.37
| NCU01204 | tropomyosin (162 aa)	0.94	0.73	-0.43	-0.17
| NCU07914 | phosphoglycerate kinase (419 aa)	0.94	0.73	1.37	1.18
| NCU01861 | short chain dehydrogenase/reductase family (360 aa)	0.93	0.72	1.05	0.94
| NCU03100 | 6-phosphogluconate dehydrogenase (493 aa)	0.93	0.72	0.65	0.64
| NCU09862 | ubiquinone biosynthesis methyltransferase coq5 (342 aa)	0.92	0.71	0.86	0.80
| NCU00936 | succinate semialdehyde dehydrogenase (537 aa)	0.90	0.70	0.47	0.50
| NCU09598 | mitochondrial escape protein 2 (868 aa)	0.90	0.70	1.37	1.18
| NCU03559 | ubiquinol-cytochrome c reductase complex core protein 2 precursor (455 aa)	0.89	0.69	-0.05	0.11
| NCU07695 | conserved hypothetical protein (425 aa)	0.89	0.69	0.82	0.77
| NCU00355 | catalase-3 (720 aa)	0.86	0.67	2.64	2.14
| NCU01404 | RNA methyltransferase (645 aa)	0.86	0.67	0.65	0.64
| NCU01680 | plasma membrane ATPase-1 (921 aa)	0.86	0.67	0.35	0.41
| NCU05225 | NADH dehydrogenase 64 (674 aa)	0.86	0.67	1.55	1.32
| NCU05248 | conserved hypothetical protein (215 aa)	0.86	0.67	-1.91	-1.29

| NCU06424 | aminomethyl transferase (440 aa)	0.86	0.67	0.64	0.63
| NCU07465 | mitochondrial phosphate carrier protein 2 (383 aa)	0.86	0.67	1.33	1.15
| NCU05286 | conserved hypothetical protein (74 aa)	0.85	0.66	0.00	0.15
| NCU01307 | conserved hypothetical protein (212 aa)	0.84	0.65	-3.10	-2.17
| NCU03891 | peptide methionine sulfoxide reductase msrB (238 aa)	0.84	0.65	1.10	0.98
| NCU09257 | conserved hypothetical protein (243 aa)	0.84	0.65	0.29	0.37
| NCU00599 | 37S ribosomal protein Rsm22 (871 aa)	0.82	0.64	0.78	0.74
| NCU05008 | predicted protein (135 aa)	0.82	0.64	-0.52	-0.24
| NCU05299 | NADH:ubiquinone oxidoreductase 29.9 (274 aa)	0.81	0.63	-2.27	-1.56
| NCU07298 | CAIB/BAIF family enzyme (445 aa)	0.81	0.63	1.05	0.94
| NCU11552 | nucleic acid-binding protein (345 aa)	0.81	0.63	-1.16	-0.72
| NCU11494 | glutaredoxin domain-containing protein (109 aa)	0.80	0.62	0.68	0.66
| NCU03148 | nascent polypeptide-associated complex beta subunit (153 aa)	0.78	0.61	0.57	0.58
| NCU05076 | conserved hypothetical protein (132 aa)	0.77	0.60	-0.68	-0.36
| NCU03338 | conserved hypothetical protein (498 aa)	0.76	0.59	0.52	0.54
| NCU04142 | heat shock protein 80 (706 aa)	0.76	0.59	0.93	0.85

| NCU06749 | 60S ribosomal protein L3 (385 aa)	0.76	0.59	0.68	0.66
| NCU07494 | conserved hypothetical protein (318 aa)	0.76	0.59	-0.23	-0.02
| NCU07793 | conserved hypothetical protein (527 aa)	0.76	0.59	0.96	0.87
| NCU02936 | proline oxidase (551 aa)	0.74	0.58	0.80	0.75
| NCU04244 | syntaxin 2 (336 aa)	0.74	0.58	0.77	0.73
| NCU08823 | band (214 aa)	0.74	0.58	1.21	1.06
| NCU03737 | elongation factor Tu (438 aa)	0.72	0.56	-1.53	-1.00
| NCU03802 | trimethyllysine dioxygenase (528 aa)	0.69	0.54	-0.81	-0.46
| NCU00405 | glycyl-tRNA synthetase 1 (733 aa)	0.68	0.53	1.71	1.44
| NCU07742 | poly(p)/ATP NAD kinase (504 aa)	0.68	0.53	0.43	0.47
| NCU08676 | conserved hypothetical protein (223 aa)	0.68	0.53	0.05	0.19
| NCU05495 | CVNH domain-containing protein (112 aa)	0.66	0.52	1.17	1.03
| NCU05593 | mitochondrial outer membrane beta-barrel protein Tob55 (517 aa)	0.65	0.51	-0.64	-0.33
| NCU12112 | cell division protein ftsj (487 aa)	0.65	0.51	1.25	1.09
| NCU02580 | fumarate reductase Osm1 (617 aa)	0.64	0.50	0.64	0.63
| NCU05982 | hexaprenyldihydroxybenzoate methyltransferase (344 aa)	0.62	0.49	0.97	0.88
| NCU00695 | conserved hypothetical protein (537 aa)	0.61	0.48	1.13	1.00

| NCU01306 | conserved hypothetical protein (391 aa)	0.61	0.48	0.08	0.21
| NCU03753 | clock-controlled gene-1 (72 aa)	0.61	0.48	0.86	0.80
| NCU03893 | short-chain dehydrogenase/reductase SDR (365 aa)	0.61	0.48	-0.11	0.07
| NCU05459 | mitochondrial AAA ATPase (1105 aa)	0.61	0.48	2.22	1.82
| NCU01512 | phenylalanyl-tRNA synthetase (518 aa)	0.60	0.47	0.85	0.79
| NCU02734 | citrate lyase beta subunit (320 aa)	0.60	0.47	0.21	0.31
| NCU05427 | ATP-dependent Clp protease (641 aa)	0.60	0.47	1.33	1.15
| NCU07386 | Fe superoxide dismutase (311 aa)	0.60	0.47	0.50	0.53
| NCU07807 | fructose bisphosphate aldolase (363 aa)	0.60	0.47	1.71	1.44
| NCU02727 | glycine cleavage system T protein (478 aa)	0.58	0.46	0.85	0.79
| NCU03080 | conserved hypothetical protein (588 aa)	0.58	0.46	-0.24	-0.03
| NCU05512 | copper resistance protein Crd2 (113 aa)	0.58	0.46	-0.57	-0.28
| NCU06588 | conserved hypothetical protein (182 aa)	0.58	0.46	-1.95	-1.32
| NCU04117 | ATP-dependent permease MDL2 (800 aa)	0.57	0.45	-0.69	-0.37
| NCU12023 | 37S ribosomal protein MRP4 (429 aa)	0.56	0.44	-0.77	-0.43
| NCU00122 | aspartyl aminopeptidase (538 aa)	0.53	0.42	0.60	0.60
| NCU00562 | conserved hypothetical protein (579 aa)	0.53	0.42	1.24	1.08

| NCU02623 | mitochondrial hypoxia responsive domain-containing protein (242 aa)	0.53	0.42	0.04	0.18
| NCU00057 | ubiquinol cytochrome-c reductase assembly protein Cbp3 (369 aa)	0.52	0.41	0.49	0.52
| NCU02565 | hypothetical protein (509 aa)	0.52	0.41	1.50	1.28
| NCU03231 | mitochondrial chaperone BCS1 (474 aa)	0.50	0.40	0.24	0.33
| NCU04510 | aldose reductase (327 aa)	0.50	0.40	1.22	1.07
| NCU08477 | small GTP-binding protein (204 aa)	0.50	0.40	0.21	0.31
| NCU09091 | mitochondrial inner membrane magnesium transporter mrs2 (548 aa)	0.50	0.40	0.53	0.55
| NCU04081 | GTP binding protein (505 aa)	0.49	0.39	0.23	0.32
| NCU01523 | GTP-binding protein ypt3 (215 aa)	0.48	0.38	1.73	1.45
| NCU06880 | AhpC/TSA family protein (197 aa)	0.48	0.38	-1.67	-1.11
| NCU11285 | cytosolic Fe-S cluster assembling factor NBP35 (310 aa)	0.48	0.38	1.42	1.22
| NCU00278 | conserved hypothetical protein (272 aa)	0.47	0.37	0.13	0.25
| NCU04140 | FK506 resistant-2 (176 aa)	0.47	0.37	-1.62	-1.07
| NCU00395 | mRNA processing protein (528 aa)	0.45	0.36	0.35	0.41
| NCU00905 | N-acylethanolamine amidohydrolase (611 aa)	0.44	0.35	0.35	0.41
| NCU02095 | conserved hypothetical protein (315 aa)	0.44	0.35	1.38	1.19
| NCU03147 | assembly factor cbp-4 (126 aa)	0.44	0.35	0.33	0.40

| NCU03173 | HAD superfamily hydrolase (459 aa)	0.44	0.35	-0.44	-0.18
| NCU04347 | pyruvate formate lyase activating enzyme (254 aa)	0.44	0.35	1.67	1.41
| NCU03870 | conserved hypothetical protein (834 aa)	0.43	0.34	0.23	0.32
| NCU07423 | conserved hypothetical protein (748 aa)	0.43	0.34	0.03	0.17
| NCU08299 | 60S ribosomal protein L3 (440 aa)	0.41	0.33	-0.09	0.08
| NCU09057 | conserved hypothetical protein (274 aa)	0.41	0.33	-2.09	-1.42
| NCU02536 | ubiquinone biosynthesis monooxygenase COQ6 (491 aa)	0.40	0.32	0.93	0.85
| NCU03488 | pyrimidine-4 (398 aa)	0.40	0.32	0.43	0.47
| NCU04013 | yellow-1 (517 aa)	0.40	0.32	0.44	0.48
| NCU04225 | 60S ribosomal protein L20 (226 aa)	0.40	0.32	-0.57	-0.28
| NCU02310 | conserved hypothetical protein (803 aa)	0.39	0.31	-0.41	-0.16
| NCU02499 | DNL zinc finger domain-containing protein (239 aa)	0.39	0.31	-0.25	-0.04
| NCU01485 | conserved hypothetical protein (397 aa)	0.37	0.30	0.00	0.15
| NCU02127 | methylcrotonoyl-CoA carboxylase subunit beta (609 aa)	0.37	0.30	1.49	1.27
| NCU03739 | ERP38 protein (370 aa)	0.37	0.30	1.01	0.91
| NCU03793 | conserved hypothetical protein (493	0.37	0.30	0.21	0.31

aa)				
| NCU04768 | electron transfer flavoprotein-ubiquinone oxidoreductase (646 aa)	0.37	0.30	0.00	0.15
| NCU09741 | NADPH-cytochrome P450 reductase (693 aa)	0.37	0.30	0.61	0.61
| NCU06450 | mitochondrial ribosomal protein (259 aa)	0.36	0.29	0.07	0.20
| NCU06760 | pyruvate dehydrogenase kinase (438 aa)	0.36	0.29	0.09	0.22
| NCU07915 | integral membrane protein (280 aa)	0.36	0.29	0.11	0.23
| NCU11176 | actin cytoskeleton organization protein App1 (855 aa)	0.36	0.29	-1.09	-0.67
| NCU00051 | conserved hypothetical protein (367 aa)	0.35	0.28	0.57	0.58
| NCU01528 | glyceraldehyde-3-phosphate dehydrogenase-1 (339 aa)	0.35	0.28	0.88	0.81
| NCU05118 | vacuolar membrane ATPase-10 (116 aa)	0.35	0.28	-0.37	-0.13
| NCU00135 | phosphatidyl synthase (347 aa)	0.33	0.27	-0.24	-0.03
| NCU00225 | conserved hypothetical protein (319 aa)	0.33	0.27	0.28	0.36
| NCU06881 | succinyl-CoA:3-ketoacid-coenzyme A transferase subunit A (517 aa)	0.33	0.27	-0.43	-0.17
| NCU01997 | ABC transporter (719 aa)	0.32	0.26	0.00	0.15
| NCU06748 | hypothetical protein (215 aa)	0.32	0.26	0.80	0.75
| NCU00475 | 40S ribosomal protein S18 (157 aa)	0.31	0.25	1.69	1.42

| NCU09732 | acetyl-CoA acetyltransferase (431 aa)	0.31	0.25	-0.73	-0.40
| NCU01469 | conserved hypothetical protein (286 aa)	0.29	0.24	0.04	0.18
| NCU04636 | cysteine desulfurase (506 aa)	0.29	0.24	0.60	0.60
| NCU05601 | cytochrome-2 (347 aa)	0.29	0.24	1.04	0.93
| NCU07549 | mitochondrial ribosomal protein L43 (139 aa)	0.29	0.24	-0.07	0.10
| NCU11889 | ADP-ribose 1"-phosphate phosphatase (862 aa)	0.29	0.24	-0.15	0.04
| NCU01516 | mitochondrial co-chaperone GrpE (239 aa)	0.28	0.23	-2.78	-1.94
| NCU02571 | acetyl-CoA acetyltransferase (400 aa)	0.28	0.23	1.32	1.14
| NCU04069 | 3'-phosphoadenosine 5'-phosphatase isoform B (429 aa)	0.28	0.23	-0.03	0.13
| NCU06542 | mitochondrial 30S ribosomal protein S12 (175 aa)	0.28	0.23	0.01	0.16
| NCU08120 | mitochondrial ribosomal protein DAP3 (470 aa)	0.28	0.23	0.17	0.28
| NCU08269 | pyridoxamine 5'-phosphate oxidase (299 aa)	0.28	0.23	0.27	0.35
| NCU09594 | seryl-tRNA synthetase (552 aa)	0.28	0.23	-0.19	0.01
| NCU00726 | cyclosporin-resistant-1 (224 aa)	0.27	0.22	-1.30	-0.83
| NCU10007 | malate synthase (543 aa)	0.27	0.22	0.25	0.34
| NCU00371 | mitochondrial import inner membrane translocase subunit tim23 (239 aa)	0.25	0.21	0.19	0.29
| NCU04764 | conserved hypothetical protein (480 aa)	0.25	0.21	0.33	0.40

| NCU09770 | acetyl-coa hydrolase (526 aa)	0.25	0.21	-0.09	0.08
| NCU01800 | 37S ribosomal protein S5 (478 aa)	0.24	0.20	-0.45	-0.19
| NCU03439 | conserved hypothetical protein (356 aa)	0.24	0.20	0.04	0.18
| NCU05623 | translocase of mitochondrial inner membrane 17 (156 aa)	0.24	0.20	0.61	0.61
| NCU08004 | electron transfer flavoprotein alpha-subunit (349 aa)	0.24	0.20	-2.80	-1.96
| NCU05517 | mitochondrial genome maintenance protein MGM101 (338 aa)	0.23	0.19	-0.23	-0.02
| NCU03516 | mitochondrial ribosomal protein subunit L32 (130 aa)	0.21	0.18	1.05	0.94
| NCU05302 | GTP-binding protein Obg (592 aa)	0.21	0.18	-0.15	0.04
| NCU11170 | mitochondrial translation optimization protein (718 aa)	0.21	0.18	-0.03	0.13
| NCU02133 | superoxide dismutase (155 aa)	0.20	0.17	-0.57	-0.28
| NCU04412 | conserved hypothetical protein (348 aa)	0.20	0.17	-0.04	0.12
| NCU00895 | RAB GTPase Ypt5 (221 aa)	0.19	0.16	1.37	1.18
| NCU00903 | conserved hypothetical protein (351 aa)	0.19	0.16	0.21	0.31
| NCU06783 | ATP citrate lyase (488 aa)	0.19	0.16	0.50	0.53
| NCU08336 | succinate dehydrogenase flavoprotein subunit (649 aa)	0.19	0.16	-0.81	-0.46
| NCU11181 | Ras superfamily GTPase (190 aa)	0.19	0.16	0.37	0.43
| NCU00959 | succinate dehydrogenase iron-sulfur	0.17	0.15	-2.33	-1.60

protein (283 aa)				
| NCU03284 | conserved hypothetical protein (184 aa)	0.17	0.15	0.40	0.45
| NCU05635 | conserved hypothetical protein (585 aa)	0.17	0.15	0.92	0.84
| NCU05772 | translocase of outer mitochondrial membrane 6 (61 aa)	0.17	0.15	-0.44	-0.18
| NCU07852 | ribosomal protein L13 (184 aa)	0.17	0.15	-0.53	-0.25
| NCU11834 | tryptophanyl-tRNA synthetase (422 aa)	0.17	0.15	-0.56	-0.27
| NCU00680 | 2-methylcitrate dehydratase (566 aa)	0.16	0.14	1.98	1.64
| NCU03827 | 40S ribosomal protein S9 (316 aa)	0.16	0.14	0.53	0.55
| NCU01484 | rho-type GTPase (196 aa)	0.15	0.13	-0.44	-0.18
| NCU03283 | 2-keto-4-pentenoate hydratase (242 aa)	0.15	0.13	-1.37	-0.88
| NCU09143 | conserved hypothetical protein (100 aa)	0.15	0.13	-2.23	-1.53
| NCU06008 | conserved hypothetical protein (427 aa)	0.13	0.12	0.98	0.89
| NCU07682 | arginine-14 (713 aa)	0.13	0.12	0.50	0.53
| NCU02585 | aspartyl-tRNA synthetase (645 aa)	0.12	0.10	-0.16	0.03
| NCU05488 | RNA-binding protein Vip1 (284 aa)	0.12	0.10	1.20	1.05
| NCU07756 | succinate dehydrogenase cytochrome b560 subunit (181 aa)	0.12	0.10	-0.19	0.01
| NCU08350 | conserved hypothetical protein (302 aa)	0.12	0.10	0.07	0.20
| NCU00173 | esterase D	0.11	0.09	-0.21	-0.01

(296 aa)				
| NCU02572 | U5 small nuclear ribonucleoprotein component (938 aa)	0.11	0.09	1.69	1.42
| NCU04578 | ATP-dependent Clp protease proteolytic subunit 1 (259 aa)	0.11	0.09	0.45	0.49
| NCU06606 | iron-sulfur subunit-1 (232 aa)	0.11	0.09	-1.61	-1.06
| NCU04380 | acyl-CoA synthetase (707 aa)	0.09	0.08	0.01	0.16
| NCU07733 | electron transfer flavoprotein beta-subunit (257 aa)	0.09	0.08	-1.51	-0.99
| NCU11345 | conserved hypothetical protein (471 aa)	0.09	0.08	-0.07	0.10
| NCU11996 | conserved hypothetical protein (503 aa)	0.09	0.08	0.07	0.20
| NCU01023 | 50S ribosomal protein L17 (194 aa)	0.08	0.07	-2.01	-1.36
| NCU02319 | aminopeptidase (1060 aa)	0.08	0.07	-0.08	0.09
| NCU04138 | conserved hypothetical protein (220 aa)	0.08	0.07	-0.50	-0.23
| NCU04817 | electron transfer protein 1 (493 aa)	0.08	0.07	-0.17	0.02
| NCU05813 | mitochondrial large ribosomal subunit (365 aa)	0.08	0.07	0.00	0.15
| NCU07446 | vacuolar membrane ATPase-4 (231 aa)	0.07	0.06	1.41	1.21
| NCU07670 | CYT-19 DEAD-box protein (627 aa)	0.07	0.06	0.16	0.27
| NCU08130 | conserved hypothetical protein (163 aa)	0.07	0.06	0.44	0.48
| NCU00114 | 30S ribosomal protein S10 (269 aa)	0.05	0.05	-0.12	0.06

| NCU02599 | BAP31 domain-containing protein (213 aa)	0.05	0.05	-0.62	-0.32
| NCU02955 | elongation factor G 1 (658 aa)	0.05	0.05	-0.05	0.11
| NCU03177 | sco1 (283 aa)	0.05	0.05	-1.14	-0.71
| NCU04336 | 60S ribosomal protein L19 (159 aa)	0.05	0.05	0.29	0.37
| NCU05552 | conserved hypothetical protein (444 aa)	0.05	0.05	0.07	0.20
| NCU03296 | F1 ATPase assembly protein 11 (342 aa)	0.04	0.04	-0.35	-0.11
| NCU11301 | mitochondrial translation initiation factor (1271 aa)	0.04	0.04	0.41	0.46
| NCU11908 | hypothetical protein (62 aa)	0.04	0.04	-0.36	-0.12
| NCU00884 | NAD dependent epimerase/dehydratase (417 aa)	0.03	0.03	0.45	0.49
| NCU01758 | YdiU domain-containing protein (685 aa)	0.03	0.03	0.74	0.71
| NCU02064 | hypothetical protein (281 aa)	0.03	0.03	-0.12	0.06
| NCU06069 | conserved hypothetical protein (132 aa)	0.03	0.03	0.00	0.15
| NCU09999 | conserved hypothetical protein (301 aa)	0.03	0.03	0.07	0.20
| NCU03579 | alanine racemase (263 aa)	0.01	0.02	0.37	0.43
| NCU05714 | 50S ribosomal subunit protein L15 (313 aa)	0.01	0.02	-0.19	0.01
| NCU06924 | kynurenine 3-monooxygenase (513 aa)	0.01	0.02	0.17	0.28
| NCU08272 | cytochrome b2 (502 aa)	0.01	0.02	0.33	0.40
| NCU09892 | prolyl-tRNA synthetase (588 aa)	0.01	0.02	-0.20	0.00

| NCU00977 | aconitate hydratase (218 aa)	0.00	0.01	-0.20	0.00
| NCU03112 | NADH-cytochrome b5 reductase 2 (344 aa)	0.00	0.01	-0.52	-0.24
| NCU04171 | 50S ribosomal protein L5 (353 aa)	0.00	0.01	-0.44	-0.18
| NCU05390 | mitochondrial phosphate carrier protein (320 aa)	0.00	0.01	-0.08	0.09
| NCU06877 | CRAL/TRIO domain-containing protein (492 aa)	0.00	0.01	-0.20	0.00
| NCU07608 | ribose 5-phosphate isomerase A (365 aa)	0.00	0.01	-0.25	-0.04
| NCU09462 | conserved hypothetical protein (155 aa)	0.00	0.01	0.08	0.21
| NCU01779 | HIRA-interacting protein 5 (327 aa)	-0.01	0.00	-0.24	-0.03
| NCU02804 | mitochondrial 60S ribosomal protein L25 (164 aa)	-0.01	0.00	0.07	0.20
| NCU03156 | NUO (95 aa)	-0.01	0.00	-1.36	-0.87
| NCU06786 | 50S ribosomal protein L30 (162 aa)	-0.01	0.00	-0.21	-0.01
| NCU08661 | pantoate-beta-alanine ligase (362 aa)	-0.01	0.00	-0.09	0.08
| NCU11950 | 50S ribosomal protein L24 (275 aa)	-0.01	0.00	-0.03	0.13
| NCU00596 | lipoyltransferase (385 aa)	-0.03	-0.01	0.09	0.22
| NCU01506 | conserved hypothetical protein (330 aa)	-0.03	-0.01	0.74	0.71
| NCU04173 | actin (376 aa)	-0.03	-0.01	-0.11	0.07
| NCU04644 | conserved hypothetical protein (265 aa)	-0.03	-0.01	0.35	0.41

| NCU02108 | BolA domain-containing protein (163 aa)	-0.04	-0.02	-0.21	-0.01
| NCU03006 | sterol 24-C-methyltransferase (380 aa)	-0.04	-0.02	-1.58	-1.04
| NCU03339 | glutathione reductase (504 aa)	-0.04	-0.02	0.00	0.15
| NCU04280 | aconitate hydratase (810 aa)	-0.04	-0.02	-0.05	0.11
| NCU05778 | iron sulfur cluster assembly protein 1 (186 aa)	-0.04	-0.02	-1.67	-1.11
| NCU08893 | 60S ribosomal protein L1 (304 aa)	-0.04	-0.02	-0.07	0.10
| NCU00489 | cytoplasmic ribosomal protein-10 (263 aa)	-0.05	-0.03	0.82	0.77
| NCU02063 | mitochondrial intermediate peptidase (806 aa)	-0.05	-0.03	-0.94	-0.56
| NCU02107 | AMP-binding enzyme (619 aa)	-0.05	-0.03	-0.07	0.10
| NCU03624 | conserved hypothetical protein (677 aa)	-0.05	-0.03	-0.17	0.02
| NCU03926 | 37S ribosomal protein Rsm24 (405 aa)	-0.05	-0.03	-1.17	-0.73
| NCU08707 | iron sulfur assembly protein (315 aa)	-0.05	-0.03	1.28	1.11
| NCU01371 | UPF0660 protein (219 aa)	-0.07	-0.04	-0.29	-0.07
| NCU01859 | NADH:ubiquinone oxidoreductase 20.9kD subunit (190 aa)	-0.07	-0.04	-0.48	-0.21
| NCU02705 | F1F0 ATP synthase assembly protein Atp10 (370 aa)	-0.07	-0.04	-0.03	0.13
| NCU05221 | NADH:ubiquinone oxidoreductase 21kD subunit (219 aa)	-0.07	-0.04	-0.53	-0.25

| NCU06532 | dihydroorotate reductase PyrE (501 aa)	-0.07	-0.04	-0.04	0.12
| NCU01102 | mitochondrial export translocase Oxa1 (463 aa)	-0.08	-0.05	0.01	0.16
| NCU01854 | conserved hypothetical protein (215 aa)	-0.08	-0.05	0.15	0.26
| NCU02007 | iron-sulfur cluster biosynthesis protein Isd11 (111 aa)	-0.08	-0.05	-0.29	-0.07
| NCU03004 | pyruvate dehydrogenase E1 component (380 aa)	-0.08	-0.05	-3.00	-2.10
| NCU04212 | conserved hypothetical protein (512 aa)	-0.08	-0.05	-0.20	0.00
| NCU06308 | DNA-directed RNA polymerase (1424 aa)	-0.08	-0.05	0.00	0.15
| NCU00484 | NADH:ubiquinone oxidoreductase 18.4kD subunit (166 aa)	-0.09	-0.06	-1.85	-1.24
| NCU02193 | cellular filament polypeptide (549 aa)	-0.09	-0.06	1.38	1.19
| NCU03343 | 37S ribosomal protein S25 (241 aa)	-0.09	-0.06	0.39	0.44
| NCU00075 | mitochondrial import inner membrane translocase subunit tim-14 (106 aa)	-0.11	-0.07	0.00	0.15
| NCU00204 | conserved hypothetical protein (215 aa)	-0.11	-0.07	0.00	0.15
| NCU00958 | 5-azacytidine resistance protein azr1 (459 aa)	-0.11	-0.07	-0.32	-0.09
| NCU01219 | glutaredoxin (125 aa)	-0.11	-0.07	0.00	0.15
| NCU01975 | complex I intermediate associated protein 30 (279 aa)	-0.11	-0.07	-0.03	0.13
| NCU03979 | biotin	-0.11	-0.07	-0.20	0.00

synthase (440 aa)				
| NCU03094 | conserved hypothetical protein (219 aa)	-0.12	-0.08	-0.16	0.03
| NCU05202 | conserved hypothetical protein (361 aa)	-0.12	-0.08	-0.15	0.04
| NCU06556 | thioredoxin II (148 aa)	-0.12	-0.08	-0.09	0.08
| NCU02504 | DUF1640 domain-containing protein (275 aa)	-0.13	-0.09	0.03	0.17
| NCU02534 | NADH:ubiquinone oxidoreductase 49kD subunit (479 aa)	-0.13	-0.09	0.17	0.28
| NCU04754 | branched-chain-amino-acid aminotransferase (406 aa)	-0.13	-0.09	-0.01	0.14
| NCU06876 | adenosine 5'-monophosphoramidase (141 aa)	-0.13	-0.09	0.47	0.50
| NCU08138 | cytochrome C1 heme lyase (315 aa)	-0.13	-0.09	0.41	0.46
| NCU08329 | mitochondrial ribosomal protein subunit L23 (229 aa)	-0.13	-0.09	-0.89	-0.52
| NCU06617 | myosin regulatory light chain cdc4 (140 aa)	-0.15	-0.10	0.35	0.41
| NCU07263 | carnitine/acyl carnitine carrier (343 aa)	-0.15	-0.10	0.00	0.15
| NCU09602 | heat shock protein 70-1 (647 aa)	-0.15	-0.10	-0.11	0.07
| NCU00385 | ATP synthase subunit delta (166 aa)	-0.16	-0.11	-2.90	-2.02
| NCU04044 | NADH2 dehydrogenase flavoprotein 1 (494 aa)	-0.16	-0.11	-0.21	-0.01
| NCU06768 | 60S ribosomal protein L16 (250 aa)	-0.16	-0.11	-0.11	0.07
| NCU11421 | conserved hypothetical protein (460 aa)	-0.16	-0.11	-0.16	0.03

| NCU06546 | conserved hypothetical protein (554 aa)	-0.17	-0.12	-0.15	0.04
| NCU08354 | conserved hypothetical protein (514 aa)	-0.17	-0.12	-0.09	0.08
| NCU00443 | ran-specific GTPase-activating protein 1 (251 aa)	-0.19	-0.13	0.62	0.62
| NCU01894 | conserved hypothetical protein (349 aa)	-0.19	-0.13	-0.07	0.10
| NCU01983 | conserved hypothetical protein (309 aa)	-0.19	-0.13	0.77	0.73
| NCU02407 | dihydrolipoyl dehydrogenase (505 aa)	-0.19	-0.13	-0.98	-0.59
| NCU02701 | dipeptidyl peptidase (707 aa)	-0.19	-0.13	1.32	1.14
| NCU11237 | prenylated Rab acceptor 1 (177 aa)	-0.19	-0.13	-1.50	-0.98
| NCU02757 | 60S ribosomal protein L2 (384 aa)	-0.20	-0.14	-1.14	-0.71
| NCU03653 | conserved hypothetical protein (237 aa)	-0.20	-0.14	0.03	0.17
| NCU04588 | conserved hypothetical protein (223 aa)	-0.20	-0.14	0.81	0.76
| NCU06914 | histidyl-tRNA synthetase (547 aa)	-0.20	-0.14	-0.56	-0.27
| NCU07794 | 2Fe-2S iron-sulfur cluster binding domain-containing protein (192 aa)	-0.20	-0.14	-0.80	-0.45
| NCU08994 | conserved hypothetical protein (417 aa)	-0.20	-0.14	0.23	0.32
| NCU09243 | conserved hypothetical protein (389 aa)	-0.20	-0.14	0.40	0.45
| NCU00641 | cytochrome c oxidase-assembly factor cox-16 (115 aa)	-0.21	-0.15	-0.44	-0.18

| NCU03229 | translocase of inner mitochondrial membrane 44 (527 aa)	-0.21	-0.15	-2.56	-1.78
| NCU08861 | conserved hypothetical protein (448 aa)	-0.21	-0.15	-1.58	-1.04
| NCU00264 | hypothetical protein (163 aa)	-0.23	-0.16	-1.61	-1.06
| NCU09119 | ATP synthase subunit gamma (300 aa)	-0.23	-0.16	-1.06	-0.65
| NCU11753 | conserved hypothetical protein (203 aa)	-0.23	-0.16	-0.25	-0.04
| NCU02160 | small GTPase RAC (201 aa)	-0.24	-0.17	0.54	0.56
| NCU03008 | conserved hypothetical protein (112 aa)	-0.24	-0.17	-0.15	0.04
| NCU08071 | cytochrome-21 (108 aa)	-0.24	-0.17	-0.04	0.12
| NCU08923 | zinc knuckle domain-containing protein (184 aa)	-0.24	-0.17	1.14	1.01
| NCU09539 | 40S ribosomal protein S13 (120 aa)	-0.24	-0.17	-0.43	-0.17
| NCU02162 | SURF-family protein (341 aa)	-0.25	-0.18	0.25	0.34
| NCU11171 | ssDNA binding protein (153 aa)	-0.25	-0.18	-1.58	-1.04
| NCU01473 | mitochondrial large ribosomal subunit YmL35 (450 aa)	-0.27	-0.19	-0.25	-0.04
| NCU01673 | conserved hypothetical protein (240 aa)	-0.27	-0.19	-0.24	-0.03
| NCU05522 | PaaI_thioesterase (171 aa)	-0.27	-0.19	-0.31	-0.08
| NCU05890 | conserved hypothetical protein (166 aa)	-0.27	-0.19	-0.49	-0.22
| NCU06721 | peptide chain release factor 1 (431 aa)	-0.27	-0.19	-0.88	-0.51

| NCU08326 | mitochondrial carrier protein LEU5 (391 aa)	-0.27	-0.19	0.56	0.57
| NCU08824 | molybdopterin binding domain-containing protein (290 aa)	-0.27	-0.19	-0.03	0.13
| NCU00211 | mitochondrial ribosomal protein subunit L31 (111 aa)	-0.28	-0.20	-0.88	-0.51
| NCU00431 | mitochondrial import receptor subunit Tom22 (155 aa)	-0.28	-0.20	-0.47	-0.20
| NCU08960 | hypothetical protein (110 aa)	-0.29	-0.21	0.20	0.30
| NCU09058 | enoyl-CoA hydratase (344 aa)	-0.29	-0.21	-2.23	-1.53
| NCU03030 | tyrosyl-tRNA synthetase (670 aa)	-0.31	-0.22	0.25	0.34
| NCU04068 | 60S ribosomal protein L6 (256 aa)	-0.31	-0.22	0.05	0.19
| NCU05454 | glycerol-3-phosphate dehydrogenase (695 aa)	-0.31	-0.22	-1.34	-0.86
| NCU05541 | conserved hypothetical protein (380 aa)	-0.31	-0.22	-0.21	-0.01
| NCU06451 | conserved hypothetical protein (397 aa)	-0.31	-0.22	-0.65	-0.34
| NCU06469 | 54S ribosomal protein L12 (177 aa)	-0.31	-0.22	-4.52	-3.24
| NCU00111 | conserved hypothetical protein (214 aa)	-0.32	-0.23	-0.25	-0.04
| NCU00654 | conserved hypothetical protein (275 aa)	-0.32	-0.23	-0.88	-0.51
| NCU01650 | conserved hypothetical protein (202 aa)	-0.32	-0.23	-0.12	0.06
| NCU01920 | conserved hypothetical protein (220 aa)	-0.32	-0.23	-0.82	-0.47

| NCU02954 | homoisocitrate dehydrogenase (358 aa)	-0.32	-0.23	-1.41	-0.91
| NCU07776 | anchored cell wall protein-5 (191 aa)	-0.32	-0.23	-0.56	-0.27
| NCU01467 | NADH:ubiquinone oxidoreductase 10.4kD subunit (93 aa)	-0.33	-0.24	-0.29	-0.07
| NCU04481 | mitochondrial ATPase (556 aa)	-0.33	-0.24	0.66	0.65
| NCU05075 | mitochondrial tricarboxylate transporter (305 aa)	-0.33	-0.24	-0.45	-0.19
| NCU06017 | thiosulfate sulfurtransferase (334 aa)	-0.33	-0.24	-0.62	-0.32
| NCU07659 | pyruvate dehydrogenase complex (459 aa)	-0.33	-0.24	-2.34	-1.61
| NCU02451 | mitochondrial hypoxia responsive domain-containing protein (279 aa)	-0.35	-0.25	-1.18	-0.74
| NCU03394 | ribosomal protein S15 (321 aa)	-0.35	-0.25	-1.10	-0.68
| NCU05029 | iron-sulfur clusters transporter atm-1 (717 aa)	-0.35	-0.25	0.40	0.45
| NCU06403 | conserved hypothetical protein (673 aa)	-0.35	-0.25	-0.08	0.09
| NCU01454 | mitochondrial hydrolase (349 aa)	-0.36	-0.26	-1.12	-0.69
| NCU00676 | F1-ATP synthase assembly protein (432 aa)	-0.37	-0.27	-0.69	-0.37
| NCU01007 | conserved hypothetical protein (257 aa)	-0.37	-0.27	-0.43	-0.17
| NCU06300 | guanylate kinase (216 aa)	-0.37	-0.27	0.33	0.40
| NCU08002 | carnitine acetyl transferase (644 aa)	-0.37	-0.27	-0.84	-0.48
| NCU07727 | COPI-coated vesicle protein (131 aa)	-0.39	-0.28	-0.09	0.08

| NCU05119 | conserved hypothetical protein (117 aa)	-0.40	-0.29	-1.55	-1.02
| NCU08352 | cysteine-9 (335 aa)	-0.40	-0.29	0.23	0.32
| NCU01828 | conserved hypothetical protein (61 aa)	-0.41	-0.30	-0.24	-0.03
| NCU02003 | translation elongation factor-1 (461 aa)	-0.41	-0.30	0.19	0.29
| NCU06632 | translocase of outer mitochondrial membrane 20 (182 aa)	-0.41	-0.30	-1.05	-0.64
| NCU08954 | conserved hypothetical protein (202 aa)	-0.41	-0.30	0.29	0.37
| NCU04799 | polyadenylate-binding protein (765 aa)	-0.43	-0.31	0.17	0.28
| NCU07930 | adenosylhomocysteinase (450 aa)	-0.43	-0.31	0.50	0.53
| NCU01589 | heat shock protein 60 (575 aa)	-0.44	-0.32	-2.88	-2.01
| NCU01689 | mitochondrial DNA replication protein YHM2 (317 aa)	-0.44	-0.32	-0.21	-0.01
| NCU02566 | alanyl-tRNA synthetase (962 aa)	-0.44	-0.32	0.50	0.53
| NCU06346 | conserved hypothetical protein (102 aa)	-0.44	-0.32	-0.43	-0.17
| NCU00418 | NADH:ubiquinone oxidoreductase 14.8kD subunit (125 aa)	-0.47	-0.34	-0.32	-0.09
| NCU02545 | conserved hypothetical protein (317 aa)	-0.47	-0.34	-0.84	-0.48
| NCU06336 | N2,N2-dimethylguanosine tRNA methyltransferase (717 aa)	-0.47	-0.34	-0.17	0.02
| NCU11951 | aspartate aminotransferase (429 aa)	-0.47	-0.34	-2.39	-1.65
| NCU00565 | lipoic acid synthetase (431 aa)	-0.48	-0.35	-0.61	-0.31

| NCU01807 | conserved hypothetical protein (246 aa)	-0.48	-0.35	1.37	1.18
| NCU04074 | NADH:ubiquinone oxidoreductase 30.4 (284 aa)	-0.48	-0.35	1.21	1.06
| NCU04153 | pseudouridine synthase (487 aa)	-0.48	-0.35	-0.60	-0.30
| NCU09025 | glutamyl-tRNA(Gln) amidotransferase (648 aa)	-0.48	-0.35	0.05	0.19
| NCU00952 | mitochondrial ribosomal protein L44 (99 aa)	-0.49	-0.36	-2.99	-2.09
| NCU01304 | mitochondrial mRNA processing protein PET127 (851 aa)	-0.49	-0.36	-1.93	-1.30
| NCU07360 | DnaJ domain-containing protein (310 aa)	-0.49	-0.36	-0.89	-0.52
| NCU07724 | mitochondrial division protein 1 (635 aa)	-0.49	-0.36	-0.60	-0.30
| NCU08956 | MSP domain-containing protein (280 aa)	-0.49	-0.36	0.25	0.34
| NCU05220 | ATP synthase subunit F (102 aa)	-0.50	-0.37	-0.19	0.01
| NCU06732 | leukotriene A-4 hydrolase (668 aa)	-0.50	-0.37	2.02	1.67
| NCU02016 | conserved hypothetical protein (129 aa)	-0.52	-0.38	-1.16	-0.72
| NCU02423 | mitoferrin-1 (311 aa)	-0.52	-0.38	-0.21	-0.01
| NCU03155 | conserved hypothetical protein (166 aa)	-0.52	-0.38	-2.29	-1.57
| NCU04429 | mitochondrial import protein mmp37 (558 aa)	-0.53	-0.39	-0.89	-0.52
| NCU06051 | conserved hypothetical protein (370 aa)	-0.53	-0.39	0.05	0.19

| NCU05515 | mitochondrial import inner membrane translocase subunit tim16 (142 aa)	-0.54	-0.40	-1.38	-0.89
| NCU00636 | ATP synthase subunit D (174 aa)	-0.56	-0.41	-2.59	-1.80
| NCU06844 | conserved hypothetical protein (170 aa)	-0.56	-0.41	-0.44	-0.18
| NCU05642 | cysteinyl-tRNA synthetase (854 aa)	-0.57	-0.42	-0.01	0.14
| NCU08930 | NADH:ubiquinone oxidoreductase 21.3kD subunit a (202 aa)	-0.57	-0.42	-2.10	-1.43
| NCU09265 | calreticulin (566 aa)	-0.57	-0.42	0.77	0.73
| NCU08898 | homoaconitase (785 aa)	-0.58	-0.43	-0.57	-0.28
| NCU09693 | conserved hypothetical protein (323 aa)	-0.58	-0.43	1.17	1.03
| NCU00979 | 60S acidic ribosomal protein P2 (111 aa)	-0.61	-0.45	0.23	0.32
| NCU01808 | cytochrome c (109 aa)	-0.61	-0.45	-3.32	-2.34
| NCU02044 | GTP-binding protein (396 aa)	-0.62	-0.46	-0.37	-0.13
| NCU03020 | IdgA domain-containing protein (783 aa)	-0.62	-0.46	-0.60	-0.30
| NCU03565 | ribosomal protein L26 (137 aa)	-0.62	-0.46	-0.04	0.12
| NCU03910 | microsomal cytochrome b5 (140 aa)	-0.62	-0.46	-0.90	-0.53
| NCU06307 | multisynthetase complex auxiliary component p43 (420 aa)	-0.62	-0.46	-0.66	-0.35
| NCU01666 | acetolactate synthase small subunit (331 aa)	-0.64	-0.47	-0.40	-0.15
| NCU02948 | non-anchored cell wall protein-4 (206 aa)	-0.64	-0.47	-0.58	-0.29

| NCU05421 | lipoyltransferase and lipoate-protein ligase (434 aa)	-0.64	-0.47	0.17	0.28
| NCU05551 | conserved hypothetical protein (300 aa)	-0.64	-0.47	-1.14	-0.71
| NCU03558 | conserved hypothetical protein (79 aa)	-0.65	-0.48	-1.89	-1.27
| NCU06189 | 5-aminolevulinate synthase (630 aa)	-0.66	-0.49	-1.46	-0.95
| NCU07697 | isocitrate dehydrogenase subunit 2 (380 aa)	-0.66	-0.49	-2.67	-1.86
| NCU09599 | conserved hypothetical protein (283 aa)	-0.66	-0.49	-2.18	-1.49
| NCU09995 | hypothetical protein (104 aa)	-0.66	-0.49	0.52	0.54
| NCU00605 | ThiF domain-containing protein (511 aa)	-0.68	-0.50	-0.08	0.09
| NCU06695 | cytochrome c oxidase polypeptide VI (149 aa)	-0.69	-0.51	-2.63	-1.83
| NCU02075 | heat shock protein 70 (586 aa)	-0.70	-0.52	0.70	0.68
| NCU03953 | NADH:ubiquinone oxidoreductase 19.3 (227 aa)	-0.70	-0.52	0.11	0.23
| NCU09002 | NADH:ubiquinone oxidoreductase 10.6kD subunit (94 aa)	-0.70	-0.52	-1.97	-1.33
| NCU05430 | ATP synthase beta subunit (520 aa)	-0.73	-0.54	-2.70	-1.88
| NCU03359 | intermembrane space AAA protease IAP-1 (844 aa)	-0.74	-0.55	-0.57	-0.28
| NCU11687 | conserved hypothetical protein (203 aa)	-0.74	-0.55	-1.20	-0.75
| NCU01115 | tRNA-splicing endonuclease	-0.76	-0.56	-0.41	-0.16

subunit SEN2 (634 aa)				
| NCU03188 | sugar 1,4-lactone oxidase (557 aa)	-0.76	-0.56	-0.05	0.11
| NCU08297 | cell division control protein 3 (459 aa)	-0.77	-0.57	-0.49	-0.22
| NCU08300 | conserved hypothetical protein (92 aa)	-0.77	-0.57	-0.33	-0.10
| NCU06702 | yop-1 (169 aa)	-0.80	-0.59	-1.04	-0.63
| NCU00160 | NADH:ubiquinone oxidoreductase 6.6kD subunit (76 aa)	-0.81	-0.60	-0.64	-0.33
| NCU06482 | pyruvate dehydrogenase E1 component alpha subunit (418 aa)	-0.81	-0.60	-0.89	-0.52
| NCU08794 | UPF0041 domain-containing protein (126 aa)	-0.82	-0.61	-0.52	-0.24
| NCU01218 | conserved hypothetical protein (392 aa)	-0.84	-0.62	-1.06	-0.65
| NCU03217 | MRS7 family protein (549 aa)	-0.84	-0.62	-1.33	-0.85
| NCU03233 | hypothetical protein (60 aa)	-0.85	-0.63	-0.97	-0.58
| NCU02002 | conserved hypothetical protein (1032 aa)	-0.86	-0.64	-0.39	-0.14
| NCU04753 | NADH:ubiquinone oxidoreductase 11.6kD subunit (106 aa)	-0.86	-0.64	-0.31	-0.08
| NCU04899 | malate dehydrogenase (337 aa)	-0.86	-0.64	-3.43	-2.42
| NCU09223 | protein disulfide-isomerase (506 aa)	-0.86	-0.64	1.05	0.94
| NCU00935 | conserved hypothetical protein (582 aa)	-0.88	-0.65	-0.43	-0.17
| NCU02366 | aconitase (785 aa)	-0.88	-0.65	-2.43	-1.68

| NCU03982 | glucose regulated protein 78 (662 aa)	-0.88	-0.65	0.20	0.30
| NCU07560 | 50S ribosomal subunit L30 (369 aa)	-0.88	-0.65	-3.00	-2.10
| NCU01436 | questionable protein (84 aa)	-0.89	-0.66	-0.57	-0.28
| NCU10468 | arginine biosynthesis argJ (470 aa)	-0.89	-0.66	-0.85	-0.49
| NCU11956 | DUF1674 domain-containing protein (170 aa)	-0.90	-0.67	-0.49	-0.22
| NCU00050 | pyruvate dehydrogenase X component (427 aa)	-0.94	-0.70	-2.34	-1.61
| NCU04334 | chaperonin (105 aa)	-0.94	-0.70	-2.52	-1.75
| NCU00775 | isocitrate dehydrogenase subunit 1 (386 aa)	-0.96	-0.71	-1.58	-1.04
| NCU01241 | mitochondrial carrier protein (707 aa)	-0.96	-0.71	-0.41	-0.16
| NCU01692 | mitochondrial citrate synthase (470 aa)	-0.96	-0.71	-2.75	-1.92
| NCU08133 | carbonic anhydrase 2 (284 aa)	-0.96	-0.71	-0.21	-0.01
| NCU08471 | succinyl-CoA ligase beta-chain (448 aa)	-0.96	-0.71	-1.99	-1.35
| NCU01101 | mitochondrial import 1 (131 aa)	-0.97	-0.72	-0.23	-0.02
| NCU00969 | NADH:ubiquinone oxidoreductase 17.8kD subunit (187 aa)	-1.00	-0.74	-0.85	-0.49
| NCU07295 | mitochondrial import inner membrane translocase subunit tim-54 (469 aa)	-1.00	-0.74	-0.86	-0.50
| NCU04287 | conserved hypothetical protein (228 aa)	-1.01	-0.75	-1.62	-1.07

| NCU04945 | mitochondrial intermembrane space protein Mia40 (299 aa)	-1.01	-0.75	-0.54	-0.26
| NCU02013 | conserved hypothetical protein (164 aa)	-1.04	-0.77	-1.29	-0.82
| NCU06332 | alpha/beta hydrolase (595 aa)	-1.04	-0.77	0.13	0.25
| NCU06452 | cysteine synthase (377 aa)	-1.04	-0.77	-1.51	-0.99
| NCU01767 | phophatase 2C family protein (623 aa)	-1.05	-0.78	0.66	0.65
| NCU02438 | dihydrolipoamide succinyltransferase (422 aa)	-1.05	-0.78	-2.56	-1.78
| NCU06201 | cell wall biogenesis protein Ecm15 (157 aa)	-1.08	-0.80	-1.55	-1.02
| NCU00303 | smr domain-containing protein (256 aa)	-1.09	-0.81	0.57	0.58
| NCU00567 | arginine-6 (872 aa)	-1.09	-0.81	-0.70	-0.38
| NCU04245 | translocase of outer mitochondrial membrane 70 (623 aa)	-1.09	-0.81	-2.72	-1.90
| NCU07493 | conserved hypothetical protein (415 aa)	-1.09	-0.81	-1.30	-0.83
| NCU08627 | cytoplasmic ribosomal protein-7 (88 aa)	-1.10	-0.82	0.12	0.24
| NCU03637 | CaaX prenyl protease Ste24 (463 aa)	-1.12	-0.83	-0.85	-0.49
| NCU05009 | NADH:ubiquinone oxidoreductase 21.3 (220 aa)	-1.14	-0.85	-1.91	-1.29
| NCU03129 | threonyl-tRNA synthetase (498 aa)	-1.16	-0.86	-0.19	0.01
| NCU00644 | ATP synthase subunit G (188 aa)	-1.18	-0.88	-1.29	-0.82
| NCU09228 | aminopeptidase 2 (972 aa)	-1.18	-0.88	-1.70	-1.13
| NCU12061 | UDP-glucose:sterol	-1.18	-0.88	0.48	0.51

glycosyltransferase (1554 aa)				
| NCU00670 | NADH:ubiquinone oxidoreductase 9.5 (83 aa)	-1.20	-0.89	-0.73	-0.40
| NCU05425 | 2-oxoglutarate dehydrogenase E1 component (1044 aa)	-1.24	-0.92	-0.77	-0.43
| NCU02475 | glycine dehydrogenase (1101 aa)	-1.25	-0.93	-1.18	-0.74
| NCU07982 | acetolactate synthase (690 aa)	-1.25	-0.93	-1.33	-0.85
| NCU02280 | NADH:ubiquinone oxidoreductase 21.3kD subunit b (201 aa)	-1.26	-0.94	0.54	0.56
| NCU10008 | fumarate hydratase (534 aa)	-1.29	-0.96	-2.35	-1.62
| NCU11238 | mitochondrial 2-methylisocitrate lyase (619 aa)	-1.30	-0.97	-1.42	-0.92
| NCU03211 | conserved hypothetical protein (362 aa)	-1.32	-0.98	-1.41	-0.91
| NCU04698 | spermine/spermidine synthase (623 aa)	-1.32	-0.98	-0.61	-0.31
| NCU06512 | methionine synthase (770 aa)	-1.32	-0.98	0.52	0.54
| NCU09299 | NADH:ubiquinone oxidoreductase 14kD subunit (122 aa)	-1.32	-0.98	-0.07	0.10
| NCU09477 | ADP, ATP carrier protein (314 aa)	-1.33	-0.99	-2.33	-1.60
| NCU03199 | ATP synthase subunit H (125 aa)	-1.40	-1.04	-2.92	-2.04
| NCU02514 | ATPase-1 (552 aa)	-1.41	-1.05	-3.15	-2.21
| NCU01343 | TPR repeat protein (222 aa)	-1.42	-1.06	-2.10	-1.43
| NCU09460 | NADH:ubiquinone oxidoreductase 20.1kD	-1.42	-1.06	-1.90	-1.28

subunit (178 aa)				
| NCU01142 | NADH:ubiquinone oxidoreductase 13.4kD subunit (138 aa)	-1.44	-1.07	-2.25	-1.54
| NCU08940 | ubiquinol-cytochrome c reductase complex protein (124 aa)	-1.44	-1.07	-1.53	-1.00
| NCU06247 | conserved hypothetical protein (1354 aa)	-1.45	-1.08	-3.22	-2.26
| NCU06495 | UPF0327 protein (94 aa)	-1.45	-1.08	-2.05	-1.39
| NCU00030 | mitochondrial nuclease (333 aa)	-1.46	-1.09	-0.37	-0.13
| NCU01969 | conserved hypothetical protein (199 aa)	-1.46	-1.09	-0.07	0.10
| NCU05279 | conserved hypothetical protein (222 aa)	-1.50	-1.12	-2.05	-1.39
| NCU04843 | predicted protein (324 aa)	-1.55	-1.16	-1.01	-0.61
| NCU02293 | conserved hypothetical protein (118 aa)	-1.59	-1.19	-2.21	-1.51
| NCU07112 | conserved hypothetical protein (459 aa)	-1.63	-1.22	-0.69	-0.37
| NCU01765 | NADH:ubiquinone oxidoreductase 78 (745 aa)	-1.65	-1.23	-1.18	-0.74
| NCU01179 | translocase of outer mitochondrial membrane 40 (350 aa)	-1.70	-1.27	-1.93	-1.30
| NCU03093 | NADH:ubiquinone oxidoreductase 12.3kD subunit (105 aa)	-1.71	-1.28	-2.09	-1.42
| NCU11755 | conserved hypothetical protein (92 aa)	-1.74	-1.30	-1.99	-1.35
| NCU05457 | cytochrome a-4 (172 aa)	-1.75	-1.31	-2.41	-1.66

| NCU04781 | NADH:ubiquinone oxidoreductase 9.8 (87 aa)	-1.77	-1.32	-1.29	-0.82
| NCU09816 | cytochrome-1 (322 aa)	-1.77	-1.32	-1.36	-0.87
| NCU10311 | mitochondrial ribosomal protein subunit S4 (688 aa)	-1.78	-1.33	-1.18	-0.74
| NCU07732 | arginine-2 (454 aa)	-1.79	-1.34	0.19	0.29
| NCU08137 | conserved hypothetical protein (131 aa)	-1.81	-1.35	0.03	0.17
| NCU03135 | conserved hypothetical protein (205 aa)	-1.82	-1.36	-0.69	-0.37
| NCU09250 | conserved hypothetical protein (81 aa)	-1.82	-1.36	-1.46	-0.95
| NCU07576 | hypothetical protein (417 aa)	-1.85	-1.38	-1.75	-1.17
| NCU04579 | dihydroxy-acid dehydratase (597 aa)	-1.86	-1.39	-3.26	-2.29
| NCU03857 | conserved hypothetical protein (463 aa)	-1.89	-1.41	-2.66	-1.85
| NCU00894 | conserved hypothetical protein (673 aa)	-1.91	-1.43	-2.06	-1.40
| NCU05410 | acetylornithine aminotransferase (462 aa)	-1.99	-1.49	-0.25	-0.04
| NCU01227 | succinyl-CoA ligase alpha-chain (334 aa)	-2.01	-1.50	-2.63	-1.83
| NCU08877 | glycine cleavage system H protein (170 aa)	-2.02	-1.51	-2.30	-1.58
| NCU03216 | adenylate kinase (274 aa)	-2.07	-1.55	-2.27	-1.56
| NCU04276 | conserved hypothetical protein (100 aa)	-2.11	-1.58	-0.28	-0.06
| NCU00436 | GTPase FZO1 (919 aa)	-2.14	-1.60	-1.94	-1.31
| NCU00103 | conserved hypothetical protein (293	-2.15	-1.61	0.80	0.75

aa)

| NCU02812 | uridylate kinase (344 aa)	-2.17	-1.62	-1.47	-0.96
| NCU06560 | conserved hypothetical protein (485 aa)	-2.19	-1.64	0.11	0.23
| NCU01379 | histone acetylase complex subunit Paf400 (3896 aa)	-2.21	-1.65	-2.64	-1.84
| NCU02217 | cytochrome c oxidase-assembly factor cox-23 (83 aa)	-2.25	-1.68	-0.08	0.09
| NCU05027 | hypothetical protein (456 aa)	-2.25	-1.68	-2.33	-1.60
| NCU08947 | ubiquinol-cytochrome-c reductase chain VIII (108 aa)	-2.25	-1.68	-2.54	-1.76
| NCU00930 | translocase of inner mitochondrial membrane 10 (91 aa)	-2.42	-1.81	-1.74	-1.16
| NCU05689 | cytochrome c oxidase polypeptide IV (187 aa)	-2.43	-1.82	-3.95	-2.81
| NCU04114 | conserved hypothetical protein (72 aa)	-2.44	-1.83	-1.85	-1.24
| NCU02530 | cytochrome c oxidase copper chaperone Cox17 (79 aa)	-2.46	-1.84	-3.47	-2.45
| NCU03695 | phosphatidylserine decarboxylase proenzyme 1 (533 aa)	-2.64	-1.98	-1.16	-0.72
| NCU03608 | ketol-acid reductoisomerase (403 aa)	-2.78	-2.08	-3.07	-2.15
| NCU02677 | arginine-3 (1169 aa)	-2.92	-2.19	-1.53	-1.00
| NCU06244 | translocase of inner mitochondrial membrane, subunit 13 (87 aa)	-2.95	-2.21	-3.00	-2.10
| NCU01667 | arginine-12 (386 aa)	-2.96	-2.22	-1.21	-0.76
| NCU02115 | conserved hypothetical protein (954	-3.03	-2.27	-1.53	-1.00

aa)

| NCU01283 | conserved hypothetical protein (1418 aa)	-3.11	-2.33	-2.41	-1.66
| NCU04202 | nucleoside diphosphate kinase-1 (153 aa)	-3.14	-2.35	-3.55	-2.51
| NCU02472 | NADH:ubiquinone oxidoreductase 20.8kD subunit (184 aa)	-3.16	-2.37	-1.04	-0.63
| NCU03561 | mitochondrial carrier protein (305 aa)	-3.16	-2.37	-1.41	-0.91
| NCU06740 | conserved hypothetical protein (97 aa)	-3.27	-2.45	-2.83	-1.98
| NCU00153 | pyridine nucleotide-disulphide oxidoreductase (557 aa)	-3.32	-2.49	-0.43	-0.17
| NCU02149 | cytochrome c oxidase assembly protein (133 aa)	-3.34	-2.50	-2.18	-1.49
| NCU01546 | coproporphyrinogen III oxidase (410 aa)	-3.39	-2.54	-1.32	-0.84
| NCU11311 | small zinc finger protein Tim8 (93 aa)	-3.43	-2.57	-1.83	-1.23
| NCU02373 | NADH-ubiquinone oxidoreductase 40 kDa subunit (376 aa)	-3.44	-2.58	1.67	1.41
| NCU10048 | 3-methyl-2-oxobutanoate hydroxymethyltransferase (384 aa)	-3.44	-2.58	-1.63	-1.08
| NCU11339 | cytochrome c oxidase subunit VIb (85 aa)	-3.44	-2.58	-1.16	-0.72
| NCU01360 | NADH:ubiquinone oxidoreductase 11.5kD subunit (106 aa)	-3.72	-2.79	-1.91	-1.29
| NCU01550 | adenylate kinase cytosolic (279 aa)	-3.84	-2.88	-3.80	-2.70
| NCU00227 | mitochondrial cation transporter (341 aa)	-3.85	-2.89	0.13	0.25

| NCU01024 | conserved hypothetical protein (314 aa)	-3.93	-2.95	-1.53	-1.00
| NCU11348 | NADH-ubiquinone oxidoreductase B18 subunit (88 aa)	-4.04	-3.03	-2.02	-1.37
| NCU01962 | conserved hypothetical protein (137 aa)	-4.42	-3.32	-1.65	-1.09
| NCU11397 | NAD(P)H dehydrogenase (external)-2 (578 aa)	-5.10	-3.83	-2.38	-1.64
| NCU11655 | outer mitochondrial membrane protein porin (284 aa)	-5.99	-4.50	-4.32	-3.09
| NCU05989 | conserved hypothetical protein (142 aa)	-6.22	-4.67	-3.40	-2.40
| NCU01272 | mitochondrial presequence protease (1013 aa)	n/d	n/d	1.13	1.00

† $\log_2$ ratios are given for WS004 (iTRAQ species 116) over FGSC 9718 (iTRAQ species 114)

§ z score for each $\log_2$ ratio is calculated as ($\log_2$ ratio - mean of all $\log_2$ ratios) / standard deviation of all $\log_2$ ratios.

n/d not determined

References

Abu-Hamad, S., Zaid, H., Israelson, A., Nahon, E. and Shoshan-Barmatz, V. (2008). "Hexokinase-I protection against apoptotic cell death is mediated via interaction with the voltage-dependent anion channel-1: mapping the site of binding." J Biol Chem **283**(19): 13482-90.

Arzoine, L., Zilberberg, N., Ben-Romano, R. and Shoshan-Barmatz, V. (2009). "Voltage-dependent anion channel 1-based peptides interact with hexokinase to prevent its anti-apoptotic activity." J Biol Chem **284**(6): 3946-55.

Bainbridge, G., Armstrong, G. A., Dover, L. G., Whelan, K. F. and Lakey, J. H. (1998). "Displacement of OmpF loop 3 is not required for the membrane translocation of colicins N and A in vivo." FEBS Lett **432**(3): 117-22.

Baines, C. P., Kaiser, R. A., Sheiko, T., Craigen, W. J. and Molkentin, J. D. (2007). "Voltage-dependent anion channels are dispensable for mitochondrial-dependent cell death." Nat Cell Biol **9**(5): 550-5.

Baker, M. A., Lane, D. J., Ly, J. D., De Pinto, V. and Lawen, A. (2004). "VDAC1 is a transplasma membrane NADH-ferricyanide reductase." J Biol Chem **279**(6): 4811-9.

Bay, D. C. and Court, D. A. (2002). "Origami in the outer membrane: the transmembrane arrangement of mitochondrial porins." Biochem. Cell Biol. **80**(5): 551-62.

Bay, D. C., O'Neil, J. D. and Court, D. A. (2008). "Two-step folding of recombinant mitochondrial porin in detergent." Biophys. J. **94**: 457-468.

Bayrhuber, M., Meins, T., Habeck, M., Becker, S., Giller, K., Villinger, S., Vonrhein, C., Griesinger, C., Zweckstetter, M. and Zeth, K. (2008). "Structure of the human voltage-dependent anion channel." Proc Natl Acad Sci U S A **105**(40): 15370-5.

Belogrudov, G. I., Lee, P. T., Jonassen, T., Hsu, A. Y., Gin, P. and Clarke, C. F. (2001). "Yeast COQ4 encodes a mitochondrial protein required for coenzyme Q synthesis." Arch Biochem Biophys **392**(1): 48-58.

Benz, R. (1994). "Permeation of hydrophilic solutes through mitochondrial outer membranes: review on mitochondrial porins." Biochim Biophys Acta **1197**(2): 167-96.

Bertrand, H. and Kohout, J. (1977). "Nuclear suppressors of the (poky) cytoplasmic mutant in Neurospora crassa. II. Mitochondrial cytochrome systems." Can J Genet Cytol **19**(1): 81-91.

Bertrand, H. and Pittenger, T. H. (1969). "Cytoplasmic Mutants Selected from Continuously Growing Cultures of NEUROSPORA CRASSA." Genetics **61**(3): 643-59.

Beverly, K. N., Sawaya, M. R., Schmid, E. and Koehler, C. M. (2008). "The Tim8-Tim13 complex has multiple substrate binding sites and binds cooperatively to Tim23." J Mol Biol **382**(5): 1144-56.

Blachly-Dyson, E., Baldini, A., Litt, M., McCabe, E. R. and Forte, M. (1994). "Human genes encoding the voltage-dependent anion channel (VDAC) of the outer mitochondrial membrane: mapping and identification of two new isoforms." Genomics **20**(1): 62-7.

Blachly-Dyson, E., Peng, S., Colombini, M. and Forte, M. (1990). "Selectivity changes in site-directed mutants of the VDAC ion channel: structural implications." Science **247**(4947): 1233-6.

Blachly-Dyson, E., Song, J., Wolfgang, W. J., Colombini, M. and Forte, M. (1997). "Multicopy suppressors of phenotypes resulting from the absence of yeast VDAC encode a VDAC-like protein." Mol Cell Biol **17**(10): 5727-38.

Bohnert, M., Pfanner, N. and van der Laan, M. (2007). "A dynamic machinery for import of mitochondrial precursor proteins." FEBS Letters **581**: 2802-2810.

Bullock, W., Fernandez, J. and Short, J. (1987). "XL1-Blue: A high efficiency plasmid transforming *recA Escherichia coli* strain with beta-galactosidase selection." Biotechniques **5**: 376-379.

Casadio, R., Jacoboni, I., Messina, A. and De Pinto, V. (2002). "A 3D model of the voltage-dependent anion channel (VDAC)." FEBS Lett **520**(1-3): 1-7.

Chae, M. S. and Nargang, F. E. (2009). "Investigation of regulatory factors required for alternative oxidase production in Neurospora crassa." Physiol Plant **137**(4): 407-18.

Chen, Q., Vazquez, E. J., Moghaddas, S., Hoppel, C. L. and Lesnefsky, E. J. (2003). "Production of reactive oxygen species by mitochondria: central role of complex III." J Biol Chem **278**(38): 36027-31.

Colombini, M. (1980). "Pore size and properties of channels isolated from mitochondria isolated from *Neurospora crassa*." J. Membrane Biol. **53**: 79-84.

Colombini, M. (1989). "Voltage gating in the mitochondrial channel, VDAC." J Membr Biol **111**(2): 103-11.

Colot, H. V., Park, G., Turner, G. E., Ringelberg, C., Crew, C. M., Litvinkova, L., Weiss, R. L., Borkovich, K. A. and Dunlap, J. C. (2006). "A high-throughput gene knockout procedure for Neurospora reveals functions for multiple transcription factors." Proc Natl Acad Sci U S A **103**(27): 10352-7.

Court, D. A., Kleene, R., Neupert, W. and Lill, R. (1996). "Role of the N- and C-termini of porin in import into the outer membrane of *Neurospora* mitochondria." FEBS Lett **390**(1): 73-7.

Czub, J. and Baginski, M. (2006). "Comparative molecular dynamics study of lipid membranes containing cholesterol and ergosterol." Biophys J **90**(7): 2368-82.

Davis, R. H. and De Serres, F. J. (1970). "Genetic and microbiological research techniques for *Neurospora crassa*." Methods in Enzymology **17**: 79-143.

De Pinto, V., Messina, A., Schmid, A., Simonetti, S., Carnevale, F. and Benz, R. (2000). "Characterization of channel-forming activity in muscle biopsy from a porin-deficient human patient." J Bioenerg Biomembr **32**(6): 585-93.

De Pinto, V., Prezioso, G., Thinnes, F. P., Link, T. A. and Palmieri, F. (1991). "Peptide-specific antibodies and proteases as probes of the transmembrane topology of the bovine heart mitochondrial porin." Biochemistry **30**: 10191-10200.

De Pinto, V., Tomasello, F., Messina, A., Guarino, F., Benz, R., La Mendola, D., Magri, A., Milardi, D. and Pappalardo, G. (2007). "Determination of the conformation of the human VDAC1 N-terminal peptide, a protein moiety essential for the functional properties of the pore." Chembiochem **8**(7): 744-56.

Dihanich, M., Benz, R. and Mannella, C. A. (1990). "Pore-forming proteins of biological membranes." Experientia **46**(2): 131-201.

Dihanich, M., Suda, K. and Schatz, G. (1987). "A yeast mutant lacking mitochondrial porin is respiratory-deficient, but can recover respiration with simultaneous accumulation of an 86-kd extramitochondrial protein." Embo J **6**(3): 723-8.

Dolder, M., Zeth, K., Tittmann, P., Gross, H., Welte, W. and Wallimann, T. (1999). "Crystallization of the human, mitochondrial voltage-dependent anion-selective channel in the presence of phospholipids." J Struct Biol **127**(1): 64-71.

Fleissner, A., Sarkar, S., Jacobson, D. J., Roca, M. G., Read, N. D. and Glass, N. L. (2005). "The so locus is required for vegetative cell fusion and postfertilization events in Neurospora crassa." Eukaryot Cell **4**(5): 920-30.

Forte, M., Adelsberger-Mangan, D. and Colombini, M. (1987). "Purification and characterization of the voltage-dependent anion channel from the outer mitochondrial membrane of yeast." J Membr Biol **99**(1): 65-72.

Freitag, H., Neupert, W. and Benz, R. (1982). "Purification and characterisation of a pore protein of the outer mitochondrial membrane from *Neurospora crassa*." Eur. J. Biochem. **123**(3): 629-36.

Fuchs, F., Prokisch, H., Neupert, W. and Westermann, B. (2002). "Interaction of mitochondria with microtubules in the filamentous fungus Neurospora crassa." J Cell Sci **115**(Pt 9): 1931-7.

Galagan, J. E., Calvo, S. E., Borkovich, K. A., Selker, E. U., Read, N. D., Jaffe, D., FitzHugh, W., Ma, L. J., Smirnov, S., Purcell, S., Rehman, B., Elkins, T., Engels, R., Wang, S., Nielsen, C. B., Butler, J., Endrizzi, M., Qui, D., Ianakiev, P., Bell-Pedersen, D., Nelson, M. A., Werner-Washburne, M., Selitrennikoff, C. P., Kinsey, J. A., Braun, E. L., Zelter, A., Schulte, U., Kothe, G. O., Jedd, G., Mewes, W., Staben, C., Marcotte, E., Greenberg, D., Roy, A., Foley, K., Naylor, J., Stange-Thomann, N., Barrett, R., Gnerre, S., Kamal, M., Kamvysselis, M., Mauceli, E., Bielke, C., Rudd, S., Frishman, D., Krystofova, S., Rasmussen, C., Metzenberg, R. L., Perkins, D. D., Kroken, S., Cogoni, C., Macino, G., Catcheside, D., Li, W., Pratt, R. J., Osmani, S. A., DeSouza, C. P., Glass, L., Orbach, M. J., Berglund, J. A., Voelker, R., Yarden, O., Plamann, M., Seiler, S., Dunlap, J., Radford, A., Aramayo, R., Natvig, D. O., Alex, L. A., Mannhaupt, G., Ebbole, D. J., Freitag, M., Paulsen, I., Sachs, M. S., Lander, E. S., Nusbaum, C. and Birren, B. (2003). "The genome sequence of the filamentous fungus Neurospora crassa." Nature **422**(6934): 859-68.

Goncalves, R. P., Buzhynskyy, N., Prima, V., Sturgis, J. N. and Scheuring, S. (2007). "Supramolecular assembly of VDAC in native mitochondrial outer membranes." J Mol Biol **369**(2): 413-8.

Grad, L. I., Descheneau, A. T., Neupert, W., Lill, R. and Nargang, F. E. (1999). "Inactivation of the Neurospora crassa mitochondrial outer membrane protein TOM70 by repeat-induced point mutation (RIP) causes defects in mitochondrial protein import and morphology." Curr Genet **36**(3): 137-46.

Gray, M. W., Burger, G. and Lang, B. F. (2001). "The origin and early evolution of mitochondria." Genome Biol **2**(6): REVIEWS1018.

Guo, X. W., Smith, P. R., Cognon, B., D'Arcangelis, D., Dolginova, E. and Mannella, C. A. (1995). "Molecular design of the voltage-dependent, anion-selective channel in the mitochondrial outer membrane." J Struct Biol **114**(1): 41-59.

Guthrie, C. (2002). Guide to Yeast Genetics and Molecular and Cell Biology, Part B. San Diego, Academic Press.

Hanahan, D. (1983). "Studies on transformation of *Escherichia coli* with plasmids." J Mol Biol **166**(4): 557-80.

Harkness, T. A., Metzenberg, R. L., Schneider, H., Lill, R., Neupert, W. and Nargang, F. E. (1994). "Inactivation of the Neurospora crassa gene encoding the mitochondrial protein import receptor MOM19 by the technique of "sheltered RIP"." Genetics **136**(1): 107-18.

Harkness, T. A., Nargang, F. E., van der Klei, I., Neupert, W. and Lill, R. (1994). "A crucial role of the mitochondrial protein import receptor MOM19 for the biogenesis of mitochondria." J Cell Biol **124**(5): 637-48.

Hiller, S., Garces, R. G., Malia, T. J., Orekhov, V. Y., Colombini, M. and Wagner, G. (2008). "Solution structure of the integral human membrane protein VDAC-1 in detergent micelles." Science **321**(5893): 1206-10.

Hoppins, S. C., Go, N. E., Klein, A., Schmitt, S., Neupert, W., Rapaport, D. and Nargang, F. E. (2007). "Alternative Splicing Gives Rise to Different Isoforms of the Neurospora crassa Tob55 Protein That Vary in Their Ability to Insert {beta}-Barrel Proteins Into the Outer Mitochondrial Membrane." Genetics **177**(1): 137-49.

Hoppins, S. C. and Nargang, F. E. (2004). "The Tim8-Tim13 complex of Neurospora crassa functions in the assembly of proteins into both mitochondrial membranes." J Biol Chem **279**(13): 12396-405.

Horowitz, N. H. (1991). "Fifty years ago: the Neurospora revolution." Genetics **127**(4): 631-5.

Innocenti, F. D., Pohl, U. and Russo, V. E. (1983). "Photoinduction of protoperithecia in Neurospora crassa by blue light." Photochem Photobiol **37**(1): 49-51.

Kennell, J. C., Collins, R. A., Griffiths, A. J. F. and Nargang, F. E. (2004). "Mitochondrial Genetics of *Neurospora*." The Mycota **Vol. 2**(Genetics and Biotechnology): 95-112.

Kleene, R., Pfanner, N., Pfaller, R., Link, T. A., Sebald, W., Neupert, W. and Tropschug, M. (1987). "Mitochondrial porin of *Neurospora crassa*: cDNA cloning, in vitro expression and import into mitochondria." Embo J **6**(9): 2627-33.

Kmita, H. and Budzinska, M. (2000). "Involvement of the TOM complex in external NADH transport into yeast mitochondria depleted of mitochondrial porin1." Biochim Biophys Acta **1509**(1-2): 86-94.

Koebnik, R., Locher, K. P. and Van Gelder, P. (2000). "Structure and function of bacterial outer membrane proteins: barrels in a nutshell." Mol Microbiol **37**(2): 239-53.

Konstantinova, S. A., Mannella, C. A., Skulachev, V. P. and Zorov, D. B. (1995). "Immunoelectron microscopic study of the distribution of porin on outer membranes of rat heart mitochondria." J Bioenerg Biomembr **27**(1): 93-9.

Koppel, D. A., Kinnally, K. W., Masters, P., Forte, M., Blachly-Dyson, E. and Mannella, C. A. (1998). "Bacterial expression and characterization of the mitochondrial outer membrane channel. Effects of n-terminal modifications." J. Biol. Chem. **273**(22): 13794-800.

Kutik, S., Stojanovski, D., Becker, L., Becker, T., Meinecke, M., Kruger, V., Prinz, C., Meisinger, C., Guiard, B., Wagner, R., Pfanner, N. and Wiedemann, N. (2008). "Dissecting membrane insertion of mitochondrial beta-barrel proteins." Cell **132**(6): 1011-24.

Lambowitz, A. M. and Slayman, C. W. (1971). "Cyanide-resistant respiration in Neurospora crassa." J Bacteriol **108**(3): 1087-96.

Le Hir, H., Izaurralde, E., Maquat, L. E. and Moore, M. J. (2000). "The spliceosome deposits multiple proteins 20-24 nucleotides upstream of mRNA exon-exon junctions." Embo J **19**(24): 6860-9.

Lee, B., Yoshida, Y. and Hasunuma, K. (2006). "Photomorphogenetic characteristics are severely affected in nucleoside diphosphate kinase-1 (ndk-1)-disrupted mutants in Neurospora crassa." Mol Genet Genomics **275**(1): 9-17.

Lee, B., Yoshida, Y. and Hasunuma, K. (2009). "Nucleoside diphosphate kinase-1 regulates hyphal development via the transcriptional regulation of catalase in Neurospora crassa." FEBS Lett **583**(19): 3291-5.

Lemeshko, S. V. and Lemeshko, V. V. (2000). "Metabolically derived potential on the outer membrane of mitochondria: a computational model." Biophys J **79**(6): 2785-800.

Liu, M. Y. and Colombini, M. (1992). "Regulation of mitochondrial respiration by controlling the permeability of the outer membrane through the mitochondrial channel, VDAC." Biochim Biophys Acta **1098**(2): 255-60.

Liu, X. H., Chen, P. Q., Wang, B. L., Li, Y. H., Wang, S. H. and Li, Z. M. (2007). "Synthesis, bioactivity, theoretical and molecular docking study of 1-cyano-N-substituted-cyclopropanecarboxamide as ketol-acid reductoisomerase inhibitor." Bioorg Med Chem Lett **17**(13): 3784-8.

Ludwig, O., Krause, J., Hay, R. and Benz, R. (1988). "Purification and characterization of the pore forming protein of yeast mitochondrial outer membrane." Eur Biophys J **15**(5): 269-76.

Malia, T. J. and Wagner, G. (2007). "NMR structural investigation of the mitochondrial outer membrane protein VDAC and its interaction with antiapoptotic Bcl-xL." Biochemistry **46**(2): 514-25.

Mannella, C. A. (1982). "Structure of the outer mitochondrial membrane: ordered arrays of porelike subunits in outer-membrane fractions from Neurospora crassa mitochondria." J Cell Biol **94**(3): 680-7.

McDonald, B. M., Wydro, M. M., Lightowlers, R. N. and Lakey, J. H. (2009). "Probing the orientation of yeast VDAC1 in vivo." FEBS Lett **583**(4): 739-42.

Meisinger, C., Rissler, M., Chacinska, A., Szklarz, L. K., Milenkovic, D., Kozjak, V., Schonfisch, B., Lohaus, C., Meyer, H. E., Yaffe, M. P., Guiard, B., Wiedemann, N. and Pfanner, N. (2004). "The mitochondrial morphology protein Mdm10 functions in assembly of the preprotein translocase of the outer membrane." Dev Cell **7**(1): 61-71.

Michea-Hamzehpour, M. and Turian, G. (1987). "GMP-stimulation of the cyanide-insensitive mitochondrial respiration in heat-shocked conidia of Neurospora crassa." Experientia **43**(4): 439-40.

Mihara, K. and Sato, R. (1985). "Molecular cloning and sequencing of cDNA for yeast porin, an outer mitochondrial membrane protein: a search for targeting signal in the primary structure." Embo J **4**(3): 769-74.

Nargang, F. E., Bertrand, H. and Werner, S. (1978). "A nuclear mutant of Neurospora crassa lacking subunit 1 of cytochrome c oxidase." J Biol Chem **253**(18): 6364-9.

Nargang, F. E., Kunkele, K. P., Mayer, A., Ritzel, R. G., Neupert, W. and Lill, R. (1995). "'Sheltered disruption' of Neurospora crassa MOM22, an essential component of the mitochondrial protein import complex." Embo J **14**(6): 1099-108.

Nicholas, K. B. and Nicholas, H. B. J. (1997). "GeneDoc: A tool for editing and annotating multiple sequence alignments." 2.5.010. from http://www.psc.edu/biomed/genedoc.

Ninomiya, Y., Suzuki, K., Ishii, C. and Inoue, H. (2004). "Highly efficient gene replacements in Neurospora strains deficient for nonhomologous end-joining." Proc Natl Acad Sci U S A **101**(33): 12248-53.

Park, Y. C., San, K. Y. and Bennett, G. N. (2007). "Characterization of alcohol dehydrogenase 1 and 3 from Neurospora crassa FGSC2489." Appl Microbiol Biotechnol **76**(2): 349-56.

Pavlov, E., Grigoriev, S. M., Dejean, L. M., Zweihorn, C. L., Mannella, C. A. and Kinnally, K. W. (2005). "The mitochondrial channel VDAC has a cation-selective open state." Biochim Biophys Acta **1710**(2-3): 96-102.

Peng, S., Blachly-Dyson, E., Forte, M. and Colombini, M. (1992). "Large scale rearrangement of protein domains is associated with voltage gating of the VDAC channel." Biophys J **62**(1): 123-31; discussion 131-5.

Pollastri, G., Przybylski, D., Rost, B. and Baldi, P. (2002). "Improving the prediction of protein secondary structure in three and eight classes using recurrent neural networks and profiles." Proteins **47**(2): 228-35.

Pon, L., Moll, T., Vestweber, D., Marshallsay, B. and Schatz, G. (1989). "Protein import into mitochondria: ATP-dependent protein translocation activity in a submitochondrial fraction enriched in membrane contact sites and specific proteins." J Cell Biol **109**(6 Pt 1): 2603-16.

Popp, B., Court, D. A., Benz, R., Neupert, W. and Lill, R. (1996). "The role of the N and C termini of recombinant *Neurospora* mitochondrial porin in channel formation and voltage-dependent gating." J. Biol. Chem. **271**(23): 13593-9.

Popp, B., Gebauer, S., Fischer, K., Flügge, U. I. and Benz, R. (1997). "Study of structure and function of recombinant pea root plastid porin by biophysical methods." Biochemistry **36**(10): 2844-52.

Prokisch, H., Neupert, W. and Westermann, B. (2000). "Role of MMM1 in maintaining mitochondrial morphology in Neurospora crassa." Mol Biol Cell **11**(9): 2961-71.

Rauch, G. and Moran, O. (1994). "On the structure of mitochondrial porins and its homologies with bacterial porins." Biochem Biophys Res Commun **200**(2): 908-15.

Reina, S., Palermo, V., Guarnera, A., Guarino, F., Messina, A., Mazzoni, C. and De Pinto, V. (2010). "Swapping of the N-terminus of VDAC1 with VDAC3 restores full activity of the channel and confers anti-aging features to the cell." FEBS Lett **584**(13): 2837-44.

Roman, I., Figys, J., Steurs, G. and Zizi, M. (2005). "In vitro interactions between the two mitochondrial membrane proteins VDAC and cytochrome c oxidase." Biochemistry **44**(39): 13192-201.

Roman, I., Figys, J., Steurs, G. and Zizi, M. (2006). "Hunting interactomes of a membrane protein: obtaining the largest set of VDAC-interacting protein epitopes." Mol Cell Proteomics **9**: 1667-80.

Roman, I., Figys, J., Steurs, G. and Zizi, M. (2006). "Hunting interactomes of a membrane protein: obtaining the largest set of voltage-dependent anion channel-interacting protein epitopes." Mol Cell Proteomics **5**(9): 1667-80.

Rostovtseva, T. K., Antonsson, B., Suzuki, M., Youle, R. J., Colombini, M. and Bezrukov, S. M. (2004). "Bid, but not Bax, regulates VDAC channels." J Biol Chem **279**(14): 13575-83.

Rostovtseva, T. K. and Bezrukov, S. M. (2008). "VDAC regulation: role of cytosolic proteins and mitochondrial lipids." J Bioenerg Biomembr **40**(3): 163-70.

Runke, G., Maier, E., Summers, W. A., Bay, D. C., Benz, R. and Court, D. A. (2006). "Deletion variants of Neurospora mitochondrial porin: electrophysiological and spectroscopic analysis." Biophys J **90**(9): 3155-64.

Runke, G., Maier, E., Summers, W. A. T., Bay, D. C., Benz, R. and Court, D. A. (2006). "Deletion variants of *Neurospora* mitochondrial porin: Electrophysiological and spectroscopic analysis." Biophys. J. **90**: 3155-3164.

Sambrook, J. (2001). Molecular cloning: a laboratory manual. Cold Spring Harbor Cold Spring Harbor Laboratory Press.

Scharfe, C., Zaccaria, P., Hoertnagel, K., Jaksch, M., Klopstock, T., Dembowski, M., Lill, R., Prokisch, H., Gerbitz, K. D., Neupert, W., Mewes, H. W. and Meitinger, T. (2000). "MITOP, the mitochondrial proteome database: 2000 update." Nucleic Acids Res **28**(1): 155-8.

Schein, S. J., Colombini, M. and Finkelstein, A. (1976). "Reconstitution in planar lipid bilayers of a voltage-dependent anion-selective channel obtained from paramecium mitochondria." J Membr Biol **30**(2): 99-120.

Schmitt, S., Prokisch, H., Schlunck, T., Camp, D. G., 2nd, Ahting, U., Waizenegger, T., Scharfe, C., Meitinger, T., Imhof, A., Neupert, W., Oefner, P. J. and Rapaport, D. (2006). "Proteome analysis of mitochondrial outer membrane from Neurospora crassa." Proteomics **6**(1): 72-80.

Selker, E. U. (1990). "Premeiotic instability of repeated sequences in Neurospora crassa." Annu Rev Genet **24**: 579-613.

Selker, E. U., Cambareri, E. B., Jensen, B. C. and Haack, K. R. (1987). "Rearrangement of duplicated DNA in specialized cells of Neurospora." Cell **51**(5): 741-52.

Shanmugavadivu, B., Apell, H. J., Meins, T., Zeth, K. and Kleinschmidt, J. H. (2007). "Correct folding of the beta-barrel of the human membrane protein VDAC requires a lipid bilayer." J. Mol. Biol. **368**(1): 66-78.

Shao, L., Kinnally, K. W. and Mannella, C. A. (1996). "Circular dichroism studies of the mitochondrial channel, VDAC, from *Neurospora crassa*." Biophys. J. **71**(2): 778-86.

Simossis, V. A. and Heringa, J. (2005). "PRALINE: a multiple sequence alignment toolbox that integrates homology-extended and secondary structure information." Nucleic Acids Res **33**(Web Server issue): W289-94.

Song, J., Midson, C., Blachly-Dyson, E., Forte, M. and Colombini, M. (1998b). "The sensor regions of VDAC are translocated from within the membrane to the surface during the gating processes." Biophys J **74**(6): 2926-44.

Song, J., Midson, C., Blachly-Dyson, E., Forte, M. and Colombini, M. (1998a). "The topology of VDAC as probed by biotin modification." J Biol Chem **273**(38): 24406-13.

Staben, C., Jensen, B., Pollock, J., Schechtman, M., Kinsey, J. and Selker, E. U. (1989). "Use of a bacterial Hygromycin B resistance gene as a dominant selectable marker in *Neurospora crassa* transformation." Fungal Gene. Newslett **36**: 79-81.

Stanley, S., Dias, J. A., D'Arcangelis, D. and Mannella, C. A. (1995). "Peptide-specific antibodies as probes of the topography of the voltage-gated channel in the mitochondrial outer membrane of *Neurospora* crassa." J Biol Chem **270**(28): 16694-700.

Summers, W. A. and Court, D. A. (2010). "Origami in outer membrane mimetics: correlating the first detailed images of refolded VDAC with over 20 years of biochemical data." Biochem Cell Biol **88**(3): 425-38.

Tanton, L. L., Nargang, C. E., Kessler, K. E., Li, Q. and Nargang, F. E. (2003). "Alternative oxidase expression in Neurospora crassa." Fungal Genet Biol **39**(2): 176-90.

Taylor, R. D., McHale, B. J. and Nargang, F. E. (2003). "Characterization of Neurospora crassa Tom40-deficient mutants and effect of specific mutations on Tom40 assembly." J Biol Chem **278**(2): 765-75.

Thomas, L., Blachly-Dyson, E., Colombini, M. and Forte, M. (1993). "Mapping of residues forming the voltage sensor of the voltage-dependent anion-selective channel." Proc Natl Acad Sci U S A **90**(12): 5446-9.

Thomas, L., Kocsis, E., Colombini, M., Erbe, E., Trus, B. L. and Steven, A. C. (1991). "Surface topography and molecular stoichiometry of the mitochondrial channel, VDAC, in crystalline arrays." J Struct Biol **106**(2): 161-71.

Tsujimoto, Y. and Shimizu, S. (2007). "Role of the mitochondrial membrane permeability transition in cell death." Apoptosis **12**(5): 835-40.

Ujwal, R., Cascio, D., Colletier, J. P., Faham, S., Zhang, J., Toro, L., Ping, P. and Abramson, J. (2008). "The crystal structure of mouse VDAC1 at 2.3 A resolution reveals mechanistic insights into metabolite gating." Proc Natl Acad Sci U S A **105**(46): 17742-7.

Vanderleyden, J., Peeters, C., Verachtert, H. and Bertrand, H. (1980). "Stimulation of the alternative oxidase of Neurospora crassa by Nucleoside phosphates." Biochem J **188**(1): 141-4.

Xie, G. C. and Wilson, J. E. (1988). "Rat brain hexokinase: the hydrophobic N-terminus of the mitochondrially bound enzyme is inserted in the lipid bilayer." Arch Biochem Biophys **267**(2): 803-10.

Young, M. J., Bay, D. C., Hausner, G. and Court, D. A. (2007). "The evolutionary history of mitochondrial porins." BMC Evol Biol **7**: 31.

Young, M. J. and Court, D. A. (2008). "Effects of the S288c genetic background and common auxotrophic markers on mitochondrial DNA function in Saccharomyces cerevisiae." Yeast **25**(12): 903-12.

Zaid, H., Abu-Hamad, S., Israelson, A., Nathan, I. and Shoshan-Barmatz, V. (2005). "The voltage-dependent anion channel-1 modulates apoptotic cell death." Cell Death Differ **12**(7): 751-60.